

E&G

Eiszeitalter und Gegenwart
Quaternary Science Journal



Vol. 61
No 1
2012

LEHNMÜHLE RESERVOIR, EASTERN ERZGEBIRGE [Germany]
NORTHERN CALCAREOUS ALPS [Austria]
SCHWALBENBERG II [Germany]
LOWER RHINE EMBAYMENT [Germany]
SPIEGELBERG, KANTON SCHWYZ [Switzerland]
JUNGMORÄNENGEBIET SÜD-HOLSTEIN [Germany]
PERMAFROST SIBERIA [Russia]

E&G

Eiszeitalter und Gegenwart Quaternary Science Journal

Volume 61 / Number 1 / 2012 / DOI: 10.3285/eg.61.1 / ISSN 0424-7116 / www.quaternary-science.net / Founded in 1951

EDITOR

DEUQUA
Deutsche Quartärvereinigung e.V.
Office
Stilleweg 2
D-30655 Hannover
Germany
Tel: +49 [0]511-643 36 13
E-Mail: info [at] deuqua.de
www.deuqua.org

PRODUCTION EDITOR

SABINE HELMS
Geozon Science Media
Postfach 3245
D-17462 Greifswald
Germany
Tel. +49 [0]3834-80 14 60
E-Mail: helms [at] geozon.net
www.geozon.net

EDITOR-IN-CHIEF

HOLGER FREUND
ICBM – Geoecology
Carl-von-Ossietzky Universität Oldenburg
Schleusenstr. 1
D-26382 Wilhelmshaven
Germany
Tel.: +49 [0]4421-94 42 00
Fax: +49 [0]4421-94 42 99
E-Mail: holger.freund [at] uni-oldenburg.de

ASSOCIATE EDITORS

PIERRE ANTOINE, Laboratoire de Géographie Physique, Université Paris i Panthéon-Sorbonne, France
MARKUS FUCHS, Department of Geography, Justus-Liebig-University Giessen, Germany
RALF DIETRICH KAHLKE, Senckenberg Research Institute, Research Station of Quaternary Palaeontology Weimar, Germany

THOMAS LITT, Steinmann-Institute of Geology, Mineralogy and Paleontology, University of Bonn, Germany

LESZEK MARKS, Institute of Geology, University of Warsaw, Poland

HENK J. T. WEERTS, Physical Geography Group, Cultural Heritage Agency Amersfoort, The Netherlands

FORMER EDITORS-IN-CHIEF

PAUL WOLDSTEDT [1951–1966]
MARTIN SCHWARZBACH [1963–1966]
ERNST SCHÖNHALS [1968–1978]
REINHOLD HUCKRIEDE [1968–1978]
HANS DIETRICH LANG [1980–1990]
JOSEF KLOSTERMANN [1991–1999]
WOLFGANG SCHIRMER [2000]
ERNST BRUNOTTE [2001–2005]

ADVISORY EDITORIAL BOARD

FLAVIO ANSELMETTI, Department of Surface Waters, Eawag (Swiss Federal Institute of Aquatic Science & Technology), Dübendorf, Switzerland

KARL-ERNST BEHRE, Lower Saxonian Institute of Historical Coastal Research, Wilhelmshaven, Germany

PHILIP GIBBARD, Department of Geography, University of Cambridge, Great Britain

VOLLI E. KALM, Institute of Ecology and Earth Sciences, University of Tartu, Estonia

CESARE RAVAZZI, Institute for the Dynamics of Environmental Processes, National Research Council of Italy, Italy

JAMES ROSE, Department of Geography, Royal Holloway University of London, Great Britain

CHRISTIAN SCHLÜCHTER, Institute of Geological Sciences, University of Bern, Switzerland

DIRK VAN HUSEN, Altmünster, Austria

JEF VANDENBERGHE, Faculty of Earth and Life Sciences, VU University Amsterdam, The Netherlands

ANDREAS VÖTT, Institute of Geography, Johannes Gutenberg-Universität Mainz, Germany

AIMS & SCOPE

The *Quaternary Science Journal* publishes original articles of quaternary geology, geography, palaeontology, soil science, archaeology, climatology etc.; special issues with main topics and articles of lectures of several scientific events.

MANUSCRIPT SUBMISSION

Please upload your manuscript at the online submission system at our journal site www.quaternary-science.net. Please note the instructions for authors before.

FREQUENCY

2 numbers per year

SUBSCRIPTION

Free for DEUQUA-Members! Prices for standing order: single number 27,- Euro; double number 54,- Euro; plus shipping costs. We offer discounts for libraries and bookstores. Please subscribe to the journal at the publisher *Geozon Science Media*.

JOURNAL EXCHANGE

If you are interested in exchange your journal with the *Quaternary Science Journal*, please contact: Universitätsbibliothek Halle Tauschstelle, Frau Winther August-Bebel-Straße 13 D-06108 Halle (Saale), Germany

Tel. +49 [0]345-55 22 183

E-Mail: [tausch \[at\] bibliothek.uni-halle.de](mailto:tausch [at] bibliothek.uni-halle.de)

REORDER

Reorders are possible at the publishing house. See full list and special prices of available numbers on next to last page.

PUBLISHING HOUSE

Geozon Science Media UG (haftungsbeschränkt)
Postfach 3245
D-17462 Greifswald
Germany
Tel. +49 [0]3834-80 14 80
E-Mail: [info \[at\] geozon.net](mailto:info [at] geozon.net)
www.geozon.net

PRINT

Printed in Germany on 100% recycled paper climate neutral produced

COVER FIGURE

Frank Haubrich "Flood in Tharandt (Saxony, Germany), August 13th 2002"

RIGHTS

Copyright for articles by the authors

LICENSE

Distributed under a Creative Commons Attribution License 3.0

<http://creativecommons.org/licenses/by/3.0/>



Sediment imprint of the severe 2002 summer flood in the Lehnmühle reservoir, eastern Erzgebirge (Germany)

Lucas Kämpf, Achim Brauer, Peter Dulski, Karl-Heinz Feger, Frank Jacob, Eckehard Klemt

How to cite: KÄMPF, L., BRAUER, A., DULSKI, P., FEGER, K.-H., JACOB, F. & KLEMT, E. (2012): Sediment imprint of the severe 2002 summer flood in the Lehnmühle reservoir, eastern Erzgebirge (Germany). – E&G Quaternary Science Journal, 61 (1): 3–15. DOI: 10.3285/eg.61.1.01

Abstract: A series of 18 short cores has been obtained from the Lehnmühle reservoir (operation since 1932) in eastern Erzgebirge (Germany) in order to investigate the effects of the severe flood event in August 2002 on sedimentation by combining microfacies and high resolution μ -XRF scanning techniques. A distinct graded detrital layer, unique for the whole record, appears in almost the entire reservoir basin, ranging in thickness from 33 mm at proximal sites close to the river inflow to 5 mm at distal sites. The total sediment influx during this event was estimated to approximately 2,400 tons. Around two-thirds of the sediment was deposited in the southern-central part of the basin (approx. 32 % of the basin area) due to basin morphometry and proximity to the inflow. An enhanced flux of fine silt and clays to areas near the dam was observed and is likely driven by a steady current towards the dam. Occurrence of detrital material in a lateral bay reveals that sediment derived not only from the main inflow but also from surface runoff through non-permanently water bearing stream channels around the reservoir. In addition to the exceptional 2002 flood layer, 22 microscopically thin detrital layers were detected in the sediment cores, most of them at the deepest core locations close to the main dam. A chronology of detrital layers was established by ^{137}Cs dating of three core sequences and was transferred to other cores by detailed correlation based on four lithological markers. The comparison with instrumental data reveals that 64 % of the total 22 flood events over the last three decades with a daily discharge $> 8 \text{ m}^3\text{s}^{-1}$ of the main inflowing stream resulted in deposition of a layer of detrital material in the reservoir basin.

Sedimenteintrag durch das Augsthochwasser 2002 in die Talsperre Lehnmühle (Osterzgebirge)

Kurzfassung: Anhand von 18 Kurzkernen aus der Talsperre Lehnmühle (Inbetriebnahme 1932) im Osterzgebirge (Deutschland) wurden mittels mikrofaziellen und hochauflösenden μ -XRF Scanning Verfahren Auswirkungen des extremen Augsthochwassers 2002 auf den Sedimenteintrag untersucht. Fast über den gesamten Talsperrenboden hinweg wurde eine für die gesamte Sedimentsequenz einmalig markante detritische Lage detektiert, welche eine Mächtigkeit von 5 mm an der Staumauer bis 33 mm nahe dem Zufluss misst. Die eingetragene Sedimentmenge dieser Lage wird auf ca. 2.400 Tonnen geschätzt, wovon etwa zwei Drittel im südlich-zentralen Teil des Beckens (ca. 32 % der Gesamtfläche) abgelagert wurden, begründet durch die Beckenmorphologie und die Lage zum Zufluss. Feine Silt- und Tonpartikel wurden dagegen vornehmlich weiter in Richtung Staumauer transportiert, forciert durch eine ständige Wasserströmung durch das Staubecken. Eine erhöhte Akkumulation von detritischem Material in einer seitlichen Bucht zeigt, dass Sedimente nicht nur durch den Hauptzufluss eingetragen wurden, sondern ebenfalls durch Oberflächenabfluss in nicht ständig wasserführenden Rinnen um die Talsperre herum. Neben der markanten Lage des Jahres 2002, wurden 22 weitere, mikroskopisch dünne detritische Lagen in den Sedimentkernen nachgewiesen, die meisten im Profundbereich nahe der Staumauer. Eine Chronologie der detritischen Lagen wurde an drei ^{137}Cs datierten Kernsequenzen erstellt und durch detaillierte Korrelation mittels vier lithologischer Marker auf die übrigen Kerne übertragen. Der Vergleich mit instrumentellen Abflussdaten des Hauptzuflusses zeigt, dass während der letzten drei Jahrzehnte 64 % von insgesamt 22 Hochwasserereignissen mit einem Tagesabfluss $> 8 \text{ m}^3\text{s}^{-1}$ in die Ablagerung von detritischem Material resultierten.

Keywords: lake sediments, flood events, detrital layers, microfacies analysis, eastern Erzgebirge, water supply reservoir

Addresses of authors: L. Kämpf*, A. Brauer, P. Dulski, GFZ German Research Centre for Geosciences, Section 5.2 Climate Dynamics and Landscape Evolution, D-14473 Potsdam, Germany. K.-H. Feger, F. Jacob, Dresden University of Technology, Institute of Soil Science and Site Ecology, D- 01737 Tharandt, Germany. E. Klemt, Hochschule Ravensburg-Weingarten, University of Applied Sciences, D-88250 Weingarten, Germany. *Corresponding author: L. Kämpf, GFZ German Research Centre for Geosciences, Section 5.2 Climate Dynamics and Landscape Evolution, 14473 Potsdam, Germany. E-Mail: lucask@gfz-potsdam.de

1 Introduction

Establishing long flood time series from geoarchives has become a main issue of modern palaeoclimatic research (BAKER 2006, CHAPRON et al. 2005, CZYMIK et al. 2010, THORNDYCRAFT et al. 2003). Particularly valuable archives are lakes because they form ideal traps in the landscape, continuously recording land surface processes in the catchment including extreme events (BRAUER 2004, BRAUER & CASANOVA 2001, THORNDYCRAFT et al. 1998). Discrete flood-triggered sediment fluxes of detrital channel, bank

and catchment material into lakes result in long chronologies of detrital event layers (e.g. CHAPRON et al. 2005, CZYMIK et al. 2010, STØREN et al. 2010). Comparisons with instrumental hydrological data have revealed that sediment flux is not linearly related to discharge strength and that even strong flood events can miss in the sediment records (LAMOUREUX 2000, SWIERCZYNSKI et al. 2009). Sediment input to the lake can be minimized, for example due to wash out of river channel material by former floods (SCHIEFER et al. 2011) or by reduced erosion due to a dense vegetation cover or a frozen ground (CZYMIK et al. 2010, GILLI et

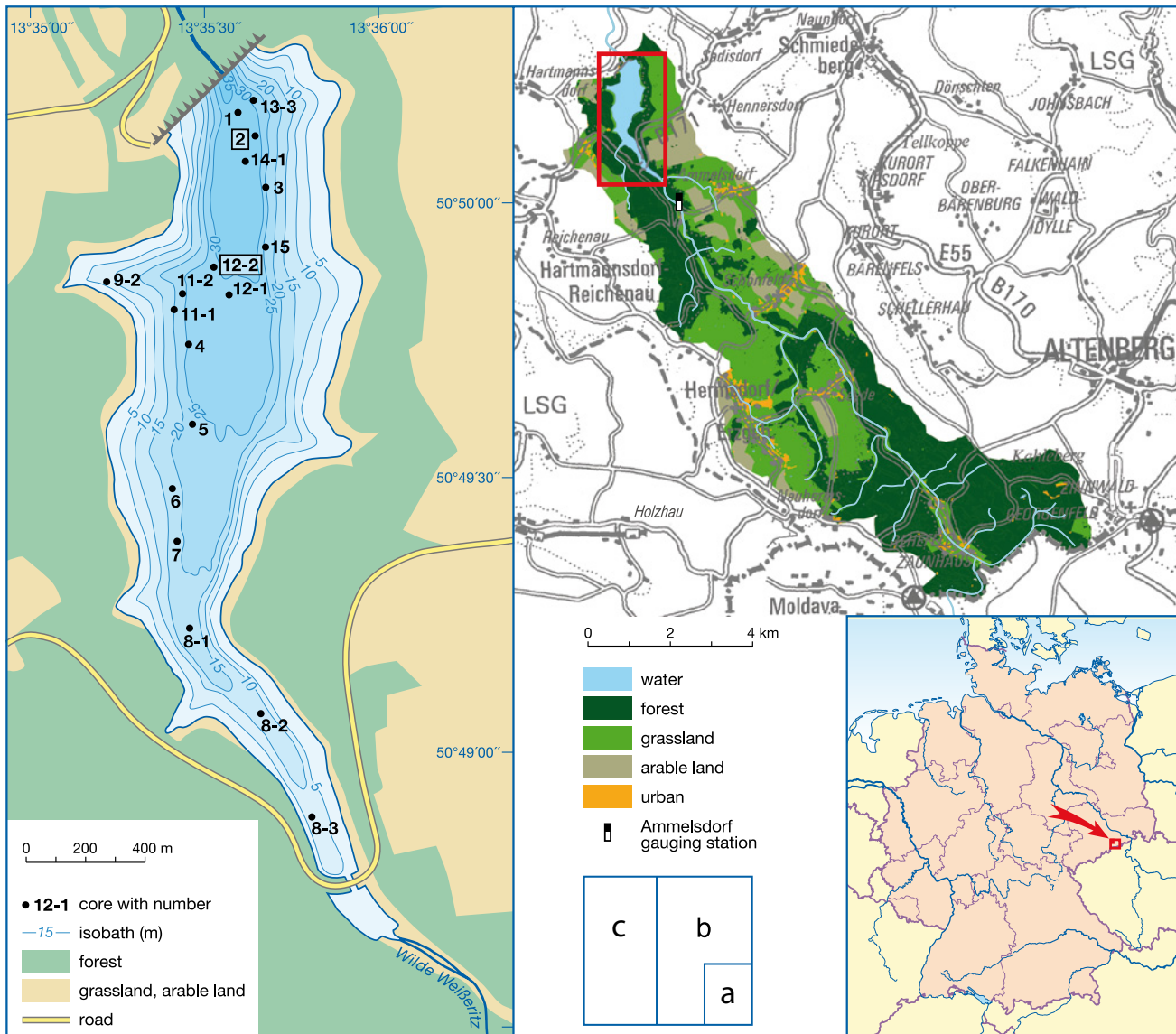


Fig. 1: Location of the Lehnsmühle reservoir and the Wilde Weißeritz catchment in the eastern Erzgebirge. (a) Location within Germany. (b) Land use of the Weißeritz catchment, based on CIR-GIS data from 2005 and a topographic map 1: 50 000, supplied by LfULG. (c) Core locations within the reservoir (black dots); locations of master cores TSLM 2 and TSLM 12-2 are stressed.

Abb. 1: Talsperre Lehnsmühle und Einzugsgebiet des Hauptzuflusses Wilde Weißeritz im Osterzgebirge. (a) Lage innerhalb Deutschlands. (b) Landnutzung im Einzugsgebiet der Wilden Weißeritz basierend auf CIR-GIS Daten (Stand: 2005) und topographischer Karte 1: 50 000, bereitgestellt vom LfULG. (c) Positionen der Sedimentkerne in der Talsperre (schwarze Punkte); hervorgehoben sind die Leitprofile TSLM 2 und TSLM 12-2.

al. 2003). Since sediment records often are obtained from a single location in the lake, missing detrital layers can also be caused by variability in sediment dispersion due to lake internal currents, stratification and basin morphometry (BEST et al., 2005, LAMB et al. 2010, WEIRICH 1986). Advancing the knowledge about the entire chain of sedimentary processes, leading to generation of detrital layers in lake sediments is crucial for improving their hydrological interpretation.

Besides natural lakes, reservoirs are suitable research objects, since in-depth monitoring provides a large variety of instrumental data, enabling a verification of sedimentological information (SHOTBOLT et al. 2005, SNYDER et al. 2006). Furthermore, flood events are of particular interest for reservoir management due to the consequences of an enhanced sediment delivery and the potential impact on water quality (DE CESARE et al. 2001, EFFLER et al. 2006). Therefore, this study aims to provide basic information

about flood related sediment transport and deposition in a reservoir.

The main objective was to investigate the deposits of the severe 2002 summer flood in the Lehnsmühle reservoir, located in eastern Erzgebirge (Germany). This flood occurred in the Elbe catchment and caused major damages (BfG 2002, LfULG 2004). It provides an ideal case study to investigate the impact of floods on sedimentation and to attempt to estimate total sediment flux into the reservoir during this single hydrometeorological event. It was a further objective to compare these deposits with the entire sediment record, formed since the operation started in 1932, to test if similar events have occurred in the past decades.

2 Site description

Lehnsmühle reservoir was built from 1927 to 1931 in the upper eastern Erzgebirge (Germany), approx. 25 km south-

Lehnsmühle reservoir	
Built	1927-1931
Reservoir volume	$23.73 \times 10^6 \text{ m}^3$
Dam water level	522.2 m.a.s.l.
	520.0 m.a.s.l. in Aug 2008 (date of coring)
Dam crest	525.6 m.a.s.l.
Reservoir surface area	135.0 ha
Mean depth	14.0 m
Maximum depth	35.6 m
Trophy status	Mesotroph
Open pre-dam	
Height	8 m
Outlet diameter	4 m
Wilde Weißeritz	
Mean discharge	$1.1 \text{ m}^3 \text{s}^{-1}$
Catchment size	60.4 km ² (thereof 12.3 km ² in Czech Republic)
Geology	Gneiss (60 %), phyllite (20 %), felsic magmatites (15 %), floodplain sediments (5 %)
Land use (German part)	Forest (62 %), grassland (18 %), arable land (13 %), water bodies (2.2 %), urban (2.0 %)

Tab. 1: Characteristics of Lehnsmühle reservoir and its tributary Wilde Weißeritz. Data from LTV (2002, 2009), LfULG.

Tab. 1: Daten zur Talsperre Lehnsmühle und Hauptzufuss Wilde Weißeritz. Daten von LTV (2002, 2009), LfULG.

east of Dresden (Fig. 1, Tab. 1). It is the upper of a chain of two reservoirs and was built (1) to reduce flood severity downstream and (2) to provide constant water supply for the downstream drinking water reservoir Klingenberg. In result of the latter, the water level of the Lehnsmühle reservoir has been intensively regulated and underwent strong fluctuations. Even an almost complete emptying took place in autumn 1975, because of technical reasons (KAULFUSS 1979).

The reservoir is fed by the tributary Wilde Weißeritz, entering the main basin from the south after passing an open dam (Fig. 1c), consisting of a stone wall, approx. 8 m in height with an open gate at the center of the wall, which is around 4 m in diameter. The dam was built as traffic link and to trap sediments in a flat, approx. 400 m long basin in front of the open dam. Downstream of the reservoir the stream enters into the Elbe River in the city of Dresden. The watershed of the upper Wilde Weißeritz (Fig. 1b), feeding the reservoir with a long-term mean of $1.1 \text{ m}^3 \text{s}^{-1}$, covers 60.4 km² and is characterized by smooth plateaus and steep hill slopes ranging from 522 m above sea level (a.s.l.) at the reservoir to 890 m a.s.l. at the main mountain crest. The land cover is mainly forest (62 %), grassland (18 %) and arable land (13 %), with forest dominating high altitude areas and left streambank areas next to the reservoir, respectively (LTV 2002). Dominant soils are poorly developed cambisols and podzols, which have developed from periglacial cover beds mainly above gneiss, phyllite and rhyolite (KAULFUSS 1979) and, thus, are characterized by dominance of siliciclastic minerals, mainly mica, quartz and feldspars. Annual mean precipitation ranges from approx. 880 mm at Lehnsmühle reservoir to 1000 mm at high altitude areas of the catchment (KAULFUSS 1979, BERNHOFER et al. 2008). Maximum rainfall amounts are recorded in summer and are caused by instantaneous, often intense convective rainfall. A second maximum in winter relates to more persistent precipitation, often as snowfall, which is driven by westerlies (BERNHOFER et al. 2008). The latter is the reason for maximum mean discharges during the snow melt sea-

son from March to April, attended by the highest flood frequency (Fig. 2). Additionally, intense discharges frequently occur in summer due to heavy short term precipitation, like in the case of the August 2002 flood (BERNHOFER et al. 2008).

3 Methods

In total, 18 short cores were taken from Lehnsmühle reservoir in August 2008, using a Ghilardi Gravity Corer Type KGH 94. These cores were 13.5 to 62.0 cm long and have been collected in water depths between 8.8 and 33.0 m (Tab. 2). After cutting the cores into two halves, lithological description, digital photographs and magnetic susceptibility scanning on the split core surface (Barington MS2E Sensor) were carried out for each sediment core. The core sequences were correlated, using distinct lithological markers (Fig. 3), except the shallow water cores TSLM 8-2 and TSLM 8-3.

A series of cores from different parts of the basin has been selected for detailed microfacies analyses: TSLM 1 and TSLM 2 close to the dam, TSLM 12-1, TSLM 12-2 and TSLM 4 in the center of the basin as well as TSLM 6 and TSLM 7 in the southern proximal area closer to the river inflow (Fig. 1, Tab. 2). In addition, the uppermost 10 to 18 cm have been analyzed from most other cores (Tab. 2). Microfacies analyses have been carried out on large format thin sections. For this, overlapping samples (10 cm x 2 cm x 1 cm) were taken from the fresh sediment surface of a split core half. The procedure of thin section preparation is described in detail by BRAUER & CASANOVA (2001) and MANGILI et al. (2005). Analyses have been carried out under magnifications between 12.5x and 100x, using a petrographic microscope (Carl Zeiss Axiophot). Thin-section images were obtained with a digital camera (Carl Zeiss AxioCam) and the software Carl Zeiss Axiovision 2.0.

In addition, high-resolution semi-quantitative geochemical data were obtained by micro X-ray fluorescence (μ -XRF) measurements on impregnated sediment slabs from thin section preparation of cores TSLM 2, TSLM 12-2 and from the upper 10 cm of core TSLM 12-1, allow-

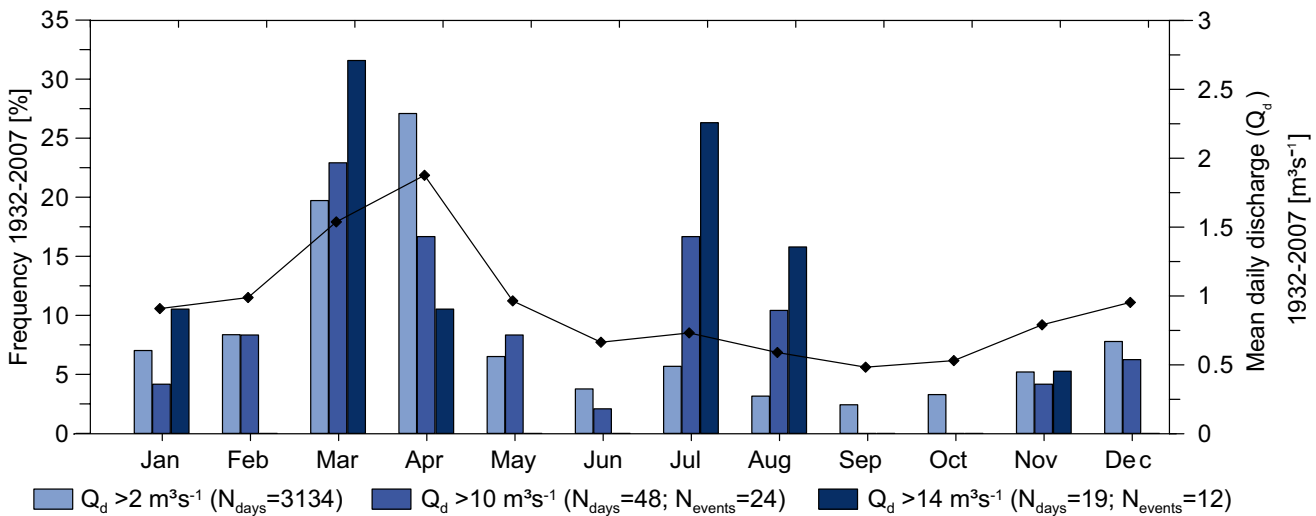


Fig. 2: Mean monthly discharge (line) and annual frequency distribution of Wilde Weißeritz discharge events of different intensities (bars), based on daily discharge values (Q_d), recorded at Ammelsdorf gauge station located approx. 1 km upstream of the inflow to Lehnsmühle reservoir (11/01/1931 to 10/31/2007).

Abb. 2: Mittlerer monatlicher Abfluss (Linie) und jährliche Häufigkeitsverteilung von unterschiedlich starken Abflussereignissen der Wilden Weißeritz (Balken) basierend auf Tagesmittelwerten (Q_d) vom Pegel Ammelsdorf, ca. 1 km vor dem Eintritt des Flusses in die Talsperre (01.11.1931 bis 31.10.2007).

Tab. 2: List of 18 gravity cores, taken from Lehnsmühle reservoir in August 2008 (water level: 520.0 m a.s.l.). Water level drawdown has led to exposure of coring locations (most recently notified). I/II trans. is the border between sediment units I and II. Age of each core basis (sediment unit II) refers either to the I/II transition (1932) or to correlated lithological markers. Underlined are the two dated master cores TSLM 2 close to the dam and TSLM 12-2 in the basin center.

Tab. 2: Liste der 18 Sedimentkerne aus der Talsperre Lehnsmühle (entnommen im August 2008, Wasserstand: 520.0 m ü. NN). Exposure: Jüngstes Trockenfallen der Kernposition bei niedrigem Wasserstand. I/II trans.: Grenze zwischen Sedimenteinheiten I und II. Basis age: Das Alter der Kernbasis (Sedimenteneinheit II) bezieht sich entweder auf die I/II Grenze (1932) oder auf korrelierte lithologische Markerpunkte. Unterstrichen sind die zwei datierten Hauptprofile TSLM 2 am Hauptdamm und TSLM 12-2 in der Beckenmitte.

Name	Lat	Lon	Water depth	Exposure	Core length	I/II trans.	Basis age	Microfacies	μ-XRF	¹³⁷ Cs
TSLM	[50° N]	[13° E]	[m]	[yr AD]	[cm]	[cm]	[yr AD]	[cm]	[cm]	[cm]
1	49°58.9"	35°36.1"	33.0	(-)	33.2	> 33.2	1932-1954	0 - 33		
2	49°56.6"	35°39.0"	32.0	(-)	30.5	> 30.5	1932-1954	0 - 30.5	0 - 30.5	0 - 30.5
3	49°51.6"	35°41.1"	26.0	1975	23.2	> 23.2	1932-1987	0 - 18		
4	49°36.4"	35°28.3"	26.0	1975	51.0	25.2	1932	0 - 26		
5	49°28.6"	35°28.8"	24.0	1976	53.4	25.0	1932	0 - 26		
6	49°22.4"	35°25.9"	17.0	1980	37.3	19.5	1932	0 - 26		
7	49°17.3"	35°26.6"	17.2	1980	35.0	19.8	1932	0 - 26		0 - 21
8-1	49°8.8"	35°29.0"	17.5	1980	62.0	unclear		0 - 18		
8-2	49°0.5"	35°38.9"	13.3	2003	34.5	28.0	1932	-		
8-3	48°50.3"	35°48.2"	9.3	2003	13.5	unclear		-		
9-2	49°42.5"	35°14.7"	8.8	2003	33.8	unclear		0 - 10		
11-1	49°39.8"	35°26.0"	21.7	1976	32.8	21.0	1932	0 - 26		
11-2	49°41.3"	35°27.4"	23.8	1976	42.4	17.5	1932	0 - 10		
12-1	49°41.2"	35°35.1"	28.5	1975	46.2	25.2	1932	0 - 26	0 - 10	
<u>12-2</u>	49°43.9"	35°31.8"	29.0	1975	38.0	29.0	1932	0 - 34	0 - 34	0 - 30
13-1	50°00.0"	35°38.8"	29.0	1975	23.4	> 23.4	1932-1987	0 - 10		
14-1	49°54.1"	35°37.3"	31.0	(-)	26.3	> 26.3	1932-1983	0 - 10		
15	49°45.8"	35°41.2"	24.1	1975	33.0	14.5	1932	0 - 10		

ing direct comparison of geochemical and microfacies data (BRAUER et al. 2009). Micro-XRF scanning has been carried out using an EAGLE III XL μ-XRF spectrometer with a low power Rh X-ray tube at 40 kV and 300 μA. All measurements were performed under vacuum on a single scan line with 250 μm spot size, 200 μm step width and a counting time of 60 s. The fluorescent radiation emitted from the

sample was recorded by an energy dispersive Si (Li) detector and transformed into element information for each measuring point. Each data point reflects the mean element intensity, expressed in counts per second (cps).

For complementary bulk sediment analyses, volumetric samples were taken in 1 cm intervals from master cores TSLM 2 and TSLM 12-2. Samples were freeze dried and

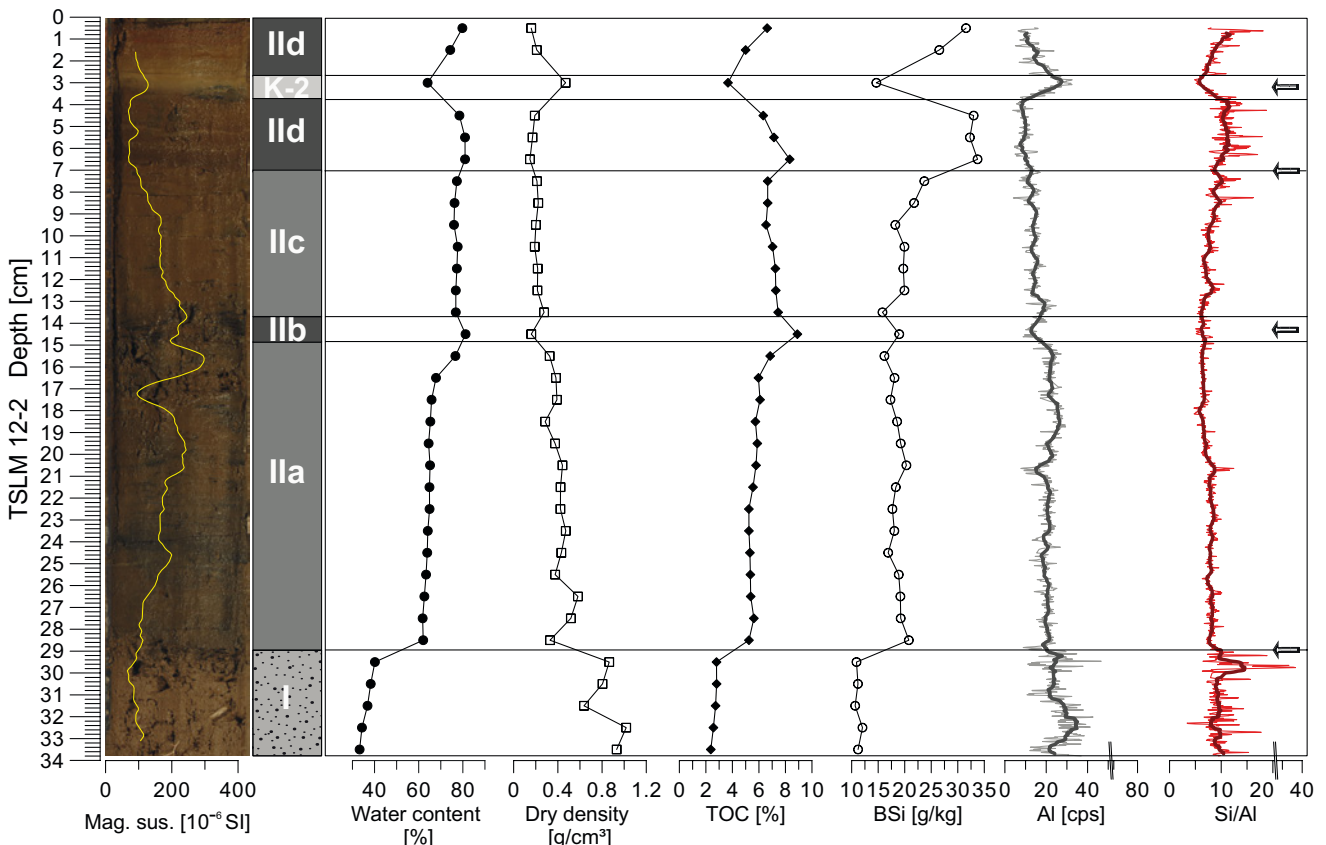


Fig. 3: Lithology of the master core sequence TSLM 12-2 from the basin center: core photo with magnetic susceptibility, water content, bulk density, contents of total organic carbon (TOC) and biogenic silica (BSi) and μ -XRF values of aluminum (Al) and the silicon:aluminum ratio (Si/Al). Arrows mark the lithological markers used for core-to-core correlation.

Abb. 3: Lithologie des Leitprofils TSLM 12-2 (Beckenmitte): Kernfoto mit den Parametern magnetische Suszeptibilität (Mag. sus.), Wassergehalt (Water content), Dichte (Bulk density), Gehalte des organischen Kohlenstoffs (TOC) und des biogenen Siliziums (BSi) und μ -XRF Werte von Aluminium (Al) und des Silizium:Aluminium Verhältnisses (Si/Al). Die Pfeile markieren die lithologischen Markerhorizonte für die Korrelation der Kernprofile.

their water contents were determined. Bulk density was calculated by dividing dry mass by volume of the sample (HÅKANSON & JANSSON 1983). The most prominent detrital layer has been sub-sampled separately for calculating the accumulated sediment mass by multiplying bulk density with layer thickness as measured in thin sections.

Measurements of total organic carbon (TOC) were performed with an elemental analyzer Euro Vector EA (EuroEA 3000 Series). Sample preparation included homogenizing 3 mg dried material, treatment with 3% and 20% HCl and further heating to 70 °C. Biogenic silica (BSi) was extracted from the dried samples, following instructions of ENGSTROM & WRIGHT (1984), modified by JACOB et al. (2009) and was determined, using a ICP-AES (CIROS, Spectro) at Dresden University of Technology.

The chronology has been established by measuring ^{137}Cs activity on homogenized samples from cores TSLM 2, TSLM 7 and TSLM 12-2, using a High Purity Germanium detector (well type) (Canberra-Eurysis) at Ravensburg-Weingarten University of Applied Sciences.

Runoff data of Wilde Weißeritz were used for interpretation of investigated sedimentological data and are based on mean daily discharge values, recorded at Ammelsdorf gauging station (Fig. 1). Data were supplied by the LfULG (Saxony State Office for the Environment, Agriculture and Geology). The gauging station was destroyed by water masses of the flood in August 2002 and data from this time

derive from the LTV (The State Reservoir Administration of Saxony), calculated to daily means by water level change and withdrawal. No discharge data are available in the time periods November 1943 to October 1945 and November 1962 to October 1963. Daily water level data measured at the main dam of Lehnsmühle reservoir since January 1st 1962 were supplied by the LTV.

4 Results

4.1 Lithology

In the sediment record from Lehnsmühle reservoir two main lithological units (I and IIa-d) have been distinguished in 10 from 18 cores (Tab. 2, Fig. 3). The lowermost sediment unit I was found in cores TSLM 4, 5, 6, 7, 8-2, 11-1, 11-2, 12-1, 12-2 and 15 (Tab. 2) and is characterized by a light colored and poorly sorted sediment with grain sizes up to fine pebbles and abundance of roots and plant remains. High bulk density (around 1 g cm⁻³) and low contents of water and total organic carbon (TOC) (< 3 %) indicate high minerogenic contents. Sediment unit II is characterized by a generally higher content of organic matter and finer grain sizes, ranging from clay to coarse silt.

The sharp boundary between the two main units I and II (Fig. 3) is interpreted as the transition from the old land surface before the reservoir construction (unit I) to lacus-

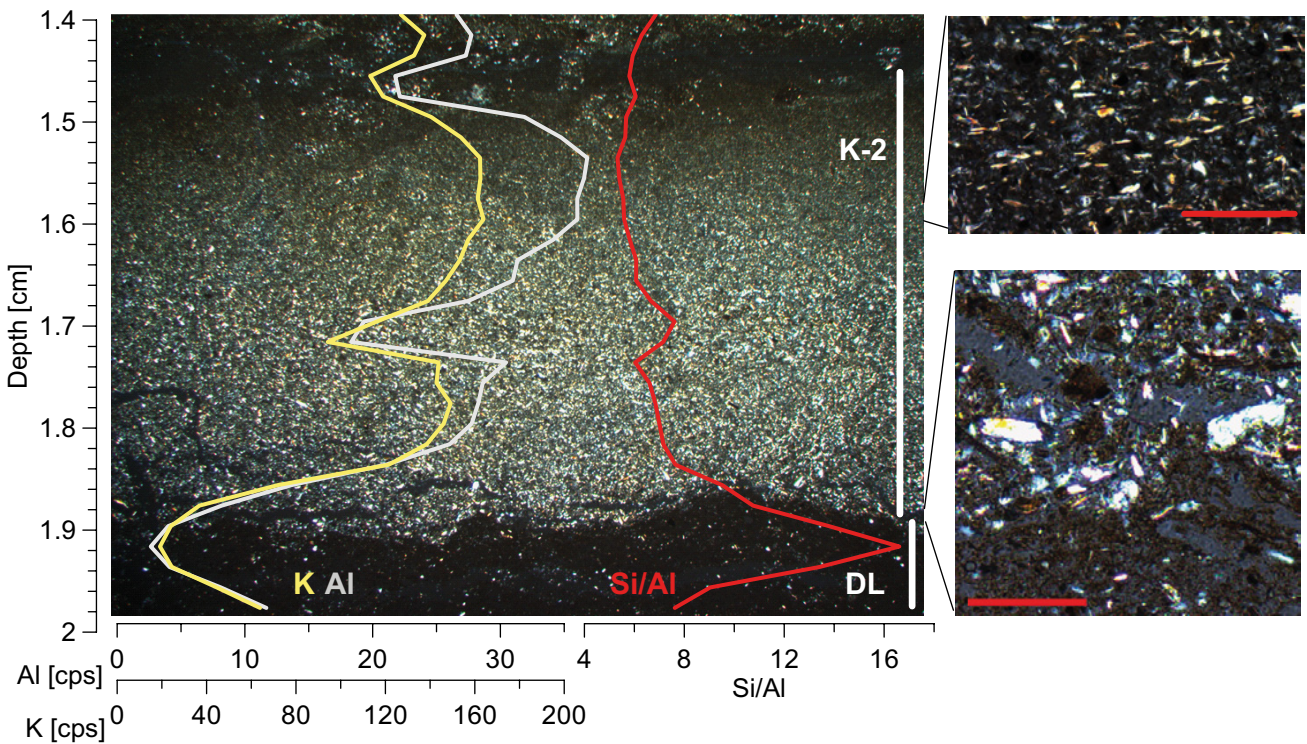


Fig. 4: Microfacies of the thick detrital layer K-2 with μ -XRF profiles of Al (grey line), K (yellow line) and Si/Al ratio (red line) obtained from core TSLM 12-1 (basin center). Note the diatom layer DL underlying K-2. Thin section images were taken under crossed polarized light with 12.5x magnification (big image) and 100x magnification (small images), red scale bars: 100 μm .

Abb. 4: Mikrofazies der detritischen Lage K-2 mit μ -XRF Profilen von Al (graue Linie), K (gelbe Linie) und Si/Al (rote Linie), gemessen am Kern TSLM 12-1 (Beckenmitte). DL markiert eine Diatomeenlage, unterhalb von K-2. Dünnschliffbilder wurden unter gekreuzt polarisiertem Licht mit 12.5x Vergrößerung (großes Bild) bzw. 100x Vergrößerung (kleine Bilder) aufgenommen, rote Skalen: 100 μm .

trine sediments formed since infilling the reservoir in 1932 (unit II). This boundary was observed in sediment depths between 14.5 cm at marginal locations (TSLM 15) and 29.0 cm in the central basin (TSLM 12-2) and is expected even deeper in locations near the dam where it has not been found in cores reaching a sediment depth of 30.5 cm (TSLM 2) and 33.0 cm (TSLM 1), respectively. For those and seven other cores (Tab. 2) it is assumed that they did not reach the base of lacustrine sediments.

The lacustrine sediment sequence (unit II) was divided into four subunits IIa-d, based on variations in sediment color, bulk density, TOC, biogenic silica (BSi), aluminum (Al), silicon:aluminum ratio (Si/Al) and abundance of organic matter (Fig. 3).

Sediment unit IIa is characterized by a light brownish color and consists of a predominantly minerogenic, fine-grained homogenous matrix. Water contents, TOC, BSi, Al and Si/Al remain almost constant within this unit. Low values of TOC (5 %) and water content (65 %) and high Al count rates confirm higher minerogenic contents compared to the upper subunits.

Sediment unit IIb represents a thin and dark brownish horizon, ranging in thickness from 0.5 cm in the basin center (TSLM 4) to 2.6 cm close to the dam (TSLM 2) and was observed only at coring sites exceeding 25.0 m water depth (TSLM 1, 2, 4, 12-1, 12-2). The horizon predominantly consists of plant remains and amorphous organics, resulting in a sharp increase in TOC values of about 2 % (Fig. 3).

Sediment unit IIc is light brownish and macroscopically rather similar to sediment unit IIa. The total thickness of

sediment units IIa-c ranges from 11.6 cm at the distal site TSLM 7 to > 27.0 cm next to the dam (TSLM 1), where the basis of sediment unit IIa, the onset of lacustrine sedimentation, is below the base of the core. Compared to sediment unit IIa, unit IIc is characterized by a higher content of organic matter, displayed in higher TOC between 6 and 7 %, lower Al count rates and a decreased bulk density (0.3 g cm^{-3}). A slight increase in diatom abundance within sediment unit IIc was observed in thin sections. This is confirmed by slightly increasing BSi values of around 4% and Si/Al, used as a proxy for biogenic silica (FRANCUS et al. 2009).

A sharp boundary between the light brownish sediment unit IIc and the uppermost darker unit IId was detected in all cores in depths between 4 cm at the basin center (TSLM 5) and 5.4 cm near the dam (TSLM 2) to 8.2 cm at the proximal position TSLM 7. Compared to lower sediment units, unit IId is characterized by higher organic matter contents reflected in an increase of TOC of about 1.5 % and abundance of diatoms, entailing a sharp rise of BSi values of more than 10%. Only in this sediment unit diatom frustules form discrete layers (Fig. 4, Fig. 5), which causes distinct peaks in the Si/Al ratio (Fig. 3).

A characteristic feature of sediment unit IId is an intercalated light-colored detrital layer (Fig. 4), found at all locations except in two shallow water cores located in the southernmost, channel-like part of the basin close to the inflow of the Wilde Weißeritz river (TSLM 8-2: 13.3 m water depth, TSLM 8-3: 9.3 m water depth). The layer ranges in thickness from 5 mm in near dam locations (TSLM 13-1:

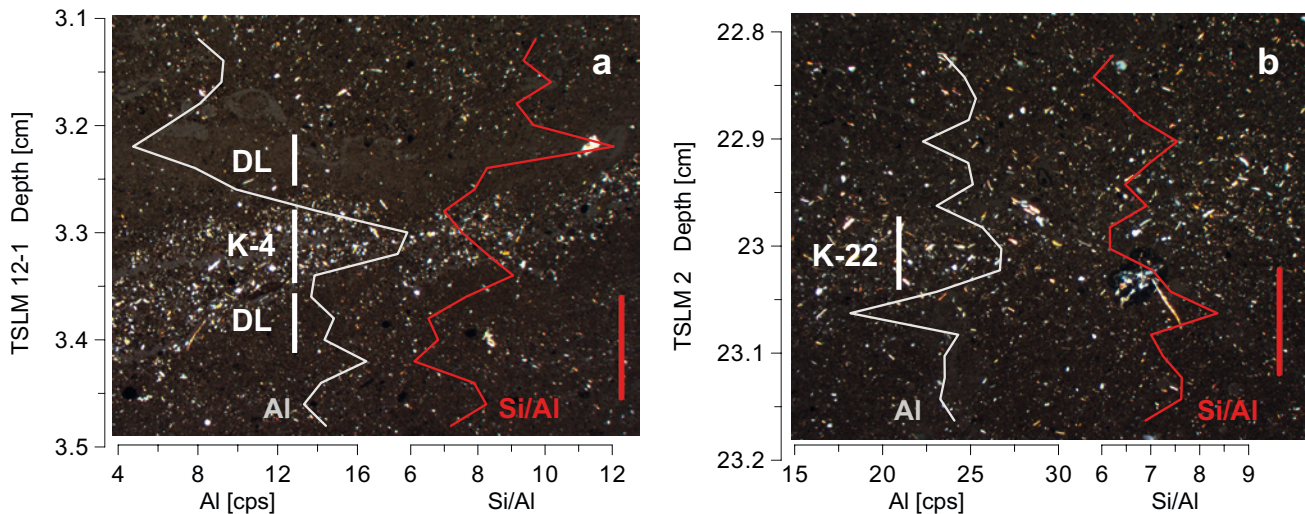


Fig. 5: Microfacies of thin detrital layers and μ -XRF profiles of Al (grey line) and Si/Al ratio (red line). (a) Detrital layer K-4 in sediment unit II_d with over- and underlying diatom layers (DL) (TSLM 12-1). (b) Detrital layer K-22 in sediment unit II_a (TSLM 2). Thin section images were taken under crossed polarized light with 12.5x magnification, scale bar: 1mm.

Abb. 5: Mikrofazies dünner detritischer Lagen und μ -XRF Profile von Al (graue Linie) und Si/Al (rote Linie). (a) Detritische Lage K-4 in Sedimenteinheit II_d mit Diatomeenlagen (DL) darüber und darunter (TSLM 12-1). (b) Detritische Lage K-22 in Sedimenteinheit II_a (TSLM 2). Dünnschliffbilder wurden unter gekreuzt polarisiertem Licht mit 12.5x Vergrößerung aufgenommen, Skala: 1 mm.

29.0 m water depth) to 33 mm closer to the inflow of the Wilde Weißeritz river (TSLM 7: 17.2 m water depth) and is mainly composed of detrital, minerogenic matter (Fig. 4). Most abundant minerals are mica, quartz, feldspar and clay minerals. The structure of this layer is characterized by normal grading, shown in decreasing grain sizes upwards within the layer, as measured in thin sections. Grain diameters in the basal part range from 40 to 60 μ m and only occasionally individual grains exceed 100 μ m in diameter. Quartz and feldspar minerals are dominating the coarse grained fraction, whereas in the upper part of the layer, more fine grained horizontally arranged mica minerals are abundant (Fig. 4). The mineralogical sorting upwards within the layer is illustrated by increasing Al and potassium (K) counts, reflecting an upward increase of clay mineral and mica contents. In general, the thickness of the top clay layer is increasing towards the dam at the expense of the silt-sized part and is absent in the most proximal sediment cores TSLM 6, 7 and 8-1.

The total sediment input through this discrete detrital-minerogenic layer into the reservoir has been calculated to approx. 2,400 t by multiplying the measured density of the layer with the estimated volume. A total volume of 4,800 m^3 was calculated by linear interpolation of layer thickness between sample points and rough extrapolation of the layer up to the rising lateral slopes (Fig. 8). More than 65 % of the sediment load was deposited between the core locations TSLM 6 and TSLM 8-1 encompassing the southern-central part of the basin, where accumulation rates reach 14.0 kg m^{-2} in contrast to 3.4 kg m^{-2} close to the dam.

In addition to this exceptional layer, microfacies analyses enabled to identify 22 further detrital layers (Fig. 5), of which 16 are intercalated in sediment units IIc and II_d (Fig. 7). Within sediment unit II_a seven layers appear in two cores close to the dam in water depth > 30.0 m (TSLM 1, 2) and three in the basin center (TSLM 4: 26.0 m water depth). All these additional detrital layers range in thick-

ness from 0.5 mm to 3.5 mm (Fig. 7) and are mainly composed of minerogenic medium to fine silt grains. In some cases, plant remains are also included. Internal structures like grading have not been observed. Due to their detrital-minerogenic composition, even thin detrital layers can be distinguished from matrix sediments in the Al scan (Fig. 5, Fig. 7).

The abundance of detrital layers in different cores varies depending on their location within the basin (Tab. 3). The largest number of detrital layers has been observed in cores > 25.0 m water depth (TSLM 1, 2, 4, 12-1, 12-2, 13-1, 14-1), proving a bottom wide distribution of these layers in the deepest part of the reservoir. In shallow water locations (TSLM 7, 8-1, 9-2) thin detrital layers are absent, likely due to erosion during low water levels (HÅKANSON 1982).

4.2 Chronology

^{137}Cs chronologies were established for three cores: TSLM 2 (water depth: 30.5 m) close to the main dam, TSLM 12-2 (water depth: 29.0 m) in the basin center and TSLM 7 (water depth: 17.2 m) in the southern part close to the river inflow (Fig. 6). The profiles from the two deep cores clearly exhibit two peaks in ^{137}Cs activity, related to nuclear weapon tests in 1963 and to the Chernobyl fallout in 1986 (PUTYRSKAYA et al. 2009). These ^{137}Cs peaks do not appear distinctly in core TSLM 7, likely due to the shallow-water location (water depth: 17.2 m). Similar observations were made in sediment cores from shallow water locations in Lago Maggiore by PUTYRSKAYA et al. (2009). It is assumed that the signal faded out due to sediment mixing during times of lower water levels. Water depth at this location was at maximum 4.0 m between 1989 and 1992 and in 2001 and 2003. In the years 1975, 1976 and 1980 this location dried up completely. The topmost sediments at this site (core TSLM 7) consist of intermixed clastic material typically indicating sediment reworking (unit X in Fig. 6).

Tab. 3: List of runoff events of the Wilde Weißeritz river ($Q_d > 8 \text{ m}^3 \text{s}^{-1}$) from 1932 to 2007 and coincided detrital layers (K-1 to K-23) correlated between different coring sites (TSLM 1 to TSLM 15). Thickness of K-2 (in mm) was measured in thin sections.

Tab. 3: Abflussereignissen der Wilden Weißeritz $Q_d > 8 \text{ m}^3 \text{s}^{-1}$ (1932–2007) und Zuordnung zu detritische Lagen (K-1 bis K-23) in verschiedenen Kernsequenzen (TSLM 1 bis TSLM 15). Die Dicke der Lage K-2 (in mm) wurde in Dünnschliffen gemessen.

Hydrological data		Sedimentological data															
Year	Month	Q_d [$\text{m}^3 \text{s}^{-1}$]	Detrital layer	Core name and water depth [m]													
				1 33.0	2 32.0	3 26.0	4 26.0	5 24.0	6 17.0	7 17.2	8-1 17.5	9-2 8.8	11-2 23.8	11-1 21.7	12-1 28.5	12-2 29.0	13-1 31.0
2006	April	16.6															
2005	March	19.1															
2004	November	9.96															
2004	February	12.70	K-1		x		x								x		
2002	August	58.90	K-2	5.5	6.8	8.0	6.5	9.0	19.0	33.0	31.0	2.2	10.5	3.2	4.0	7.5	5.0
2002	January	8.60														3.5	7.6
2000	March	19.10	K-3	x	x		x		x					x	x	x	x
1999	March	11.20	K-4	x			x	x	x					x	x	x	x
1998	March	8.59	K-5	x	x	x								x		x	x
1996	July	8.48	K-6		x	x								x	x	x	x
1995	June	6.23	K-7	x	x		x		x					x	x	x	x
1993	March	9.54	K-8	x	x	x								x		x	x
1991	December	7.47	K-9	x	x		x		x					x		x	x
1988	April	9.54	K-10		x	x	x		x					x		x	x
1987	March-April	15.80	K-11		x	x	x		x					x	x	x	x
1987	January	8.48															
1986	May	10.70	K-12				x										
1983	August	19.20	K-13	x	x	x	x										x
1981	November	11.50															
1981	July	13.20															
1981	March	16.30	K-14		x		x							x	x		
1980	July	14.50	K-15				x										
1978	August	8.23															
1976	January	8.83	K-16	x	x										x		
1974	December	13.60	K-17	x	x		x							x			
1970	April	10.30	K-18		x		x										
1967	December	10.70	K-19		x		x										
1967	February	9.65															
1966	June	8.37															
1965	May	12.00	K-20			x											
1958	July	15.20	K-21	x	x												
1957	July	18.50	K-22	x	x												
1954	December	8.66															
1954	July	16.20	K-23		x												
1948	February	8.15															
1948	January	9.18															
1946	February	11.90															
1941	September	8.50															
1941	May	12.30															
1941	April	8.75															
1940	July	9.50															
1940	March	10.00															
1939	June	12.10															
1937	July	9.96															
1932	January	24.80															

The 1963 and 1986 ^{137}Cs peaks in cores TSLM 2 and TSLM 12-2 form two anchor points for the chronology. In addition, the base of the lacustrine sedimentation (transition between sediment units I and IIa) in core TSLM 12-2 marks the initial infilling of the reservoir in 1932. The conspicuous thick detrital layer K-2 intercalated in sediment unit IIId (Fig. 6) is interpreted as deposit of the exceptional flood event in August 2002. The age-depth model was performed by linear interpolation between these anchor points.

Core-to-core correlation based on three further lithological markers allowed transferring this chronology to the other investigated cores (Fig. 6). Two of these markers ap-

pear in each core: (1) the detrital layer K-2 deposited in 2002 and (2) the boundary between the two sediment units IIc and IIId dated to 1995. Besides the aforementioned transition between sediment units I and II (1932), a fourth macroscopically discernible marker, found in locations $> 25.0 \text{ m}$ water depth (TSLM 1, 2, 4, 12-1, 12-2), is the base of the dark colored sediment unit IIb. Linear interpolation dates this shift to 1975, at the time when the reservoir was almost completely emptied. This is in agreement with the interpretation of this layer as resuspended littoral material. The core chronologies are further confirmed by correlation of other thin detrital layers (Fig. 6, Fig. 7).

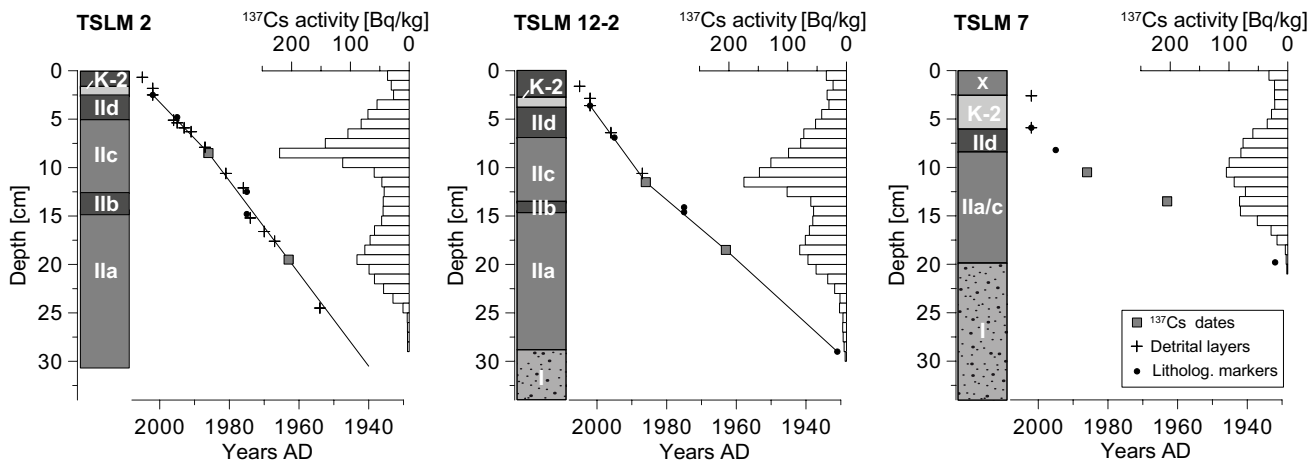


Fig. 6: Chronology of sediment sequences TSLM 2, TSLM 12-2 and TSLM 7 based on linear interpolation between the ^{137}Cs peaks in 1963 and 1986 (squares). Core-to-core correlation was done applying distinct lithological markers (dots): the detrital layer K-2 within sediment unit Ild, the border between sediment units IIc and Ild, sediment unit IIb and the border between sediment units I/Ila marking the onset of lacustrine sedimentation in 1932. Crosses mark the positions of further thin detrital layers coincided to instrumentally documented floods.

Abb. 6: Chronologie der Sedimentsequenzen TSLM 2, TSLM 12-2 und TSLM 7 basierend auf linearer Interpolation zwischen ^{137}Cs Maxima 1963 und 1986 (Quadrate). Korrelation der Kerne anhand lithologischer Markerhorizonte (Punkte): detritische Lage K-2 in Sedimenteneinheit Ild, Grenze zwischen Sedimenteinheiten IIc und Ild, Sedimenteneinheit IIb und Grenze zwischen Sedimenteneinheiten I und Ila, welche den Beginn der lakustrinen Sedimentation markiert (Talsperre in Betrieb seit 1932). Die Kreuze markieren weitere dünne detritische Lagen, die mit Hochwasserereignissen korreliert wurden.

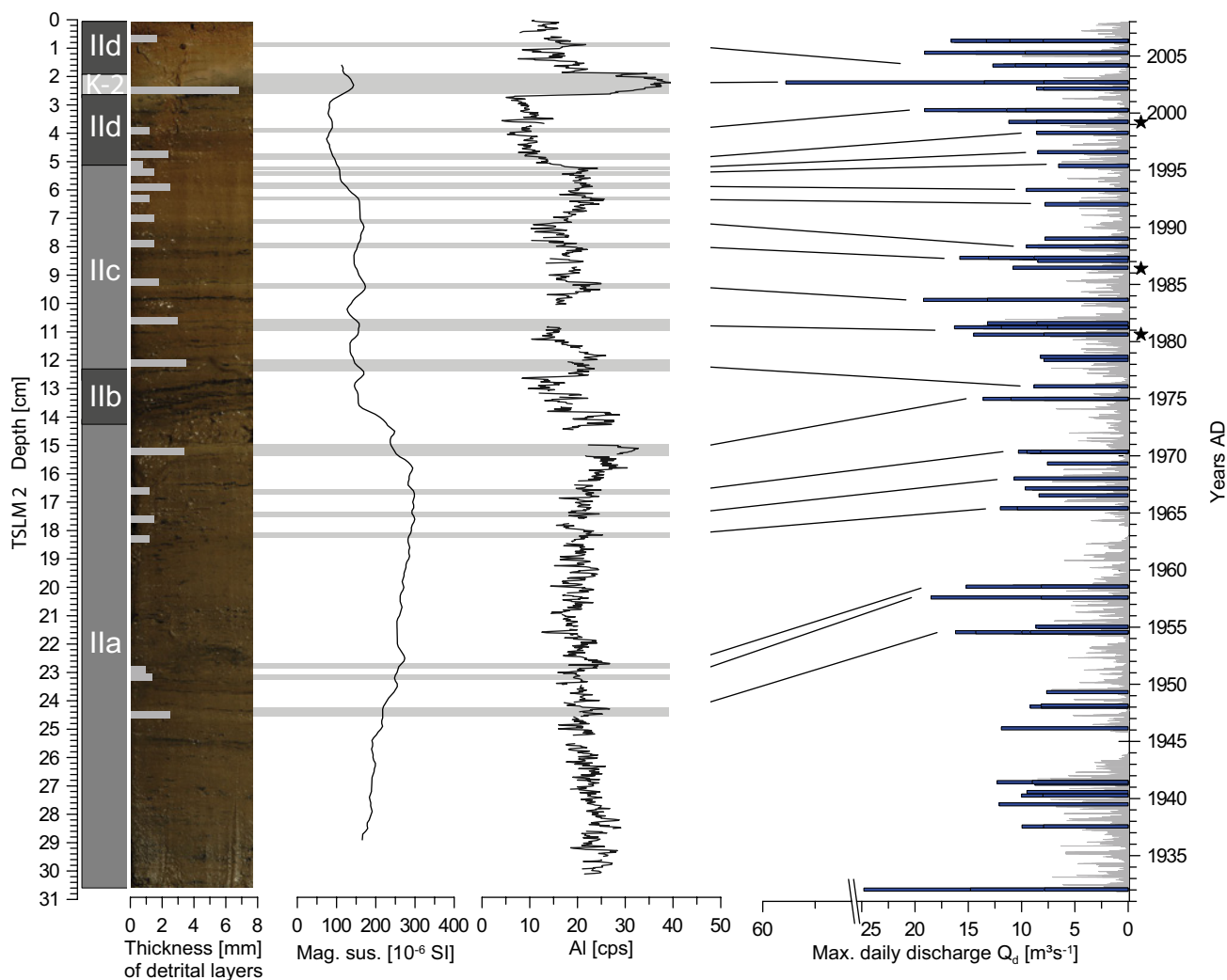


Fig. 7: Chronology of detrital layers in core TSLM 2: left hand: core photo and thickness of detrital layers, magnetic susceptibility and μ -XRF counts of Al. Right hand: daily discharge values (Q_d) of Wilde Weißeritz (blue bars: $Q_d > 8 \text{ m}^3\text{s}^{-1}$) and correlation to detrital layers (black lines). Stars mark three floods which do not correlate to detrital layers in TSLM 2 but to layers in other cores (Tab. 3).

Abb. 7: Chronologie detritischer Lagen in Kern TSLM 2: links: Kernfoto mit Lagenmächtigkeit und Profile der magnetischen Suszeptibilität (Mag. sus.) und Al (μ -XRF). Rechts: mittlere Tagesabflüsse (Q_d) der Wilden Weißeritz (blaue Balken: $Q_d > 8 \text{ m}^3\text{s}^{-1}$) und Zuordnung zu detritischen Lagen (schwarze Linien). Drei Hochwasserereignisse (schwarze Sterne) korrelieren nicht mit detritischen Lagen im Kern TSLM 2 aber mit Lagen in anderen Kernen (Tab. 3).

4.3 Detrital layers versus hydrological data

Flood events during the period 1932–2007 were identified by maximum values of daily discharges (Q_d) of the main tributary Wilde Weißeritz. In order to relate the identified 23 detrital layers to instrumentally observed flood events the strongest 24 floods with $Q_d > 10 \text{ m}^3\text{s}^{-1}$ are chosen for comparison. According to the established age model 16 detrital layers coincide with runoff events $> 10 \text{ m}^3\text{s}^{-1}$ (Tab. 3). Five of the seven other detrital layers occurring in sediment units IIb-d coincide to floods with $Q_d = 8\text{--}10 \text{ m}^3\text{s}^{-1}$, while only two detrital layers appear to be in accord with floods with $Q_d < 8 \text{ m}^3\text{s}^{-1}$. This suggests that a daily runoff of ca $8\text{--}10 \text{ m}^3\text{s}^{-1}$ represents a threshold for the deposition of a detrital layer at the reservoir floor (Tab. 3, Fig. 7).

In general, clastic-detrital layers are best recognizable in the more organic sediment units IIb-d (1975–2007) because of the higher contrast of these darker matrix sediments to the very fine minerogenic layers. From the eight floods, not detected there, five occur in years with more than one flood event (2004, 2000, 1987, 1981). One further event, not found in the sediment record, is rather weak close to the lower threshold ($Q_d = 8.2 \text{ m}^3\text{s}^{-1}$ in September 1978) and thus likely did not lead to detrital layer deposition in the main basin. The two remaining non-detected flood layers in 2005 and 2006 might be diminished with matrix sediments in the uppermost unconsolidated centimeters of the sediment cores and thus are not detectable as distinct layers. In the lower, more minerogenic sediment unit IIA (1932–1975) only seven detrital layers have been detected likely triggered by floods $> 10 \text{ m}^3\text{s}^{-1}$ (Tab. 3, Fig. 7).

Outstanding in the runoff record since 1932 is the flood event taking place in August 2002. Torrential rainfall events in Central Europe were caused by the persistence of a specific weather regime, called “Trough over Central Europe”, which caused transport of very moist air from the Mediterranean Sea to eastern Central Europe. Enhanced by orographic effects, extreme precipitation amounts fell in eastern Erzgebirge between 11th and 13th of August. The maximum of 321 mm in 24 h was reported from weather station Zinnwald-Georgenfeld, approx. 15 km southeast of the Lehnsmühle Reservoir (LfULG 2004, Fig. 1). The daily discharge on August 12th was calculated to 59 m^3s^{-1} and the modeled peak discharge reached 133 m^3s^{-1} (LfULG 2004). The second strongest daily discharge since building of the Lehnsmühle dam amounts to some 24 m^3s^{-1} and was measured in January 1932, emphasizing the exceptional intensity of the 2002 flood event. The thickness of the resulting detrital layer ranges from 5 mm in distal locations to 33 mm in proximal areas and, thus, by far exceeds the thickness of all other detrital layers in the record, reaching 3.5 mm in maximum (Fig. 7).

5 Discussion

5.1 Processes of detrital layer deposition

Detrital layers in lake sediments commonly are interpreted as natural flood records deposited by turbidity currents of the inflowing stream (e.g. CZYMZIK et al. 2010, GILBERT et al. 2006, GILLI et al. 2003, LAMOUREUX 2000, LUDLAM

1974, MANGILI et al. 2005, STURM & MATTER 1978). Here we present, for the first time, a multiple core record of flood layers deposited during the last three decades in a reservoir. Except one all detrital layers were less than 5 mm thick and thus could only be detected by microscopic techniques indicating low sediment input during these events and therefore low density over- or interflows (MULDER & ALEXANDER 2001, STURM & MATTER 1978) are the ordinary sediment transport mechanisms within the reservoir basin following floods due to sediment loss by braking of the sediment laden stream in the upstream pre-basin (Fig. 1c).

Overall 16 detrital layers were correlated with runoff events back to 1976, resulting in a ‘recording rate’ (deposition of a detrital layer) of 64 %. Most of the non-detected layers appear in years with more than one flood event (Tab. 3). The fine grained particles likely accumulated from the different floods without discernible borders in between (SIEGENTHALER & STURM 1991). An increase in layer thickness towards the dam was observed in nine cases likely caused by focusing of suspended sediments (HÄKANSON 1982). Compared to natural lakes sediment focusing in reservoirs is directed towards the dam rather than the centre of the lake. This is due to water level drawdown and water outlet at the dam wall, generating a steady motion of water and suspended sediment towards the dam (SHOTBOLT et al. 2005). Consequently, the record of flood layers is most complete in the near dam area (TSLM 2).

The occurrence of detrital layers related to two thirds of all discharge events proves that the pre-basin does not fully impede detrital matter flux into the main basin. The effect of the pre-dam, however, also depends on the water level. During water levels below the base level of the pre-dam (approx. 515 m a.s.l.), the basin in front loses its function and the inflowing stream directly enters the reservoir, resulting in thicker deposits. Thus layer thickness depends on core location and water level during the flood event (SNYDER et al. 2006) and is not directly related to flood intensity as observed in some lakes (e.g. SCHIEFER et al. 2011).

An exceptionally thick detrital layer was formed in 2002 after the major hydrometeorological event that was responsible also for the catastrophic flood of the Elbe River (BfG 2002, LfULG 2004). In contrast to our expectation, no coarse sand and gravel has been found even in most proximal locations. The absence of coarser material can be explained with the existence of the pre-dam, which reduced the discharge velocity leading to the deposition of coarser sediments in the small basin in front of the dam. This proves that the dam effectively traps sediments before entering the reservoir. Although the magnitude of this flood resulted in an unprecedented short-term sediment input into the reservoir, a much higher sediment flux must be assumed without the dam.

Sediment transport into the reservoir likely took place by high turbidity currents (MULDER & ALEXANDER 2001, STURM & MATTER 1978) as inferred from the graded structure of the detrital layer and a decreasing layer thickness in distal direction. Traces of small-scale erosion by the sediment laden current appear in the proximal core TSLM 8-1, where the layer reaches 31 mm in thickness. An approx. 1 mm thick diatom layer directly beneath the flood layer, observed in all other more distal cores (Fig. 4), is missing

at this location. This indicates that density of the sediment laden stream exceeded surrounding water density, resulting in a high density turbidity current, which moved along the basin floor after entering the reservoir (FINGER et al. 2006, MULDER & ALEXANDER 2001, STURM & MATTER 1978). The absence of the detrital layer in the narrow bay on the southern margin of the reservoir (TSLM 8-2, TSLM 8-3) probably is due to the high flow velocity of the sediment laden current in this channel-like part of the basin preventing from sediment deposition (DE CESARE et al. 2001). Moreover, eventually deposited detrital material could have been eroded from this location in summer 2003 when the lake level was so low, that this part of the basin became exposed and thus vulnerable to erosion.

5.2 Intra-basin distribution of the 2002 flood layer

The thickness distribution of the 2002 flood layer (Fig. 8) reveals maximum sediment deposition between the proximal core locations TSLM 8-1 and TSLM 6, representing the southern part of the N-S directed central part of the basin directly north of the junction with the NW-SE directed narrow channel which forms an elongation of the inflowing stream. Layer thickness in the area of maximum deposition ranges from 19 to 33 mm. Around 65 % of the sediment load is accumulated in this area, which accounts for approx. one third of the reservoir floor. The high deposition in this area is caused by the particular basin morphometry. The widening of the basin at this point causes a slow-down of the sediment laden water plume, which in turn leads to immediate sediment deposition. The slow-down effect was further enhanced by the kink of the basin at the junction of the main basin and the channel-like part in the south. To the north of the area of maximum sediment accumulation, the sediments are distributed almost evenly over the reservoir floor, contrasting an expected thinning of flood layers in distal direction as observed in many natural lakes (e.g. DROHMAN & NEGENDANK 1993, MANGILI et al. 2005, STURM & MATTER 1978). Detailed microscopic analysis, however, has proven that the thickness of the coarser grained basal section indeed decreased in distal direction, but this decrease was compensated by an increasing thickness of the fine-grained clay top. A high clay accumulation rate in the distal near-dam area is favored by a water current through the basin towards the dam due to water release through outlets in the middle and upper parts of the dam wall in order to discharge the reservoir during the flood event (PAUL & SCHEIFHACKEN 2010). A secondary maximum in sediment deposition has been found in front of a small bay in the northwestern part of the basin (Fig. 8). Despite plantation of trees around the reservoir to prevent from erosion, sediments have been transported into the basin through a non-permanently water bearing stream channel. Comparable sediment fluxes can be expected also through three further channels on the eastern shoreline, but since no cores have been obtained from this area this remains speculative.

The grid of available sediment cores allows an approximation of total sediment influx during the 2002 summer flood, calculated to 2,400 tons. This value is a minimum estimate, because of the aforementioned expected higher

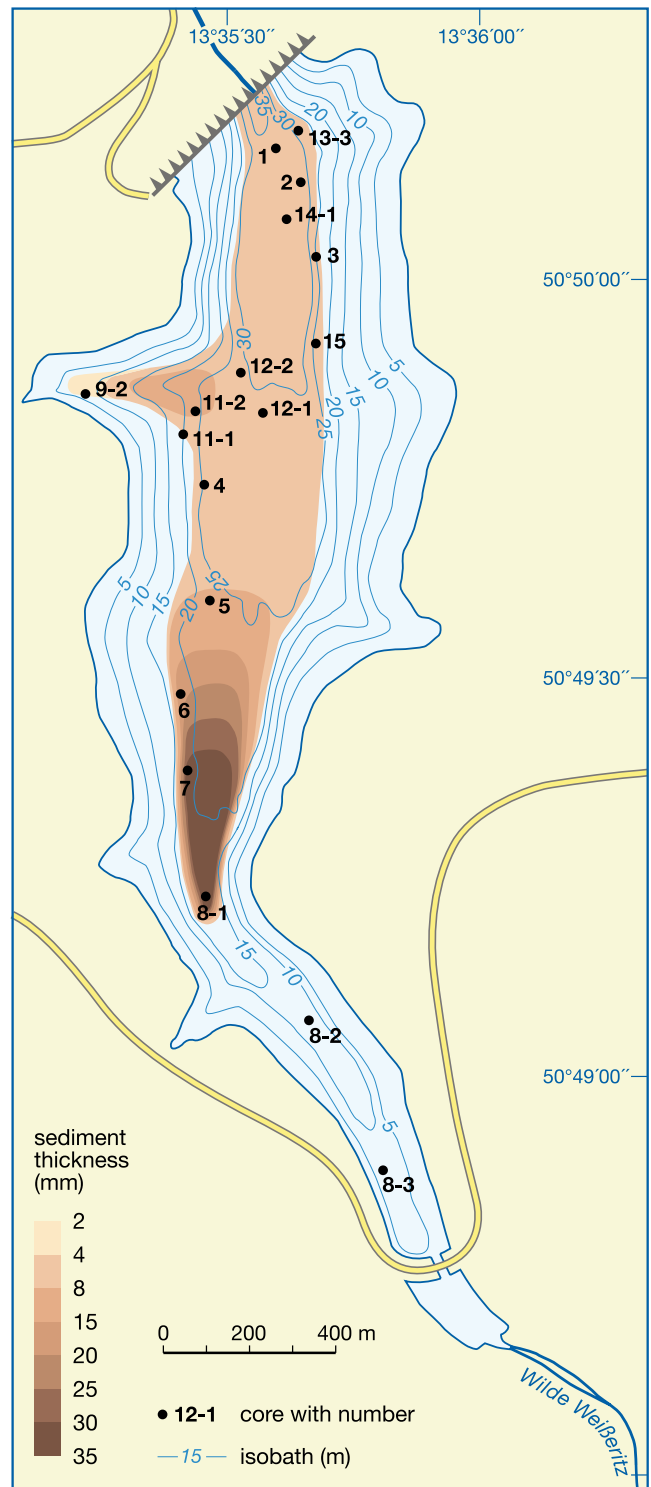


Fig. 8: Spatial distribution map of the 2002 detrital layer (K-2) as measured in thin sections. Black dots mark the different coring sites.

Abb. 8: Verteilungskarte der detritischen Lage des Jahres 2002 aus Messungen der Lagenmächtigkeit in Dünnabschliffen. Kernpositionen im Talsperrenbecken sind mit schwarzen Punkten markiert.

deposition rates in front of small channels on the eastern shoreline which have not been taken into account. Moreover, our mass estimation is only based on the in-situ deposits and does not consider any kind of reworking which has been observed only in one core (TSLM 7) where a 26 mm thick layer of reworked detrital material overlays

the K-2 flood layer. Also not included in our calculation is the amount of sediment trapped in the pre-basin. Information about the trap efficiency during the exceptional high magnitude floods is not available so far.

The accumulated mass of the 2002 flood layer was furthermore compared with the total accumulated sediment in the two master cores (TSLM 2, TSLM 12-2), where dry weight was measured on volumetric samples from the detrital layer and the complete core sequence. Sediment delivery in 2002 reached around 0.28 g cm^{-2} close to the dam (TSLM 2) and 0.38 g cm^{-2} in the middle of the basin (TSLM 12-2), where it accounts for 6.2 % of the cumulated sediment yield since 1932 (6.0 g cm^{-2}). The accumulation exceeds the annual mean by 4.5 times at the basin center (TSLM 12-2: $0.09 \text{ g cm}^{-2} \text{a}^{-1}$) and by 2.2 times in the near dam area (TSLM 2: $0.13 \text{ g cm}^{-2} \text{a}^{-1}$). The lower imprint of the flood event at the distal site (TSLM 2) primarily relates to the higher sediment ratio since 1932 caused by sediment focusing to the deepest parts close to the dam. Sediment focusing is favored by water level drawdown and the steady water flow driven by the continuous water withdrawal for drinking water supply (SHOTBOLT et al. 2005).

6 Conclusions

Investigating multiple sediment cores enabled detailed insights into processes of sediment deposition in the Lehn-mühle reservoir caused by the severe 2002 summer flood. The sediment flux into the reservoir resulted in a 5 to 33 mm thick layer of detrital catchment material in the entire basin, equivalent to approximately 2,400 tons. In the basin center the flood deposits accounts for approximately 6 % of the total sediment yield since the construction of the reservoir in 1932. Without the upstream construction of an open dam, which effectively trapped coarser material, the sediment input most likely would have been much higher. Besides the tributary Wilde Weißenitz as the primary sediment source, secondary sediment transport pathways have been identified through a non-permanently water bearing stream channel, entering the reservoir from the western shore. The distribution of sediments in the reservoir is controlled by the shape and morphometry of the basin as well as water management controlling the water flow through the reservoir and the water level.

Although depositional processes and sediment delivery related to the 2002 summer flood were exceptional for the entire history of the reservoir since the operation start date in 1932, microfacies analyses in combination with μ -XRF element scanning enabled to identify another 22 discrete, but thin detrital layers. Detailed comparison with instrumental data revealed that all these layers were triggered by minor runoff events during the last decades.

In many aspects the sedimentation regime in the Lehn-mühle reservoir resembles natural lake systems, however, modified by (1) the artificial sediment trap upstream in the main tributary, (2) the particular basin morphometry with the deepest part not located in the center but on the margin near the dam, and, (3) water management determining the water flow through the basin and strong water level fluctuations.

7 Acknowledgements

We are thankful to R. Sudbrack, T. Ihle, I. Werner and B. Böhme from the State Reservoir Administration of Saxony (LTV) for supporting sediment coring and providing useful information about Lehn-mühle reservoir. For reviewing early drafts of the manuscript and stimulating discussions we thank N. Scheifhacken and C. Lorz. The State Reservoir Administration of Saxony (LTV) and the Saxony State Office for the Environment, Agriculture and Geology (LfULG) are acknowledged for providing runoff data of the Wilde Weißenitz. We would like to thank D. Berger and G. Arnold for preparing high-quality thin sections, N. Nowaczyk for magnetic susceptibility measurements, B. Plessen and P. Meier for TOC measurements, K. Speth for performing the gamma-spectrometric measurements and C. Kaulfuss, S. Pinkerneil, M. Kuntzsch and T. Junker for their support during sediment coring and subsampling. A. Hendrich helped with the layout of the figures. This is a contribution to the PROGRESS joint project funded by the German Federal Ministry of Education and Research (BMBF).

References

- BAKER, V. R. (2006): Palaeoflood hydrology in a global context. – *Catena*, 66: 161–168. DOI:10.1016/j.catena.2005.11.016.
- BERNHOFER, C., GOLDBERG, V., FRANKE, J., HÄNTZSCHEL, J., HARMANSA, S., PLUNTKE, T., GEIDEL, K., SURKE, M., PRASSE, H., FREYDANK, E., HÄNSEL, S., MELLENTIN, U. & KÜCHLER, W. (eds., 2008): Sachsen im Klimawandel – Eine Analyse. – 211 S.; Dresden.
- BEST, J. L., KOSTASCHUK, R. A., PEAKALL, J., VILLARD, P. V. & FRANKLIN, M. (2005): Whole flow field dynamics and velocity pulsing within natural sediment-laden underflows. – *Geology*, 33(10): 765–768. DOI: 10.1130/G21516.1.
- BFG (Federal Institute of Hydrology) (2002): Das Augusthochwasser 2002 im Elbegebiet. – 49 S.; Koblenz.
- BRAUER, A. (2004): Annually laminated lake sediments and their palaeoclimatic relevance. – In: FISCHER, H., KUMKE, T., LOHMANN, G., FLÖSER, G., MILLER, H., VON STORCH, H. & NEGENDANK, J. F. W. (eds.), *The Climate in Historical Times: Towards a Synthesis of Holocene Proxy Data and Climate Models*: 109–128; Berlin, Heidelberg (Springer).
- BRAUER, A. & CASANOVA, J. (2001): Chronology and depositional processes of the laminated sediment record from Lac d'Annecy, French Alps. – *Journal of Paleolimnology*, 25: 163–177. DOI: 10.1023/A:1008136029735.
- BRAUER, A., DULSKI, P., MANGILI, C., MINGRAM, J. & LIU, J. (2009): The potential of varves in high-resolution paleolimnological studies. – *Pages News*, 17: 96–98.
- CHAPRON, E., ARNAUD, F., NOEL, H., REVEL, M., DESMET, M. & PERDEREAU, L. (2005): Rhone River flood deposits in Lake Le Bourget: a proxy for Holocene environmental changes in the NW Alps, France. – *Boreas*, 34: 404–416. DOI: 10.1080/03009480500231260.
- CZYMZIK, M., DULSKI, P., PLESSEN, B., VON GRAFENSTEIN, U., NAUMANN, R. & BRAUER, A. (2010): A 450-year record of spring/summer flood layers in annually laminated sediments from Lake Ammersee (Southern Germany). – *Water Resources Research*, 46: W11528. DOI: 10.1029/2009WR008360.
- DE CESARE, G., SCHLEISS, A. & HERMANN, F. (2001): Impact of turbidity currents on reservoir sedimentation. – *Journal of Hydraulic Engineering*, 127: 6–16.
- FRANCUS, P., LAMB, H., MARSHALL, M. & BROWN, E. (2009): The potential of high-resolution X-ray fluorescence core scanning: Applications in paleolimnology. – *Pages News*, 17: 93–95.
- DROHMAN, D. & NEGENDANK, J. F. W. (1993): Turbidites in the sediments of Lake Meerfelder Maar (Germany) and the explanation of suspension sediments. – In: NEGENDANK, J. F. W. & ZOLITSCHKA, B. (eds.): *Paleolimnology of European Maar Lakes*: 195–208; Berlin, Heidelberg (Springer).
- ENGSTROM, D. R. & WRIGHT, H. E. (1984): Chemical stratigraphy of lake sediments as a record of environmental change. – In: HAYWORTH,

- E. Y. & LUND, J. W. G. (eds): Lake Sediments and Environmental History: Studies in Palaeolimnology and Palaeoecology: 11–67; Leicester (Leicester University Press).
- EFFLER, S. W., MATTHEWS, D. A., KASER, J. W., PRESTIGIACOMO, A. R. & SMITH, D. G. (2006): Runoff impacts on a water supply reservoir: suspended sediment loading, turbid plume behavior, and sediment deposition. – *Journal of the American Water Resources Association*, 42: 1697–1710. DOI: 10.1111/j.1752-1688.2006.tb06030.x.
- FINGER, D., SCHMID, M. & WÜEST, A. (2006): Effects of upstream hydro-power operation on riverine particle transport and turbidity in downstream lakes. – *Water Resources Research*, 42: W08429. DOI: 10.1029/2005WR004751.
- GILBERT, R., CROOKSHANKS, S., HODDER, K. R., SPAGNOL, J. & STULL, R. B. (2006): The record of an extreme flood in the sediments of montane Lillooet Lake, British Columbia: Implications for paleoenvironmental assessment. – *Journal of Paleolimnology*, 35: 737–745. DOI: 10.1007/s10933-005-5152-8.
- GILLI, A., ANSELMETTI, F. S., ARIZTEGUI, D. & MCKENZIE, J. A. (2003): A 600-year sedimentary record of flood events from two sub-alpine lakes (Schwendisee, Northeastern Switzerland). – *Eclogae Geologicae Helvetiae*, 96: 49–58.
- HÄKANSON, L. (1982): Bottom dynamics in lakes. – *Hydrobiologia*, 91–92: 9–22.
- HÄKANSON, L. & JANSSON, M. (eds., 1983): Principles of Lake Sedimentology. – 316 S.; Berlin, Heidelberg (Springer).
- JACOB, F., FEGER, K.H., RÖSCH, M. & KLINGER, T. (2009): Akkumulation von amorphem Silizium in holozänen Seesedimenten des Herrenwieser Sees (Nordschwarzwald). – In: Böden – eine endliche Ressource – Jahrestagung der DBG, September 2009. – 4 S.; Bonn.
- KAULFUSS, W. (1979): Sedimentbelastung und Sedimentverteilung in der Talsperre Lehnsmühle. – *Wissenschaftliche Zeitschrift der Pädagogischen Hochschule K.F.W. Wander Dresden*, 3: 71–79.
- LAMB, M. P., McELROY, B., KOPRIVA, B., SHAW J. & MOHRIG, D. (2010): Linking river-flood dynamics to hyperpycnal-plume deposits: Experiments, theory, and geological implications. – *Geological Society of America Bulletin*, 122 (9–10): 1389–1400. DOI: 10.1130/B30125.1.
- lamoureux, S. (2000): Five centuries of interannual sediment yield and rainfall-induced erosion in the Canadian High Arctic recorded in lacustrine varves. – *Water Resources Research*, 36: 309–318.
- LfUG (Saxony State Office for the Environment, Agriculture and Geology) (eds., 2004): Ereignisanalyse – Hochwasser August 2002 in den Osterzgebirgszuflüssen. – 188 S.; Dresden.
- LTV (The State Reservoir Administration of Saxony) (2002): Nitratbericht sächsischer Trinkwassertalsperren. – 52 S.; Dresden (Dr. Uwe Miersch Verlag).
- LTV (The State Reservoir Administration of Saxony) (2009): Die Talsperre Lehmühle. – 2 S.; Pirna.
- LUDLAM, S. D. (1974): Fayetteville Green Lake, New York. 6. The role of turbidity currents in lake sedimentation. – *Limnology and Oceanography*, 19: 656–664.
- MANGILI, C., BRAUER, A., MOSCARIELLO, A. & NAUMANN, R. (2005): Microfacies of detrital event layers deposited in quaternary varved lake sediments of the Pianico-Sellere Basin (northern Italy). – *Sedimentology*, 52: 927–943. DOI: 10.1111/j.1365-3091.2005.00717.x.
- MULDER, T. & ALEXANDER, J. (2001): The physical character of subaqueous sedimentary density flows and their deposits. – *Sedimentology*, 48: 269–299. DOI: 10.1046/j.1365-3091.2001.00360.x.
- PAUL, L. & SCHEIFFACKEN, N. (2010): Einfluss der Wassermengenbewirtschaftung auf die vertikale Verteilung allochthoner Trübstoffe in Trinkwassertalsperren nach Hochwässern. – In: Deutsche Gesellschaft für Limnologie (DGL) – Erweiterte Zusammenfassung der Jahrestagung 2008 (Konstanz), Oldenburg: 144–149.
- PUTYRSKAYA, V., KLEMT, E. & RÖLLIN, S. (2009): Migration of ¹³⁷Cs in tributaries, lake water and sediment of Lago Maggiore – analysis and comparison to Lago di Lugano and other lakes. – *Journal of Environmental Radioactivity*, 100: 35–48. DOI: 10.1016/j.jenvrad.2008.10.005.
- SCHIEFER, E., GILBERT, R. & HASSAN, M. A. (2011): A lake sediment-based proxy of floods in the Rocky Mountain Front Ranges, Canada. – *Journal of Paleolimnology*, 45: 137–149. DOI: 10.1007/s10933-010-9485-6.
- SHOTBOLT, L. A., THOMAS, A. D. & HUTCHINSON, S. M. (2005): The use of reservoir sediments as environmental archives of catchment inputs and atmospheric pollution. – *Progress in Physical Geography*, 29: 337–361. DOI: 10.1191/0309133305pp452ra.
- SNYDER, N. P., WRIGHT, S. A., ALPERS, S. N., FLINT, L. E., HOLMES, C. W. & RUBIN, D. M. (2006): Reconstructing depositional processes and history from reservoir stratigraphy: Englebright Lake, Yuba River, northern California. – *J. Geophys. Res.*, 111: F04003. DOI: 10.1029/2005JF000451.
- SIEGENTHALER, C. & STURM, M. (1991): Die Häufigkeit von Ablagerungen extremer Reuss-Hochwasser: Die Sedimentationsgeschichte im Urnersee seit dem Mittelalter. – *Mitteilungen Bundesamt für Wasserwirtschaft*, 4: 127–139.
- STØREN, E. N., DAHL, S. O., NESJE, A. & PAASCHE, Ø. (2010): Identifying the sedimentary imprint of high-frequency Holocene river floods in lake sediments: development and application of a new method. – *Quaternary Science Reviews*, 29: 3021–3033. DOI: 10.1016/j.quascirev.2010.06.038.
- STURM, M. & MATTER, A. (1978): Turbidites and varves in Lake Brienz (Switzerland): Deposition of clastic detritus by density currents. – *Special Publications International Association of Sedimentologists*, 2: 147–178.
- SWIERCZYNSKI, T., LAUTERBACH, S., DULSKI, P. & BRAUER, A. (2009): Die Sedimentablagerungen des Mondsees (Oberösterreich) als ein Archiv extremer Abflussereignisse der letzten 100 Jahre. – In: SCHMIDT, R., MATULLA, C. & PSENNER, R. (eds.): Klimawandel in Österreich – Die letzten 2000 Jahre und ein Blick voraus. – *Alpine Space – Man & Environment*, 6: 115–126.
- THORNDYCRAFT, V., HU, Y., OLDFIELD, F., CROOKS, P. R. J. & APPLEBY, P. G. (1998): Individual flood events detected in the recent sediments of the Petit Lac d'Annecy, eastern France. – *The Holocene*, 8: 741–746. DOI: 10.1191/095968398668590504.
- THORNDYCRAFT, V. R., BENITO, G., BARRIENDOS, M. & LLASAT, M. C. (2003): Palaeofloods, Historical Floods & Climatic Variability: Applications in Flood Risk Assessment. – In: THORNDYCRAFT, V. R., BENITO, G., BARRIENDOS, M. & LLASAT, M. C. (eds.): Palaeofloods, Historical Floods & Climatic Variability: Applications in Flood Risk Assessment. – Proceedings of the PHEFRA Workshop Barcelona, 16–19th October 2002: 4–9; Madrid.
- WEIRICH, F. H. (1986): A Study of the Nature and Incidence of Density Currents in a Shallow Glacial Lake. – *Annals of the Association of American Geographers*, 76(3): 396–413.

Effects of deglacial sedimentation pulse, followed by incision: A case study from a catchment in the Northern Calcareous Alps [Austria]

Diethard Sanders

How to cite: SANDERS, D. (2012): Effects of deglacial sedimentation pulse, followed by incision: A case study from a catchment in the Northern Calcareous Alps (Austria). – E&G Quaternary Science Journal, 61 (1): 16–31. DOI: 10.3285/eg.61.1.02

Abstract: In the ‘Giessenbach’ catchment (Northern Calcareous Alps, NCA), a thick sedimentary succession accumulated during to shortly after deglaciation. The catchment is located on faulted and jointed Triassic dolostones. Up-section, the Quaternary succession consists of: (a) redeposited till with index clasts of the Last Glacial Maximum (LGM), (b) pebbly alluvium supplied from the dolostone substrate, (c) fluvial deposits veneering terraces, and (d) large scree slopes. Today, the pre-LGM upstream half of the Giessenbach course is a dry, elevated valley filled by deglacial to Holocene sediments. The present Giessenbach stream shows a convex longitudinal profile, with a bedrock gorge in its lower reach; the gorge was probably blocked by dead ice when deglacial sedimentation started. Aside of glacially-shaped surfaces and former nunataks, the present catchment morphology is characterized by: (a) mass-wasting deposits derived from a pulse of rapid deglaciation and, after slope stabilization, by (b) stream incision. Strong sedimentation was favoured by the structurally deformed dolostone substrate that weathers under copious production of clastic material. In the NCA, records of similar histories from rapid, deglacial sedimentation to prolonged post-glacial incision are widespread.

Auswirkungen starker spätglazialer Sedimentation, gefolgt von Erosion: Eine Fallstudie aus den Nördlichen Kalkalpen [Österreich]

Kurzfassung: Im Einzugsgebiet des ‘Giessenbaches’ (Nördliche Kalkalpen, NKA) lagerte sich eine mächtige Sedimentabfolge während bis wenig nach dem Zerfall des hochglazialen Eispanzers ab. Das Einzugsgebiet liegt auf gestörten, geklüfteten triassischen Dolomitgesteinen. Die quartäre Abfolge besteht aus, (a) aufgearbeitetem Till mit Leitgeschieben des Letzten Glazialen Maximums (LGM), (b) alluvialen Kiesen, die vom Dolomitgestein-Untergrund gespeist wurden, (c) Decklagen von Flusssedimenten auf Terrassen, und (d) grossen Schutthalde. Die ehemalige (Vor-LGM) obere Hälfte des Giessenbach-Laufs ist noch heute ein trockenes, erhöhtes Tal das wesentlich durch spätglaziale bis holozäne Sedimente verfüllt ist. Der heutige Giessenbach zeigt ein konkavex Längsprofil mit einer Klamm im Unterlauf; diese Klamm war wahrscheinlich teilweise durch Toteis versperrt während die Sedimentation der Eiszerfallsphase bereits eingesetzt hatte. Außerdem überformten Felsflächen und ehemaligen Nunatakern ist die heutige Morphologie des Einzugsgebiets im wesentlichen bestimmt durch (a) einen ‘Schub’ sehr rascher Sedimentation vom Eiszerfall bis ins frühe Spätglazial, gefolgt von (b) Hangstabilisierung durch Bewachung, und Einschneiden von Gerinnen. Die rasche Sedimentation wurde durch den Untergrund aus tektonisch verformtem Dolomitgestein gefördert, das unter reichlicher Schuttbildung abwittert. Ähnliche Verläufe von rapider Sedimentation vom Eiszerfall bis zum Spätglazial hin zu einem längeren Zeitabschnitt vorwiegend mit Einschneiden von Gerinnen sind in den NKA weit verbreitet.

Keywords: Alps, deglacial, paraglacial, Eastern Alps, late glacial, sedimentation, erosion

Address of author: D. Sanders, Institute of Geology and Palaeontology, Faculty of Geo- and Atmospheric Sciences, University of Innsbruck, A-6020 Innsbruck, Austria. E-Mail: Diethard.G.Sanders@uibk.ac.at

1 Introduction

In the Alps, thick proglacial sediment accumulations in valleys blocked by advancing ice streams are described in different studies (e. g., FLIRI 1973; VAN HUSEN 1977, 2000; DE GRAAFF 1996; GRUBER et al. 2011). The proglacial deposystems were characterized by high sediment accumulation rates chiefly as a result of climatic deterioration, hillslope stripping and associated increase in physical weathering (VAN HUSEN 1983). Similarly strong intramontane sedimentation was associated with decay of the ice streams of the Last Glacial Maximum (VAN HUSEN 1997; MÜLLER 1999; HINDERER 2001). The deglacial ‘sedimentation pulse’ and its impacts on sediment distribution, morphology and drainage, however, are little documented to

date. Most deglacial deposystems such as rock glaciers, alluvial fans, valley fans, talus slopes and lakes today are abandoned or in a state of low activity, and in many cases undergo erosion (REITNER 2007; SANDERS, OSTERMANN & KRAMERS 2009; SANDERS & OSTERMANN 2011). For a short valley within the NCA, based on seismic surveys, SCHROTT et al. (2004) conclude that post-LGM alluvial fans and talus slopes comprise the largest sediment storage in that valley, and that this should be similar in comparable valleys. Except for active talus slopes today located typically higher than about 1800–2000 m a.s.l. in the present NCA, most alluvial fans and scree slopes mainly began to accumulate during deglacial time (SANDERS, OSTERMANN & KRAMERS 2009; SANDERS & OSTERMANN 2011). At many sites within the NCA, the deglacial sediment bodies are

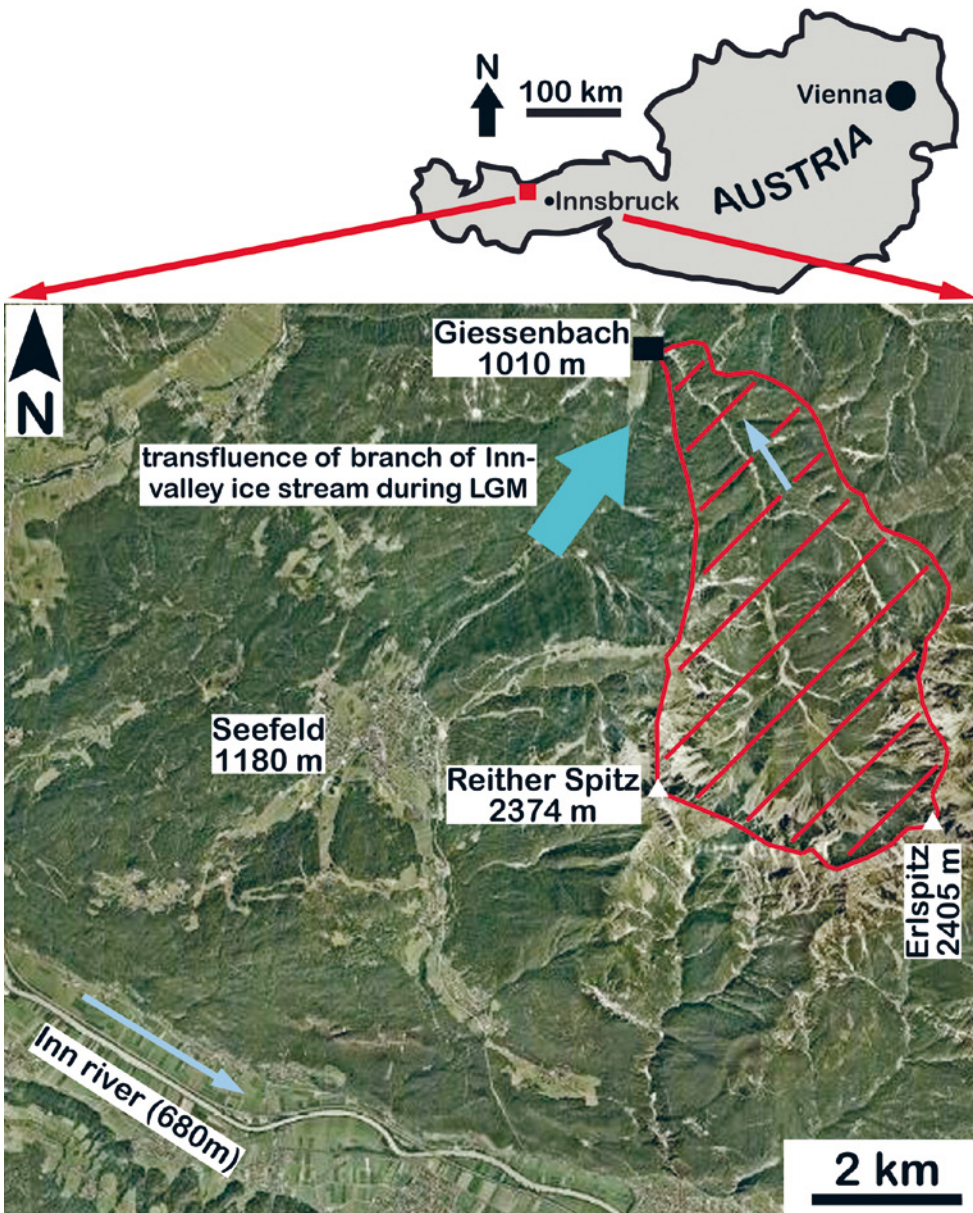


Fig. 1: Above: Position of investigated area in Austria. Below: Satellite image of catchment (red cross-hatch) and its surrounding area (source: Google Maps). During the Last Glacial Maximum, the Inn valley hosted a major ice stream. Part of the ice stream flowed towards the North over the low rock ridge in the area of Seefeld village and also affected the investigated drainage area.

Abb. 1: Oben: Lage des Untersuchungsgebiets in Österreich. Unten: Satellitenbild des Einzugs-Gebiets (rote Kreuzschraffur) und seiner Umgebung (Quelle: Google Maps). Während des Letzten Glazialen Hochstandes verlief im Inntal ein mächtiger Eisstrom. Ein Teil des Eises floss über den niederen Felsrücken im Bereich des Dorfes Seefeld nach Norden und beeinflusste damit auch das hierin betrachtete Einzugs-Gebiet.

well-preserved or are still only partially removed by later erosion.

In the Eastern Alps, the Last Glacial Maximum (LGM; 24–21.1 ka, PREUSSER 2004) was followed by rapid collapse of ice streams down to about 50% of LGM ice volume. This, early late glacial ice decay^c (ELGID) is bracketed to 21.1–19 ka BP (VAN HUSEN 2004). Due to its distinct sedimentary records, the ELGID now can be distinguished as a separate post-glacial episode (REITNER 2007; IVY-OCHS et al. 2009). Upon debuttressing from pleniglacial ice cover, small glaciers supplied from local catchments in the NCA advanced for a short period of time, before retreating, too (REITNER 2007). The ELGID was followed by the late glacial

that, in present terminology, would last from ~19 ka to the onset of the Holocene. The late glacial was characterized by stadial-interstadial cycles with progressively smaller outreach of valley glaciers (VAN HUSEN 2004; IVY-OCHS et al. 2009). Herein, in analogy to other studies of glacial to post-glacial deposits on land and in the sea (e.g., HEIN et al. 2010; BARD et al. 1996), the term ‚deglacial‘ is used as an umbrella for sediments accumulated between the end of the LGM to the start of the Holocene; the term thus comprises both the ELGID and the late glacial as outlined. Over the past ten years or so the term ‚paraglacial‘, defined as ‚processes directly conditioned by glaciation‘ (CHURCH & RYDER 1972), has seen a renaissance. Today, catastrophic rockslides and

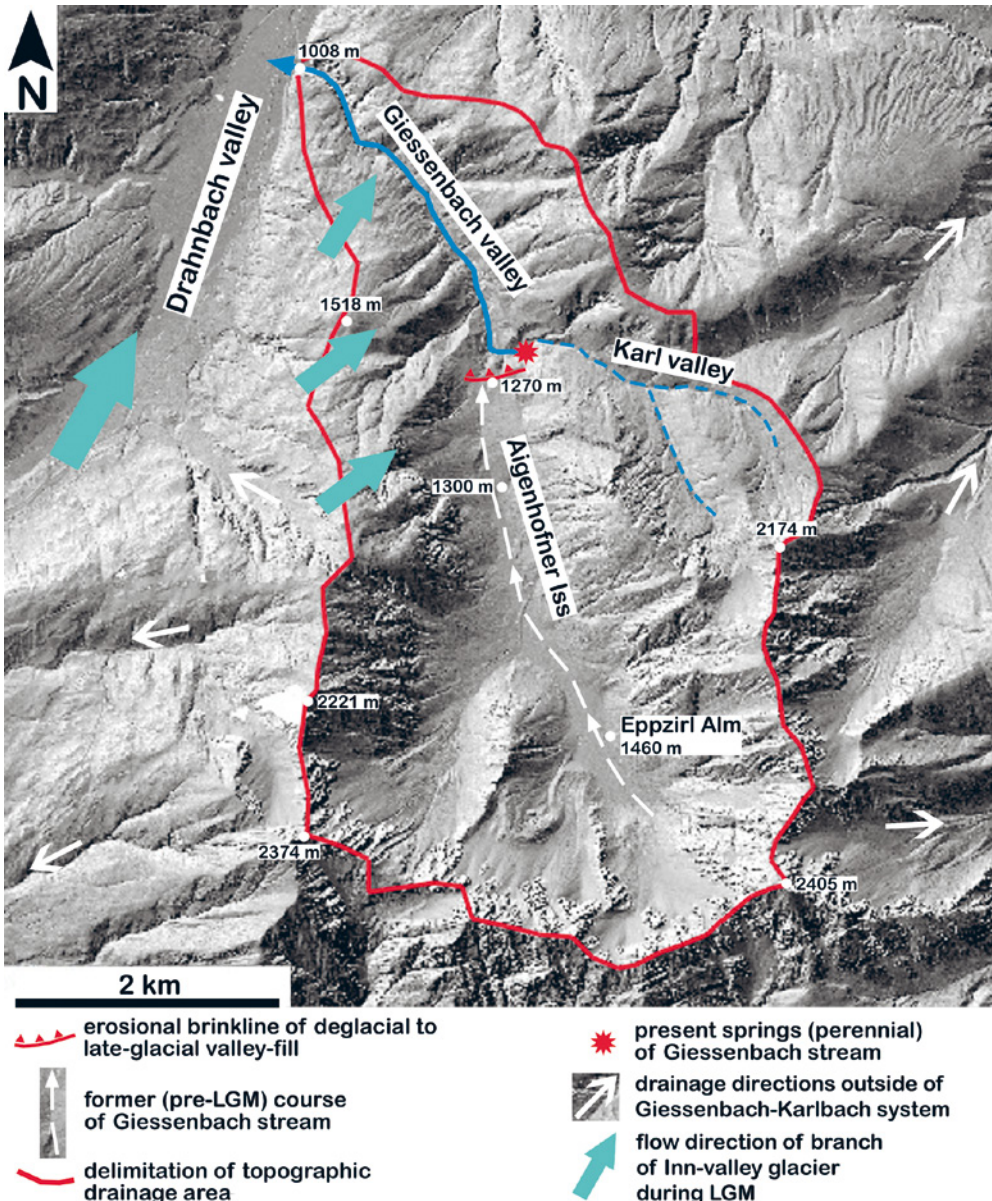


Fig. 2. Laserscan image with topographic drainage area of Giessenbach-Karl valley system (source: www.tirol.gv.at). Gießenbach is a perennial stream that originates from several adjacent springs. Karlbach is ephemeral, and water-run only after heavy rains and/or during prolonged foul weather. The larger, upper part of the drainage area of Gießenbach is a dry valley filled by sediments (Aigenhofner Iss to Eppzirl Alm). The valley-fill terminates along an erosional brinkline towards present Giessenbach.

Abb. 2: Laserscan des topographischen Einzugsgebiets des Giessenbach-Karltal systems (Quelle: www.tirol.gv.at). Giessenbach ist ein perenniauer Fluss der aus mehreren benachbarten Quellen entspringt. Der ephemerale Karlbach ist nur nach Starkniederschlägen und während langer Schlechtwetter-Phasen wasserführend. Der längere, obere Teil des Einzugsgebiets des Giessenbachs ist ein Trockental, das von Sedimenten verfüllt ist (Aigenhofner Iss bis Eppzirler Alm); diese Sedimentfüllung endet scharf an einer Erosionskante und einem Steilabfall zum heutigen Giessenbach.

slow deep-seated gravitational mass movements occurring more than 10–15 ka after glaciation are subsumed as paraglacial phenomena (BALLANTYNE 2002; KELLERER-PIRKLBAUER, PROSKE & STRASSER 2010). Paraglacial sedimentation, that is, mainly reworking of glacial deposits through debris flows and alluvium, starts immediately after ice retreat at site (CHURCH & RYDER 1972; BALLANTYNE 1995; CURRY & BALLANTYNE 1999). With respect to alluvial systems, however, a termination of paraglacial sedimentation can be hardly defined because it is a gradual fadeout in space and time, superposed by stadial-interstadial cy-

cles (ORWIN & SMART 2004; cf. TUNNICLIFFE & CHURCH 2011). Therefore, the sedimentation patterns described in the present paper are preferably characterized as deglacial rather than paraglacial. In this paper, an example of deglacial sedimentation is described that presently has a profound influence on the morphology and hydrology of a typical NCA catchment. Rapid deglacial sedimentation was followed by linear erosion, resulting in complicated stratigraphic and geomorphic patterns. The results are discussed in relation to similar, widespread deglacial deposits in the NCA.

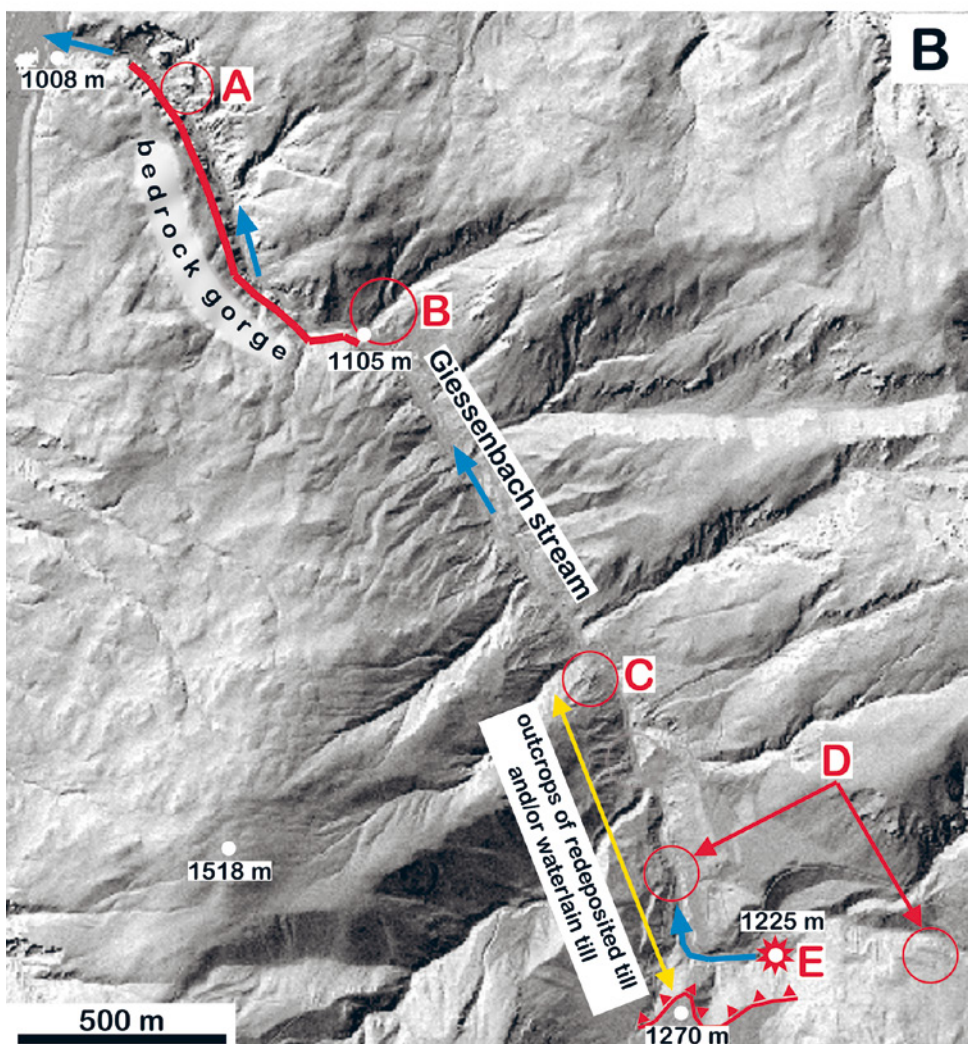
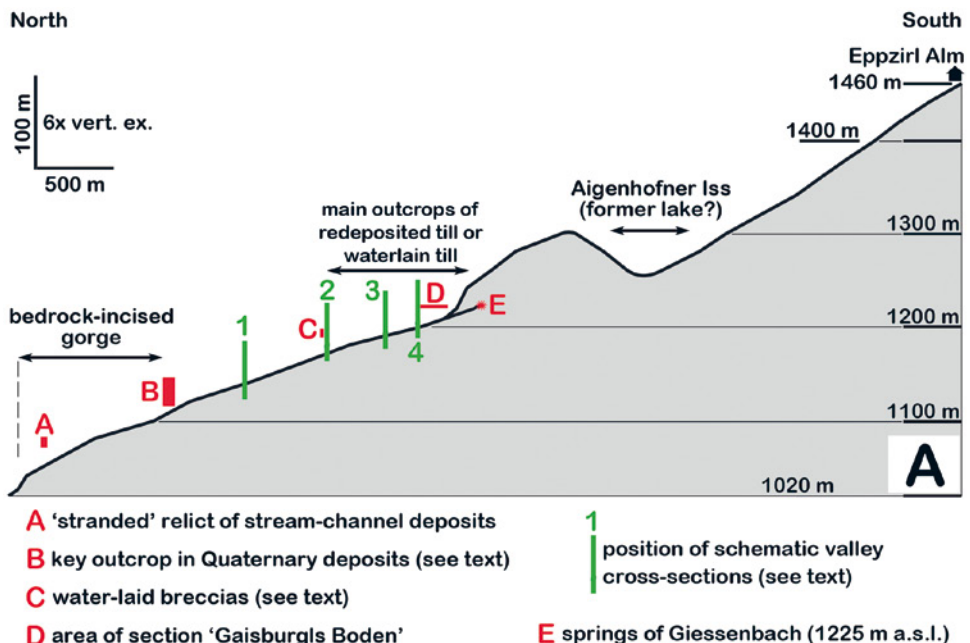


Fig. 3. A. Longitudinal section through Giessenbach valley to Eppzirl Alm (cf. Fig. 1). Note (a) overall convex longitudinal stream profile, (b) knick in stream profile in the distal reach of the bedrock gorge, and (c) the 'swell' of valley-fill deposits. B. Laserscan image (source: www.tirol.gv.at) of present Giessenbach course, with features labeled A to E as in subfigure A above.

Abb. 3. A. Längsschnitt durch das Giessenbachtal bis zur Eppzirler Alm (vgl. Abb. 1). Beachte, (a) das konvexe Längsprofil, (b) den Profilknick im distalen Abschnitt der Klamm, sowie (c) die 'Schwelle' aus Talfüllungs-Sedimenten. B. Laserscan (Quelle: www.tirol.gv.at) des heutigen Giessenbach-Laufes, mit den wichtigen Stellen A bis E wie in Subfigur A erläutert.

2 Setting

The NCA are part of the Upper Austroalpine structural unit of the Eastern Alps, and consist of stacked cover-thrust nappes dominated by Triassic platform carbonates (e.g., NEUBAUER, GENSER & HANDLER 1999; SCHMID et al. 2004). The rock substrate of the studied area (Fig. 1) consists of a thick, folded and faulted succession of Upper Triassic dolostones (Hauptdolomit unit). The Hauptdolomit accumulated in banktop environments of a large carbonate platform (BRANDNER 1984). In the specific area, the Hauptdolomit contains intercalated packages a few tens of meters in thickness of black shales and limestones of an oxygen-deficient intra-platform basin (Seefeld Formation; DONOFRIO, BRANDNER & POLESCHINSKI 2003). During Alpine folding and faulting, in the relatively low-tempered portions of the thrust-nappe stack, the Hauptdolomit reacted brittlely and was subject to dense jointing; as a result, it typically degrades under copious production of scree (SANDERS, OSTERMANN & KRAMERS 2009).

During buildup of the LGM, a bedrock swell with an altitude of about 1100–1200 m ('Seefeld Sattel') was overridden by a northward flowing branch of the Inn-valley ice stream; this branch then advanced northward along present Drahnbach valley (Fig. 1). Transfluence of Inn-glacier ice, across the low rock ridge between Giessenbach valley and Drahnbach valley, is recorded by the presence of index clasts (see below) (Fig. 2). In the investigated area, the reconstructed ice surface of the LGM was located between about 2100–2200 m a.s.l.; as a result the southern, higher crest of the topographic drainage area, with summits between about 2200 to 2400 m a.s.l. (Fig. 2), comprised a crescent-shaped nunatak (VAN HUSEN 1987, 2004). The deposits of the LGM Inn glacier are characterized by three types of index clasts: (a) dark-green garnet amphibolites and eclogites derived from the Engadin area along the uppermost reach of the Inn; (b) granites with green-coloured feldspar, derived from the Julier massif also along the uppermost reach of the Inn valley, and (c) light-green to whitish, diablastic garnet amphibolites rich in feldspar; this latter lithology originated from Alpine retrograde metamorphism of Variscan eclogites, and is derived from source areas in the Oetztal-Stubai basement unit only about 70 km upstream of the area considered herein.

The exposed Quaternary succession along the Gießenbach-Karlbach drainage system (Fig. 2) is up to at least about 100–120 m in cumulative thickness, and consists of distinct units to be described herein. For sake of communication, the most significant units are mentioned beforehand; they include, (1) a basal interval of redeposited glacial till with index clasts of the LGM, overlain by (2) a thick succession of alluvial gravels accumulated from a braided-stream system, and (3) comparatively thin intervals of fluvial deposits (rich in index clasts of LGM) that veneer terraces incised into the deposits mentioned above. In its upper and middle reaches, Giessenbach stream runs on a sediment bed (from about 1100 m a.s.l.). The lower reach is a bedrock gorge (Fig. 3). Today, the Gießenbach stream is supplied by several perennial springs emerging in a small area at 1225 m a.s.l. (Fig. 3). The springs emerge along the top of the lowermost stratigraphic unit (1) mentioned above; else-

where, this level is also characterized by numerous seepages. Conversely, Karl valley is water-run only during and closely after rainstorms. The Giessenbach valley abuts a very steep erosional slope of a valley-fill composed mainly of stratigraphic units (1) and (2) (Fig. 3A). The top of this valley-fill is situated at about 1270 m a.s.l. (Fig. 2, Fig. 3B). Above 1270 m, the valley is floored by talus slopes, and at approximately 1250–1260 m a.s.l. a subhorizontal plane is present that comprises an ephemeral pond during spring and summer (Aigenhofner Iss; Fig. 2, Fig. 3A); as outlined below, the Aigenhofner Iss may have been filled by a lake during the early deglacial interval. Still higher up, the valley is filled by a valley-fan, scree slopes, and fossil rock glaciers (Fig. 2, Fig. 3A).

3 Methods

The area was investigated during repeated field visits over an interval of eleven years; this reduced bias from seasonally-changing outcrop conditions as typical of unlithified sedimentary successions. Isohypsed satellite orthophotographs and laserscan images (both down to 1/1.000), provided free by the federal government of Tyrol (www.tirol.gv.at), improved precision in mapping and altitude leveling of outcrops. Columnar sections, documentation of key outcrops, and consideration of geomorphic features supported reconstruction of the deglacial to interglacial history of the considered area. Cut slabs and thin sections of a few lithified intervals within the Quaternary succession supplemented description and interpretation of facies. X-ray powder diffractometry used to determine the mineralogical composition of fine-grained deposits was undertaken on a Bruker-AXS D8 diffractometer with Bragg-Brentano geometry, CuK α radiation at 40kV and 40mA acceleration voltage, with parallel-beam optics and an energy-dispersive detector. The data was collected between 2 and 70° 2 θ , with a step size of 0,02° 2 θ and a detecting time of four seconds per step. Crystalline phase identification was achieved with the program Eva.Ink and the PDF4 data base 8.0.113 of ICDD. The x-ray spectra of two samples were analysed with the programs DIFFRAC PLUS (phase identification) and TOPAS (quantitative assessment).

4 Sedimentary facies

4.1 Description

The sedimentary facies, their composition and interpretation are summarized in Tables 1 and 2. Along Giessenbach, between approximately 1170 to 1230 m a.s.l., the stratigraphically deepest exposed deposits include two facies types: facies 1 consists of unlaminated and unbedded carbonate-rich silt to -mud that locally contains scattered, disoriented clasts of metamorphic rocks and/or of carbonate rocks (Fig. 4A–D, Tab. 1). The carbonate rock clasts are derived from the Hauptdolomit unit and the Seefeld Formation, and typically range from coarse-sand to medium gravel size; locally, clasts of cobble size are present (Fig. 4B). Rounding of the carbonate-lithic clast fraction is highly variable (Fig. 4A–D). Carbonate rock clasts may show surfaces with scratch marks (Fig. 4B, inset). Clasts of metamorphic rocks

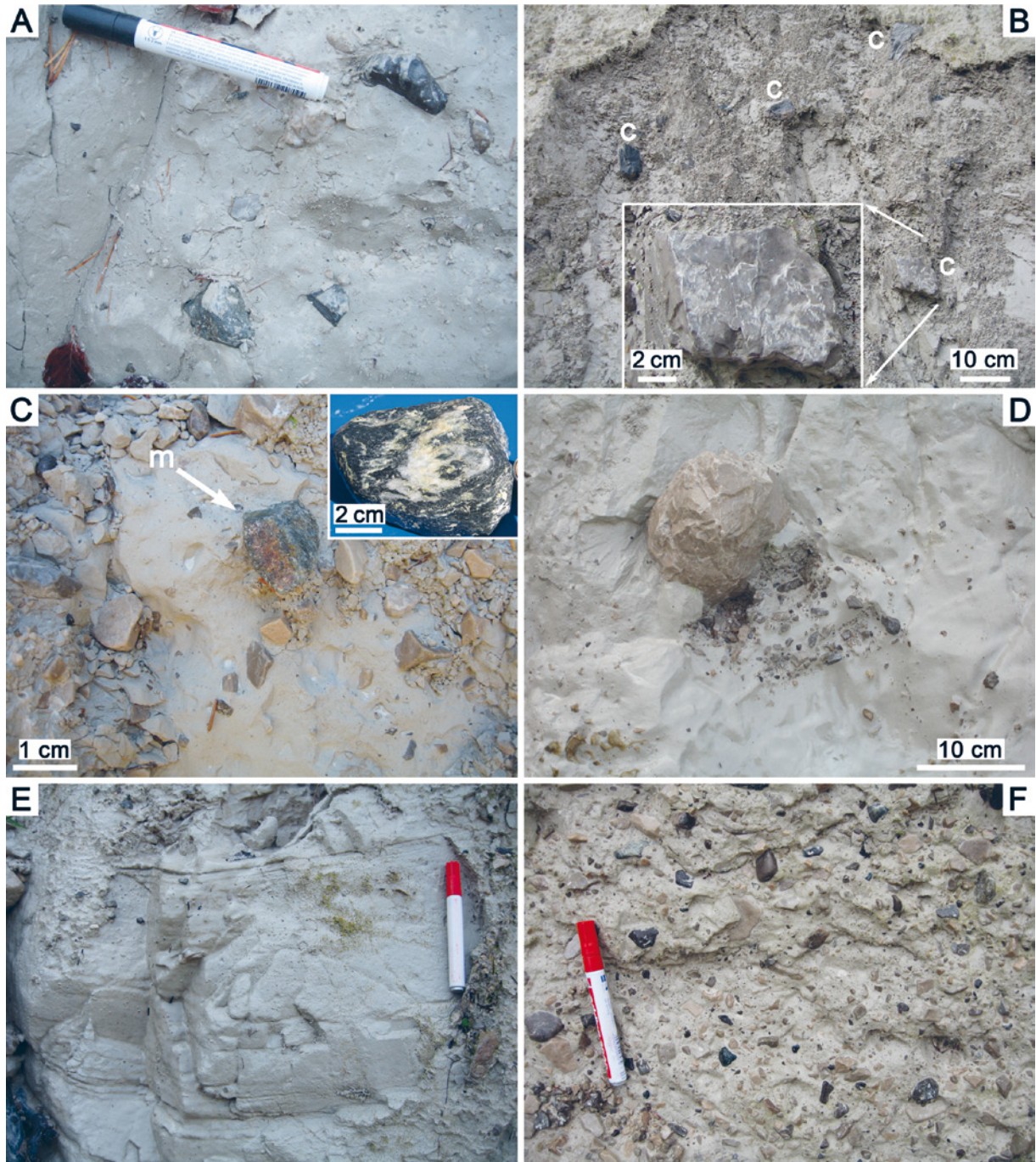


Fig. 4. A. Diamict with disordered, subangular clasts of carbonate rocks. The groundmass of the diamict is a dolomud to -silt with a few percent of siliciclastic material (Table 2). Left bank of Gießenbach, 1195 m a.s.l. Pen is 14 cm long. B. Diamict with angular coarse gravels to cobbles (some labeled with c) derived from the Hauptdolomit unit and the Seefeld Formation. Inset shows clast surface with scratch marks. Left bank of Giessenbach, 1210 m a.s.l. C. Diamict rich in carbonate rock clasts, and with a clast of metamorphic rock (shown by arrow labeled m). Inset shows clast of amphibolite excavated from the same location. Right bank of Giessenbach, 1210 m a.s.l. D. 'Cluster' of carbonate rock clasts, floating in a matrix of carbonate-rich mud to -silt. Left bank of Giessenbach, 1215 m a.s.l. E. Interval of faintly parallel-laminated, carbonate-rich mud to -silt. Left bank of Giessenbach, 1215 m a.s.l. F. Diamict of disordered carbonate-rock fragments (from Hauptdolomit unit) and fragments of metamorphic rocks derived by pleniglacial drift. Matrix is a dolomud to -silt with a few percent of siliciclastic material (see Table 2). Left bank of Gießenbach, 1185 m a.s.l. Pen is 14 cm long.

Abb. 4. A. Diamikt mit disorientierten Bruchstücken aus Karbonatgestein. Die Grundmasse ist ein halbverfestigter Dolomitschlamm von Ton- bis Siltkorngrösse mit wenigen Prozent an siliklastischem Material (Tabelle 2). Linkes Ufer des Giessenbaches, 1195 m über NN. Stift ist 14 cm lang. B. Diamikt mit angulären Klasten von Grobkies- bis Stein-Grösse (einige mit c markiert), die aus der Hauptdolomit Einheit und der Seefeld-Formation stammen. Das eingesetzte Bild zeigt Schurfmarken an der Oberfläche eines der Klasten. Linkes Ufer des Giessenbaches, 1210 m über NN. C. Diamikt mit vielen Klasten aus Karbonatgestein sowie einem Klasten aus Metamorphit (Pfeil m). Das eingesetzte Bild zeigt einen Klasten aus Amphibolit, der an dieser Örtlichkeit aus dem Diamikt geborgen wurde. Rechtes Ufer des Giessenbaches, 1210 m über NN. D. Lose Ansammlung von Karbonatgesteins-Klasten, die in einer Matrix aus halbverfestigtem Dolomitschlamm von Ton- bis Siltkorngrösse schwimmt. Linkes Ufer des Giessenbaches, 1215 m über NN. E. Lage aus undeutlich parallel-laminierter, halbverfestigtem karbonatreichem Schlamm bis Silt. Linkes Ufer des Giessenbaches, 1215 m über NN. F. Diamikt aus disorientierten Karbonatolithoklasten (aus der Haupidolomit-Einheit) und Fragmenten von Metamorphen von hochglazialer Drift. Die Grundmasse ist ein halbverfestigter Dolomitschlamm von Ton- bis Siltkorngrösse mit wenigen Prozent an siliklastischem Material (siehe Tabelle 2). Linkes Ufer des Giessenbachs, 1185 m über NN. Stift ist 14 cm lang.

Tab. 1: Prevalent facies types along Gießenbach stream. Facies types of minor significance and/or minor extent are described in the text only, or in figure captions. Facies of outcrop B (see Fig. 3) are described in Table 3. See text for description of index clasts of Inn glacier of Last Glacial Maximum.

Tab. 1: Vorwiegende Faziestypen entlang des Giessenbachs. Faziestypen von geringerer Bedeutung und/oder Ausdehnung werden im Text oder in Figurenbeschreibungen behandelt. Die Fazies des Aufschlusses B (siehe Abb. 3) werden in Tabelle 3 gesondert beschrieben. Siehe Text für die Beschreibung der Leit-Lithologien des Inn-Gletschers des Letzten Glazialen Maximums.

Facies number Designation	Description	Interpretation of sediment Interpretation within sequence of events	Remarks
#1 Diamicton with sparse lithoclasts to unbedded, carbonate-rich silt to mud	Unbedded, unlaminated carbonate silt to mud, locally with floating, disoriented lithoclasts of carbonate rocks and few clasts of metamorphic rocks [e. g. index clasts of LGM, garnet amphibolite, amphibolite, quartzite]. Some lithoclasts show polished and striated surfaces. Deposit lacks: [a] shear bands, [b] vertical joints. Intercalated interval [few dm in thickness] of banded carbonate silt to mud [facies 1a, see text].	Interpretation A: Subaerial, paraglacial redeposition of glacial till of LGM by mudflows [facies 1] and cohesive debris flows [facies 2] OR: Interpretation B: Facies 1 and 2 represent a waterlain till associated with a late-glacial local-sourced glacier. Level of postulated lake had to be located at least at about 1225–1230 m a.s.l.	Facies 1 and 2 are: [a] vertically associated with each other, [b] similar in mineralogical composition of their matrix (see Tab. 2). Unit composed of facies 1 and 2 exposed in upper reach of Gießenbach valley between about 1170–1230 m a.s.l. [Fig. 3, Fig. 9]
#2 Diamicton rich in lithoclasts [typically clast-supported]	Unbedded to faintly stratified, clast- to matrix-supported gravelly deposits with a matrix of carbonate silt to mud. Lithoclasts include local-derived carbonate rocks and metamorphic rocks from glacial drift [e. g. index clasts of LGM, amphibolite, garnet mica schist]. Some lithoclasts show polished, faceted and striated surfaces. Deposit lacks: [a] shear bands, [b] vertical joints, [c] 'overcompaction', [d] clasts fractured at point contacts.		
#3 Stratified alluvial gravels	Stratified, clast-supported gravels of angular to subrounded clasts of carbonate rocks. Indistinct strata dip subhorizontally to about 5–15° down-valley, and are typically 10–30 cm in thickness. Clasts of metamorphic rocks [including index clasts of LGM] are rare but persistently present throughout. Matrix is a carbonate-muddy sand of carbonate-rock fragments, with scarce siliciclastic grains. Locally, this facies is lithified into breccias (facies 3a) contained within.	Sheet-flow deposits of braided stream dominated by carbonate gravels. After a first phase of reworking of till and/or deposition of waterlain till ahead of a local-sourced glacier [facies 1+2], massive shedding of scree from local bedrock hillslopes started, perhaps in addition to continued redeposition of basal till. Combined with a probably elevated base-level as a result of decaying Inn-valley ice stream (see also text), this led to strong aggradation along Gießenbach valley.	Facies 3 comprises the majority of sediment volume along Gießenbach valley Stratified alluvial breccias: see Fig. 5A to 5D
#3a Alluvial breccias	Of identical characteristics than facies 3, but lithified by: [a] fringes of micrite and/or [b] thin fringes of calcitic dog tooth spar, and/or [c] by lithification of carbonate-muddy matrix	Localized lithification of alluvial gravels in a meteoric-vadose to essentially phreatic environment [SANDERS, OSTERMANN & KRAMERS 2010]	
#4 Cohesive debris-flow deposits	Layers up to a few decimeters thick of angular to subrounded clasts of carbonate rocks, with a matrix of cohesive carbonate mud to carbonate-muddy lithic sand; typically clast-supported. Rare clasts of metamorphic rocks [including index clasts of LGM]. Intercalated in lower part of successions composed of facies 3	Deposits of cohesive debris flows	Facies of minor significance with respect to volume
#5 Gravelly to bouldery fluvial deposits rich in LGM index clasts	Stratified, clast-supported, gravelly to bouldery deposits composed of subequal amounts of: [a] very well-rounded gravels to small boulders of metamorphic rocks [including index clasts of LGM], and [b] subangular to well-rounded gravels to cobbles of local carbonate rocks. Clast imbrication of a[p,t]b[i,p]-type common. This facies comprises veneers a few decimeters to about 2 meters in thickness atop terrace surfaces [at different levels] alongside the present Gießenbach and Karlbach streams.	Fluvial deposits of re-incision phase of Gießenbach-Karlbach streams, down to their present level Sheet-flow deposits (terrace veneers) and channel deposits Represents the late-glacial to Holocene state of Gießenbach-Karlbach drainage system.	A relict patch of this facies is present on a strath terrace of Gießenbach stream near the exit of the bedrock-incised gorge [outcrop A in Fig. 3].

such as garnet amphibolite, amphibolite, mica schist and gneiss are rare and confined to a few matrix-supported layers. The clasts of metamorphic rocks are in the coarse sand- to medium-gravel size range; a single amphibolite clast of coarse gravel size was found (Fig. 4C). Locally, lithoclasts are present in matrix- to clast-supported 'clusters' floating in the diamict (Fig. 4D). At 1210 m a.s.l., near the base of outcrop on the orographic right bank of Giessenbach, an interval about 30 cm in thickness of banded, carbonate silt to -mud is intercalated into the diamict (facies 1a; Fig. 4E, Tab. 1). Throughout the interval of facies 1, no evidence for 'overcompaction', vertical jointing and shear bands was found. Facies 2 is represented by clast- to matrix-supported diamicton rich in clasts of metamorphic rocks, in addition to abundant carbonate rock clasts derived from the local drainage area (Fig. 4F, Tab. 1). Clast rounding ranges from angular to well-rounded. Most of the carbonate rock clasts are of subangular shape. In facies 2, clasts with striated surfaces are relatively common. Facies 2 is locally intercalated into facies 1, but mainly comprises the upper part of the interval composed of both facies 1 and 2. In both facies, stratification surfaces are absent or only faintly expressed. Where visible, stratification dips with a few degrees down-valley; no steeply inclined bedsets were observed. With respect to mineralogical composition the fine-grained matrices of facies 1 and 2 are closely similar: aside of a percentage of ~80–91 wt% dolomite, some 9–20 wt% consist of silicic minerals such as muscovite, chlorite and albite (Tab. 2). The intercalated interval of banded carbonate silt to -mud (Fig. 4E) contains slightly less of muscovite, quartz and chlorite than the diamict facies (Tab. 2).

Over most of Giessenbach valley, above facies 1 and 2, a thick succession ('alluvial succession') is present that is composed angular to subrounded gravels of carbonate rocks from the local drainage area, and an accessory but persistent content in clasts of metamorphic rocks, including index clasts of the LGM. The succession consists of two types of facies (Tab. 1): facies 3, represented by stratified gravels with openwork fabric or with a matrix of carbonate mud to winnowed, carbonate-lithic sand; clasts prevalently are arranged with their [a,b]-plane subparallel to stratification, but downstream-imbricated clast fabrics of (a)p,(b)i type are present, too. In outcrop C (cf. Fig. 3), the stratified gravels of facies 3 became locally lithified into breccias to conglomeratic breccias (=facies 3a; Tab. 1). The breccias are of identical composition, fabric and texture than their unlithified host deposits, including a low but persistent content of LGM index clasts (Fig. 5A, 5B). The breccias are lithified by: (a) thin fringes of micritic cement, and/or (b) thin fringes of dog tooth spar and, subordinate, (c) by lithification of carbonate mud (Fig. 5C). Rounded interstitial pores within a matrix of lithified carbonate mud may be fringed by micrite and/or dog tooth spar (Fig. 5D).

Facies 4 is closely similar in lithoclast fractions and clast sorting to the former one, but contains a matrix of carbonate mud; facies 4 commonly is clast-supported, but clasts are disoriented and no clast fabrics are obvious (Tab. 1). Finally, facies 5 is present as veneers a few decimeters to a few meters in thickness atop terraces incised into the older deposits (facies 1 to 4). Facies 5 consists of roughly equal

amounts of gravels to boulders of metamorphic rocks (including index clasts of the LGM) derived from glacial drift, and of carbonate rocks from the local drainage area. In this facies stratification, clast support, and downstream imbrication of clasts (fabrics of (a)p,(b)i type) up to cobble or small boulder size are common; the matrix typically is a winnowed carbonate-lithic sand.

In outcrop B (Fig. 3), above 1105 m a.s.l. along the right flank of a ravine at the right bank of Giessenbach, a succession containing a record of the LGM is present. In this outcrop, six distinct depositional units G1 to G6 were distinguished. For characterization of depositional units, the reader is referred to Figure 6 and Table 3. By inference, the depositional units terminate in onlap onto the rock substrate a few tens of meters towards the north, where the incised bedrock gorge starts (Fig. 3). Conversely, about 20–25 meters towards the south, starting with the left (southern) flank of the incised ravine, outcrops are dominated by facies 3 to 5 as prevalent in the middle reach of Giessenbach valley (cf. Fig. 3).

4.2 Facies interpretation

Both facies 1 and 2 accumulated subsequent to the LGM. This is indicated by the presence of clasts of metamorphic rocks transported within the pleniglacial Inn glacier, combined with an absence of 'overcompaction', vertical joints and shear bands. As mentioned, the siliciclastic fractions of the fine-grained sediments of facies 1 and 2 are characterized by muscovite, chlorite and albite. Because each of these minerals is readily eradicated by chemical weathering (BERNER & BERNER 1996), this supports the hypothesis that the origin of the sediment fraction is from pleniglacial drift. The features of facies 1 suggest that it accumulated mainly from subaerial mudflows supplied by paraglacial redeposition of basal till. In facies 2, the prevalence of clast support combined with: (a) the presence of a matrix of silt to mud, and (b) the disoriented embedding of clasts indicates that it accumulated from cohesive debris flows. In consequence, the interval of faintly banded silt to -mud (facies 1a, Fig. 4E, Tab. 2) intercalated into facies 1 may record an ephemeral small lake or pond. An interpretation of facies 1 in terms of subaerial paraglacial mudflows is compatible with the intercalated layers of facies 2. Observations of melting glaciers in Norway show that redeposition of glacial till proceeds immediately after deglaciation at site, resulting mainly in debris flows and mud flows (BALLANTYNE & BENN 1994; CURRY & BALLANTYNE 1999).

Alternatively, facies 1 and 2 together may represent a waterlain till of a Late glacial local-sourced glacier that debouched into an ice-marginal lake (cf. REITNER 2007). This glacier may have filled the former upper part of the drainage area from Gaisburgls Boden to Eppzirl Alm (Fig. 3). A local glacier that advanced immediately after decay of pleniglacial ice cover at site would redeposit glacial till inherited from the immediately preceding ice cover. Both, *subaqueous* mudflows and rapid suspension fallout of mud and stones from the base of glaciers facing into proglacial lakes are common. The lack of vertical jointing and shear banding, the disoriented embedding of clasts, and the intercalated interval of banded silt in facies 1 are all com-

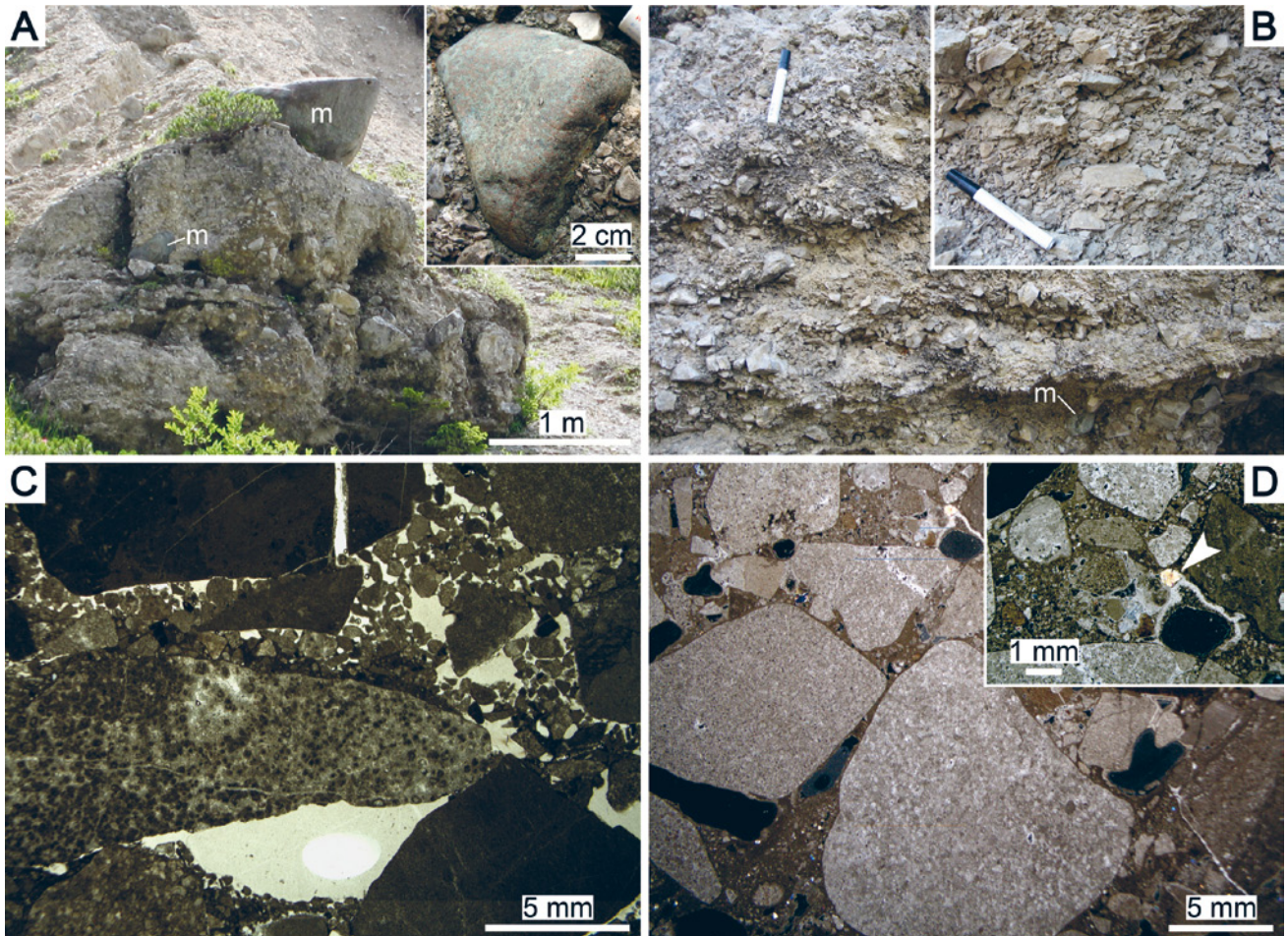


Fig. 5. A. Lithosome of breccia produced by local cementation of stratified alluvial gravels (facies 3; see Table 1). The breccia consists of clasts from the Hauptdolomit unit and of a few gravels to small boulders of metamorphic rocks (marked with ‚m‘). Note gently-dipping stratification. Inset shows clast of garnet amphibolite, an index lithology of the Inn-valley ice stream of the Last Glacial Maximum (see text), embedded in the breccia. Outcrop C, 1185–1190 m a.s.l. (cf. Fig. 3). B. Detail of breccia shown in Fig. 5A. Note faint stratification, local downstream-imbricated clast fabrics, and composition mainly of angular clasts of Hauptdolomit and a few clasts of metamorphic rocks (labeled ‚m‘). Pen is 14 cm long. C. Thin section of breccia shown in Fig. 5A. The interstitial pores of the breccia contain winnowed carbonate-lithic sand to silt cemented by very thin fringes of micrite or calcite spar. Parallel nicols. D. Thin section of breccia shown in Fig. 5A. This sample shows a matrix of carbonate-lithic silt with a few silt- to sand-sized grains of siliciclastic material (labeled by arrowtip 1 in inset photo). Note rounded pores clad by thin fringes of dog tooth spar. Crossed nicols.

Abb. 5. A. Brekzienkörper, entstanden durch örtliche Zementation geschichteter alluvialer Kiese (Fazies 3, siehe Tabelle 1). Die Brekzie besteht aus Klasten der Hauptdolomit Einheit und einigen wenigen, kies- bis block-großen Metamorphit-Klasten (mit ‚m‘ angezeigt). Beachte die sanft einfallende Stratifikation. Das Kleinbild rechts oben zeigt einen Klasten aus Granat-Amphibolit, einem Leitgestein des Inntal-Eisstroms des Letzten Glazialen Hochstands (siehe Text), eingebettet in die Brekzie. Aufschluss C, 1185–1190 m über NN (vgl. Abb. 3). B. Ausschnitt der Brekzie von Abb. 5A. Beachte die undeutliche Stratifikation, örtliche Dachziegellagerung von Klasten, und die Zusammensetzung vorwiegend aus angulären Klasten aus der Hauptdolomit-Einheit und einigen wenigen Klasten von Metamorphiten („m“). Stift ist 14 cm lang. C. Dünnschliff der Brekzie aus Abb. 5A. Die Zwickelräume sind mit ausgewaschenem karbonat-lithischem Sand bis -Silt gefüllt, der durch sehr dünne Säume von Mikrit oder Kalzitsparit verfestigt ist. Parallele Nicols. D. Dünnschliff der Brekzie aus Abb. 5A. Diese Probe enthält eine Grundmasse von karbonat-lithischem Silt mit einigen silt- bis sand-großen Körnern von siliziklastischem Material (angezeigt durch Pfeilspitze 1 im Kleinbild oben rechts). Beachte die gerundeten Poren, die mit dünnen Säumen von Hundezahn-Zement ausgekleidet sind. Gekreuzte Nicols.

patible with waterlain till (MENZIES & SHILTS 2002; Wood et al. 2010). The local interbedding of facies 1 and 2 might even result from subaqueous deposition in a ‚till delta‘ (cf. DREIMANIS 1995; BENN & EVANS 2010); this, however, can not be tested due to limited outcrop. An interpretation of facies 1 as a waterlain till implies that the level of a hypothetical ice-marginal lake was at least about 1225–1230 m a.s.l. (cf. Fig. 9). The morphology of the rock substrate would allow for a lake level at this altitude. However, because no corresponding interval is exposed farther down valley, the potential down-valley extent of that lake cannot be assessed. A narrow, elongate ice-marginal lake would receive copious sediment (chiefly reworked till and scree) not only

from the front of a late-glacial ‚Giessenbach glacier‘, but also from the very steep mountain flanks alongside. With respect to the interpretation of facies 1 and 2 in Giessenbach valley, I see no unequivocal criteria to differentiate between an interpretation in terms of: (a) subaerially redeposited pleniglacial till, and/or (b) deposition as a waterlain till ahead of a local glacier that advanced shortly after decay of the pleniglacial ice cover.

Facies 3 and its lithified equivalent (facies 3A) represents alluvial gravels. In this facies, no lenticular channel-fills (cf. SANDERS, OSTERMANN & KRAMERS 2009) were observed. Instead, the facies is characterized by low-dipping, more or-less constant stratification without major verti-

Tab. 2: Mineralogical composition of facies 1 and of the fine-grained matrices of facies 2 (see Tab. 1), determined by X-ray diffractometry.

Tab. 2: Mineralogische Zusammensetzung der Fazies 1 und der feinkörnigen Matrix von Fazies 2 (siehe Tab. 1), bestimmt mit Röntgen-Diffraktometrie.

Sample # Altitude a.s.l.	#1 1165 m	#2 1170 m	#3 1180 m	#4 1190 m	#5 1200 m	#6 1210 m	#7 1210 m
Facies [cf. Tab. 1]	#2	#2	#1	#2	#1	#1a	#1a
Dolomite	87.0	79.9	81.2	76.3	80.5	91	91
Calcite	3.9	2.9	4.3	3.5	3.6	3	4
Muscovite	3.5	5.7	6.1	4.5	4.8	2	1
Albite	2.5	4.4	2.8	5.5	4.1	< 1	< 1
Chlorite	0.7	3.0	2.5	5.7	2.3	< 2	2
Quartz	2.4	4.1	3.1	4.5	4.7	< 2	2
Total carbonate minerals:	90.9	82.8	85.5	79.8	84.1	~ 94	~ 95
Total siliciclastic minerals:	9.1	17.2	14.5	20.2	15.9	~ 6	~ 5

Tab. 3: Characterization and interpretation of units G1 to G6 in Figure 6.

Tab. 3: Charakterisierung und Deutung der Einheiten G1 bis G6 in Abbildung 6.

Depositional unit Interpretation	Characterization	Remarks
Unit G1 Pre-LGM talus slope	Faintly stratified deposit of angular gravels derived exclusively from Hauptdolomit; strata dip with about 25–30° [cf. Fig. 6]; deposit shows openwork layers, vertically changing with layers more rich in a matrix of winnowed carbonate-lithic sand to silt	Overlain by unit G2 along a truncation surface
Unit G2 Basal till of LGM	Diamicton of fine-grained, compacted, grey matrix rich in clasts of rounded, polished and faceted metamorphic rock fragments including index clasts of LGM Inn glacier	–
Unit G3 Diamicton formed by redeposition of basal till of LGM, mixed with lithoclasts derived from local rock cliffs	Diamicton of light-grey matrix rich in: [a] clasts of rounded, polished and faceted metamorphic rock fragments including index clasts of LGM, and [b] angular gravels to small boulders of clasts of Hauptdolomit.	–
Unit G4 Fluvial deposits of re-incision phase	Clast-supported gravelly to cobblely deposit of: [a] well-rounded clasts of metamorphic rocks [including index clasts of LGM], and [b] surrounded to well-rounded gravels to cobbles of Triassic carbonate rocks [Hauptdolomit unit, Seefeld Fm]; matrix is winnowed lithic sand	G4 overlies the other deposits along a surface that dips steeply towards Giessenbach stream [Fig. 6]
Unit G5 Post-glacial talus slope	Stratified deposit of angular gravels to small boulders derived from Hauptdolomit unit; rare clasts of metamorphic rocks are present, too; strata dip with about 30° towards the valley	Downlaps onto unit G4
Unit G6 Veneer of hillslope colluvium/hillslope creep deposit; topped by forested soil	Veneer, up to about 1 meter thick, of isolated lithoclasts and ‘stringers’ of clasts embedded in brown to blackish, sandy to silty groundmass rich in particulate organic matter	–

cal or lateral change in mean grain size. The characteristics of facies 3 suggest deposition from episodic, shallow flows (sheet flow; GALLOWAY & HOBDAY 1983) in an aggrading braided stream. A braided-stream setting for facies 3 is also supported by the fact that it comprises successions tens of meters in thickness that had previously filled the valley at a much higher level than present (see section 5. below). Facies 4, in turn, represents deposits of cohesive debris flows. These deposits seem to be more common in the basal part of the alluvial succession, but do not comprise a major fraction. Finally, facies 5 building terrace veneers of gravelly to bouldery deposits rich in well-rounded clasts of metamorphic rocks is interpreted as deposition from a per-

ennial, or quasi-perennial, ancestral Giessenbach stream that incised progressively deeper into the older Quaternary deposits. For the interpretation of depositional units G1 to G6 in outcrop B, the reader is referred to Table 3. In the following section, significant morphological features of the considered drainage area and their relation to facies and their relative stratigraphic position is described.

5 Morphostratigraphy

In the lowest part of Giessenbach valley, an erosional relic about 15 m in width comprising a gravelly to cobblely stream-channel deposit rich in index clasts of the LGM

SW

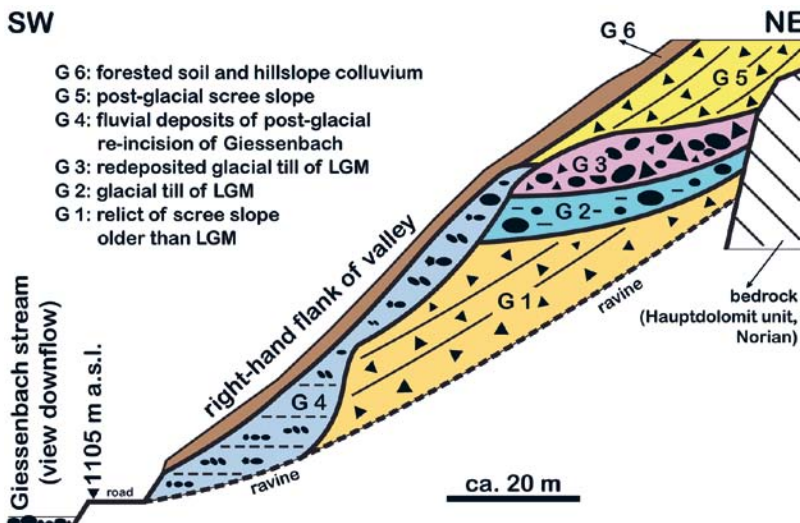


Fig. 6. Scheme of outcrop B (see Fig. 3) in a ravine at right bank of Giessenbach. See Table 3 for further characterization and interpretation of depositional units G1 to G6. Horizontal distance roughly to scale; vertical scale exaggerated.

Abb. 6: Schema des Aufschlusses B (siehe Abb. 3) in einer Rinne rechtseitig des Giessenbaches. Siehe Tafel 3 für weitere Charakterisierung und Deutung der Ab-lagerungs-Einheiten G1 bis G6. Horizontale Entfernung grob maßstäblich; vertikal versteilt.

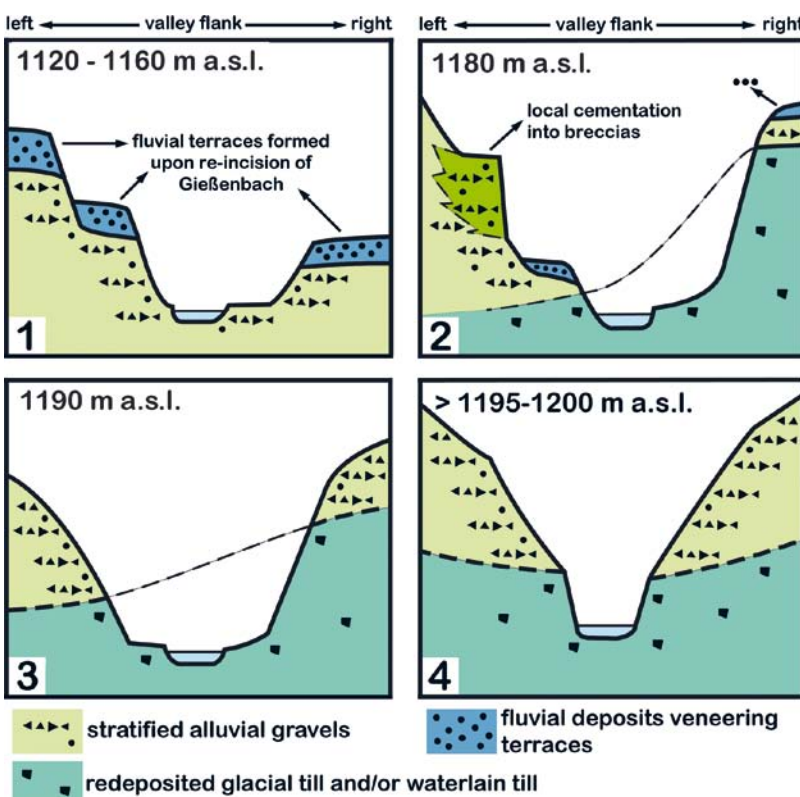


Fig. 7. Schematic cross-sections of Giessenbach valley at different locations a.s.l. (see Fig. 3A for positions). See text for description and discussion.

Abb. 7: Schematische Querschnitte des Giessenbach-Tals bei verschiedenen Höhen über NN (vgl. Abb. 3A für Lagen). Siehe Text für Beschreibung und Erörterung.

is ‘stranded’ directly on Hauptdolomit bedrock, about 25 meters above the present floor of the gorge (outcrop A in Fig. 3). At this location, the gorge is most narrow, consisting essentially of a bedrock channel about 1 meter in width incised into Hauptdolomit. In the middle reach of Giessenbach valley, outcrops are represented by thick packages of alluvial gravels and debris-flow deposits (facies 3 and 4), and by terraces veneered by fluvial deposits rich in LGM index clasts (facies 5) (Fig. 7, section 1). In the upper part of the present Giessenbach valley, above approximately 1180 m a.s.l., exposures along both valley flanks indicate that the contact between facies 1 and 2 and the overlying unit of alluvial gravels and debris-flow deposits (facies 3 and 4) is a three-dimensional surface (Fig. 7, sections 2 to 4).

In the upper part of the present Giessenbach valley a system of terraces is well-identifiable in laserscan images (Fig. 8A). Field inspection of the surface named ‘Gaisburgls Boden’ (ca. 1260 to 1290 m a.s.l.; Fig. 8A) yielded scattered clasts of metamorphic rocks as well as of Lower Triassic red beds (Verrucano or Alpiner Buntsandstein) derived by glacial drift from distant source areas, in addition to abundant carbonate-rock clasts derived from the local drainage area. On the opposite, right-hand side of Giessenbach valley, another large surface is present between about 1270 to 1300 m. a.s.l., at nearly the same level. This latter surface also is littered with gravels to cobbles of glacial drift (metamorphic rocks, red beds). The roadcut indicates that the major part of the sediment is again represented by carbonate-rock clasts from the local environs. This surface terminates

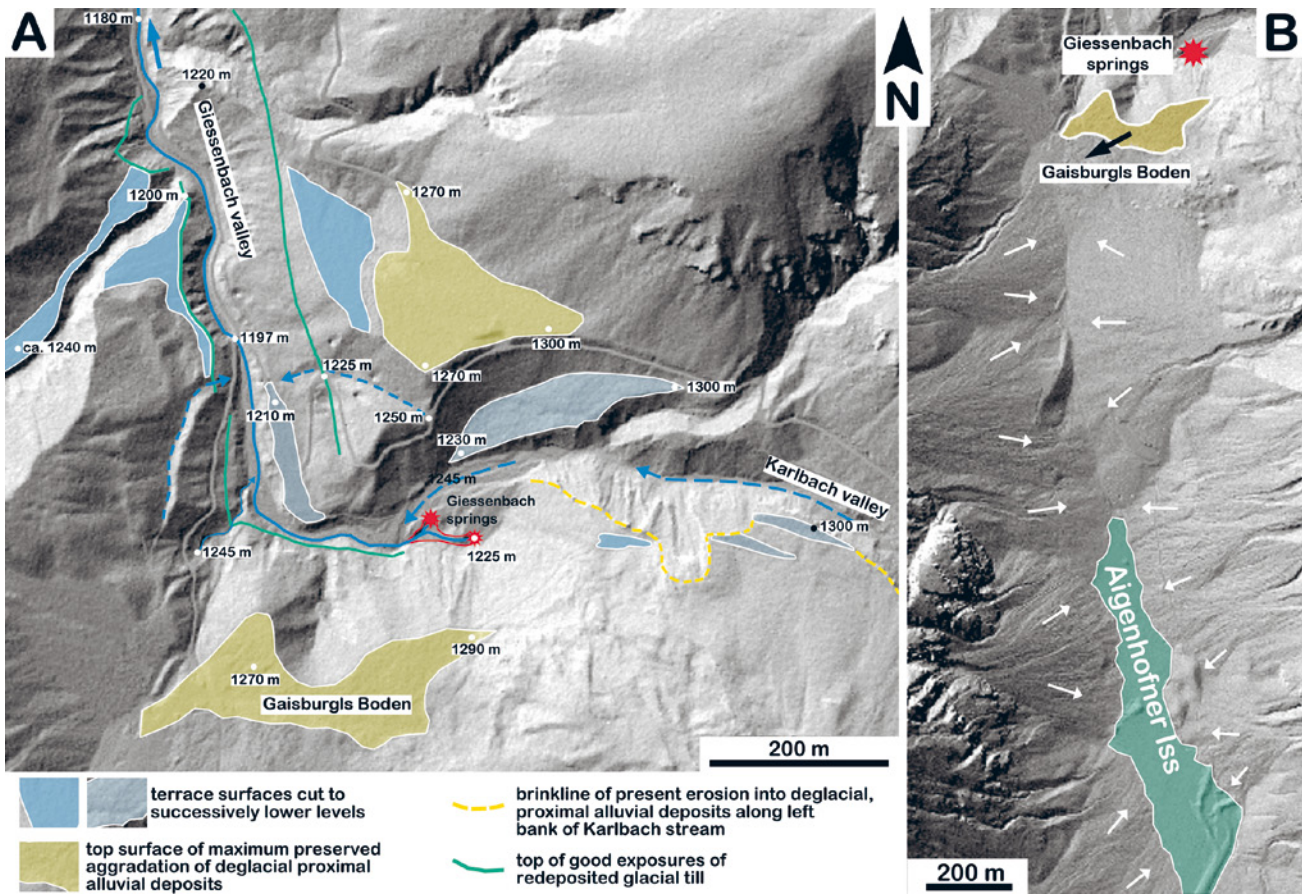


Fig. 8. A. Laserscan of upper reach of present Gießenbach (source: www.tirol.gv.at). On both valley sides, large terraces (light yellow; 'Gaisburgls Boden', and its opposite equivalent) are present between 1270 to 1300 m a.s.l.; these represent the highest and oldest terraces. Down slope along the valley flanks, lower-lying terraces (light blue hues) are present that step down up to a few meters above the present level of Gießenbach. The top of the unit of facies 1 and 2 (Tab. 1) can be placed at 1225 to 1230 m altitude (green line). B. Up-valley of the terrace Gaisburgls Boden, large scree slopes have shed onto the aggraded, raised floor of the dry valley (compare Fig. 3A). Farther up-valley, a vegetated remnant of a subhorizontal plane (Aigenhofner Iss; green hue) is preserved between prograding scree slopes; this plane may record a former lake.

Abb. 8. A. Laserscan (Quelle: www.tirol.gv.at) des Oberlaufs des heutigen Giessenbaches. Auf beiden Talseiten finden sich zwischen 1270 m bis 1300 m über NN grosse Terrassen (hellgelb; 'Gaisburgls Boden', und seine gegenüberliegende Entsprechung); diese bilden die höchstegelegenen und ältesten Terrassen. Hangabwärts finden sich an den Talflanken bis wenige Meter über der Sohle des heutigen Giessenbaches weitere Terrassen (hellblaue Farbtöne). Die Oberkante der Einheit aus Fazies 1 und 2 (Taf. 1) tritt zwischen 1225 bis 1230 m über NN auf (grüne Linie). B. Talaufwärts der Terrasse Gaisburgls Boden wurden große Schutthalden über den erhöhten Boden des Trockentals geschüttet (vgl. Abb. 3A). Weiter talauf findet sich der bewachsene Rest einer fast söligen Talfläche (Aigenhofner Iss; grüner Farbton) zwischen vorbauenden Schutthalden; diese fast sölige Fläche könnte auf einen verlandeten See zurückzuführen sein.

sharply against scree slopes that, today, are abandoned and completely forested; the scree slopes do not show evidence for a knick in the distal part of slope or erosion along their toe. In addition to the described two large surfaces, a system of smaller terraces (surfaces shown in blue hues in Fig. 8A) is identified in lower positions. These latter terraces are veneered by fluvial deposits of facies 5. From the highest terraces to the lowest, and down to the present stream bed, the fluvial facies overall becomes richer in clasts of metamorphic rocks relative to carbonate-rock clasts; in addition, cobbles to boulders of metamorphic rocks become gradually more common: whereas these are comparatively rare in the alluvial gravels (see Fig. 5A), the present stream bed is rich therein.

Schematically summarizing deposits and stratigraphic relations in the upper part of Giessenbach valley into a composite section results in a thickness of the deglacial to early late-glacial succession of more than some 100–120 meters (Fig. 9). It is obvious that the deglacial deposits re-

present the major sediment body in this valley. The cohesive nature of the redeposited glacial tills probably lowered the rate of headward erosion of Giessenbach, to result in the distinct 'blockade' of the upper half of the former Giessenbach valley by sediments. The springs of Giessenbach are characterized by perennial shedding of an estimated few hundreds of liters per second in total. Today, the springs discharge a few meters higher than the present bed of Karlbach, from a comparatively young, but vegetated terrace of gravelly to cobblely alluvial deposits. Up-valley of Gaisburgls Boden, shedding of large talus slopes from both valley flanks resulted in a local inversion of gradient, down to Aigenhofner Iss at about 1260–1270 m (Fig. 8B). Today, Aigenhofner Iss is characterized by an ephemeral pond falling dry during autumn and during longer fairweather periods in summer. Today, talus slopes downlap and prograde over the fine-grained ephemeral-lacustrine deposits that floor Aigenhofner Iss.

6 Interpretation and discussion

The segmentation of Giessenbach valley into: (a) a lower reach with a bedrock gorge of high gradient, and (b) a moderately steep middle to upper reach with bedload channel is a common in the NCA; Giessenbach valley, however, differs from many other valleys in that its former upper half (i. e., Gaisburgls Boden to Eppzirler Alm) is still clogged by a sedimentary succession at least a few tens of meters in thickness. By analogy to the outcrops along the present Giessenbach stream, it is assumed that at least the stratigraphically lower part of the valley-fill consists mainly of deposits of the deglacial phase. In the upper part of the valley, however, below cliffs of Hauptdolomit, large scree slopes added significantly to total sediment volume. Taking into account that Giessenbach does not receive major input from tributaries along its course, the overall convex shape of the longitudinal valley profile (Fig. 3A) indicates that the stream is off geomorphic equilibrium. The convex profile is probably related to, both, the increase in mean channel gradient and the knick associated with the bedrock-incised gorge in the lower reach.

To explain the sheer thickness of the stratified alluvial gravels, three hypotheses can be forwarded: (1) sediment delivery was so rapid that drainage could not keep pace, resulting in aggradation of the valley floor; (2) Giessenbach valley was blocked by decaying ice in the trunk valley; and (3) some combination of these two. The entire drainage area is situated on Hauptdolomit. Because of its dense jointing, the Hauptdolomit weathers quite easily and represents an efficient source of scree. Thus, under conditions of fresh deglacial exposure, copious sediment delivery from the Hauptdolomit by physical weathering can safely be assumed. Standing at the location of the 'stranded' relict of stream-channel deposits (outcrop A in Fig. 3), and projecting a gravelly stream bed with a gradient of about 5° down-valley may suggest that the nearby trunk valley (cf. Fig. 2) was filled by at least some 60–80 meters of sediment. Today, along both flanks of Drahnbach valley, there is no evidence for relicts of a valley-fill of this height. North and south of the debouch of Giessenbach valley, the only record of the LGM along the right flank of Drahnbach valley is represented by relicts of a veneer of basal till directly above Hauptdolomit substrate. In addition, laserscan images do not show an alluvial fan, or relicts thereof, of required size connected to the debouch of Giessenbach gorge; instead, the stream enters into Drahnbach valley along the top of an alluvial fan (now largely blocked by buildings) with the apex at about 1015 m a.s.l. The stream-channel deposits (now preserved as relict) were probably adjusted to an intermittent base-level provided by dead ice in the trunk valley.

In the upper reach of Giessenbach valley, the three-dimensional shape of the transition between redeposited tills and overlying alluvial deposits (Fig. 7) may in part represent an 'original' surface of differentiated relief. During rapid deglacial mass-wasting of till down valley flanks, a differentiated small-scale topography expectably formed. On the other hand, downslope creep of the thick sedimentary packages upon fluvial incision may have produced, or amplified, the three-dimensional aspect of the contact. Laserscan images, however, do not show evidence for sig-

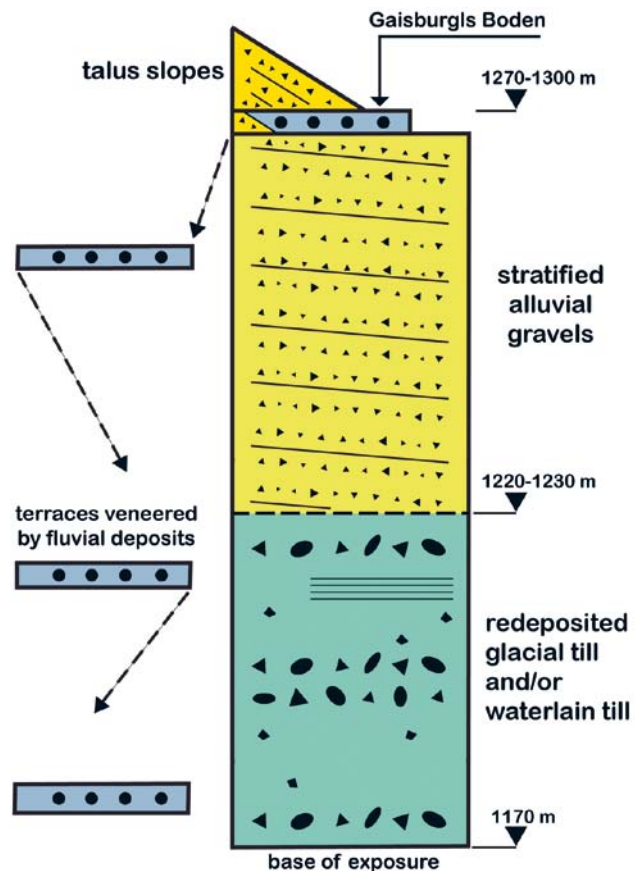


Fig. 9. Composite section of depositional units along Giessenbach valley from 1170 m a.s.l. up to the top of maximum sediment aggradation in this area ('Gaisburgls Boden', 1270–1300 m a.s.l., and its equivalent on the right-hand side of valley, see Fig. 8A).

Abb. 9: Zusammengesetztes Profil der Ablagerungs-Einheiten im Giessenbach-Tal von 1170 m über NN bis zum Dach der höchsten Sediment-Aggradation in diesem Bereich ('Gaisburgls Boden', 1270–1300 m über NN, und seine Entsprechung auf der rechten Talseite; siehe Abb. 8A).

nificant slow gravitational mass-wasting after deposition of the alluvial gravels; it is thus assumed that the contact between the redeposited tills and the alluvial sediments is largely original. Alternatively, the onset of deposition of alluvial gravels may have been associated with local erosion of the redeposited till. This, in turn, would imply a sharp vertical contact between redeposited tills and overlying alluvial gravels, in contrast to a vertical transition as suggested.

As described, along the uppermost part of Giessenbach stream two opposite terraces between 1270–1300 m a.s.l. were identified (Fig. 8A). These two terraces are interpreted to indicate the maximum preserved sediment aggradation; at that time, the valley had a comparatively wide and plane, high-positioned floor with a braided stream system. For the surface at the right side of the valley, the observation that the scree slopes do not show knicks or erosional brinklines along their toes strongly suggests that they downlap the terrace over a limited distance (Fig. 9). The 'blue' veneers in Figure 7, section 1, represent younger terraces formed during a later stage of fluvial re-incision. The increase in both relative percentage and mean diameter of clasts of metamorphic rocks with progressively lower posi-

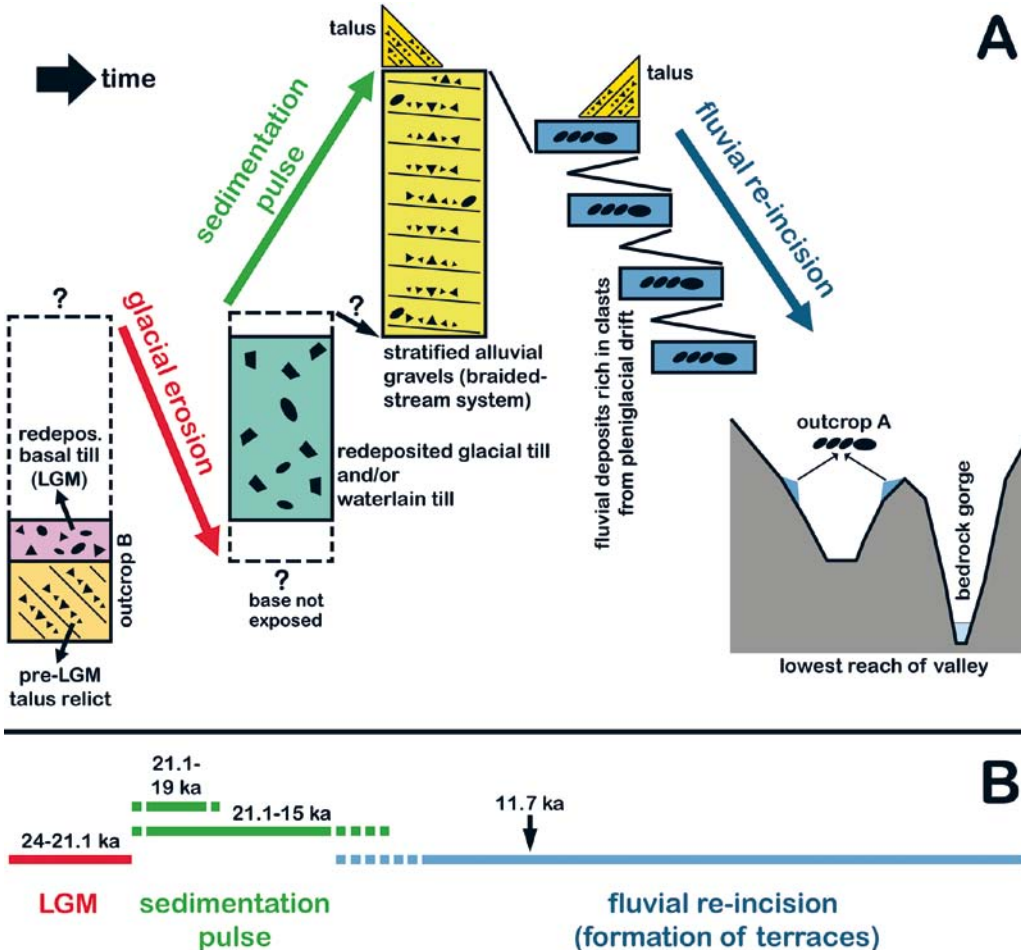


Fig. 10. Summary of geohistory as recorded along present Giessenbach stream. A. Most sedimentation took place during to shortly after decay of pleniglacial ice at the site, and probably lasted into, but faded during, the late-glacial interval. B. Possible time spans of events. For the sedimentation pulse that gave rise to the valley-fill, two time spans may be estimated, a short one from 21.1–19 ka, and a long one from 21.1–15 ka; in either case, the calculated rates of sediment accumulation are very high. See text for further discussion.

Abb. 10: Gesamtschau des geologischen Geschehens entlang des heutigen Laufes des Giessenbachs. A. Sedimentation fand hauptsächlich während bis knapp nach dem deglazialen Eis-Zerfall statt, und dauerte bis ins Spätglazial, währenddessen sie ausklang. B. Mögliche Zeitspannen der Geschehnisse. Für den Sedimentations-Schub, der die Talfüllung bildete, können zwei Zeitspannen geschätzt werden, eine kurze von 21.1–19 ka sowie eine lange von 21.1–15 ka; in beiden Fällen ergeben sich sehr hohe gerechnete Sediment-Akkumulationsraten. Siehe Text für weitere Erörterung.

tion of terraces indicates that the metamorphic clasts became relatively enriched during fluvial re-incision; enrichment is caused by four factors: (1) clasts of crystalline rocks are of higher specific weight than carbonate-rock clasts; (2) up to at least cobble size, clasts derived from glacial drift are commonly better-rounded than carbonate-rock clasts; (3) many crystalline clasts are of cobble to small-boulder size, i. e. larger than the gros of the carbonate-clastic material; and (4) except for schists, relative to carbonate clasts, crystalline clasts disintegrate extremely slowly by (a) frost action, (b) impact of bedload and suspended grains, and (c) due to abrasion in bedload transport. Repeated over thousands of flood cycles, these differences typically result in relative enrichment of crystalline rock clasts. The perennial shedding of the Giessenbach springs suggests that they are supplied from a comparatively large drainage area. In addition, their unusual location relative to the local level of ephemeral Karlbach suggests that these springs represent part of the subsurface drainage of the upper part of the Giessenbach catchment that today is clogged by sediments.

There is no evidence in surface outcrops for significant volumes of pre-LGM deposits in the Giessenbach catchment; the talus relict G1 preserved below the basal till of the LGM (= unit G2, Fig. 6) represents the only sediment accumulated before the LGM. The deglacial to Holocene history of the Giessenbach-Karl valley drainage system can thus be summarized as shown in Figure 10. Subsequent to glacial erosion during the LGM, during and immediately after decay of the pleniglacial ice cover, glacial till was redeposited from valley flanks. This partly overlapped with, and was followed by deposition of alluvial gravels and debris flows. Significant aggradation of alluvial deposits was probably favoured by: (a) high rates of physical erosion of glacially-weakened, unvegetated mountain-flanks freshly stripped of glacial ice, and (b) perhaps also by partial blocking of the exit of Giessenbach valley by dead ice (see above). The time spans and rates of sediment aggradation, however, can only be crudely estimated. It is not established when reforestation started in the considered area. The Inn valley about 12 km towards the south was perma-

nently ice-free from ~17.4 kyr cal BP over most of its extent, and became reforested at about 15 ka BP (VAN HUSEN 2000, 2004). On the other hand, due to the prolonged presence of stagnant, dead ice within the Inn valley (former Bühl „stadial“ of PENCK & BRÜCKNER 1909; now interpreted as dead ice of the ELGID; VAN HUSEN 1997, 2004; IVY-OCHS et al. 2005; REITNER 2007), reforestation of the Inn valley may have been retarded relative to other areas. Colonization of the Giessenbach catchment with shrubby vegetation thus might have already started at about 19–17 ka BP (compare maps of late-glacial ice extent in VAN HUSEN 2000, 2004). In the Giessenbach drainage area, redeposition of glacial till followed by aggradation of gravelly alluvium may be bracketed to between 21–19 ka BP to 17–15 ka BP, or between 6 ka (21–15 ka) to 2 ka (21–19 ka) in duration. Taking the altitude difference between the highest terraces (Fig. 8A) and present Giessenbach as a proxy for total aggradation, the mean sediment aggradation rate is calculated as 8.3 mm/a ('minimum') to 25 mm/a ('maximum'). An accumulation rate of 8–25 mm/a is one to two orders of magnitude higher than deglacial denudation rates of Alpine catchments as deduced from sediment volume (see MÜLLER 1999; HINDERER 2001). At least to a large part, this disparity results from the much larger scale in space of the cited studies relative to the present one (compare TUNNICLIFFE & CHURCH 2011). The aggradation rate 8–25 mm/a, however, is: (a) in the same range of accumulation rates deduced for historical paraglacial accumulation of debris cones following glacial retreat (BALLANTYNE 1995), (b) in the same range of the highest documented denudation rates of individual catchments in orogens (up to 5–18 mm/a; HOVIUS et al. 1997; see NORTON et al. 2010, for rates of 3–7.6 mm/a of denudation by debris flows and rockfalls in tributary catchments of the upper Rhone since the last deglaciation at site), (c) in the same range of high rates of rock cliff retreat (HÉTU & GRAY 2000), and (d) in the same range of high rates of talus accumulation in the NCA (SANDERS & PATZELT 2011); overall, this correspondence of rates may suggest that the estimate of deglacial sediment accumulation rate in the Giessenbach catchment is roughly correct. It is also possible that some of the low-lying terraces along Giessenbach were produced by minor aggradation during stadials (e. g., Gschätz stadial, > 15.4 ka; Egesen maximum, ~ 12.4–12.3 ka; KERSCHNER & IVY-OCHS 2008), but there is no positive evidence for this.

In the NCA, the upper reaches of many catchments are aggraded valleys with a comparatively wide, gently-dipping floor, in some cases with an abrupt transition from valley floor to cliffs (depending on the rate of scree shedding). In addition, due to gradient reversal in longitudinal valley profile (cf. Fig. 3A), lakes or ephemeral ponds and/or disappearance of streams by percolation may occur; overall, however, gradient reversals are relatively rare. The described case study from Giessenbach shows that rapid deglacial sedimentation can be of lasting and profound impact on the morphology and hydrology of intramontane catchments. A similar development from rapid deglacial to late-glacial aggradation followed by abandonment, vegetation, and linear erosion is observed for many scree slopes of the NCA (SANDERS & OSTERMANN 2011).

7 Conclusions

(1) The post-LGM development of the Giessenbach catchment was characterized by: (a) a deglacial aggradation phase with rapid sediment accumulation, followed by (b) an incision phase dominated by fluvial erosion.

(2) The aggradation phase records redeposition of glacial till from hillslopes, and/or deposition of waterlain till ahead of a local-sourced late-glacial glacier. (Re)deposition of till was followed by rapid accumulation of pebbly alluvium supplied from the local rock substrate. During the incision phase, in turn, down-stepping terraces formed while scree slopes became progressively stabilized.

(3) The springs supplying the present Giessenbach stream emerge from within the deglacial sediment succession about half way along the pre-LGM extent of the valley. The upper half of the pre-LGM course of Giessenbach is still a dry, elevated, wide-floored valley with an ephemeral pond. The sedimentary succession that fills or blocks the upper half of the former stream course mainly accumulated from deglacial to late-glacial time.

(4) Along its actual extent, Giessenbach stream shows a convex longitudinal profile with a bedrock gorge in the lowermost reach. Within the gorge, an erosional remnant of fluvial deposits (with LGM index clasts) on a bedrock terrace well-above the present floor suggests that the canyon was blocked by dead ice during ice decay.

(5) Because of their large volume and incomplete erosion, deglacial deposits still coin the morphology and hydrology of the Giessenbach catchment. Similarly thick deglacial sediment bodies, and a corresponding influence on surface runoff, are common in catchments of the Northern Calcareous Alps.

Acknowledgements

The paper gained from comments of Bernhard Salcher, Swiss Federal Institute of Technology, and an anonymous reviewer. Waltraud Wendl and Daniela Schmidmair, Institute of Mineralogy, University of Innsbruck, determined the mineralogical composition of fine-grained sediments by XRD. Gina Moseley, Institute of Geology, University of Innsbruck, is thanked for checking the English. Financial support from project 16114-NO6 of the Austrian Research Foundation is gratefully acknowledged.

References

- BALLANTYNE, C. K. (1995): Paraglacial debris-cone formation on recently deglaciated terrain, western Norway. – *The Holocene*, 5: 25–33.
- BALLANTYNE, C. K. (2002): A general model of paraglacial landscape response. – *The Holocene*, 12: 371–376.
- BALLANTYNE, C. K. & BENN, D. I. (1994): Paraglacial slope adjustment and resedimentation following recent glacier retreat, Fabergstolsdalen, Norway. – *Arctic and Alpine Research*, 26: 255–269.
- BARD, E., HAMELIN, B., ARNOLD, M., MONTAGGIONI, L. F., CABIOCH, G., FAURE, G. & ROUGERIE, F. (1996): Deglacial sea-level record from Tahiti corals and the timing of global meltwater discharge. – *Nature*, 382: 241–244.
- BENN, D. I. & EVANS, D. J. A. (2010): Glaciers and glaciation. – 802 S.; London (Hodder Education).
- BERNER, E. K. & BERNER, R. A. (1996): Global Environment: Water, air, and geochemical cycles. – 376 S.; New Jersey (Prentice-Hall).

- BRANDNER, R. (1984): Meeresspiegelschwankungen und Tektonik in der Trias der NW-Tethys. – *Jahrbuch der Geologischen Bundesanstalt*, 126: 435–475.
- CHURCH, M. & RYDER, J. M. (1972): Paraglacial sedimentation: a consideration of fluvial processes conditioned by glaciation. – *Geological Society of America Bulletin*, 83: 3059–3071.
- CURRY, A. M. & BALLANTYNE, C. K. (1999): Paraglacial modification of glaciogenic sediment. – *Geografika Annaler*, 81A: 409–419.
- DE GRAAFF, L. W. S. (1996): The fluvial factor in the evolution of alpine valleys and ice-marginal topography in Vorarlberg (W-Austria) during the upper Pleistocene and Holocene. – *Zeitschrift für Geomorphologie, Neue Folge*, Supplement 104: 129–159.
- DONOFRIO, D. A., BRANDNER, R. & POLESCHINSKI, W. (2003): Conodonten der Seefeld-Formation: Ein Beitrag zur Bio- und Lithostratigraphie der Hauptdolomit-Plattform (Obertrias, westliche Nördliche Kalkalpen, Tirol). – *Geologisch-Paläontologische Mitteilungen Innsbruck*, 26: 91–107.
- DREIMANIS, A. (1995): Landforms and structures of the waterlain west end of St. Thomas moraine, SW Ontario, Canada. – *Geomorphology*, 14: 185–196.
- FLIRI, F. (1973): Beiträge zur Geschichte der alpinen Würmvereisung: Forschungen am Bändertal von Baumkirchen (Inntal, Nordtirol). – *Zeitschrift für Geomorphologie, Neue Folge*, Supplement 16: 1–14.
- GALLOWAY, W. E. & HOBDAY, D. K. (1983): Terrigenous Clastic Depositional Systems. – 423 S.; New York (Springer).
- GRUBER, A., WISCHOUNIG, L. & SANDERS, D. (2011): Ablagerungs- und Flussgeschichte während des späten Quartärs im Bereich nördlich des Rofan. – In: GRUBER, A. (ed.), Arbeitstagung 2011 der Geologischen Bundesanstalt, Blatt 88 Achenkirch. Geologische Bundesanstalt, Vienna: 226–246.
- HEIN, A. S., HULTON, N. R. J., DUNAI, T. J., SUGDEN, D. E., KAPLAN, M. R. & XU, S. (2010): The chronology of the Last Glacial Maximum and deglacial events in central Argentine Patagonia. – *Quaternary Science Reviews*, 29: 1212–1227.
- HÉTU, B. & GRAY, J. T. (2000): Effects of environmental change on scree slope development throughout the postglacial period in the Chic-Choc Mountains in the northern Gaspé Peninsula, Québec. – *Geomorphology*, 32: 335–355.
- HINDERER, M. (2001): Late Quaternary denudation of the Alps, valley and lake fillings and modern river loads. – *Geodinamica Acta*, 14: 231–263.
- HOVIUS, N., STARK, C. P. & ALLEN, P. A. (1997): Sediment flux from a mountain belt derived by landslide mapping. – *Geology*, 25: 231–234.
- IVY-OCHS, S., KERSCHNER, H., KUBIK, P. W. & SCHLÜCHTER, C. (2006): Glacier response in the European Alps to Heinrich event 1 cooling: the Gschnitz stadial. – *Journal of Quaternary Science*, 21: 115–130.
- IVY-OCHS, S., KERSCHNER, H., MAISCH, M., CHRISTL, M., KUBIK, P. W. & SCHLÜCHTER, C. (2009): Latest Pleistocene and Holocene glacier variations in the European Alps. – *Quaternary Science Reviews*, 28: 2137–2149.
- KELLERER-PIRKLBAUER, A., PROSKE, H. & STRASSER, V. (2010): Paraglacial slope adjustment since the end of the Last Glacial Maximum and its long-lasting effect on secondary mass wasting processes: Hauser Kai-blung, Austria. – *Geomorphology*, 120, 65–76.
- KERSCHNER, H. & IVY-OCHS, S. (2008): Palaeoclimate from glaciers: Examples from the Eastern Alps during the Alpine Lateglacial and early Holocene. – *Global and Planetary Change*, 60: 58–71.
- MENZIES, J. & SHILTS, W. W. (2002): Subglacial environments. In: MENZIES, J. (ed.), Modern and past glacial environments. – Butterworth-Heinemann, Oxford, pp. 215–218.
- MÜLLER, B. U. (1999): Paraglacial sedimentation and denudation processes in an Alpine valley of Switzerland. An approach to the quantification of sediment budgets. – *Geodinamica Acta*, 12: 291–301.
- NEUBAUER, F., GENSER, J. & HANDLER, R. (1999): The Eastern Alps: Result of a two-stage collision process. – *Mitteilungen der Österreichischen Geologischen Gesellschaft*, 92: 117–134.
- NORTON, K. P., VON BLANCKENBURG, F. & KUBIK, P. W. (2010): Cosmogenic nuclide-derived rates of diffusive and episodic erosion in the glacially sculpted upper Rhone Valley, Swiss Alps. – *Earth Surface Processes and Landforms*, 35: 651–662.
- ORWIN, J. F. & SMART, C. C. (2004): The evidence for paraglacial sedimentation and its temporal scale in the deglaciating basin of Small River Glacier, Canada. – *Geomorphology*, 58: 175–202.
- PENCK, A. & BRÜCKNER, E. (1909): Die Alpen im Eiszeitalter. – 1199 S.; Tauchnitz, Leipzig.
- PREUSSER, F. (2004): Towards a chronology of the Late Pleistocene in the northern Alpine foreland. – *Boreas*, 33: 195–210.
- REITNER, J. M. (2007): Glacial dynamics at the beginning of Termination I in the Eastern Alps and their stratigraphic implications. – *Quaternary International*, 164–165: 64–84.
- SANDERS, D., OSTERMANN, M. & KRAMERS, J. (2009): Quaternary carbonate-rocky talus slope successions (Eastern Alps, Austria): sedimentary facies and facies architecture. – *Facies*, 55: 345–373.
- SANDERS, D. & OSTERMANN, M. (2011): Post-last glacial alluvial fan and talus slope associations (Northern Calcareous Alps, Austria): A proxy for Late Pleistocene to Holocene climate change. – *Geomorphology*, 131: 85–97.
- SANDERS, D. & PATZELT, G. (2011): Long-term accumulation rates of sub-aerial scree slopes: implications of numerical ages and field observations (abstr.). – *Geophysical Research Abstracts*, 13, EGU 2011–1612, 2011. EGU General Assembly, Vienna 2011.
- SCHMID, S. M., FÜGENSCHUH, B., KISSLING, E. & SCHUSTER, R. (2004): Tectonic map and overall architecture of the Alpine orogen. – *Elogiae geologicae Helvetiae*, 97: 93–117.
- SCHRÖTT, L., HUFSCHEIDT, G., HANKAMMER, M., HOFFMANN, T. & DIKAU, R. (2004): Spatial distribution of sediment storage types and quantification of valley fill deposits in an alpine basin, Reintal, Bavarian Alps, Germany. – *Geomorphology*, 55: 45–63.
- TUNNICLIFFE, J. F. & CHURCH, M. (2011): Scale variation of post-glacial sediment yield in Chilliwack Valley, British Columbia. – *Earth Surface Processes and Landforms*, 36: 229–243.
- VAN HUSEN, D. (1977): Zur Fazies und Stratigraphie der jungpleistozänen Ablagerungen im Trauntal. – *Jahrbuch der Geologischen Bundesanstalt*, 120: 1–130.
- VAN HUSEN, D. (1983): General sediment development in relation to the climatic changes during Würm in the eastern Alps. – In: EVENSON, E. B., SCHLÜCHTER, C. & RABASSA, J. (eds.): *Tills and Related Deposits*: 345–349; Rotterdam (Balkema).
- VAN HUSEN, D. (1987): Die Ostalpen in den Eiszeiten. – Geologische Bundesanstalt, Vienna: 24 S., 1 Karte.
- VAN HUSEN, D. (1997): LGM and Late glacial fluctuations in the Eastern Alps. – *Quaternary International*, 38/39: 109–118.
- VAN HUSEN, D. (2000): Geological Processes during the Quaternary. – *Mitteilungen der Österreichischen Geologischen Gesellschaft*, 92: 135–156.
- VAN HUSEN, D. (2004): Quaternary glaciations in Austria. – In: EHLERS, J. & GIBBARD, P. L. (eds.): *Quaternary Glaciations-Extent and Chronology*. – Developments in Quaternary Science 2: 1–13; Amsterdam (Elsevier).
- WOOD, J. R., FORMAN, S. L., PIERSON, J. & GOMEZ, J. (2010): New insights on Illinoian deglaciation from deposits of Glacial Lake Quincy, central Indiana. – *Quaternary Research*, 73: 374–384.

Rhine loess at Schwalbenberg II – MIS 4 and 3

Wolfgang Schirmer

How to cite: SCHIRMER, W. (2012): Rhine loess at Schwalbenberg II – MIS 4 and 3. – E&G Quaternary Science Journal, 61 (1): 32–47. DOI: 10.3285/eg.61.1.03

Abstract: The locality Schwalbenberg is situated in the Middle Rhine valley close to the town of Remagen. It exhibits a rather complete section of the Last Glacial loess with good tripartite subdivision of the Lower Pleniglacial (Keldach Formation, MIS 4) with one interstadial soil, excellent subdivision of the Middle Pleniglacial (Ahrgau Formation, MIS 3) with eight interstadial soils, and minor subdivision of the Upper Pleniglacial (Hesbaye and Brabant Formation). A first profile log, Schwalbenberg I, published earlier with organic carbon (Corg) and phosphorus curves, showed that the Middle Pleniglacial Schwalbenberg section represents an excellent mirror image of MIS 3 curves of ice and deep sea cores. This text presents a new profile log from a new wall, Schwalbenberg II, with tighter sampling (6 cm per sample). Grain-size and carbonate curves show the tripartition of smaller coarse silt content and carbonate content in the Keldach Formation, fluctuating coarse silt and carbonate in the Ahrgau Formation and enhanced coarse silt and carbonate in the Upper Pleniglacial. The nine interstadial soils (calcaric cambisols and one calcareous regosol) turn out to be autochthonous due to maxima of organic carbon, minima of carbonate and pedogenic top down intrasol zonation. All gelic gleysols show carbonate maxima. The Corg curve of Schwalbenberg II and $\delta^{18}\text{O}$ record of the annual-layer counted Greenland GISP 2 core show strikingly good correlation of rhythmicity and magnitude between the Ahrgau Formation and the Greenland interstadials 17 to 5. This correlation is widely confirmed by numerical dating of the Schwalbenberg II section. The boundary Ahrgau Formation/Hesbaye Formation (MIS 3/MIS 2) was drawn so far with the top of the uppermost cambisol (Sinzig 3 Soil). Lithological and chronological data speak for drawing the boundary somewhat higher at the Hesbaye Discordance. Consequently, the Schwalbenberg section misses the soil representing the GIS 5 interstadial. Nevertheless, it presents the most complete Ahrgau Formation (MIS 3) in western Europe. Loess profiles of the more continental region in the northeastern Carpathians or in Siberia are even richer in soils.

Rheinlöss von Schwalbenberg II – MIS 4 und 3

Kurzfassung: Die Lokalität Schwalbenberg bei Remagen am Mittelrhein erschließt ein sehr vollständiges Profil durch den letztglazialen Löss mit drei Großgliedern. Gut gegliedert sind der Löss der Keldach-Formation (Früh-Weichsel/Würm-Hochglazial, MIS 4) mit einem Interstadial-Boden und der Löss der Ahrgau-Formation (Mittelweichsel-/Würm-Interstadial-Komplex, MIS 3) mit acht Interstadial-Böden. Den Abschluss nach oben bildet weniger gut gliederbarer Löss des Jung-Weichsel/Würm-Hochglazials. Zu bereits veröffentlichten organischen Kohlenstoff (Corg)- und Phosphor-Kurven einer ersten Profilaufnahme, Schwalbenberg I, präsentiert dieser Text Daten des Profils Schwalbenberg II: AMS ^{14}C -Datierungen, Korngrößen, Corg- und Karbonatgehalt. Die Korngrößen spiegeln die Dreigliederung wider mit Grobsilt-ärmerem Keldach-Löss, schwankendem Siltgehalt im Ahrgau-Löss und Grobsilt-reicherem Jungwürmlöss. Auch im Karbonatgehalt spiegelt sie sich mit Karbonat-ärmerem Keldach-Löss, schwankenden Gehalten im Ahrgau-Löss und Karbonat-reicherem Jungwürmlöss. Die neun interstadialen Böden erweisen sich durch Corg-Gipfel und Karbonat-Minima vereinigt mit pedogener Zonierung bodenintern von oben nach unten als autochthone Böden. Alle Nassböden zeigen Karbonatmaxima. Der Vergleich der Corg-Kurve mit der der $\delta^{18}\text{O}$ -Kurve des jahrring-zonierten grönlandischen Eiskerns GISP 2 zeigt für die Ahrgau-Formation – wie früher schon die Kurven vom Schwalbenberg I – erneut nach Kurvenrhythmis und Magnitude hohe Gleichhäufigkeit des Klimaverlaufes zu den Grönland-Interstadialen 17 bis 5. Numerische Daten vom Schwalbenberg II unterstützen das weitgehend. Zur Frage, ob die Grenze Mittel-/Oberwürm (MIS 3/MIS 2) nach dem obersten braunen Boden (Sinzig 3-Boden) oder wenig höher mit der Hesbaye-Diskordanz zu ziehen ist, sprechen die meisten lithologischen und die chronologischen Kriterien für die Grenzziehung an der Hesbaye-Diskordanz. Ansonsten ist der Schwalbenberg unter den gut vergleichbaren Lössprofilen im westlichen Europa bisher das am detailliertesten gegliederte MIS 3-Profil. Reicher gegliedert sind nur Lössprofile des kontinentalen geprägten Raumes in der nordöstlichen Karpatenregion und in Sibirien.

Keywords: loess stratigraphy, grain size, TOC, carbonate

Address of author: W. Schirmer, Department of Geology, Heinrich Heine University Düsseldorf. Mailing address: 91320 Wolkenstein 24, Germany. E-Mail: schirmer@uni-duesseldorf.de

1 Introduction

Up to now the Schwalbenberg section exposed the most detailed loess stratigraphy of MIS 3 (Middle Würmian/Weichselian) in western Central Europe by a multiplicity of intercalated fossil soils. In 1989 the 13 m high loess section of the Schwalbenberg close to Remagen/Middle Rhine (Fig. 1) was sampled continuously by 99 samples later called

section Schwalbenberg I. (Continuous sampling means that the whole section – of here 13 m – is sampled from base to top without any gap between the single samples.) When Schwalbenberg I was analyzed, the enormous significance of the section became visible – a true mirror image of the Greenland ice curves during MIS 3 (SCHIRMER 1990a, 1991).

This gave rise to tighter sampling of this 13 m high loess section. When in 1991 the Schwalbenberg loess wall was

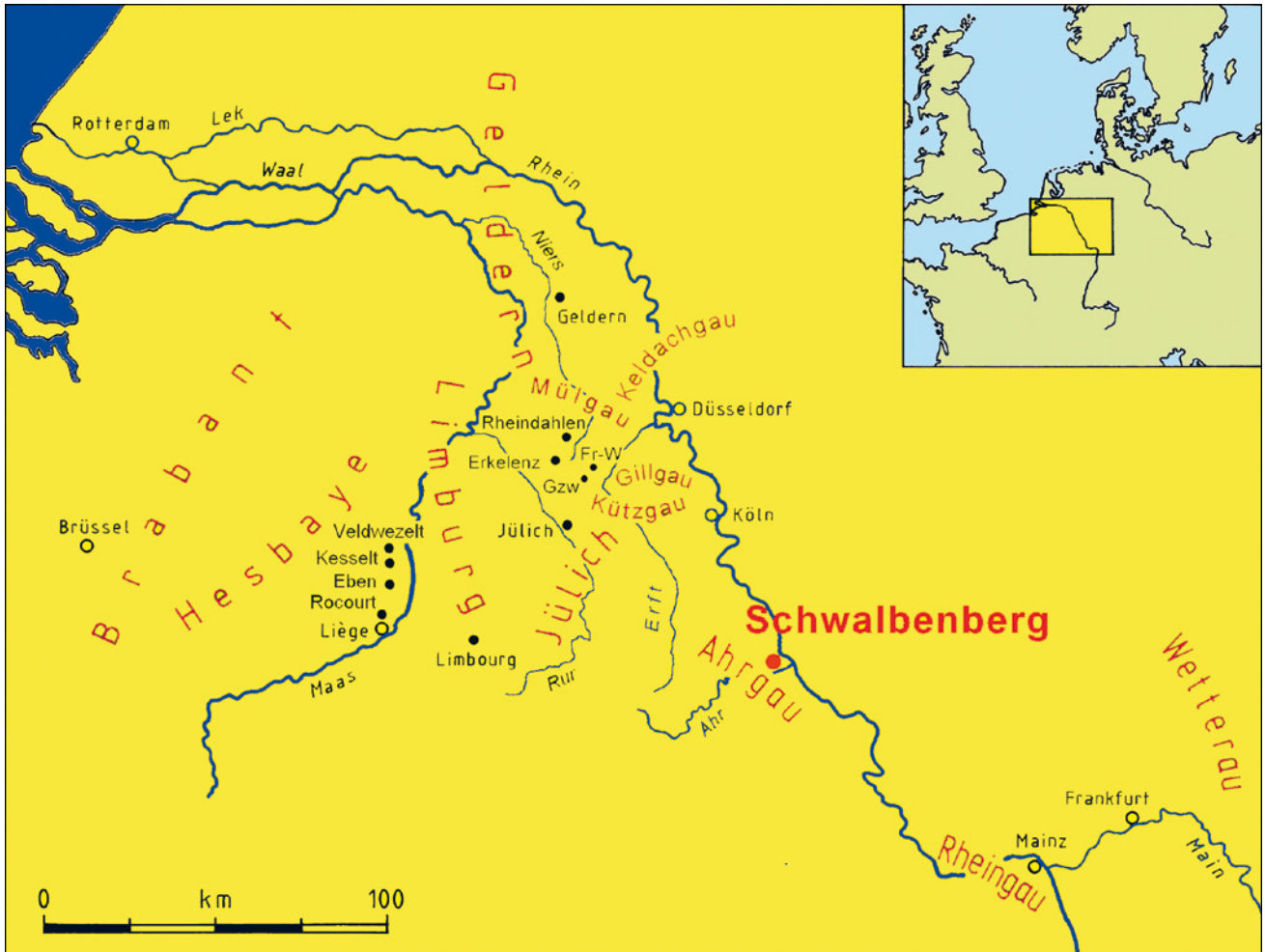


Fig. 1: Loess localities (black dots) at the Middle and Lower Rhine with the location of the Schwalbenberg section (Fr-W = Frimmersdorf-West, Gzw = Garzweiler).

Abb. 1: Löss-Lokalitäten (schwarze Punkte) am Mittel- und Niederrhein mit Lage des Schwalbenberg-Profs (Fr-W = Frimmersdorf-West, Gzw = Garzweiler).

exploited several meters backwards to enlarge a garden I took a new profile log with 216 continuous samples called Schwalbenberg II (Fig. 2). Thus, Schwalbenberg II is a newly logged section on a new wall some meters behind the wall of Schwalbenberg I.

This paper presents first proxy data of the Schwalbenberg II section in order to specify the proxy data for their comparison with other detailed MIS 3 records.

2 Location

The Schwalbenberg locality (R 258824, H 560356, 92 m a.s.l.) is situated within the Middle Rhine reach. Here, the Rhine pierces the Rhenish Shield (Rheinisches Schiefergebirge). As this shield has been rising especially since Pliocene, the Rhine had to cut in, forming a terrace staircase with the famous romantic Rhine gorge.

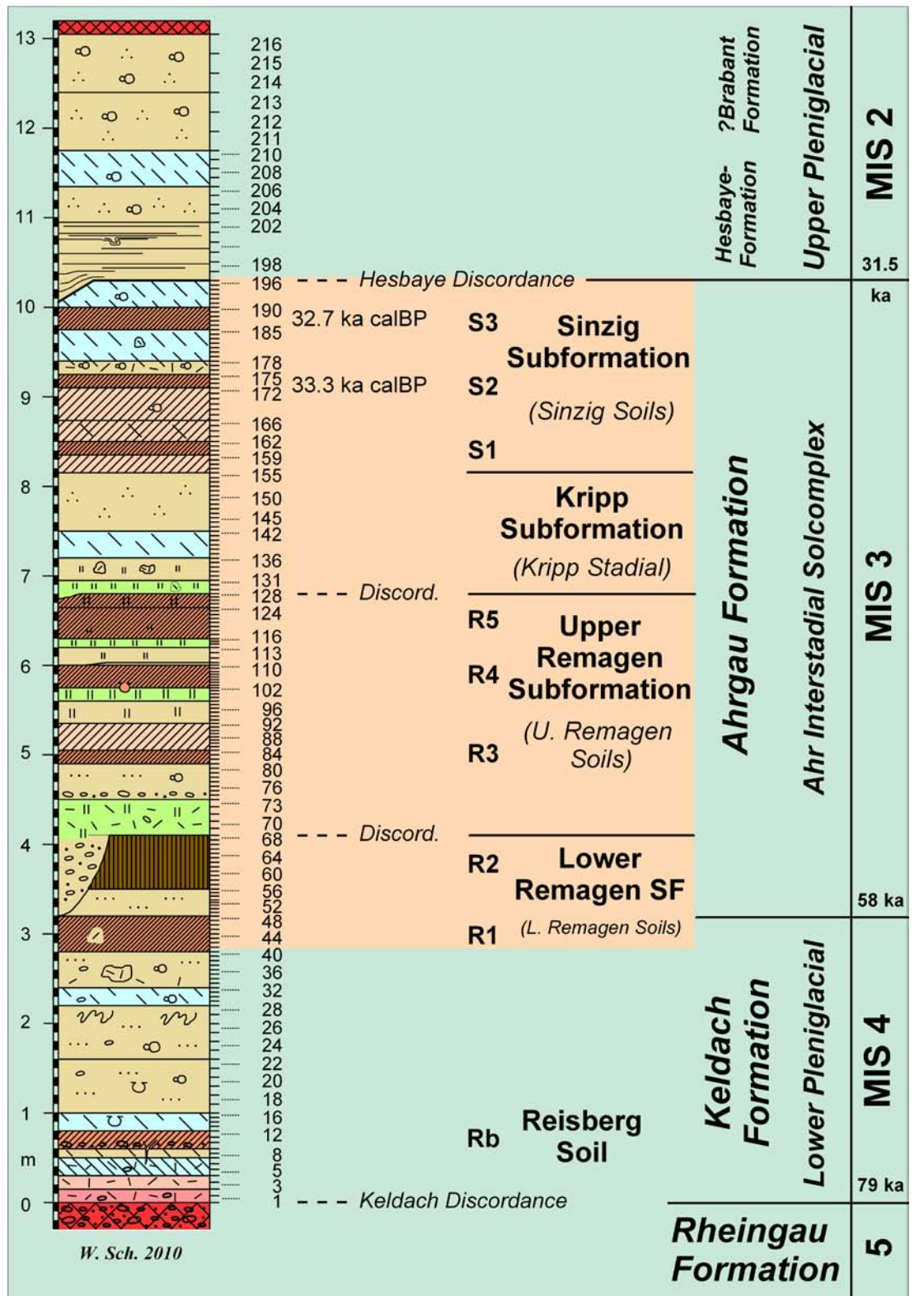
The Schwalbenberg lies on the western slope of this narrow entrenched valley at the northern corner of the mouth of a left tributary, the Ahr River (Fig. 1). The base of the loess profile lies 28 m above the Rhine river level on top of an eroded river terrace, the Lower Middle Terrace (Untere Mittelterrasse) that is attributed to the penultimate glaciation (SCHIRMER 1990a). The cliff embracing the gravel of the Lower Middle Terrace with the loess section on top joins

a 2 km wide flat plain, the so called Goldene Meile. This terrace plain represents the late Weichselian Low Terraces (Niederterrassen) and Holocene floodplain terraces at the junction of the rivers Rhine and Ahr (SCHIRMER 1990b). As the steep loess outcrop is part of a private garden, we had to plant the ledges of the cliff wall after the investigations; meanwhile the cliff is overgrown.

3 The Schwalbenberg II section – its litho-pedological composition and age

3.1 The Schwalbenberg II section and its stratigraphical frame

The profile Schwalbenberg II is drawn in Fig. 2 showing the exact position of samples 1–216 and the rough stratigraphic interpretation of the section that is explained in the sequel. The profile log is given in Tab. 1. A rough subdivision starts with a Bt horizon topping the basal gravel. It is regarded as the last interglacial soil that normally tops the Lower Middle Terrace (SCHIRMER 1990a). This soil is unconformably cut by the Keldach Discordance and overlain by a 13 m thick loess-soil sequence piling up to the recent surface. The loess-soil sequence is tripartite by a 3.2 m lower loess, preferably solifluidal, a some 7 m thick middle loess with



Legend

[Ah symbol]	Ah	humus	[Ckc symbol]	Ckc	loess dolls	[Nr symbol]	Nr	Grey Gelic Gleysol stronger/weaker	[Nr symbol]	elolian loess
[Bcv symbol]	Bcv	calcareous cambisol stronger/weaker	[Sd symbol]	Sd	pseudogley: bleached vertical streaks bounded by rust seams	[M symbol]	M	reworked soil sediment	[M symbol]	solifluidal loess/ laminated loess, colluvial loess
[Bt symbol]	Bt	luvisol: Bt horizon	[Ng symbol]	Ng	Speckled Gelic Gleysol	[crotovina symbol]		crotovina	[gravel symbol]	gravel

Fig. 2: Profile Schwalbenberg II with samples 1–216 and the stratigraphic interpretation of the section. The brown field marks the stretch of the MIS 3 interstadial soil formation. Its basal extension down into MIS 4 is due to the fact that the substratum of the R1 Soil belongs to MIS 4, whereas the soil formation correlates to MIS 3. SF = Subformation; ka after Greenland ice cores.

Abb. 2: Profil Schwalbenberg II mit den Proben 1–216 und stratigraphischer Interpretation. Das braune Feld kennzeichnet den Bereich der interstadialen Bodenbildung im MIS 3. Sein Übergreifen auf MIS 4 geschieht dadurch, dass das Substrat des R1-Bodens wohl MIS 4-zeitlich, die Bodenbildung aber MIS 3-zeitlich ist. SF = Subformation; ka gemäß Grönland-Eiskernen.

an eight-fold soil complex of mostly calcareous cambisols, and a scanty 3 m upper loess, preferably eolian loess.

The Lower Pleniglacial loess, the Keldach Formation, starts with the Keldach Discordance. The Keldach Discordance at the base of the Weichselian Lower Pleniglacial is a widespread phenomenon in central Europe cutting at many places the Rheingau Formation (MIS 5) with its Rocourt Solcomplex (SCHIRMER 2003: 49). The above following 3.2 m thick loess layer is correlated litho-pedo-stratigraphically with the Weichselian Lower Pleniglacial for the following reasons:

It is the widely distributed early loess between the Rocourt Solcomplex (MIS 5) and the soil complex of the Ahrgau Formation (MIS 3). The loess facies of this lower loess is throughout solifluidal loess, which is typical for the Keldach Formation (MIS 4) in whole central Europe. At its base occurs more or less reworked red or brown soil sediment, present here between profile meter 0–0.5; it is reworked soil material from the partly eroded Rheingau Formation that normally embraces four Bt horizons (SCHIRMER 2000a, b). The weak Reisberg cambisol fits well to two weak soils, the Jackerath and Spenrath Soil, which occur in the lower part of the Keldach Formation in the Lower Rhine basin (SCHIRMER 2002a: 19). Below and above the Reisberg Soil occur Grey Gelic Gleysols that likewise are typical for the Keldach Formation.

Thus, from facies, soils and its litho-pedo-stratigraphical position this basal loess unit is a typical representative of the Lower Pleniglacial (MIS 4). Nevertheless, bracketed by the Rocourt Solcomplex below and the Middle Pleniglacial brown soil cluster above, this thick loess unit would neither fit to the Rheingau Formation with its Bt horizon and humus zones nor to the Ahrgau Formation with its brown soils and mostly Speckled Gelic Gleysols.

The following Ahrgau Formation represents the typical brown soil bundle of the Middle Pleniglacial. This tight soil-loess sequence shows three soil groups, two Lower Remagen Soils, three Upper Remagen Soils and three Sinzig Soils. Each soil group is capped by a discordance and separated from the next group by a somewhat thicker loess layer. These two discordances at profile meter 4.1 and 6.8 effect incomplete soil sequences in several positions of the wall that make the investigation of the sheer cliff not easy (Fig. 3). The brown cambisols of the Ahrgau Formation are interbedding with gelic gleysols of two types, the rusty and grey Speckled Gelic Gleysol in the lower part and the homogeneously Grey Gelic Gleysol in the upper part.

In earlier publications it was shown that the eight-fold solcomplex of the Ahrgau Formation matches phenologically in details with MIS 3 in the Grand Pile section (Vosges), in ice cores (Dye 3, Camp Century, GRIP Summit) and deep-sea cores (DSDP-609, KET 8004). Therein it correlates to the Greenland interstadials GIS 17 to 6 thus forming an own interstadial complex, the Ahr interstadial complex, which is interbedded between the Weichselian Lower Pleniglacial loess and the Upper Pleniglacial loess (SCHIRMER 1995a: 513, 1995b: 531, 1999, 2000a, b, 2002a: 11, 19, 2002b: 318–319, 2004).

The upper boundary of the Ahrgau Formation, either drawn with the top-line of the uppermost brown soil, the Sinzig 3 Soil, or at the Hesbaye Discordance, is discussed below.



Fig. 3: Cliff of the Schwalbenberg II section. Gravel of the Lower Middle Terrace covered by a loess-soil sequence. Sampling by a mobile elevation work platform (cherry picker). Photo: W. Schirmer 30.04.1999.

Abb. 3: Kliff des Schwalbenberg II-Profil. Unten Schotter der Unteren Mittelterrasse, darüber Löss-Boden-Folge. Beprobung mit Hilfe einer Hubarbeitsbühne. Foto: W. Schirmer 30.04.1999.

The Upper Pleniglacial loess contains laminated colluvial loess in its lower part, eolian loess above it with one Grey Gelic Gleysol intercalated. The little subdivision of this 3 m thick loess unit does not allow its distribution to the Hesbaye and Brabant Formations.

3.2 datings from the Schwalbenberg II section

The litho-pedologic association of the Ahr Interstadial Solcomplex with MIS 3 is supported by the following chronological data:

In a neighboring section, some decades of meters nearby, a prehistoric excavation revealed a smaller soil sequence of cambisols. The uppermost soil of them was dated by ^{14}C of mollusks to $32,669 \pm 521$ a calBP CalPal (^{14}C : $28,100 \pm 530$ a BP, Pta-2721) and $32,487 \pm 430$ a cal BP CalPal (^{14}C : $27,900 \pm 440$ a BP, Pta-2722, both dates APP et al. 1995: 29) and by TL to 31.3 ± 2.6 ka (ZÖLLER et al. 1991: 409). A gelic gleysol quite above the cambisol had a TL age of 29.6 ± 2.7 ka (ZÖLLER et al. 1991: 409). The dated cambisol might match with the Sinzig 3 Soil of Schwalbenberg II; but it is not fully proved due to the short-distance changes of the strata sequence at the steep cliff and behind it. Therefore these data are not included in Fig. 2.

In the Schwalbenberg section II an AMS age from gastropods *Pupilla sterri* of the Sinzig 3 Soil yielded $32,653 \pm 377$ a calBP CalPal ($28,200 +300/-290$ ^{14}C a BP, KIA22209), and from the same gastropod species of the Sinzig 2 Soil $33,347 \pm 429$ a calBP CalPal ($28,860 +300/-290$ ^{14}C a BP, KIA22208). The agreement between the mollusk data of the Sinzig 3 Soil and that of the above mentioned section makes a correlation of both soils probable.

In the Schwalbenberg II section itself a set of 27 IRSL and TL datings gave ages of the Ahr Solcomplex between 45 and 25 ka (FRECHEN & SCHIRMER 2011: 85f.).

COFFLET (2005) finds a possible hint for the presence of the Laschamp Event by a relative low palaeointensity within the stretch of the Remagen 3-5 Soils and the following Kripp Stadial, resp. the stretch around GIS 12 to GIS 9. The worldwide Laschamp Event is settled at $40,700 \pm 950$ a before 2000 AD within GIS 10 (SINGER et al. 2009).

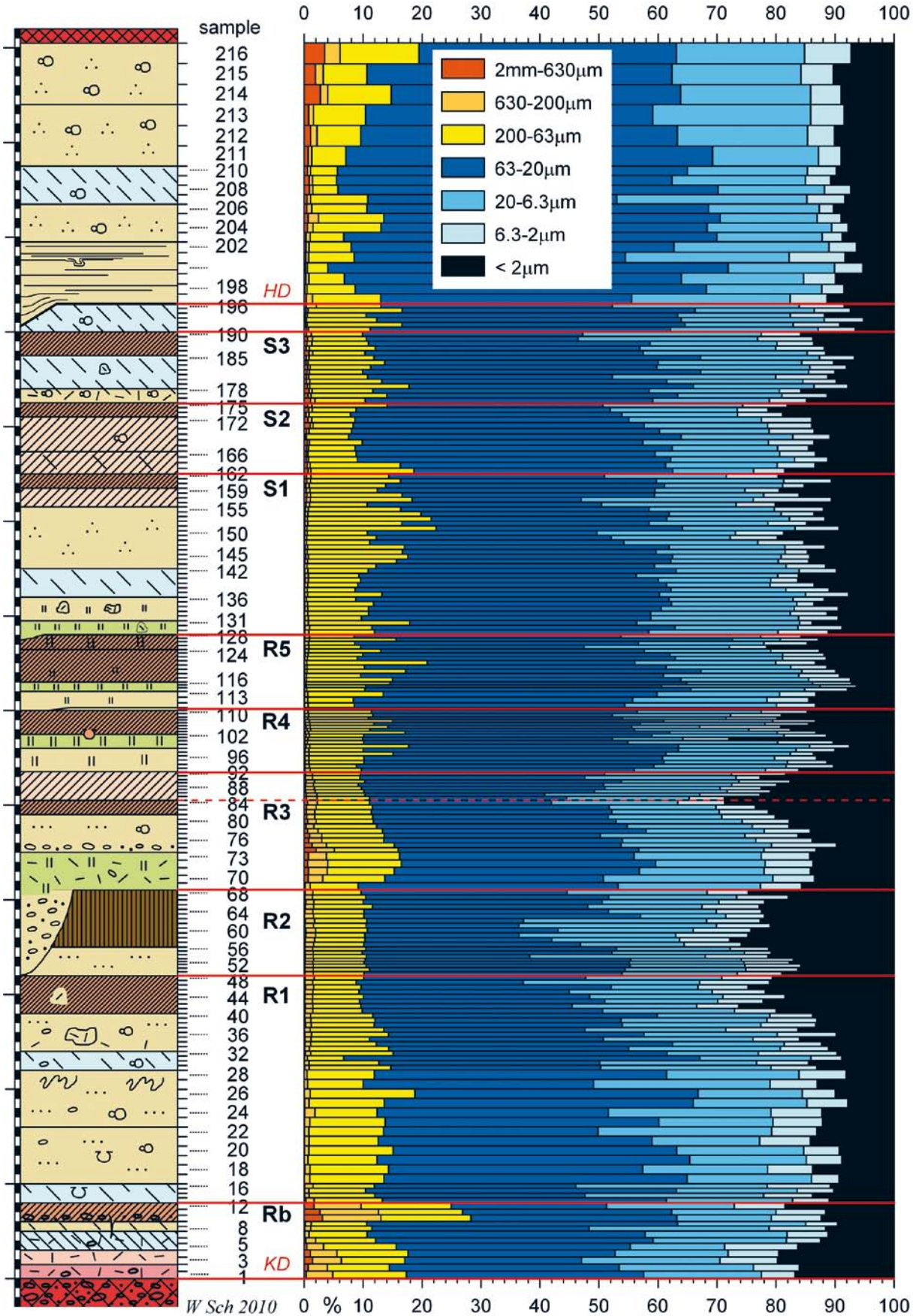
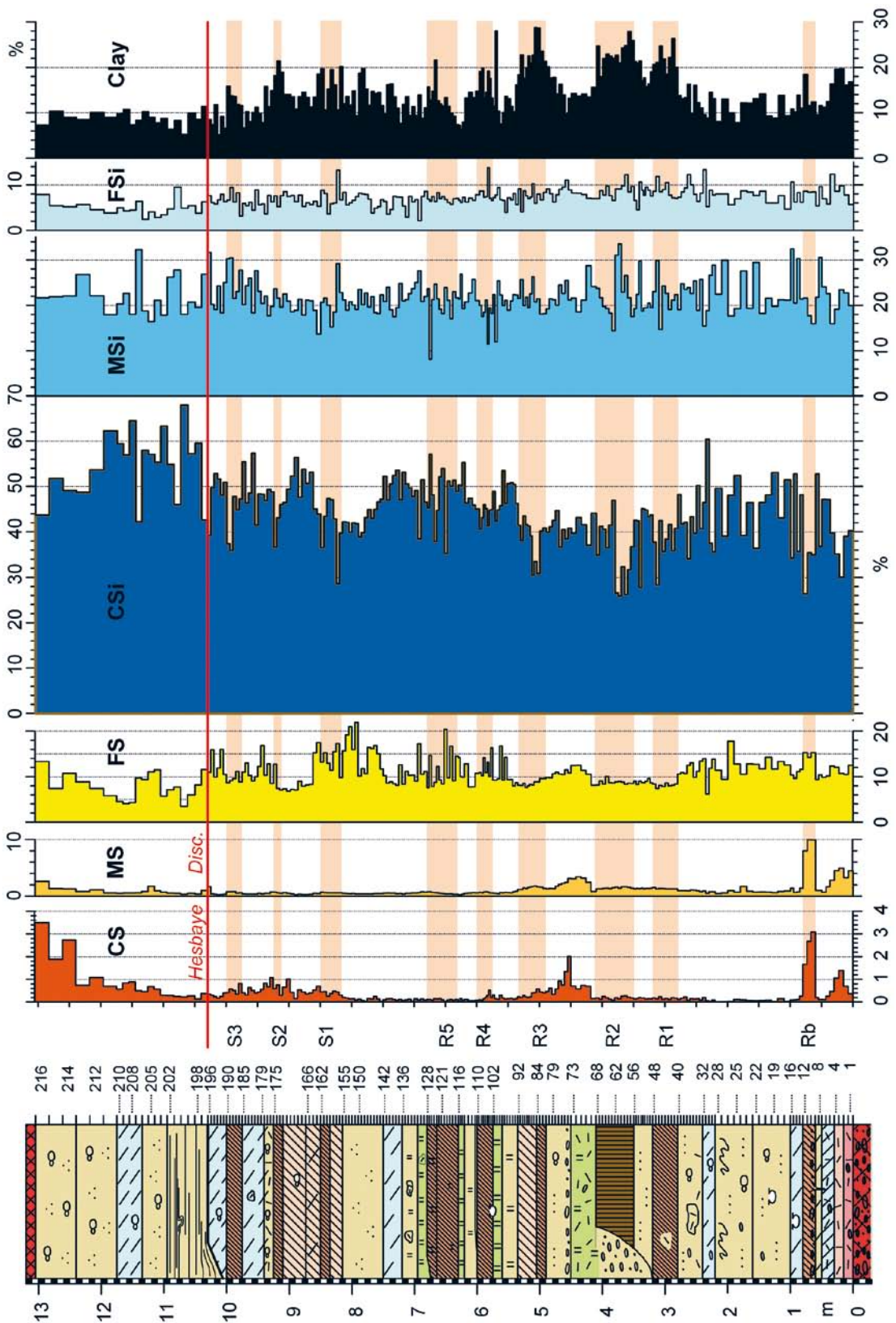


Fig. 4 Schwalbenberg II section with seven grain size fractions: 100% diagram. Red lines mark soil tops, the Hesbaye (HD) and Keldach Discordance (KD). Profile legend see Fig. 2.

Abb. 4 Profil Schwalbenberg II mit sieben Korngrößenfraktionen: 100%-Diagramm. Rote Linien kennzeichnen Bodenoberflächen und die Hesbaye- (HD) und Keldach-Diskordanz (KD), Profillegende in Abb. 2.



All datings confirm the phenological correlation of the Schwalbenberg section with long records from ice and deep sea.

The Keldach Formation within the Schwalbenberg II section was covered by 12 IRSL and TL datings, which gave ages between 55–45 ka (FRECHEN & SCHIRMER 2011). These ages contradict the assignment of the Keldach Formation to MIS 4 (see discussion in chapter 5).

4 Schwalbenberg II proxy-data and their discussion

The sampling of the Schwalbenberg II section was continuously, within the Ahrgau Formation (MIS 3) in vertical columns of 5 cm, sometimes even 3 cm, above and below the Ahrgau Formation mostly 10 cm. The heights of the sampled columns are depicted in Figs. 2 and 4–7. By sampling in vertical columns the analyse values represent the whole vertical stretch of one sampled column. Continuously sampled columns avoid gaps within the whole sedimentary record of the section.

This chapter presents the grain size analysis, organic carbon and carbonate content of the Schwalbenberg II. Paleomagnetic data are given in the PhD work of COFFLET (2005), first mollusk analyses in SCHIERMEYER (2000).

4.1 Grain size analysis

From clastic sediment < 2 mm Ø seven grain size fractions were measured: coarse sand 2 mm–630 µm, medium sand 630–200 µm, fine sand 200–63 µm, coarse silt 63–20 µm, medium silt 20–6.3 µm, fine silt 6.3–2 µm and clay < 2 µm. The whole sample was fractioned by gravity sedimentation using a fully automatic apparatus after WERNER (1973) that is pipetting the silt and clay. Subsequently the sand was wet-sieved. Pretreatment: 15.0 g of non-decalcified clastic sediment pre-dried with 80° C was peptized by Na₄P₂O₇·10 H₂O and vibromixed for 12 min.

The nine calcic cambisols resp. the regosol are each marked by clay peaks (Figs. 4 and 5). The maximum clay concentration lies within the Remagen 1–3 Soils. The clay peaks are descending from R3 to R5, which is important for the comparison with the Greenland interstadials. The Sinzig Soils show less clay formation, similar to R4–5. Among the Sinzig Soils the S2 shows the maximum clay peak as well as the maximum average clay volume.

Similar to the clay, the fine silt shows slight tendency towards increase in the soils. The medium silt is indifferent. Coarse silt retreats in the soils. It rises distinctly above the Ahrgau Formation. Fine sand retreats during the clay augmentation phases in R1–R3 and during coarse silt progression above the Ahrgau Formation.

Maxima of coarse, medium and fine sand at the base of the section between 0 and 1 m and between R2 and R3 Soils indicate enhanced sediment shift, obvious in the substratum of the Reisberg Soil, which is a solifluidal loam.

4.2 Organic carbon (Corg)

The organic Carbon content (TOC) was analysed with a Dimatec laboratory furnace by combustion at 480°. Pretreatment: The sediment < 2 mm Ø was pulverized and dried

with 80° C for 24 hours, again pulverized and dried with 105° for 2 hours.

The red Corg curve in Fig. 6 is a mean curve showing the arithmetic mean of the various analyses made from one sample. The curve shows 216 values from 459 single analyses.

All terrestrial soils are marked by maxima in Corg. Soil Remagen 3 (R3) shows the highest peak with about 0.5% Corg. The Upper Remagen Soils (R3–R5) show a descending peak sequence from older to younger soils, respectively from R3, the highest peak of the whole Ahrgau Formation, to R5, the lowest peak of this sequence. Likewise the Sinzig Soils (S1–S3) exhibit a descending peak sequence from older to younger soils, respectively from S1, the highest peak, to S3, the lowest peak. Additional Corg peaks occur in sample 2–6 presenting solifluiddally reworked soil material (M), and in sample 197 presenting colluvial loess and a possible hint for an eroded soil (see chapter 5).

The Corg levels of the Lower Pleniglacial and the Upper Pleniglacial loesses below and above the Ahrgau Formation are roughly the same. The Corg values of the cold periods in-between the Ahrgau soils exhibit a little bit higher values than the pleniglacial loesses.

4.3 Carbonate content

The sample < 2 mm Ø was analyzed with a Dimatec laboratory furnace by combustion at 1000° (TC). The carbonate content was calculated by subtraction of the combustion value at 400° (TC-TOC) and converting the C value to CaCO₃. Pretreatment: The sediment < 2 mm Ø was pulverized and dried with 80° C for 24 hours, again pulverized and dried with 105° for 2 hours.

All calcic cambisols and the regosol (brown bands behind the curve of Fig. 7) show minima of the carbonate content. In some cases the minimum lies in the soil top: Reisberg Soil (Rb), Remagen 1 Soil (R1) and Sinzig Soils S1 and S2. This indicates decalcification starting from the surface of the soils – perfect curves to give prove of the autochthony of the soils. Other cases show the minimum in the midst of the soils or somewhat below: soils R2–5. This points to a secondary carbonate infiltration from above. Moreover, decalcification of the soils causes maxima of the carbonate content at the soil base or below (downward lime illuviation), visible with R1 and R2. The maxima below the other cambisols coincide with gelic gleysols.

All in all, during soil formation all cambisols and the regosol underwent a certain decalcification process. In addition, all of them received a subsequent secondary carbonate infiltration from above. Whether they ever were completely decalcified remains unknown.

All gelic gleysols (the grey type as well as the speckled type) show maxima of the carbonate content. Peaks towards 30% occur in the gelic gleysols at samples no. 7, 112 and 140. The gelic gleysols represent thawing horizons on top of the permafrost with water stagnation. It is interesting that the terrestrial soils, cambisols and the regosol, always are topped by gelic gleysols, whether Grey or Speckled Gelic Gleysols. Hence, the cambisols work as aquiclude.

Average carbonate content of the whole Schwalbenberg section is 18.3%. Among the three subunits, Keldach loess,

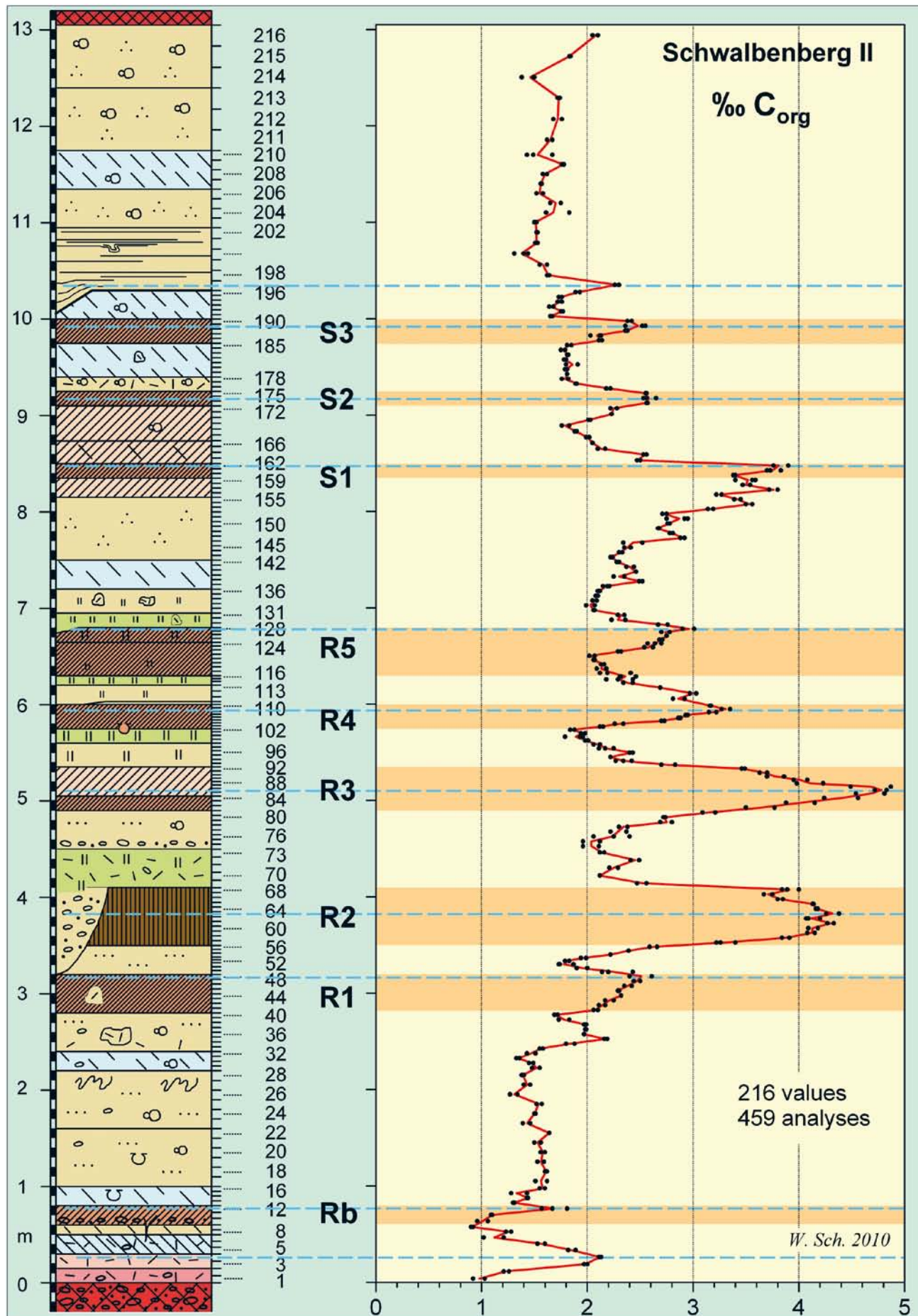


Fig. 6: Schwalbenberg II section with curve of the organic carbon. Profile legend see Fig. 2.

Abb. 6: Profil Schwalbenberg II mit Kurve des organischen Kohlenstoffs. Profillegende in Abb. 2.

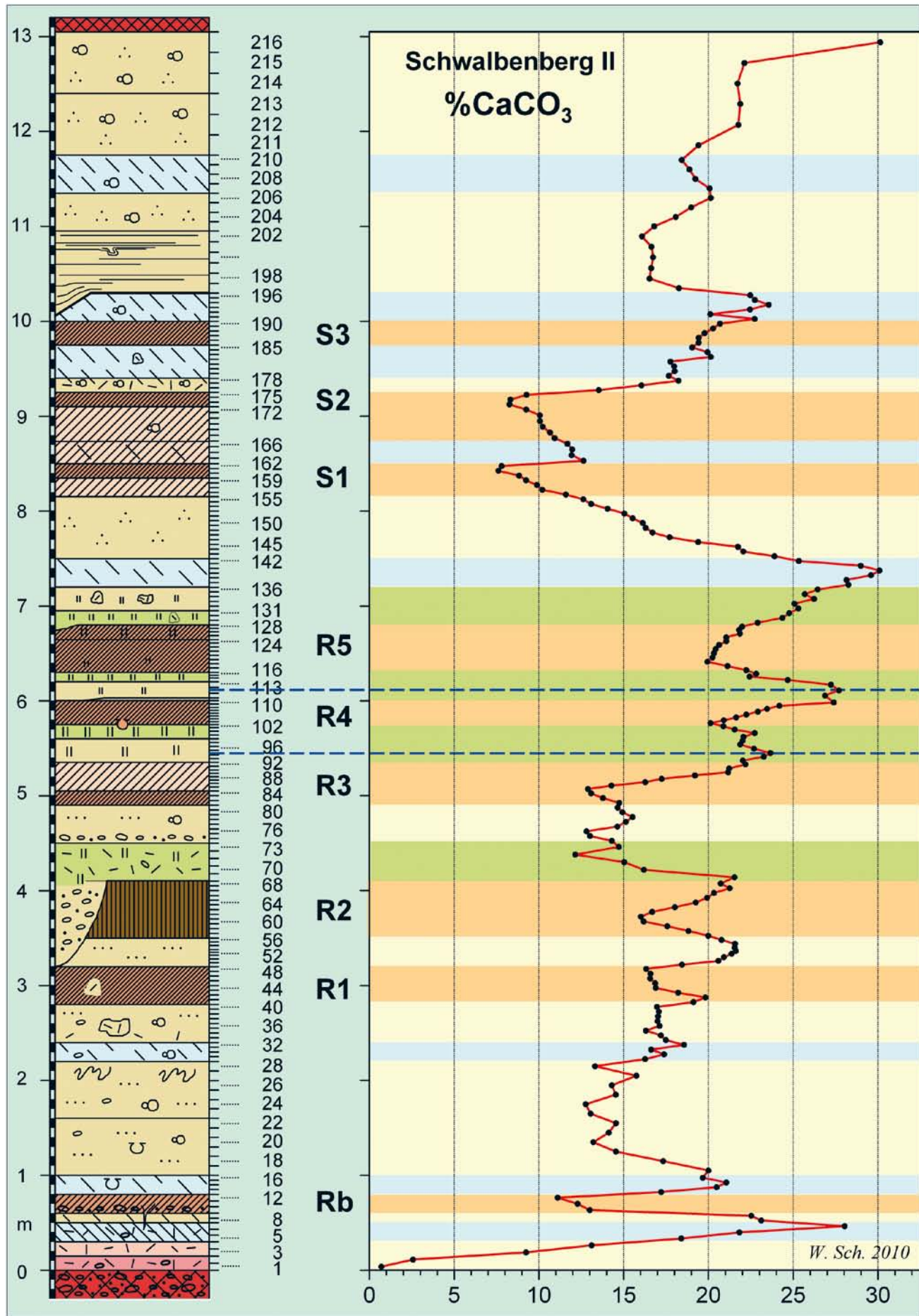


Fig. 7: Schwalbenberg II section with curve of the carbonate content. Profile legend see Fig. 2.

Abb. 7: Profil Schwalbenberg II mit Karbonat-Kurve. Profillegende in Abb. 2.

Ahrgau loess and Late Weichselian loess (Hesbaye and Brabant loess), the Keldach loess (samples no. 4–39) has the lowest average carbonate content (16.9%), the Upper Pleniglacial loess (samples no. 197–215) the highest (18.9%). The Ahrgau loess (samples no. 40–196) with its strongly varying carbonate curve has an average carbonate content of 18.8%. The lower values of the Keldach loess (Lower Pleniglacial loess) in comparison to the higher values of the Upper Pleniglacial loess is a widespread phenomenon in central Europe: see for example measurements of the Middle Rhine (BOENIGK et al. 1994), Upper Rhine (BIBUS et al. 2007: 238) and Bavaria (BRUNNACKER 1957).

5 Results and discussion

The Schwalbenberg II section is tripartite into the Weichselian Lower Pleniglacial Keldach Formation, the Middle Pleniglacial Ahrgau Formation and the Upper Pleniglacial Hesbaye and Brabant Formations.

5.1 Keldach Formation

It starts with a strong unconformity, the wide-spread Keldach Discordance, cutting and reworking a great deal of the Rheingau Formation below. Reworked soil material is present from profile meter 0–0.5 (samples 1–7). Analytically this is reflected by sand input (Fig. 4–5) and augmentation of organic carbon (Fig. 6). Additional input of fresh loess material is indicated by silt (Fig. 4) and carbonate increase (Fig. 7). This solifluction layer at the base of the Keldach Formation is well known from central Europe and supplied with local names as „Basisfließerde“ (BRUNNACKER 1954) (i. e. basal solifluidal loam), „Niedervellmar-Bodenkomplex“ (ROHDENBURG & MEYER 1966) and as „Niedereschbach-Zone“ (SEMMLER 1968).

The lower Keldach Formation is characterized by the interstadial brown Reisberg Soil. It has been formed on a solifluidal layer (sand increase in Fig. 4). The soil turns out to be autochthonous owing to a Corg peak (Fig. 4) and carbonate minimum (Fig. 7) in its very top.

In the most complete stratigraphy of the Keldach Formation on the Lower Rhine there occur two terrestrial soils, the Jackerath Soil (regosol–cambisol) and the Spenrath Soil (regosol) (SCHIRMER 2002a: 19). One of them should match with the Reisberg Soil of the Schwalbenberg section. Both soils might correlate with the Greenland Interstadials 19 and 20 (Fig. 7). These weak terrestrial soils are marker horizons for the lower part of the Keldach Formation.

Further criteria for the Keldach Formation in the Schwalbenberg section are prevalence of solifluidal loess with silt clods and crotovinas (Fig. 2), typical features for this formation in whole central Europe. Further characteristics are coarse silt prevalence of the grain size curve (Fig. 5), low values of the organic carbon curve (Fig. 6) and carbonate curve (Fig. 7). As typical marker horizons within the Keldach Formation, Grey Gelic Gleysols occur (SCHIRMER 2002a: 19).

Whereas all these criteria of the Keldach Formation are typical for the Lower Pleniglacial (MIS 4) in central Europe, the TL and IRSL dates for the Keldach Formation show ages between 55–45 ka (FRECHEN & SCHIRMER 2011) that do not match to MIS 4. Rather they would match to MIS 3.

From litho-pedological aspect it would be paradoxical to add this soil-poor loess section to the typical soil-rich Ahrgau Formation (MIS 3). The common separation of MIS 4 and MIS 3 is based on the delimitation of the cooler MIS 4 and the striking cluster of warmer and cooler spikes of MIS 3. In the terrestrial environment this is realized by MIS 4 loess against the cluster of brown soils in MIS 3. Thus, from litho-pedological view the mentioned TL/IRSL data of this part are too young. Hints for a tendency being too young give already the numerical ages in the top of the Ahrgau Formation (MIS 3). In the Sinzig 3 soil ^{14}C ages of 32.7 ± 0.4 ka calBP (Fig. 2) contrast with an IRSL/REGEN age of 24.6 ± 2.2 (FRECHEN & SCHIRMER 2011, Fig. 5). In the top of the Keldach Formation the IRSL/REGEN age no. 11 of 44.9 ± 3.7 ka was fading-corrected to 53.9 ± 4.7 ka (FRECHEN & SCHIRMER 2011, Fig. 5). The upper value of this age range, 53.9 ± 4.7 , would match excellently with the Upper boundary of MIS 4 of 58 ka calBP. It shows up: There is latitude enough to move these IRSL dates.

5.2 Ahrgau Formation

The Ahrgau Formation contains eight fossil interstadial soils, seven cambisols and one regosol. It stands to reason that the top of all fossil soils is more or less truncated – as it is generally valid for nearly all fossil soils.

Autochthony of the soils

The Corg maximum of the single interstadial soils occurs towards the top of the soils in case of the Remagen 1 (R1), R 4, R5, Sinzig 1 (S1), S2 and S3 Soils (blue dashed lines in Fig. 6). It designates these soils as autochthonous soils with soil formation from their top downwards. Only in the case of the Remagen 2 and 3 Soils the Corg maximum appears in the midst of the soils. This may be due to a ongoing soil formation process accompanied by weak sedimentation after the peak of the soil formation with quiescence of sedimentation. In case of R3 this interpretation is visible in the profile by a weakening of the soil characters in the upper part of the soil. Consequently, all peaks with maxima at the top or in the midst of the soils show that the soils represent autochthonous soils and not reworked soil material. As the multiplicity of cambisols within the Ahrgau Formation of Schwalbenberg II contrasts to other loess sections in central Europe, the question arose whether some soils could be reworked soil material. In the case of reworked soil material the Corg peaks would not appear thus well developed and should occur in all positions of the visible soil material especially close to the base of the soil bands.

Another indicator for autochthony of the soils is the de-calcification minimum at the soil top of the Remagen 1 Soil, Sinzig 1 and 2 Soils (Fig. 7; see discussion in chapter 4.3).

Age of the soils

The MIS 3 age of the Ahrgau Formation is assured by numerical datings: AMS ^{14}C ages from loess gastropods, TL and IRSL data from all horizons (FRECHEN & SCHIRMER 2011) though they are somewhat too young (see above in chapter 5.1). However, even more convincing is the phenological comparison of the litho-pedological profile and the Corg curve of the Schwalbenberg II section with Green-

land ice cores (Fig. 8) or deep-sea cores (SCHIRMER 2000a,b).

In Fig. 8 the organic carbon curve is compared with the $\delta^{18}\text{O}$ record of the annual-layer counted Greenland GISP 2 core. The $\delta^{18}\text{O}$ curve is arranged along the core depth and not along the time scale. It shows that in both, the loess section and the ice core, the sediment thickness per time is increasing upward.

The striking facts of matching with the Greenland ice cores and deep sea cores are the four Bond cycles represented by the soils R1, R2, R3-5, S1-3. In addition, in both records the Schwalbenberg and the Greenland ice cores, the widest cold gap (Kripp Stadial) lies between the third and the forth cycle. This gap is wider than the gaps between the individual peaks within the sequences. Initially, this gap was the reason for separating the Remagen Soil group from the Sinzig Soil group. A further conspicuous parallelism are the upward descending maxima spikes of the asymmetrically saw-tooth shaped peak lines of the Upper Remagen Soils (R3-5) resp. GIS 12-10, and that of the Sinzig Soils (S1-3) resp. GIS 8-6 (Fig. 7). These upward descending forms – rapid warming and long cooling – were first described by Bond et al. (1993). Consequently, R1 corresponds to the GIS group 17-16, R2 to GIS 15-14, R3 to GIS 12, R4 to GIS 11, R5 to GIS 10, S1 to GIS 8, S2 to GIS 7, S3 to GIS 6.

Moreover, Fig. 8 shows, that the highest peaks of the two curves, the Corg curve of the Schwalbenberg and the $\delta^{18}\text{O}$ curve of the GISP 2, occur in both corresponding spikes: R2 respectively GIS 14, and R3 respectively GIS 12.

Thus, shape and internal structure of the Corg curve of the Ahrgau Formation at Schwalbenberg is nearly the same than that in ice cores and marine cores. So much phenologic agreement of the Corg curve and the GISP 2 curve, together with the chronological data, leaves nearly no doubt that this loess section matches to MIS 3.

Above the Sinzig Soils there is a further Corg peak at sample 197 (Fig. 6). It is the base of a colluvial loess layer with sharp bedding planes. The colluvial loess might have reworked any soil from the Ahr Solcomplex in the hinterland. But it is also conceivable that it had reworked a theoretical Sinzig 4 Soil (S4). Looking at the Greenland interstadial group 8–5 in Fig. 8 there are 4 interstadials, the peaks of which form an upward descending range. The same picture is given in the Corg curve of the Schwalbenberg. Yet, this is a mere phenomenon and discussed below in item 5.3.

5.3 The boundary Ahrgau Formation/Hesbaye Formation

In all terrestrial investigations on the Last Glacial the upper limit of the warmer middle part of the Last Glacial (MIS 3), characterized by a cluster of interstadial soils or deposits, is drawn with the top-line of the uppermost interstadial soil or deposit. Consequently, the first (loess) bed above this interstadial soil or layer represents the beginning of the Upper Pleniglacial period (MIS 2).

Accordingly, in all former papers concerning the Schwalbenberg section, I drew the upper limit of the Ahrgau Formation at the top-line of the youngest brown soil, which is the Sinzig 3 Soil. In the Schwalbenberg section this soil is overlain by a 30 cm thick weak Grey Gelic Gleysol, which again is unconformably cut off towards the Rhine valley

by a laminated colluvial silt. The unconformable cut-off is the Hesbaye Discordance (see Fig. 2) that widely occurs at the base of the Hesbaye Formation (SCHIRMER 2003: 49) respectively at the base of the Upper Pleniglacial loess (ROHDENBURG 1968). This discordance can produce very deep erosion, sometimes down to the Rocourt Solcomplex (MIS 5) (SEMMEL 1968: 42) or deeper (SEMMEL & STÄBLEIN 1971: 26).

Thus, the Schwalbenberg section offers the possibility to draw the boundary Ahrgau/Hesbaye Formation with the Hesbaye Discordance, thus 30 cm higher than the first version. This higher situated boundary is favored by the following facts:

- In ice and deep sea curves the Bond cycle GIS 8–6 consists of four warm peaks. However, in the Schwalbenberg section only three warm peaks are present. Thus, the question arises whether the Schwalbenberg equivalent for GIS 5, the fourth warm peak, was eroded by the Hesbaye Discordance (Fig. 2). In case of its erosion, the Grey Gelic Gleysol above the Sinzig 3 Soil would belong to the Ahrgau Formation, and the following Hesbaye Discordance would indicate the beginning of the Hesbaye Formation.

- Hints for this version are given by the lithological data of the 30 cm Grey Gelic Gleysol above the Sinzig 3 Soil. This layer tends to fit more to the Ahrgau loess than to the Hesbaye loess: The grain sizes of fine silt, coarse silt and fine sand and the Corg values continue the trend of the Ahrgau loess. The lithologic break to the Hesbaye loess starts with the Hesbaye Discordance: lower values of Corg (Fig. 6), lower values of fine silt and fine sand, and higher values of coarse silt (Fig. 5).

- Moreover, there is a Corg peak at the very base of the colluvial loess overlaying the Hesbaye Discordance (Fig. 6). This peak may represent reworked Corg content of the Sinzig 4 Soil. The possible erosion of a Sinzig 4 Soil is shown in Fig. 9. However, likewise this peak may represent the Corg content of any soil that was eroded uphill by the reworking phase.

- However, there is a certain probability for the age of the Sinzig 3 Soil (S3) to match with the GIS 6 Interstadial: The AMS ^{14}C age of the S3, 28.200 +300/-290 (see item 3.2), may be corrected after NotCal04 (VAN DER PLICHT et al. 2004) to around 33–33.5 ka calBP, or 32.3–33 a calBP CalPal corresponding to GIS 6 in the GISP2 core (GROOTES & STUTVER 1997).

- Moreover, the comparison with the well-dated north-eastern Carpathian loess sections of Molodova (Ukraine) and Mitoc-Malu Galben (Romania) as well with the Siberian locality Kurtak (HAESAERTS 2003, 2009) shows that the interstadial soils referring to GIS 6 have uncalibrated ^{14}C ages gained mostly from charcoal of about 28.5 ka BP – well fitting to the Sinzig 3 age. In contrast, the ^{14}C ages of soils referring to GIS 5 are 27.5–27.7 ka BP, distinctly younger than the Sinzig 3 age of Schwalbenberg II. The ^{14}C ages of soils referring to GIS 7 have ages of 30–30.4 ka BP, evidently older than the Sinzig 3 age, rather fitting to the Sinzig 2 age of 28.860 +300/-290 ka BP.

The closest loess equivalent with good subdivision of the MIS 3/MIS 2 transition is the Nussloch section on the Upper Rhine (BIBUS et al. 2007, ANTOINE et al. 2009). The uppermost brown soil in the profiles of ANTOINE et al. (2009) is indicated as Lohne Soil, after its datings correlating to

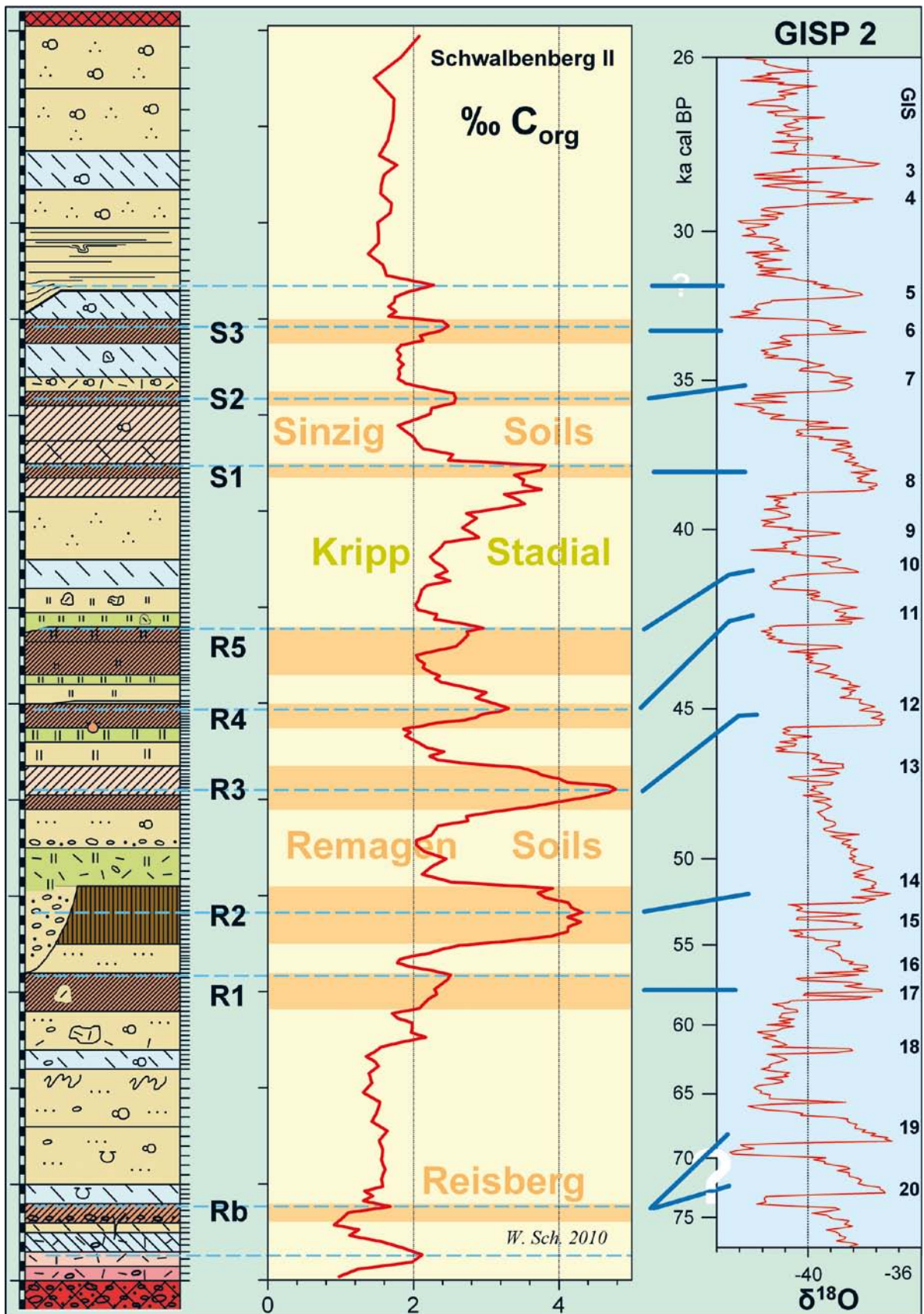


Fig. 8: Schwalbenberg II section and mean organic carbon curve of Schwalbenberg II, compared with the $\delta^{18}\text{O}$ curve of the Greenland ice core GISP 2 (GROOTES & STUIVER 1997). In the GISP 2 diagram the vertical scale (not drawn) is the ice core depth from meter 1997 down to 2640. Added is the non-linear time scale. Legend for the litho-pedo column see Fig. 2. GIS = Greenland Interstadial, Rb = Reisberg Soil, R = Remagen Soil, S = Sinzig Soil. Profile legend see Fig. 2.

Abb. 8: Profil Schwalbenberg II und Corg-Mittelkurve des Schwalbenbergs II, verglichen mit der $\delta^{18}\text{O}$ -Kurve des grönlandischen Eiskerns GISP 2 (GROOTES & STUIVER 1997). Die Vertikalskala im GISP 2-Diagramm fußt auf der Eiskerntiefe von Meter 1997 bis 2640 (nicht beschriftet); beschriftet ist die nicht-lineare Zeitskala. Legende der Litho-pedo-Säule in Abb. 2. GIS = Grönland-Interstadial, Rb = Reisberg-Boden, R = Remagen-Boden, S = Sinzig-Boden. Profillegende in Abb. 2.

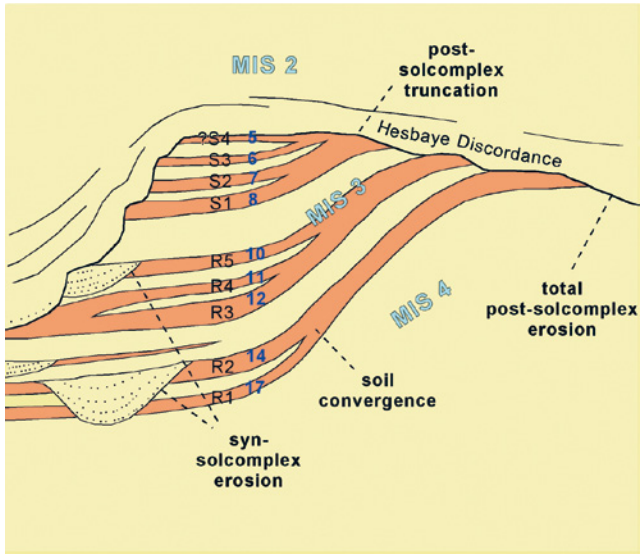


Fig. 9: Scheme of diminution of the Ahr interstadial solcomplex (MIS 3) by convergence, syn-solcomplex erosion and post-solcomplex erosion of soils. The scheme shows the solcomplex sandwiched between the Keldach Formation and the Hesbaye Formation. HD = Hesbaye Discordance, MIS = Marine Isotope Stage, R1-R5 = Remagen Soils, S1-S4 = Sinzig Soils, blue numbers 5-17 = affiliation to Greenland Interstadials 5-17. The loesses of the Keldach Formation (MIS 4) below and the Hesbaye Formation (MIS 2) on top of the Ahrgau Formation (MIS 3) are not shown differentiated (modified after SCHIRMER 2010: 34).

Abb. 9: Schema der Verminderung des Ahr-Interstadial-Solkomplexes (MIS 3) durch Konvergenz, Syn-Solkomplex-Erosion und Post-Solkomplex-Erosion von Böden. Das Schema zeigt den Solkomplex zwischen der Keldach- (MIS 4) und Hesbaye-Formation (MIS 2) gelegen, die in sich nicht mehr weiter untergliedert dargestellt sind. HD = Hesbaye Diskordanz, MIS = Marines Isotopen-Stadium, R1-R5 = Remagen Böden, S1-S4 = Sinzig-Böden, blaue Zahlen 5-17 = Verknüpfung mit den Grönland-Interstadialen 5-17 (verändert nach SCHIRMER 2010: 34).

GIS 7. Thus, it would correspond to S2 of the Schwalbenberg. Above it in Nussloch ANTOINE et al. (2009) only note gelic gleysols.

Consequently, the Sinzig 3 Soil should represent the warm phase of GIS 6. In this case the Hesbaye Discordance has cut the top part of the Ahrgau Formation. The 30 cm thick Grey Gelic Gleysol is constituent of the Ahrgau Formation and the expected Sinzig 4 Soil may appear in the reworked Corg peak at the base of the Hesbaye loess represented by the colluvial silt layer.

5.4 Hesbaye and Brabant Formations

The Hesbaye Formation starts with the Hesbaye Discordance. Within the 3 m thick loess between the Hesbaye Discordance and the surface there is only one Grey Gelic Gleysol developed. The Hesbaye Formation normally hosts up to three Grey Gelic Gleysols, the Erbenheim 1-3 Soils (SCHÖNHALS et al. 1964). Owing to the incomplete development of the Upper Pleniglacial section neither it is possible to assign this gleysol to a distinct one of the Erbenheim Soils nor it is known whether the uppermost loess contains shares of the Brabant Formation. Sand augmentation in the uppermost part of the section (samples 214-216, Fig. 3) is due to eolian sand accompanying the silt of the loess.

Up to now in the descriptions of the Hesbaye Formation

nowhere in central Europe a hint of a brown or humus soil is given that could represent an equivalent of the warming peaks GIS 3 and 4 around 28-29 ka cal BP.

6 Conclusion

A terrestrial equivalent of the marine and inland ice MIS 3 was exposed at the Schwalbenberg on the left slope of the River Rhine close to Remagen. The stadial phases are represented by loess layers, interstadial phases by eight fossil terrestrie soils, seven cambisols and one regosol. Compared with ice cores – in this paper the $\delta^{18}\text{O}$ curve of the annual-layer counted GISP 2 core – and deep sea cores it turns out that the Schwalbenberg section shows the Ahrgau Formation (MIS 3) in its most complete preservation in western central Europe. A striking phenomenon remains that this formation in most loess sections of central Europe appears more or less reduced, sometimes reduced down to one cambisol only. A possible answer for this phenomenon is given in SCHIRMER (2010: 38): The diminution of soils within the Ahr Solcomplex occurs by convergence of soils, due to thinning of loess deposition between soil formation (Fig. 9), by erosional activity of soils during the cold phases between the interstadials (syn-solcomplex truncation) and also by erosional activity after completion of the Ahr Solcomplex (post-solcomplex truncation of parts or the whole solcomplex).

Thus, elsewhere in central Europe there are three soils, two soils or even only one soil preserved. In cases of one preserved soil it remains questionable which soil of the eight-membered solcomplex has been preserved at the place described, and whether this one soil is always the same soil among the variety of members of the whole solcomplex. The strongest interstadials of the Schwalbenberg section are Remagen 1, Remagen 2 and Remagen 3 concerning the clay formation (Fig. 5). Concerning the amount of Corg, Remagen 2, Remagen 3 and Sinzig 1 are dominant (Fig. 8). The warmest interstadials in the ice cores (Fig. 8) are GIS 17+16 (corresponding to Remagen 1), GIS 14 (corresponding to Remagen 2), GIS 12 (corresponding to Remagen 3) and GIS 8 (corresponding to Sinzig 1) – even here appears conformity between Schwalbenberg and ice core. Consequently, the warmer part of MIS 3 is not the uppermost part, rather the lower section. Therefore, regarding the probability of preservation of the fossil soils from erosion this lower section is favored.

As shown in this paper it turns out that even the soil-rich Schwalbenberg section is not complete. The equivalent of the GIS 5 interstadial seems to be eroded by the Hesbaye Discordance – the case of post-solcomplex truncation (as shown in Fig. 9). On the other hand, there exist sections of the Ahrgau Formation presenting a more detailed stratigraphy than that of the Schwalbenberg, for example the sections Molodova (Ukraine) and Mitoc-Malu Galben (Romania) as well as the Siberian locality Kurtak (HAESAERTS et al. 2003, 2009). Thus, the more continental areas of Eurasia seem to be less affected by erosional processes causing syn-solcomplex or post-solcomplex mutilations. Regarding the Schwalbenberg in this light, its plentiful configuration of members seems to be a happy coincidence for the western part of central Europe.

Tab. 1: Profile log Schwalbenberg II.

Tab. 1: Profilbeschreibung Schwalbenberg II.

The pedologic abbreviations follow the German pedological soil labeling (AG Boden 2005). In addition, letter M is used for reworked soils or soil sediment, letter N stands for Nassboden (gelic gleysol), N' means weak gelic gleysol and N'' means very weak gelic gleysol. The number behind a soil horizon gives its thickness in cm. Following numbers in brackets are the soil samples (see Fig. 2).

Surface

BtM up to 1.5 m Bt horizon, slightly reworked: Loam, silty, reddish brown, non-carbonaceous

Ckc 65 cm [samples 216–214] Loess: Loam, silty, light yellow-brown, carbonaceous, numerous loess dolls

Ckc 65 [213–211] Loess: Loam, silty, light grey-yellow, carbonaceous, copious loess dolls

CkcfNr'' 40 [210–207] Weak Grey Gelic Gleysol: Loam, silty, light grey-yellow, slightly grey streaked, very weak rusty streaks, carbonaceous, loess dolls

Ckc 40 [206–203] Loess: Loam, silty, light grey-yellow, carbonaceous, loess dolls

C 65 [202–197] Colluvial loess: Loam, silty, light brown-yellow and light grey-yellow banded, carbonaceous, small cryoturbations; towards east downcutting into the underlying gelic gleysol

Erosional discordance

fNr' 30 [196–191] Weak Grey Gelic Gleysol: Loam, silty, light brown-grey, very few rusty speckles, carbonaceous, little carbonate pseudo-mycelia, few small loess dolls, small Fe-Mn-concretions

fBcv 25 [190–186] Weak calcic cambisol [*Sinzig 3 Soil*]: Loam, silty, brown, carbonaceous, carbonate pseudo-mycelia, worm dike internal casts [-4 mm Ø], Fe-Mn-coated root tracks, coherent structure, burrows up to 1 cm Ø and 15 cm depth

fNr 35 [185–179] Weak Grey Gelic Gleysol: Loam, silty, light brown-grey, carbonaceous, some loess dolls, very few carbonate pseudo-mycelia, worm dike casts [-4 mm Ø], Fe-Mn-coated root tracks, some clods of reworked brown soil material up to 10 cm Ø

Nr+BM 15 [178–176] Weak Grey Gelic Gleysol: Loam, silty, light brown-grey, carbonaceous, some loess dolls, very few carbonate pseudo-mycelia, worm dike casts [-4 mm Ø], Fe-Mn-coated root tracks, rich in reworked brown soil material of the underlying bed, loess doll layer at the top

fBcv1 15 [175–173] Calcic cambisol [*Sinzig 2 Soil*]: Loam, silty, slightly clayey, brown, carbonaceous, few carbonate pseudo-mycelia, some loess dolls, worm dike internal casts [2–4 mm Ø], small Fe-Mn-coated root tracks

Bcv2 35 [172–167] Loam, silty light brown, carbonaceous, few carbonate pseudo-mycelia, some loess dolls [-2 cm Ø], small Fe-Mn-coated root tracks

fNrBcv2 25 [166–163] Loam, silty, light brown-grey, grey spots up to 5 cm Ø, carbonaceous, few carbonate pseudo-mycelia, some loess dolls [-2 cm Ø], small Fe-Mn-coated root tracks

fBcv1 15 [162–160] Calcic cambisol [*Sinzig 1 Soil*]: Loam, silty, brown, carbonaceous, carbonate pseudo-mycelia, Fe-Mn-coated root tracks

Bcv2 20 [159–156] Loam, silty, light brown, carbonaceous, carbonate pseudo-mycelia, Fe-Mn-coated root tracks

C 65 [155–143] Loess: Loam, silty, light yellow-brown, carbonaceous, carbonate pseudo-mycelia

fNr' 30 [142–137] Weak Grey Gelic Gleysol: Loam, silty, light brown-grey, carbonaceous, carbonate pseudo-mycelia

fNg' 25 [136–132] Weak Speckled Gelic Gleysol: Loam, silty, light grey-brown, very weak grey and rusty speckles, carbonaceous, carbonate pseudo-mycelia, brownish clods of solifluidal loess up to 10 cm Ø

Ng 15 [131–129] Speckled Gelic Gleysol: Loam, silty, light brown-grey, strong grey and rusty speckles, in the lowest 5 cm the lightest speckles, carbonaceous, carbonate pseudo-mycelia, large brown clods of solifluidal loess reworked from the underlying soil; base line unconformably downcutting into the underlying soil

Erosional discordance

fSdBcv 15 [128–125] Calcic cambisol [*Remagen 5 Soil*]: Loam, silty, very weakly gravelly [-1,5 cm Ø], brown, bleached vertical streaks bounded by rust seams, carbonaceous, carbonate pseudo-mycelia, vertical worm dykes with humic brown infill up to 1 mm Ø

Bcv 35 [124–117] Loam, silty, brown, very few, weak, grey, rust-bounded speckles [1–3 cm Ø], carbonaceous, carbonate pseudo-mycelia, vertical worm dykes with humic brown infill up to 1 mm Ø

fNg' 10 [116–114] Weak Speckled Gelic Gleysol: Loam, silty, very weakly fine-gravelly, light grey-brown, little rusty and strongly grey speckled, carbonaceous, carbonate pseudo-mycelia, vertical worm dykes with humic brown infill up to 1 mm Ø

Ng'' 17 [113–111] Loam, silty, light grey-brown, very weakly rusty and grey speckled, carbonaceous, carbonate pseudo-mycelia, vertical worm dykes with humic brown infill up to 1 mm Ø

C 3 Colluvial layer: Loam, fine sandy, and Loam, silty, light yellow-brown, mm-thin bedding, carbonaceous

fBcv 25 [110–103] Calcic cambisol [*Remagen 4 Soil*]: Loam, silty, brown, sporadic gravel lines [up to 2 cm Ø], carbonaceous, carbonate pseudo-mycelia; vertical burrows, very weakly carbonaceous, baggy deepened into the underlying bed

fNg 15 [102–99] Speckled Gelic Gleysol: Loam, silty, very weakly fine-gravelly'', light grey-brown, strong grey and rusty speckling, carbonaceous, carbonate pseudo-mycelia

Ng' 25 [98–93] Loam, silty, light grey-brown, weakly grey and rusty speckled, carbonaceous, carbonate pseudo-mycelia

fBcv 30 [92–85] *Calcic cambisol [Remagen 3 Soil]*: Loam, silty, very weakly medium-gravelly, yellow brown, somewhat lighter than the horizon below, carbonaceous, carbonate pseudo-mycelia

Bcv 15 [84–82] Loam, silty, slightly clayey, very weakly fine-gravelly, yellow brown, carbonaceous, carbonate pseudo-mycelia, Fe-Mn-concretions

C 35 [81–75] *Solifluidal loess*: Loam, silty, weakly fine-gravelly, light yellow-brown, carbonaceous, carbonate pseudo-mycelia, very few loess dolls, Fe-Mn-concretions

C 5 [74] *Gravel layer*: Loam, fine-gravelly, medium to coarse sandy, light yellow-brown, carbonaceous

MfNg 40 [73–69] *Speckled Gelic Gleysol on solifluidal loess*: Loam, silty, weakly fine sandy, strongly fine gravelly, light yellow-brown, rusty and grey speckled, reddish brown reworked streaks and shreds of soil sediment, carbonaceous, carbonate pseudo-mycelia, Fe-Mn-concretions

C 0–80 Local channel filled with gravel: Fine to medium gravel, fine to medium sandy, silty, carbonaceous

Erosional discordance

fAh 60 [68–57] *Calcic regosol [Remagen 2 Soil]*: Loam, silty, slightly clayey, very weakly gravelly, grey brown, weakly humic, carbonaceous, many Fe-Mn-concretions

C 30 [56–49] *Solifluidal loess*: Loam, silty, very weakly gravelly, light grey-brown, carbonaceous

fBcv 40 [48–41] *Calcic cambisol [Remagen 1 Soil]*: Loam, silty, slightly clayey, very weakly fine-gravelly, brown, carbonaceous, light brownish grey clods of loam [-25 cm Ø]

Ckc 40 [40–33] *Light brown solifluidal loess*: Loam, silty, very weakly fine-gravelly, light brown, brown and grey clods of solifluidal loam of 0,5–2 m Ø, mm-thin light silt shreds, carbonaceous, few loess dolls

fNr" 20 [32–29] *Very weak Grey Gelic Gleysol*: Loam, silty, very weakly fine-gravelly, light brownish grey, scattered light irregular spots without traces of rust, mm-thin light silt shreds, carbonaceous, few loess dolls

Ckc 60 [28–23] *Light brown solifluidal loess*: Loam, silty, fine sandy, very weakly gravelly, light brown, carbonaceous, carbonate pseudo-mycelia, loess dolls up to 2 cm Ø, many Mn-concretions and -streaks; in the upper part strong solifluidal involutions

Ckc 60 [-40 cm] [22–17] *Light yellow-brown solifluidal loess*: Loam, silty, fine sandy, very weakly gravelly, light yellow-brown, [without Mn-spots], carbonaceous, few carbonate pseudo-mycelia, loess dolls

fCkcNr 20 [-40 cm] [16–13] *Grey Gelic Gleysol*: Loam, silty, fine sandy, very weakly fine-gravelly, light brown-grey, carbonaceous, very few loess dolls, Mn-spots, in the basal part reworked material from the underneath layer, large crotovinas

fBM 20 [12–10] *Brown solifluidal loam [Reisberg Soil]*: Loam, silty, fine sandy, brown, copious Mn-spots, carbonaceous, frost cracks; locally a basal band of fine gravel up to 10 cm in thickness

fNr" 10 [9–8] *Loess with weak Grey Gelic Gleysol*: Loam, silty, fine sandy, light grey-brown, carbonaceous

Nr' 20 [7–5] *Solifluidal Grey Gelic Gleysol*: Loam, silty, fine sandy, very weakly gravelly, light grey and light grey-brown scraps, very few rusty speckles, carbonaceous, sporadic clods of reddish brown loam

BtM 15 [4–3] *Reddish solifluidal loam*: Loam, fine sandy, silty, very weakly gravelly, light reddish brown, carbonaceous

BtM 15 cm [samples 2–1] *Red solifluidal loam*: Loam, fine sandy, silty, very weakly gravelly, reddish brown, with clods and scraps of a gelic gleysol, carbonaceous

Erosional discordance

Bt 180 cm *Fluvial channel deposit*: Medium to coarse gravel, block-bearing, top red brown, downward grey brown, copious streaks of skeleton gravel [grain-supported gravel], sand striae, little loam striae, cross-bedding, trough bedding, single pebbles with clay coating, high content of slate, decalcified, secondary slightly carbonaceous from above

Bv 500 cm Medium to coarse gravel, block-bearing, horizontal to slight trough bedding in layers of 1–2 dm in thickness, gravel rich in matrix, medium-sandy, loamy, yellow brown, interbedded with brown skeleton gravel, poorer in slate than the gravel above it, 2 m below the upper bound a drift boulder of 80x50 cm of milky quartz.

Underlying bed: not exposed.

Acknowledgements

Thanks to Dr. Antje Voelker for providing me with ice core literature, and thanks to Prof. Dr. Manfred Frechen and a further reviewer for giving useful hints that improved the manuscript.

References

- AG BODEN (2005): Bodenkundliche Kartieranleitung. – 5. Aufl., 438 S.; Hannover.
- ANTOINE, P., ROUSSEAU, D.-D., MOINE, O., KUNESCH, S., HATTÉ, C., LANG, A., TISSOUT, H. & ZÖLLER, L. (2009): Rapid and cyclic aeolian deposition during the Last Glacial in European loess: a high-resolution record from Nussloch, Germany. – *Quaternary Science Reviews*, 28 (25–26): 2955–2973.
- APP, V., AUFFERMANN, B., HAHN, J., PASDA, C. & STEPHAN, E. (1995), mit Beiträgen von BAALES, M., BIBUS, E., RÄHLE, W., ROTTÄNDER, R., SCHOCHE, W. & STEPPAN, K.-H.: Die altsteinzeitliche Fundstelle auf dem Schwalbenberg bei Remagen. – *Trierer Zeitschrift, Beiheft 20:* 11–136, Beil. 1–2; Trier.
- BIBUS, E., FRECHEN, M., KÖSEL, M. & RÄHLE, W. (2007): Das jungpleistozäne Lössprofil von Nussloch (SW-Wand) im Aufschluss der Heidelberger Zement AG. – *E&G Quaternary Science Journal*, 56 (4): 227–255.
- BOENIGK, W., FRECHEN, M. & WEIDENFELLER, M. (1994): Die mittel- und oberpleistozäne Deckschichtenfolge im Naturschutzgebiet „Eiszeitliches Lößprofil“ in Koblenz-Metternich. – *Mainzer geowissenschaftliche Mitteilungen*, 23: 287–320.
- BOND, G., BROECKER, W., JOHNSEN, S., McMANUS, J., LABAYRIE, L., JOUZEL, J. & BONANI, G. (1993): Correlations between climate records from North Atlantic sediments and Greenland ice. – *Nature*, 365: 143–147.
- BRUNNACKER, K. (1954): Löß und diluviale Bodenbildungen in Südbayern. – *Eiszeitalter und Gegenwart*, 4/5: 83–86.
- BRUNNACKER, K. (1957): Bemerkungen zur Feinstgliederung und zum Kalkgehalt des Lösses. – *Eiszeitalter und Gegenwart*, 8: 107–115.
- COFFLET, L. (2005): Paläomagnetische Untersuchungen im rheinischen Löss. – Inaugural-Dissertation Universität Düsseldorf (Abteilung Geologie): 152 S.
- FRECHEN, M. & SCHIRMER, W. (2011): Luminescence Chronology of the Schwalbenberg Loess in the Middle Rhine Valley. – *E&G Quaternary Science Journal*, 60 (1): 78–89.
- GROOTES, P. M. & STUIVER, M. (1997): Oxygen 18/16 variability in Greenland snow and ice with 10–3 to 105-year time resolution. – *Journal of Geophysical Research*, 102 (C12): 26,455–26,470.
- HAESAERTS, P., BORZIAC, I., CHEKHA, V.P., CHIRICA, V., DAMBLON, F., DROZDOV, N. I., ORLOVA, L. A., PIRSON, S. & VAN DER PLICHT, J. (2009): Climatic signature and radiocarbon chronology of middle and late Pleniglacial loess from Eurasia: Comparison with the marine and Greenland records. – *Radiocarbon*, 51, (1): 301–318.
- HAESAERTS, P., BORZIAC, I., CHIRICA, V., DAMBLON, F., KOULAKOVSKA, L. & VAN DER PLICHT, J. (2003): The East Carpathian loess record: a reference for the middle and late pleniglacial stratigraphy in central Europe. – *Quaternaire*, 14 (3): 163–88.
- ROHDENBURG, H. (1968): Jungpleistozäne Hangformung in Mitteleuropa – Beiträge zur Kenntnis, Deutung und Bedeutung ihrer räumlichen und zeitlichen Differenzierung. – *Göttinger Bodenkundliche Berichte*, 6: 3–107.
- ROHDENBURG, H. & MEYER, B. (1966): Zur Feinstratigraphie und Paläopedologie des Jungpleistozäns nach Untersuchungen an südniedersächsischen und nordhessischen Lößprofilen. – *Mitteilungen der Deutschen Bodenkundlichen Gesellschaft*, 5: 1–137.
- SCHIERMEYER, J. (2000): Würmzeitliche Lößmollusken aus der Eifel. – Inaugural-Dissertation Universität Düsseldorf (Heinrich-Heine-Universität): 125 S.
- SCHIRMER, W. (1990a): Schwalbenberg südlich Remagen. – In: SCHIRMER, W. (ed.): *Rheingeschichte zwischen Mosel und Maas*. – deuqua-Führer 1: 94–98; Hannover (DEUQUA).
- SCHIRMER, W. (1990b): Die Goldene Meile. – In: SCHIRMER, W. (Hrsg.): *Rheingeschichte zwischen Mosel und Maas*. – deuqua-Führer, 1: 94–98; Hannover (DEUQUA).
- SCHIRMER, W. (1991): Würmzeitliche Paläoböden am Mittelrhein. – 10. Tagung des Arbeitskreises Paläoböden der Deutschen Bodenkundlichen Gesellschaft vom 30. 5. – 1. 6. 1991 in Bonn, Programm und Exkursionsführer: 70–83.
- SCHIRMER, W. (1995a): The Oberrheingraben and its borders. – In: Schirmer, W. (ed.): *Quaternary field trips in Central Europe*, 1. – 511–520; München (Pfeil).
- SCHIRMER, W. (1995b): Mittelrhein Basin and lower Mittelrhein. – In: SCHIRMER, W. (ed.): *Quaternary field trips in Central Europe*, 1. – 524–537; München (Pfeil).
- SCHIRMER, W. (1999): Kaltzeiten und Warmzeiten im Löß. – In: BECKER-HAUMANN, R. & FRECHEN, M. (ed.): *Terrestrische Quartärgeologie*. – 81–100; Köln (Logabook).
- SCHIRMER, W. (2000a): Rhein loess, ice cores and deep-sea cores during MIS 2–5. – *Zeitschrift der deutschen geologischen Gesellschaft*, 151 (3): 309–332.
- SCHIRMER, W. (2000b): Eine Klimakurve des Oberpleistozäns aus dem rheinischen Löss. – *Eiszeitalter und Gegenwart*, 50: 25–49.
- SCHIRMER, W. (2002a): Compendium of the Rhein loess sequence. – In: IKINGER, A. & SCHIRMER, W. (eds.): *Loess units and solcomplexes in the Niederrhein and Maas area*. – *Terra Nostra*, 2002 (1): 8–23, 102–104.
- SCHIRMER, W. (2002b): Frühes Würm/Weichsel im Rahmen der Glazial-Interglazial-Gliederung. – *Terra Nostra*, 2002 (6): 314–321.
- SCHIRMER, W. (2003): Stadien der Rheingeschichte. – In: SCHIRMER, W. (ed.): *Landschaftsgeschichte im Europäischen Rheinland*. GeoArchaeoRhein, 4: 21–80.
- SCHIRMER, W. (2004): Terrestrischer Klimagang des MIS 3. – In: DEUQUA meeting, 30. August–3. September 2004, Nijmegen, the Netherlands. Abstract volume: 74.
- SCHIRMER, W. (2010): Interglacial complex and solcomplex. – *Central European Journal of Geosciences*, 2 (1): 32–40.
- SCHÖNHALS, E., ROHDENBURG, H. & SEMMEL, A. (1964): Ergebnisse neuerer Untersuchungen zur Würmlöß-Gliederung in Hessen. – *Eiszeitalter und Gegenwart*, 15: 199–206.
- SEMMEL, A. (1968): Studien über den Verlauf jungpleistozäner Formung in Hessen. – *Frankfurter geographische Hefte* (?), 45: 133 S.; Frankfurt am Main.
- SEMMEL, A. & STÄBLEIN, G. (1971): Zur Entwicklung quartärer Hohlformen in Franken. – *Eiszeitalter und Gegenwart*, 22: 23–24.
- SINGER, B. S., GUILLOU, H., JICHA, B. R., LAJ, C., KISSEL, C., BEARD, B. L. & JOHNSON, C. M. (2009): $^{40}\text{Ar}/^{39}\text{Ar}$, K-Ar and $^{230}\text{Th}-^{238}\text{U}$ dating of the Laschamp excursion: A radioisotopic tie-point for ice core and climate chronologies. – *Earth and Planetary Science Letters*, 286: 80–88.
- VAN DER PLICHT J. , BECK, J.W., BARD, E., BAILLIE, M.G.L., BLACKWELL, P.G., BUCK, C.E., FRIEDRICH, M., GUILDERSON, T.P., HUGHEN, K.A., KROMER, B., MCCORMAC, F.G., BRONK RAMSEY, C., REIMER, P.J., REIMER, R.W., REMMELE, S., RICHARDS, D.A., SOUTHON, J.R., STUIVER, M. & WEYHENMEYER, C.E. (2004): NotCal04 – comparison/calibration ^{14}C records 26–50 cal kyr BP. – *Radiocarbon*, 46 (3): 1225–1238.
- WERNER, H. (1973): Ein vollautomatisches Pipettiergerät für die Korngrößenbestimmung nach Köhn. – *Zeitschrift für Pflanzenernährung und Bodenkunde*, 134 (1): 52–56.
- ZÖLLER, L., CONARD, N. J. & HAHN, J. (1991): Thermoluminescence dating of middle Palaeolithic open air sites in the Middle Rhine Valley/Germany. – *Naturwissenschaften*, 78: 408–410.

Formation and geochronology of Last Interglacial to Lower Weichselian loess/palaeosol sequences – case studies from the Lower Rhine Embayment, Germany

Peter Fischer, Alexandra Hilgers, Jens Protze, Holger Kels, Frank Lehmkuhl, Renate Gerlach

How to cite:

FISCHER, P.; HILGERS, A.; PROTZE, J.; KELS, H.; LEHMKUHL, F.; GERLACH, R. (2012): Formation and geochronology of Last Interglacial to Lower Weichselian loess/palaeosol sequences – case studies from the Lower Rhine Embayment, Germany. – E&G Quaternary Science Journal, 61 (1): 48–63. DOI: 10.3285/eg.61.1.04

Abstract:

Located in the Lower Rhine area two loess/palaeosol sections were investigated focusing on the last Interglacial to Lower Weichselian pedosedimentary sequence. The sections are situated in the brown coal opencast mining area of Inden and Garzweiler, and comprise archaeological find layers from the Middle Palaeolithic. Selected ratios derived from multi-element analysis are presented for the first time for the prominent loess accumulation area north of the Rhenish Shield. In addition luminescence ages were determined based on isothermal thermoluminescence (ITL) and optically stimulated luminescence (OSL) using the quartz mineral fraction. The results indicate multiple sediment redeposition and polygenetic soil formation for both sections displaying a complex formation of the investigated sequences. Due to the polygenetic character of the loess/palaeosol sequences, interpretation in terms of stratigraphical correlation and palaeoclimatic reconstruction is not straightforward. In addition, the geomorphological position and the formation of the palaeorelief in the surrounding area of loess/palaeosol sequences have to be taken into account as important factors of the geomorphodynamic and soil forming processes of the past.

Genese und Chronologie von letztinterglazialen bis früh-weichselzeitlichen Löss-Paläoboden-Abfolgen – Beispiele aus der Niederrheinischen Bucht, Deutschland

Kurzfassung:

Anhand zweier Profile aus dem Niederrheingebiet wird die Komplexität der Genese und Chronologie letztinterglazialer bis früh-weichselzeitlicher Löss-Paläoboden-Sequenzen diskutiert. Die untersuchten Profile wurden in den Braunkohlebergbau Inden und Garzweiler aufgenommen und sind mit mittelpaläolithischen Fundkomplexen verknüpft. Erstmals werden dabei Multi-Element-Analysen neben Lumineszenz-Datierungen an Quarzen (ITL, OSL) aus niederrheinischen Lössprofilen vorgestellt und diskutiert. Die Ergebnisse offenbaren große Unsicherheiten hinsichtlich einer stratigraphischen und paläoklimatischen Interpretation von polygenetisch überprägten Sediment- und Paläobodensequenzen. Eine bedeutende Rolle nimmt dabei auch die Reliefposition in Verbindung mit der Morphogenese des Paläoreliefs ein, die in höherem Maße als bisher berücksichtigt werden sollte.

Keywords:

Loess stratigraphy, Lower Rhine area, pedocomplexes, multi element analysis, luminescence chronology, Last Interglacial, Lower Weichselian

Addresses of authors: P. Fischer, A. Hilgers, Institute for Geography, University of Cologne, Albertus-Magnus-Platz, 50923 Cologne, Germany, E-Mail: peter.fischer@uni-koeln.de; F. Lehmkuhl, H. Kels, J. Protze, Chair of Physical Geography and Geocology, Department of Geography, RWTH Aachen University, Wüllerstr. 5b, 52062 Aachen, Germany; R. Gerlach, Landschaftsverband Rheinland, Amt für Bodendenkmalpflege im Rheinland, Endenicher Str. 133, 53115 Bonn, Germany.

1 Introduction

This study is concerned with loess sediments and pedocomplexes from the Lower Rhine Embayment, which is a prominent loess accumulation area north of the Rhenish Shield in western Central Europe. The loess research in Central Europe and in Germany has a long tradition (cf. PéCSI & RICHTER 1996; SMALLEY et al. 2001; ZÖLLER & SEMMEL 2001).

For the Lower Rhine area, detailed discussions of the early stages of loess research were presented by HENZE (1998), KELS (2007) and FISCHER (2010). Especially the improvement of palaeopedological methods in the second half of the last century enabled the development of a general stratigraphical scheme for the Upper Pleistocene (e.g. SCHÖNHALS et al. 1964; ROHDENBURG & MEYER 1966; SEMMEL 1968). Essential chronostratigraphical studies from the Lower Rhine area (e.g. REMY 1960; PAAS 1968a, b; BRUNNACKER 1967) were

based on the stratigraphical relation to underlying fluvial terraces and counting of palaeosols from top to bottom. This approach did not consider erosional unconformities and hiatuses within the studied sequences (cf. SCHIRMER 2003). In the last two decades a comprehensive loess stratigraphy for the Lower Rhine area has been developed by SCHIRMER (e.g. 1999, 2000a, 2000b, 2002, 2010).

In their function as archives of climate and environmental change during the Middle and Upper Pleistocene loess/palaeosol sequences are being investigated in recent times using a wide methodological spectrum, including sedimentological, geochemical, palaeopedological and geochronological approaches. Geochemical weathering indices derived from multi-element analyses have recently been applied as promising tool for the palaeoclimatical interpretation of Pleistocene as well as Holocene pedosedimentary records (e.g. LIU, 1985, 1991; DERBYSHIRE et al. 1995;

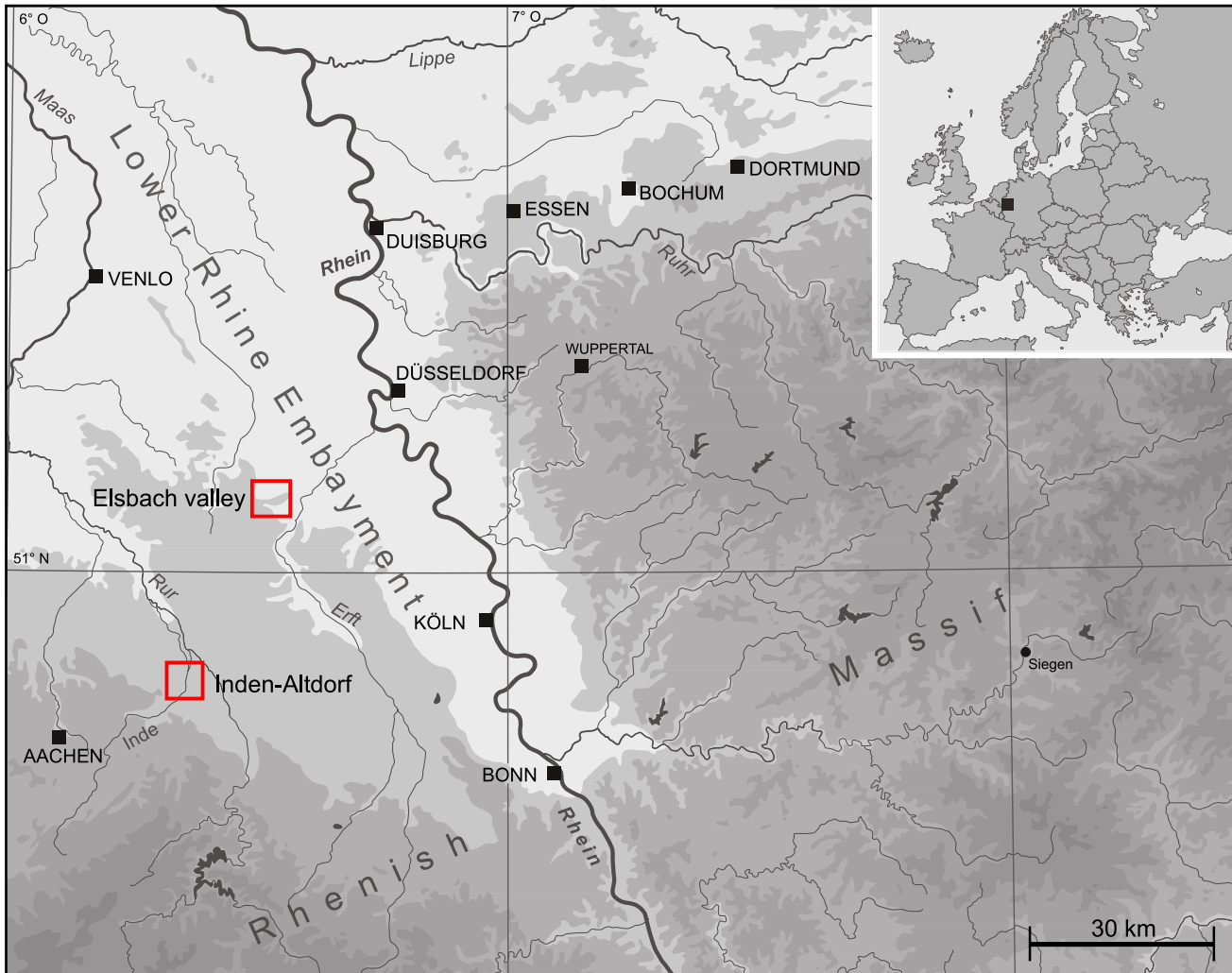


Fig. 1: Map showing the location of study sites in the Lower Rhine Embayment.

Abb. 1: Lage der Untersuchungsgebiete in der Niederrheinischen Bucht.

GALLET et al. 1996; BOKHORST et al. 2008; BUGGLE et al. 2008; BUGGLE et al. 2010). Furthermore, geochemical fingerprints can give important clues on lithological changes reflecting soil and geomorphodynamic processes during the formation of loess deposits. However, for the Rhenish loess area comparably few geochemical studies are available (SMYKATZ-KLOSS 2003; SMYKATZ-KLOSS et al. 2004).

Loess deposits were among the first sediments being systematically dated with luminescence techniques (PREUSSER et al. 2008) enabling the direct determination of their time of deposition. Overviews of the state of the art in luminescence dating on Pleistocene loess sediments are given in SINGHVI et al. (2001), KOSTER (2005), ROBERTS (2008) and PREUSSER et al. (2008). Published luminescence data obtained for loess deposits of the Lower Rhine area are mainly based on thermoluminescence (TL) and infra-red stimulated luminescence of feldspars (IRSL) and concentrate on a few type localities (ZÖLLER et al. 1988; ZÖLLER 1989; JANOTTA 1991; FRECHEN et al. 1992; BOENIGK & FRECHEN 1995). Thus, there is still a need for systematic dating of loess deposits applying different luminescence dating approaches.

The present study focuses upon the sedimentological and geochemical characteristics as well as the chronology

of pedocomplexes of Eemian and Lower Weichselian age in the Lower Rhine area. For two sites, a robust chronological frame shall be established, and the use of multi-element analyses will be tested and discussed. As the records under investigation are related to archaeological finds correlating to the Middle Palaeolithic, the results contribute to a better understanding of site formation processes (e.g. UTHMEIER 2006).

2 Regional setting and investigated loess sections

2.1 The loess/palaeosol sequence of the Elsbach valley [Garzweiler]

The investigated section of the Elsbach valley (archaeological documentation number FR 2006/0086, feature 5) is situated in the north-eastern Jülicher Börde, close to the brown coal opencast mining area Garzweiler (Fig. 1, 2). In this area the loess covered Upper Terrace of the River Rhine is dissected by numerous dry valleys. The section is located on the middle slope of the Elsbach valley facing to the south. The importance of (palaeo-) depressions for the conservation of stretched stratigraphical records in this area is well known and loess/palaeosol sequences from the

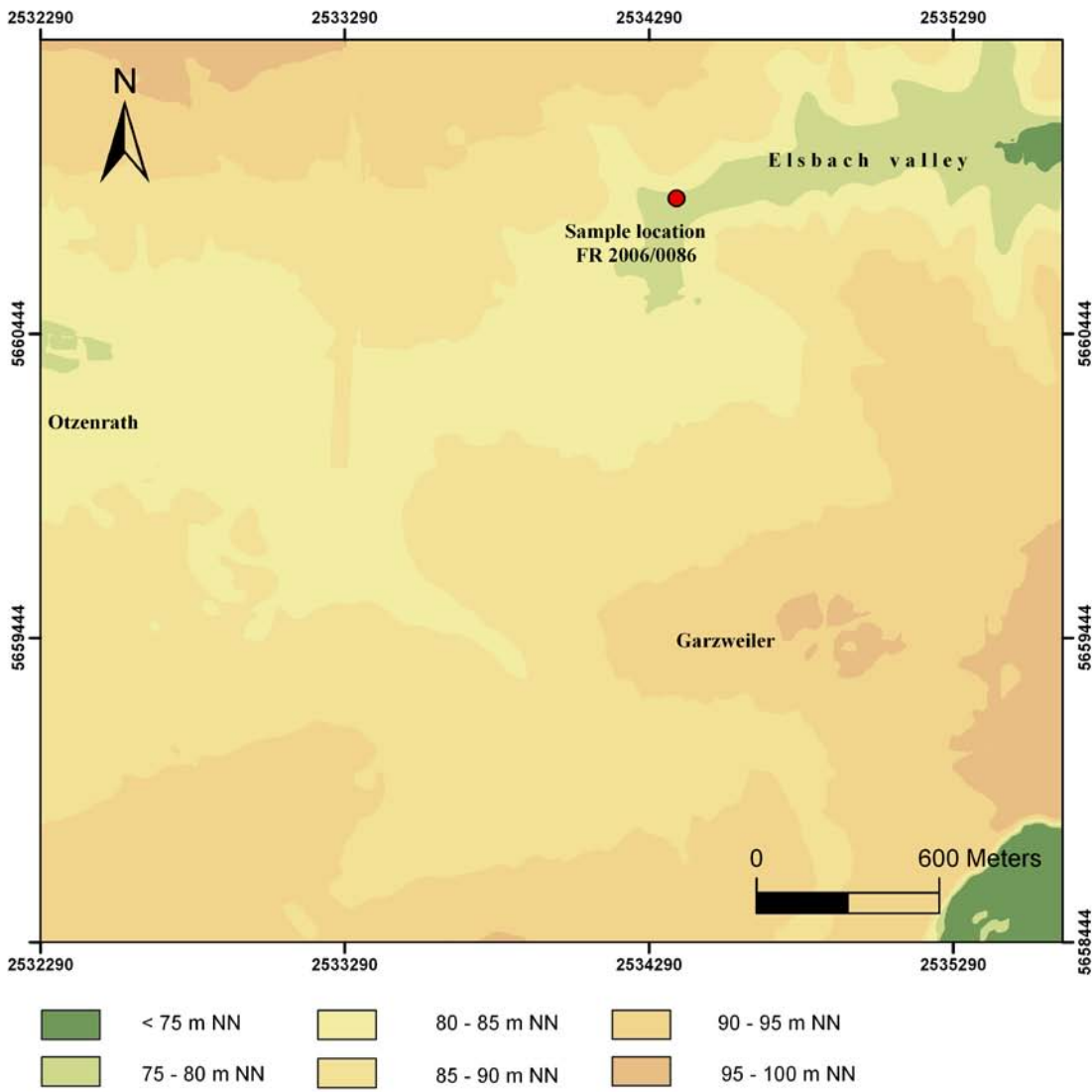


Fig. 2: Position of the loess/palaeosol record in the Elsbach valley (Garzweiler). The map shows the former morphology (prior to further mining) based on the digital elevation model (Data source: Geobasisdaten, Landesvermessungssamt NRW (2008), DEM 5, courtesy of the Rhineland Regional Council, LVR).

Abb. 2: Lage des Lössprofils im Elsbachtal. Die Karte zeigt die morphologische Situation (vor dem mittlerweile fortgeschrittenen Abbau) auf Basis des DGM 5 (Datenquelle: Geobasisdaten, Landesvermessungssamt NRW 2008, mit Genehmigung des LVR).

Garzweiler area are discussed in numerous publications (e.g. HENZE 1998; KELS 2007; SCHIRMER 2000b, SCHIRMER 2010; SCHIRMER & KELS 2002).

The section has a vertical extension of 2.7 m (Fig. 3). At its base a lamellic Bw horizon occurs, superimposed by clay illuviation from the overlying Btg horizon, which shows concretions of iron and manganese hydroxides. As based on field observations these horizons most likely correlate with a truncated Eemian soil (MIS 5e). The Btg horizon is overlain by a slightly humic Bt and a bleached stagnic horizon. The latter two are separated by an unconformity indicated by occasional gravel. The question arises, if the weak humic Bt horizon represents a soil sediment postdating the "Eemian" soil. The bleached stagnic horizon is overlain by a slightly humous, water stained AhE horizon, which shows weak Bt-features and decomposition of organic material. The following humic layers can be separated into a lower, rust spotted, clay-rich horizon and an upper horizon characterised by increasing organic carbon content and enrichment of secondary carbonate.

Small cryogenic cracks intrude from the overlying soil sediment into the Ah horizon.

The uppermost part is considerably reworked as characterised by tongue-like soil material imbedded within calcareous loess sediments.

2.2 The loess/palaeosol record of Inden-Altdorf

The site of Inden-Altdorf is situated in the south-eastern part of the Aldenhovener Platte, which is part of the southern loess landscape of the Jülicher Börde. Here, the loess belt, continuing westwards to the Zülpicher Börde, is interrupted by the River Inde, a tributary to the River Rur, both having their sources in the Rhenish Massif (Fig. 1). The Aldenhovener Platte slopes downward in northerly and north-easterly direction. Several tectonic dislocations occur, striking from northwest to southeast (cp. AHORNER 1962).

On average the loess cover reaches thicknesses between 3 and 7 metres, growing up to 11 metres in local palaeo-

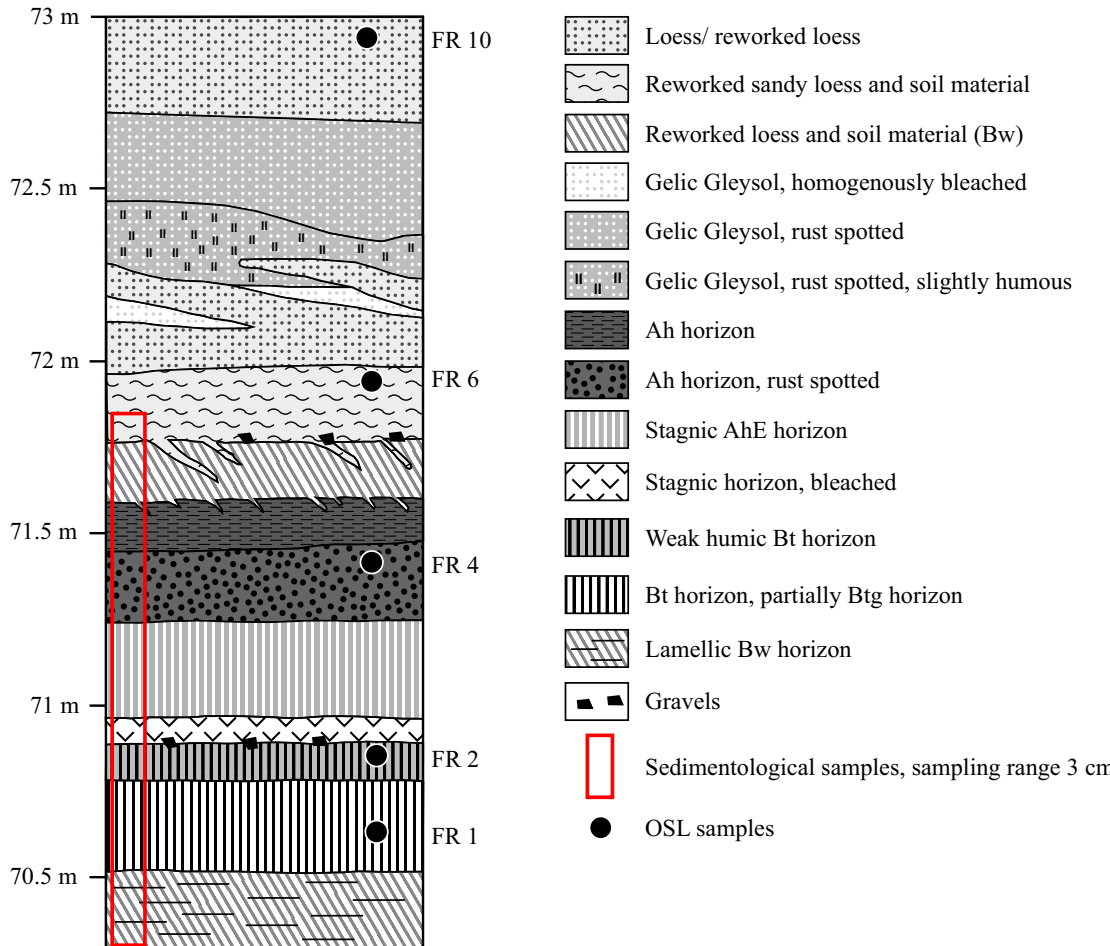


Fig. 3: Litho- and pedological composition of the loess/palaeosol record of Garzweiler/Elsbach valley (FR 2006/0086, feature 5; Position (German Grid) R: 2534381, H: 5660889, 75 m a.s.l.).

Abb. 3: Litho- und pedologischer Aufbau der Loess-Paläoboden-Sequenz aus Garzweiler/Elsbachtal (FR 2006/0086, Stelle 5; Lage (Gauß-Grüger Koordinaten) R: 2534381, H: 5660889, 75 m ü. NN).

channels (KELS 2007; PAAS 1968a, b). These palaeochannels are often connected to tectonic subsidence and represent positions of major relevance for conservation of older loess sediments and pedocomplexes in the Lower Rhine area. The loess sediments cover Early- and Mid-Pleistocene fluvial deposits of the rivers Rhine and Meuse and their tributaries. From this area only few loess sections were investigated (PAAS 1961, 1968a, b; LÖHR & BRUNNACKER 1974; HENZE 1998).

The documentation and sampling of the loess/palaeosol record of Inden-Altdorf as described in the following was conducted during an archaeological excavation (WW 2005/91) in the forefront of the brown coal mining area Inden (Fig. 4, 5). The archaeological finds were dated to the Middle Palaeolithic (THISSEN 2006, 2007; KELS et al. 2009; PAWLICK & THISSEN 2011).

Attuned to the River Inde in its function as local erosional base numerous dry valleys exist dissecting the loess landscape. These dry valleys formed under periglacial conditions during the Pleistocene and were affected by colluviation processes during the Holocene caused by human impact on the natural landscape. Taking these processes into account a considerably more accentuated relief can be presumed for the time before major soil erosion (cf. SCHULZ 2007).

The investigated record with a vertical extension of 2.3 m is located on the north-eastern inclined shoulder of

the south-eastern slope of the Altdorf dell (Fig. 4). The base comprises a Bt horizon characterised by a reddish brown colour and lamellic clay illuviation, which is overlain by a reddish brown, clay rich Btg horizon. Both horizons show strong hydromorphic staining by iron and manganese hydroxides. Based on the field evidence these horizons most likely correlate with the truncated soil of the Eemian interglacial (MIS 5e). On top of the Btg horizon a stagnic horizon is developed characterised by a light grey colour due to bleaching processes. Within this layer numerous charcoal fragments were found and Middle Palaeolithic finds were imbedded in the surrounding of the sample location. Disturbed soil structure and rounded charcoal fragments indicate reworking processes, further supported by a main artefact concentration at the foot of the slope. The stagnic horizon is overlain by a weak Bt horizon which is slightly humous in the lower part. On top of the Bt horizon a stagnic AhE horizon comprising rounded charcoal was documented. The hanging layer is characterised by reworked soil material, with increasing organic carbon content towards the top and intercalated lamellic silt indicating sheet wash processes. The organic carbon is most likely eluviated from the overlying Ah horizon. A weakly humic Bt with an angular blocky soil structure and clay coatings is superimposing the Ah horizon. This horizon is again overlain by a light brown soil sediment. This reworked soil material

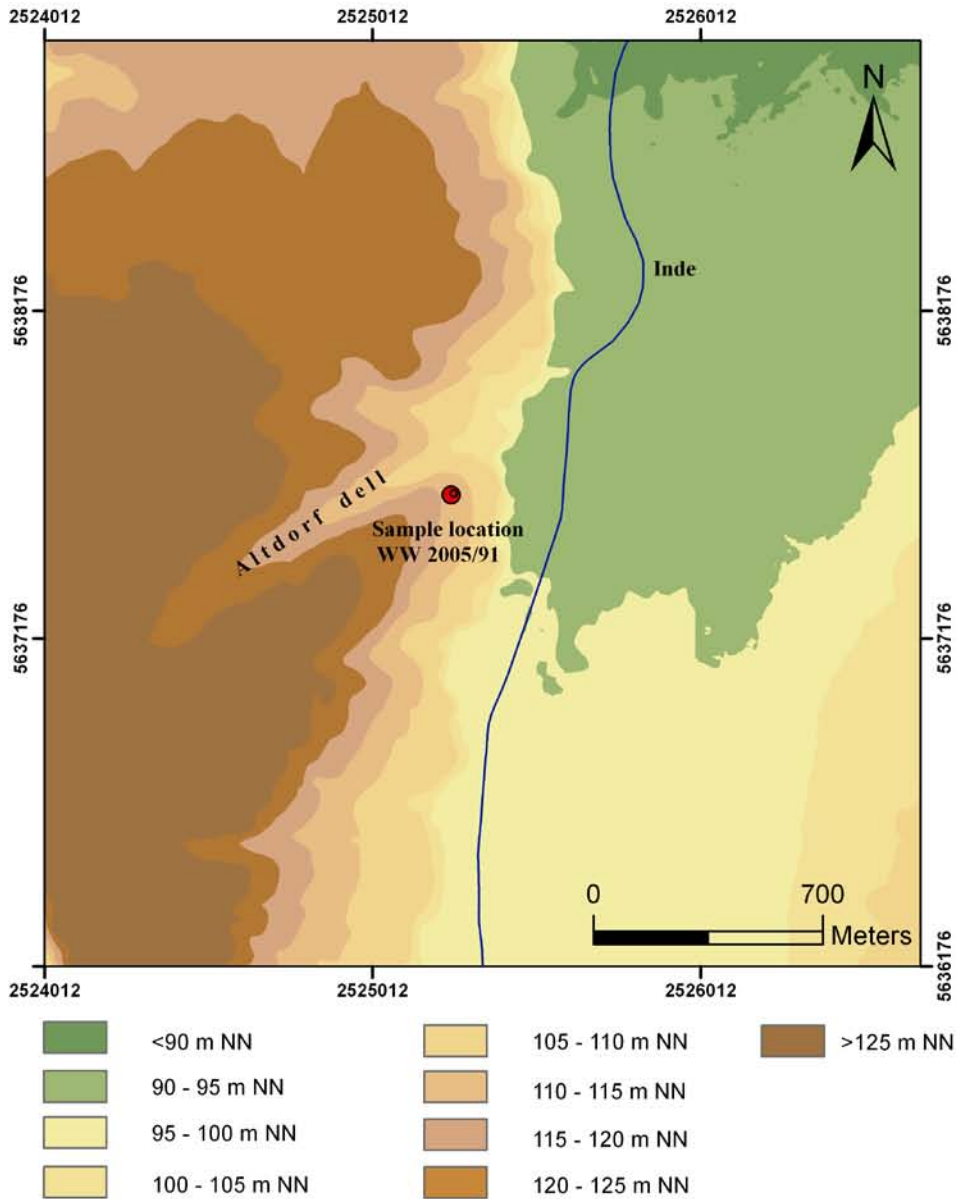


Fig. 4: Position of the loess/palaeosol record of Inden-Altdorf. Map showing the morphology (prior to further mining) based on the digital elevation model (Data source: Geobasisdaten, Landesvermessungsamt NRW (2008), DEM 5, courtesy of the Rhineland Regional Council, LVR).

Abb. 4: Lage des Lössprofils aus Inden-Altdorf. Die Karte zeigt die morphologische Situation (vor dem mittlerweile fortgeschrittenen Abbau) auf Basis des DGM 5 (Datenquelle: Geobasisdaten, Landesvermessungsamt NRW 2008, mit Genehmigung des LVR).

as well as the Bt, Ah and AhE horizons show secondary carbonate enrichment. The hanging sequence is characterized by yellowish loess sediments showing increasing carbonate content and intercalated Gelic Gleysols, which most likely correlate with the Upper Weichselian (MIS 2). Cryoturbation features with tongue-like structures intrude into the loess sediments.

Both records exhibit signs of strong reworking processes and a reduction of the stratigraphy due to superimposition of different soil formation phases.

Evidence of younger (and weaker) Bt horizons postdating the last interglacial soil is reported by SCHIRMER (e.g. 2002, 2010) for the Lower Rhine area as well as for other loess regions from Germany (e.g. FRECHEN, BOENIGK & WEIDENFELLER 1995; FRECHEN, TERHORST & RÄHLE 2007).

3 Methods

3.1 Sedimentological and geochemical analysis

In order to obtain high-resolution records, sediment samples were taken at 3 cm intervals at the lower part of the Elsbach valley sequence and at 5 cm intervals at the Inden-Altdorf sequence (cp. Figs. 3, 5). The grain size distribution of the Inden-Altdorf sequence was determined using a Sedigraph (Micromeritics 5100) measuring the fraction from 63-0.63 µm. The bulk sample was boiled with H₂O₂, resulting in the oxidation of organic matter. Carbonates were dissolved by HCl (10 %). Sediment samples were reduced to the fraction < 63 µm by sieving and 4 g per sample were dispersed in 80 ml sodium-pyrophosphate (Na₄P₂O₇ x 10 H₂O).

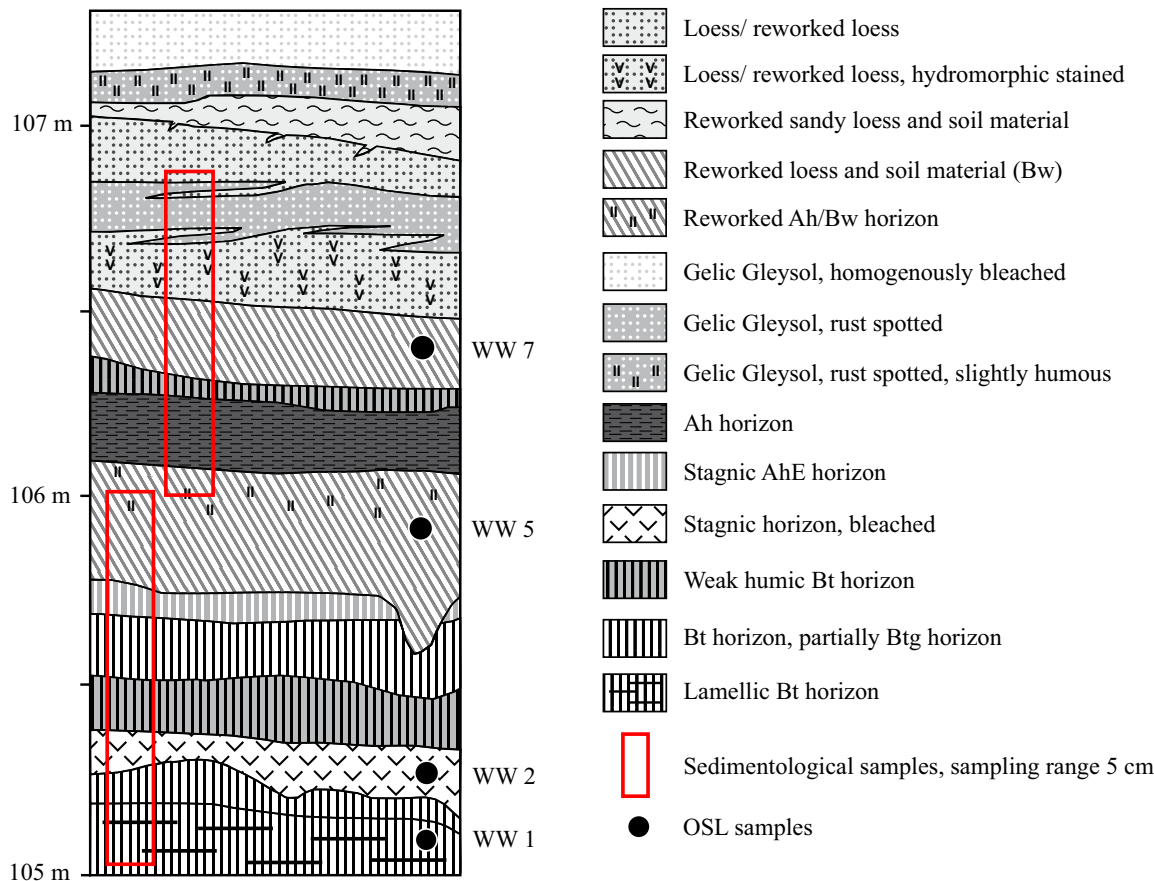


Fig. 5: Litho- and pedological composition of the loess-palaeosol record of Inden-Altdorf (WW 2005/91, feature 125; Position (German Grid) R: 2525252, H: 5637614, 107 m a.s.l.).

Abb. 5: Litho- und pedologischer Aufbau der Löss-Paläoboden Sequenz aus Inden-Altdorf (WW 2005/91, Stelle 125, Lage (Gauß-Krüger Koordinaten) R: 2525252; H: 5637614; 107 m ü. NN).

In loess/palaeosol sequences initial weathering processes result in dissolution of minerals followed by hydration and hydrolysis. The latter produces new ions and/or insoluble components due to the reaction of minerals with water in more humid periods, in contrast to cold (periglacial) arid periods with loess accumulation. In order to characterise palaeosols in loess sections ratios of soluble cations (e.g. Na, K, Rb, Mg, Sr) to relatively insoluble hydrolysates (e.g. Al_2O_3 , TiO_2) can be determined, in which the weathering processes (as basic soil formation processes) are indicated by decreasing ratios (cp. SMYKATZ-KLOSS et al. 2004). In general, with rising radius the mobility of ions decreases and the tendency to be adsorbed to fine grained sediments or soil particles increases (SMYKATZ-KLOSS et al. 2004). Thus, large cations like K and Rb are increasingly adsorbed whereas for example Na and Mg are preferentially leached. Due to intensive weathering and soil formation processes in the more humid climate of Western Central Europe as displayed in the sections under study ratios based on volatile elements such as Na and Mg are not as suitable as in loess/palaeosol sequences of more continental climate regions (cp. BOKHORST et al. 2009; BUGGLE et al. 2010; KABATA-PENDIAS 2010; HOODA, 2010).

For the present study, element contents of calcium (Ca), strontium (Sr), potassium (K), rubidium (Rb) and titanium (Ti) and correlating ratios are included (cp. Figs. 8, 9, 10, 11).

The K/Rb ratio usually decreases during in situ soil formation processes and thus indicates the weathering degree. In loess/palaeosol sequences it is suggested that increasing values in this ratio also reflect secondary potassium enrichment, interpreted as accumulation of clay due to input of pre-weathered material. The Ti/Ca ratio indicates increasing weathering degrees by increasing values and is suggested as a primary weathering index. In combination with the K/Ti ratio it allows for a detection of secondary carbonate. Secondary clay enrichment as displayed in high values of the K/Rb ratio is attended by high Ti contents. The Sr/Rb ratio indicates secondary carbonate precipitation due to a strong affinity of Sr to Ca as well as clay accumulation due to the high capacity of clay minerals to adsorb Sr (KABATA-PENDIAS 2010). In general crosschecks between selected ratios allow for assuring the deduced interpretation.

The elements were measured using a portable X-ray fluorescence (XRF) device (Nitron Xlt 700 Series). The bulk sediment samples were reduced to the fraction $< 63 \mu\text{m}$ and prepared for the analytical cuvette. Measurements were obtained in the pre-calibrated bulk mode (38 KeV, 10 W).

3.2 Luminescence dating

Luminescence dating was carried out at the luminescence dating laboratory of the Institute for Geography, University of Cologne. Here, luminescence ages of nine sediment sam-

Tab. 1: Dose rate data for the quartz fraction calculated assuming average water contents of 14 ± 5 weight-%. Radionuclide concentrations of sample set FR were determined by neutron activation analysis (NAA, Becquerel Laboratories, Canada), whereas for sample set WW low-level gamma-spectrometry was carried out (VKTA Rossendorf, Germany). The dose rates include the cosmic dose contribution which was calculated according to the present sampling depth (PRESCOTT & HUTTON, 1994). All values are shown with their 1 sigma-error.

Tab. 1: Dosisleistungswerte berechnet für die Quarz-Fraktion unter Berücksichtigung eines mittleren Wassergehaltes von 14 ± 5 Gew.-%. Radionuklid-Konzentrationen des Probensatzes „FR“ wurden mittels Neutronen-Aktivierungs-Analyse (NAA, Becquerel Laboratories, Canada) bestimmt, die des Probensatzes „WW“ mittels hochauflösender Gamma-Spektroskopie (VKTA Rossendorf). In der Dosisleistung ist der Anteil der kosmischen Dosisleistung berücksichtigt, der entsprechend der Beprobungstiefe berechnet wurde (PRESCOTT & HUTTON 1994).

Lab.-code	Sample	Depth (m)	Dose rate (Gy/ka)	U (ppm)	Th (ppm)	K (%)
C-L2019	FR 1	5.33	2.62 ± 0.19	2.19 ± 0.15	10.53 ± 0.34	1.65 ± 0.05
C-L2020	FR 2	5.07	2.67 ± 0.20	3.23 ± 0.19	9.61 ± 0.31	1.47 ± 0.05
C-L2022	FR 4	4.45	2.56 ± 0.19	2.59 ± 0.15	9.99 ± 0.32	1.47 ± 0.05
C-L2024	FR 6	3.83	2.57 ± 0.19	3.06 ± 0.17	9.37 ± 0.30	1.45 ± 0.05
C-L2028	FR 10	2.60	2.36 ± 0.18	2.47 ± 0.15	8.38 ± 0.27	1.41 ± 0.05
C-L2029	WW 1	6.37	2.62 ± 0.20	3.22 ± 0.13	11.00 ± 0.40	1.40 ± 0.07
C-L2030	WW 2	6.16	2.32 ± 0.17	2.96 ± 0.12	10.30 ± 0.30	1.16 ± 0.04
C-L2033	WW 5	5.66	2.55 ± 0.19	3.24 ± 0.13	10.40 ± 0.40	1.35 ± 0.05
C-L2035	WW 7	5.00	2.60 ± 0.19	2.82 ± 0.11	10.40 ± 0.40	1.50 ± 0.05

Tab. 2: Luminescence ages obtained for the fine sand quartz fraction using different single-aliquot regeneration dose protocols. The ages which are considered to be the most reliable are highlighted.¹ The number of aliquots measured and used to calculate the average equivalent dose.² RSD= relative standard deviation of the De-data set.³ Overdispersion of the De data set.⁴ Depending on the dispersion of the individual De-estimates the mean value of the equivalent doses is based on either the common or central age model (GALBRAITH et al. 1999). COM= common age model, CAM = central age model.⁵ All measurements were carried out on automated Risø TL/OSL readers (type TL-DA-12, -15, or -20, BØTTER-JENSEN et al. 2003) using small aliquots (~300 grains per aliquot) and the following settings: Quartz, OSL: detection U340 filter (7.5 mm thickness), pre-heat 10 s @ 240°C, cut-heat 160°C TL, 50 s @ 125°C blue stimulation, hot-bleach after test dose OSL: 40 s @ 280°C, Quartz, ITL: detection U340 filter (7.5 mm thickness), 500 s @ 310°C (hold 10 s @ 310°C before meas.). The De-errors include a 5 % uncertainty for the beta source calibration.

Tab. 2: Ergebnisse der Lumineszenz-Datierungen für die Feinsand-Quarz-Fraktion auf Basis unterschiedlicher Single-Aliquot-Regenerierungs-Protokolle. Wahrscheinlichste Alter sind hervorgehoben.¹ Anzahl der gemessenen und zur Bestimmung der mittleren Äquivalenzdosis (De) herangezogenen Teilproben.² RSD= relative Standardabweichung des De-Datensatzes.³ Ausmaß der Streuung des De-Datensatzes.⁴ Mittelwerte der Äquivalenzdosis basieren in Abhängigkeit von der Streuung der Einzelwerte entweder auf dem "common" oder "central age model" (GALBRAITH et al. 1999). COM= common age model, CAM = central age model.⁵ Alle Messungen wurden auf automatisierten Risø TL/OSL Messgeräten (type TL-DA-12, -15, oder -20, BØTTER-JENSEN et al. 2003) unter Verwendung kleiner Teilproben (~300 Körner pro Teilprobe) und folgender Messkonfiguration durchgeführt: Quarz, OSL: Detektion U340 Filter (7,5 mm), Vorheizen 10 s @ 240°C, 160°C TL, 50 s @ 125°C blaue Stimulation, thermo-optisches Bleichen nach Test-Dosis OSL: 40 s @ 280°C, Quarz, ITL: Detektion U340 Filter (7,5 mm), 500 s @ 310°C (vor der Messung Probe 10 s @ 310°C gehalten). Die De-Fehler beinhalten eine 5%ige Unsicherheit hinsichtlich der Beta-Quellen Kalibration.

Lab.-code	Sample	n ¹	RSD (%) ²	OD (%) ³	Age model ⁴	De (Gy) ⁵	OSL-age (ka)	ITL-age (ka)
C-L2019	FR 1	16	13.5	11.5	CAM	339 ± 21	---	130 ± 12
C-L2020	FR 2	17	10	---	COM	315 ± 18	---	118 ± 11
C-L2022	FR 4	18	13.5	---	COM	223 ± 13	---	87.1 ± 8.3
C-L2024	FR 6	17	13.7	10.8	CAM	203 ± 12	---	79.0 ± 7.4
		24	15.4	14.3	CAM	79.5 ± 4.8	30.9 ± 2.9	---
C-L2028	FR 10	24	21.5	17.2	CAM	59.9 ± 3.8	25.4 ± 2.5	---
C-L2029	WW 1	20	21.1	15.9	CAM	314 ± 20	---	120 ± 12
C-L2030	WW 2	11	23.3	18.0	CAM	231 ± 19	---	99.4 ± 11.0
C-L2033	WW 5	20	18.7	15.3	CAM	191 ± 12	---	74.9 ± 7.3
C-L2035	WW 7	19	15.1	13.8	CAM	188 ± 11	---	72.3 ± 6.8

ples are presented, which were taken from the site Inden-Altdorf (WW 2005/91, sample set WW) and from the loess sequence of the Elsbach valley (WW 2006/0086, sample set FR). All luminescence measurements were carried out on automated Risø TL/OSL readers (types TL-DA-12, -15, or 20) and followed single-aliquot regenerative-dose protocols (SAR). Per sample several sub-samples, or aliquots, were measured to obtain estimates of the amount of radiation

dose accumulated within the crystal lattice of a mineral grain since it was shielded from sunlight (equivalent dose, D_e). To calculate the annual dose (dose rate, D_0) derived from the decay of lithogenic radionuclides in the sediment, the concentration of uranium, thorium, and potassium in each sediment sample was determined by neutron activation analysis (sample set FR) or high-resolution low-level gamma spectrometry (sample set WW) (see Tab. 1).

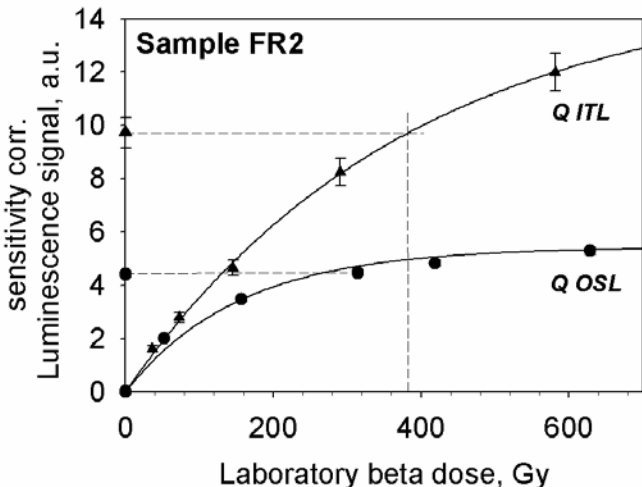


Fig. 6: Dose-response curve of sample FR2. At high doses the signal approaches a saturation level. The quartz OSL signal saturates at much lower doses than the ITL signal of the same sample (a.u. = arbitrary unit).

Abb. 6: Wachstumskurve der Probe FR2. Bei hohen Dosen zeigt sich eine Signalsättigung. Das Quarz-OSL-Signal erreicht dieses Sättigungsniveau deutlich früher als das ITL-Signal derselben Probe (a.u. = beliebige Einheit).

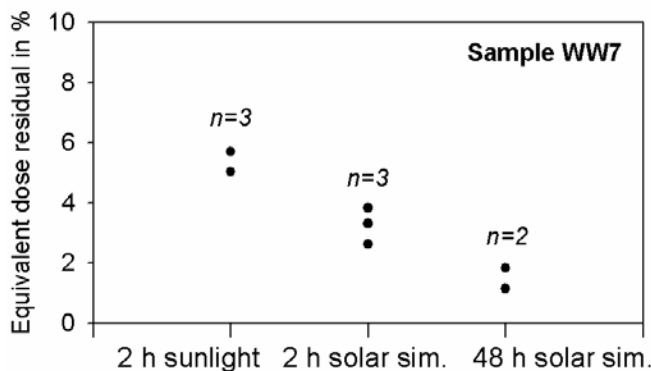


Fig. 7: Sub-samples of sample WW7 were bleached either with sunlight or solar simulator for 2 and 48 h, respectively. After bleaching the residual ITL signal was measured and is plotted here in % of the equivalent dose value. For the 2 h-sunlight bleaching two aliquots yielded the same results.

Abb. 7: Teilproben der Probe WW7 wurden sowohl mittels Sonnenlicht als auch im Solar-Simulator für 2 bzw. 48 h gebleicht. Nach der Bleichung wurde das Restsignal der ITL bestimmt und hier als prozentualer Anteil gegen die Äquivalenzdosis aufgetragen. Die 2-stündige Bleichung unter Sonnenlicht ergab für zwei Teilproben identische Ergebnisse.

All samples were prepared under subdued red light. The fine sand fraction was extracted by dry sieving and settling, and subsequently treated with 10%-hydrochloric acid, 10%-hydrogen peroxide and sodium oxalate to remove carbonates, organic material, and clay. Mineral separation was carried out using solutions of sodium polytungstate and HF etching to obtain a purified quartz fraction. For more details on the background of luminescence dating, the equipment, sample preparation, and the different measurement protocols the reader is referred to e.g. PREUSSER et al. (2008), BØTTER-JENSEN et al. (2003) and ROBERTS (2008).

For samples FR 2, 6 and 10, the De of the quartz fraction was determined using a ‘conventional’ SAR protocol as described in MURRAY & WINTLE (2000) and WINTLE & MURRAY (2006). However, as illustrated in Fig. 6 for sam-

ple FR 2, the quartz OSL dose response curve approaches saturation, thus the OSL protocol is not suitable for dating these samples. This observation is in accordance with the recommendations of BUYLAERT et al. (2008) who suggest application of the SAR-OSL procedure only for sand-sized quartz samples extracted from loess (in that case from the Chinese loess plateau) with burial doses below 120–150 Gy. In our study the signal saturation limits the practical age range for SAR-OSL to approximately 45–60 ka. As the time window beyond 80 ka is of particular interest here, other luminescence protocols rather than quartz OSL had to be tested to provide reliable age information for the two study sites. We tested a variety of new measurement protocols focussing on the extension of the upper luminescence dating limit. In Table 2 (Section 4) dating results are presented which were obtained from OSL and isothermal thermoluminescence (ITL, CHOI et al. 2006; JAIN et al. 2007) of quartz. The quartz ITL signal has a much higher saturation level than the OSL signal (Fig. 6), allowing to date further back in time. Experiments on the optical resetting and the dose recovery yield promising results with respect to the applicability of ITL for the sediments investigated in this study. Residuals of ~ 3–5 % (~6–10 Gy) were measured after 2 h of sunlight bleaching and should allow dating of aeolian sediments with sufficient transport distance, i.e. bleaching time (Fig. 7).

For a dose recovery test (sample WW7), a laboratory dose of 50 Gy was administered after 48 h bleaching in the solar simulator. The ratio given/measured dose of 0.89 ± 0.07 indicates a tendency of overestimation of a burial dose by using the ITL approach. The residual after the 48 h bleaching was only 1.5 % of the natural dose and thus is not the major cause for the overestimation. A further explanation is that sensitivity changes of the natural signal are not adequately monitored by the first test dose. BUYLAERT et al. (2006) report on sensitivity changes that occur when the first heat treatment is applied to measure the natural signal. This change is not detected by the SAR procedure and led to an overestimation of ITL ages in their samples from the Chinese loess plateau (BUYLAERT et al. 2006). For our samples, the dose recovery ratio and residuals after bleaching are considered as acceptable, and the low spread in De-values further argues for a general applicability of the applied ITL-protocol. However, a certain overestimation of our ITL ages cannot be ruled out.

4 Results

The element concentrations and calculated ratios determined for the section of the Elsbach valley (Figs. 8, 9) offer a subdivision into three geochemical units. From the top of the analytical sequence to the base of the rust spotted Ah horizon (first unit) a weak secondary carbonate precipitation can be assumed, visible in the Ti/Ca and the Sr/Rb ratio. With respect to the Ti/Ca ratio a strong weathering degree can be verified for this unit. In addition, maximal values of the K/Rb ratio, resulting from an increase of K, indicate secondary clay enrichment.

The second unit comprises the stagnic AhE horizon, the bleached stagnic horizon and the weak humic Bt horizon, characterised by significantly increasing values of the

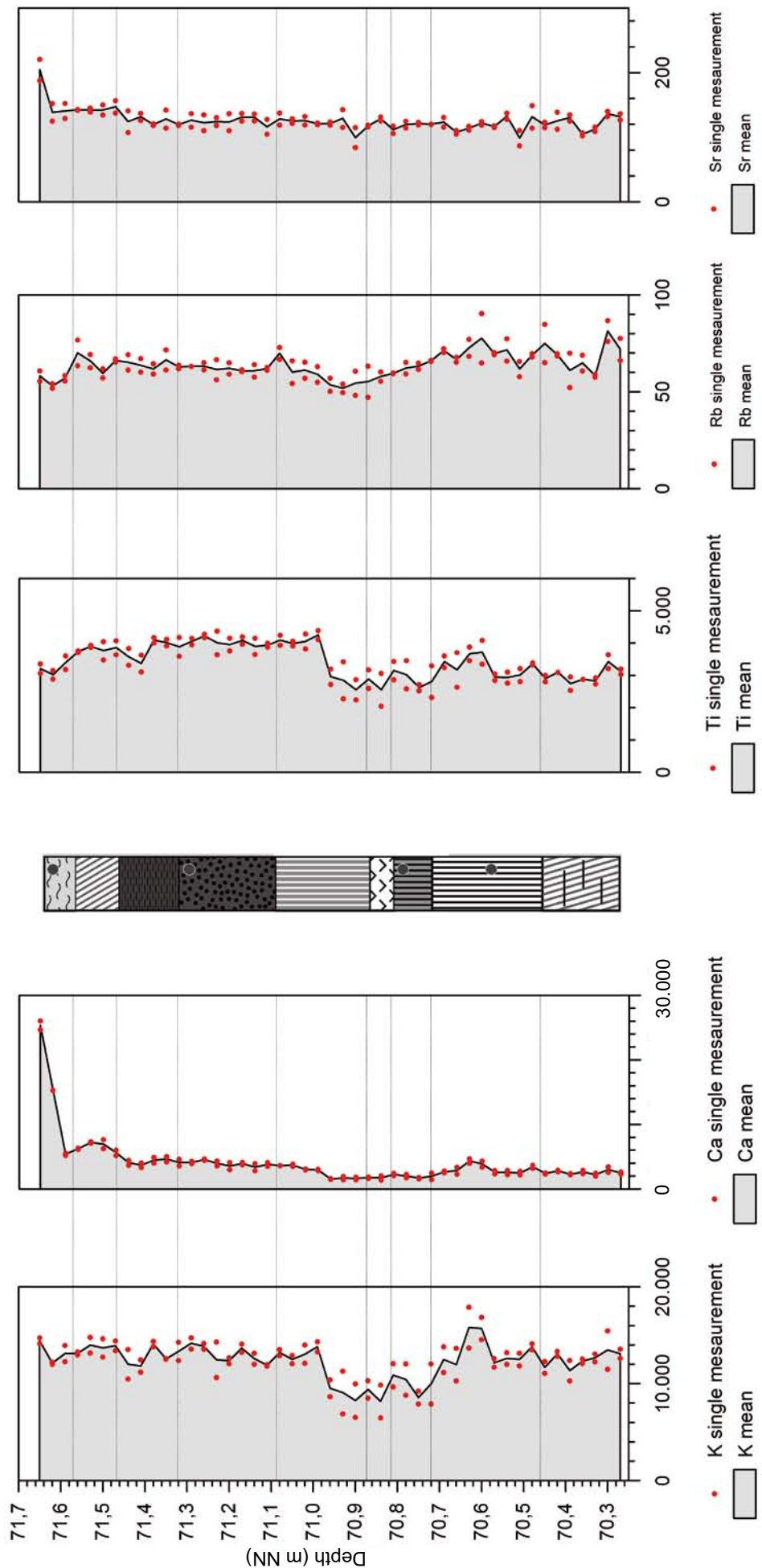


Fig. 8: Element concentrations determined for the loess/paleosol record of Gärzweiler/Elsbach valley. Each sample was measured twice and mean values were calculated. Lithological/Pedological legend according to Figure 3.
 Abb. 8: Elementgehalte der Löss-Paläoboden-Sequenz von Gärzweiler/Elsbachtal. Alle Proben wurden zweifach gemessen und Mittelwerte gebildet. Lithologisch-pedologische Legende gemäß der Darstellung in Abbildung 3.

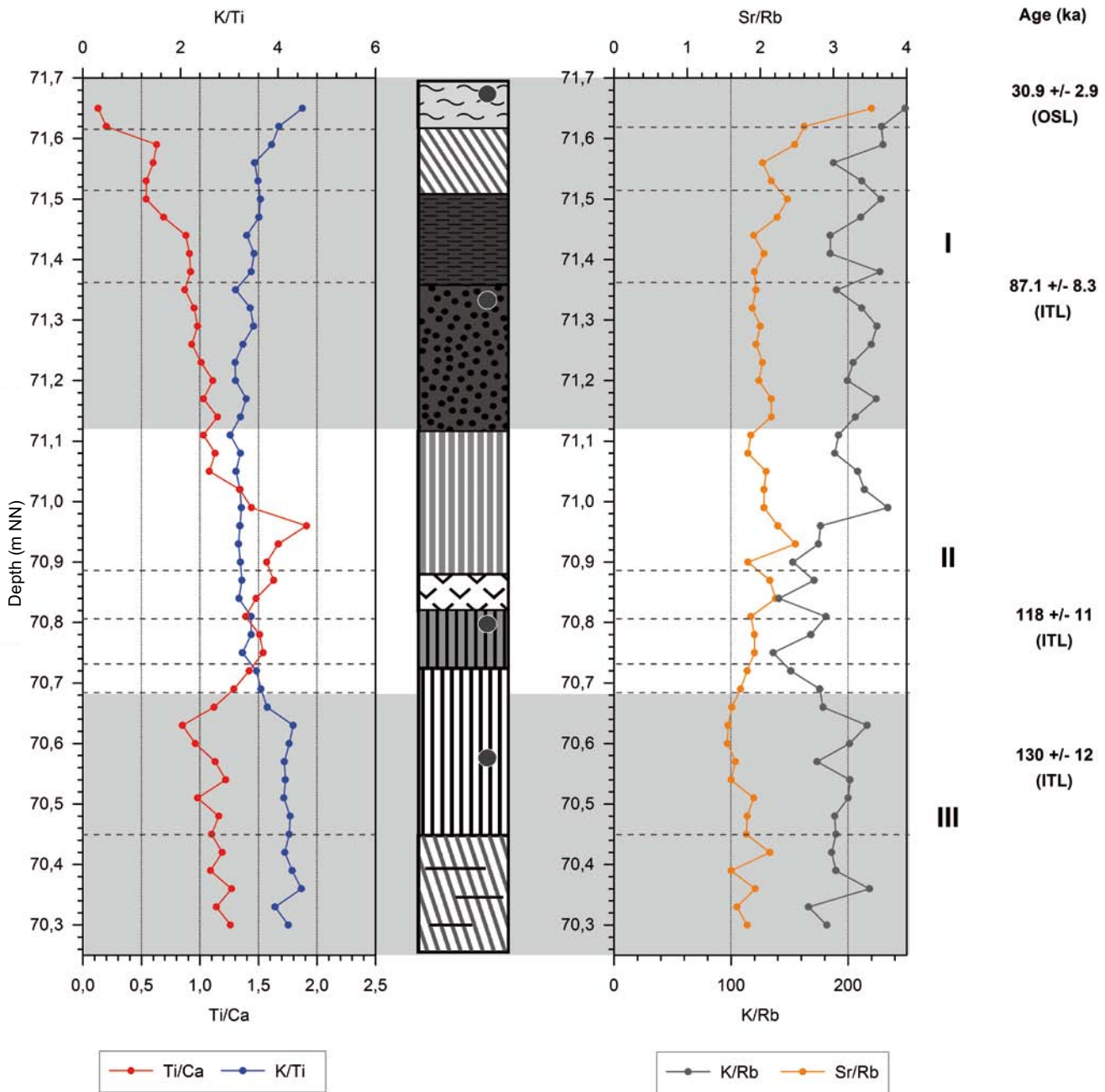


Fig. 9: Selected element ratios in the loess/palaeosol record of Garzweiler/Elsbach valley showing different soil formation processes including weathering degrees. Lithological/Pedological legend according to Figure 3. Units I-III are described in the text.

Abb. 9: Ausgewählte Elementverhältnisse aus der Löss/Paläoboden-Sequenz von Garzweiler/Elsbachtal, an denen sich bodenbildende Prozesse und Verwitterungsintensitäten ableiten lassen. Lithologisch-pedologische Legende gemäß der Darstellung in Abbildung 3. Die Einheiten I-III werden im Text erläutert.

Ti/Ca ratio and a maximum peak within the stagnic AhE horizon. This implicates in situ weathering processes for Unit II. Clay dislocation towards the weak humic Bht-horizon and the top of unit III as based on field evidence is also indicated by the decreasing trend of the K/Rb ratio.

The third unit consists of the well developed Btg horizon and the lamellic Bw horizon. Within this unit clay illuviation is reflected in the K/Ti, K/Rb and Sr/Rb ratios.

Luminescence dating (for labelling and position of the samples cp. Fig. 3) yielded quartz ITL ages of 130 ± 12 ka for the parent material of the Btg horizon (unit III, sample FR 1) and 118 ± 11 ka for the humic Bt horizon (unit II, sample FR 2), respectively.

The sediment superimposed by the rust spotted Ah horizon yielded an ITL-age of 87.1 ± 8.3 ka (unit I, sample FR 4). Sample FR 6 out of the reworked loess and soil material provided an OSL-age of 30.9 ± 2.9 ka. In this sample, the ITL-age (79.0 ± 7.4) clearly overestimates the quartz OSL age (Tab. 2). Most likely, this can be explained by the reworked nature of the sediment. The short transport distance might have been insufficient to reset the harder to bleach ITL-signal, but was adequate to effectively bleach the quartz OSL signal. In addition, the possibility of sensitivity changes during ITL-measurements has to be taken into account, which may have led to overestimation of all ITL ages (cp. Section 3.2). The uppermost sample (FR 10)

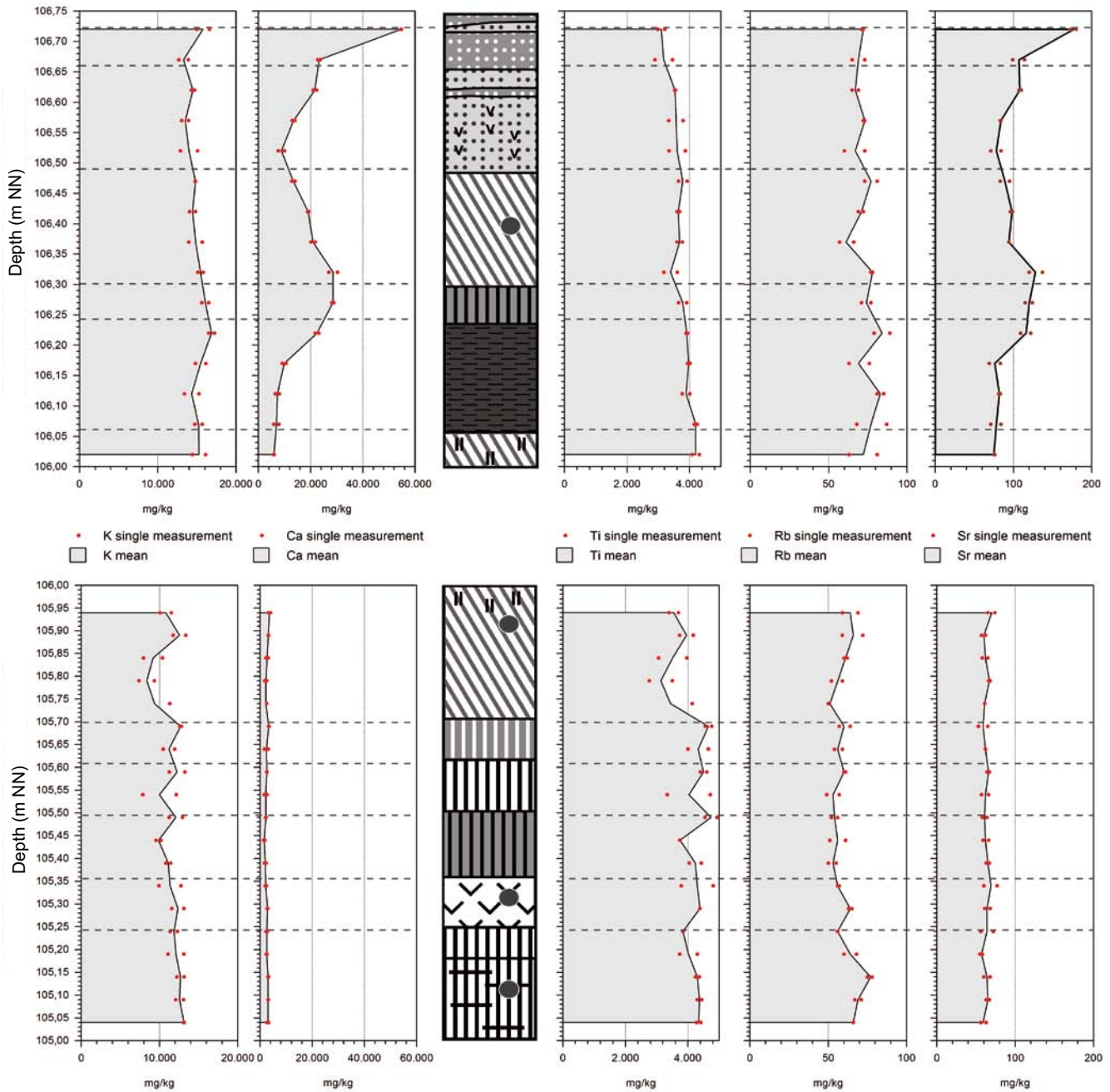


Fig. 10: Element concentrations determined for the loess/palaeosol record of Inden-Altdorf. Each sample was measured twice and mean values were calculated. Lithological/Pedological legend according to Figure 5.

Abb. 10: Elementgehalte der Löss-Paläoboden-Sequenz von Inden-Altdorf. Alle Proben wurden zweifach gemessen und Mittelwerte gebildet. Lithologisch-pedologische Legende gemäß der Darstellung in Abbildung 5.

out of reworked calcareous loess sediments yielded an OSL age of 25.4 ± 2.5 ka.

For the Inden-Altdorf sequence, five geochemical units can be differentiated based on the element contents and the calculated ratios (Figs. 10, 11). The first unit comprises hydromorphically stained loess sediments, which are superimposed by a rust spotted Gelic Gleysol in the upper part of the analytical sequence. The second unit consists of the reworked loess and soil material, the weak humic Bt horizon and the upper part of the Ah horizon. The Ti/Ca ratio shows a minimum on top of the weak humic Bt horizon correlating with a maximum in the Sr/Rb ratio. This alteration in the values is accompanied by an increasing proportion

of the sand fraction (Fig. 12, top). Within the weak humic Bt horizon an enrichment of potassium is indicated by a slight increase in the K/Ti and the K/Rb ratios correlating with a decreasing proportion of the sand fraction and an increase of the fine fraction.

The third unit comprises the lower part of the Ah horizon, the reworked layer and the underlying stagnic AhE horizon and is characterised by comparable tendencies within the ratios as described for the first unit. In contrast the Ti/Ca values are significantly higher. The humic upper part of this unit shows increasing clay content (cp. Fig. 12), which is also reflected in potassium enrichment relative to titanium.

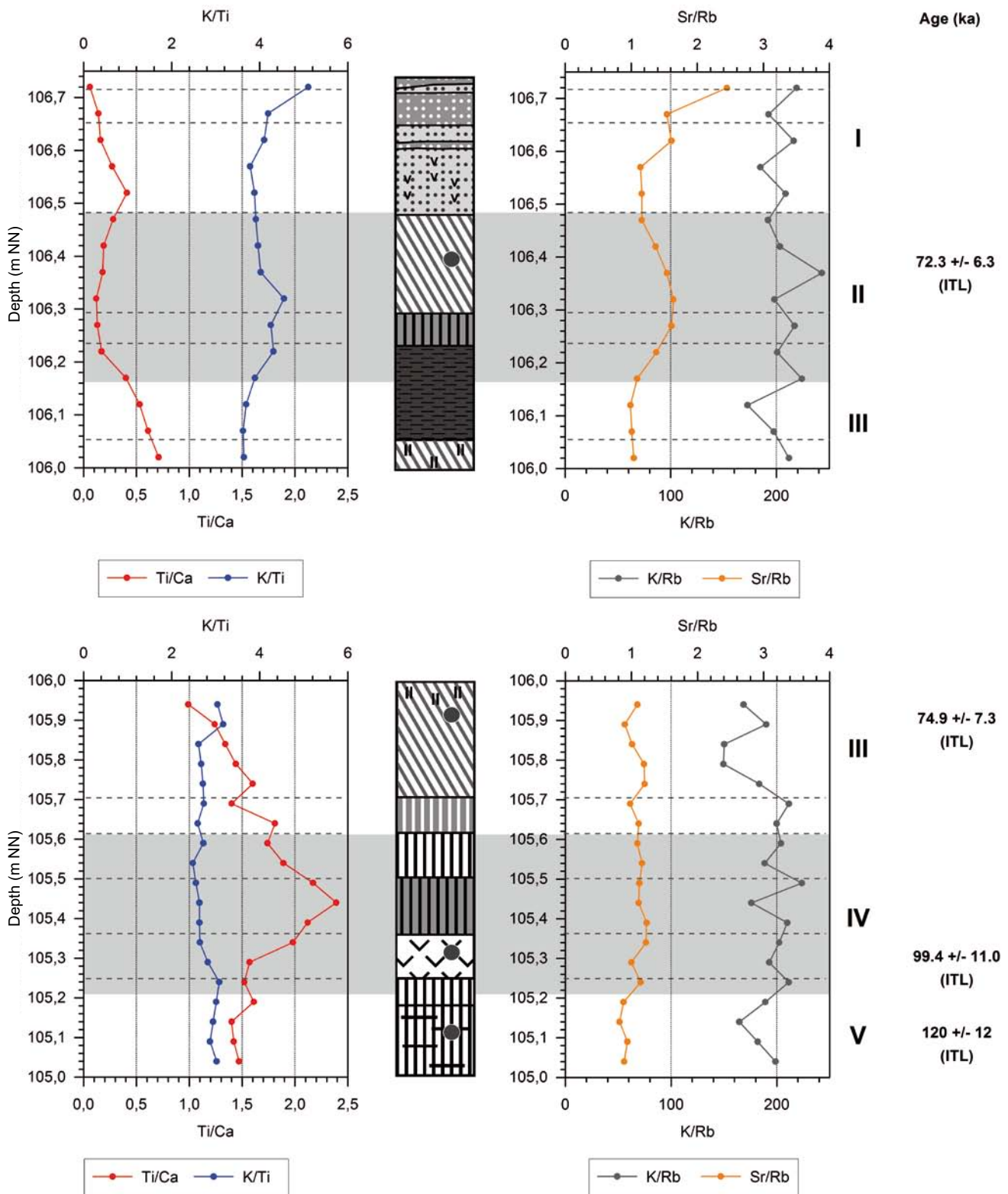


Fig. 11: Selected element ratios in the loess/palaeosol record of Inden-Altdorf showing different soil formation processes including weathering degrees. Lithological/pedological legend according to Figure 5. Units I-V are described in the text.

Abb. 11: Ausgewählte Elementverhältnisse aus der Löss/Paläoboden-Sequenz von Inden-Altdorf, an denen sich bodenbildende Prozesse und Verwitterungsintensitäten ableiten lassen. Lithologisch-pedologische Legende gemäß der Darstellung in Abbildung 5. Die Einheiten I-V werden im Text erläutert.

Within the fourth unit, containing the weak Bt, the humic Bt horizon, the bleached stagnic horizon and the uppermost part of the Btg horizon, a distinct maximum in the Ti/Ca values is noticed. Simultaneously the potassium content slightly decreases in relation to the titanium content.

Including the low K/Rb ratio this is associated with a reduced amount of clay. The lowermost unit (unit V) contains the lower part of the Btg and the lamellic Bt horizon. It is characterised by increasing clay contents. This increase is displayed in all selected ratios (cp. Fig. 11).

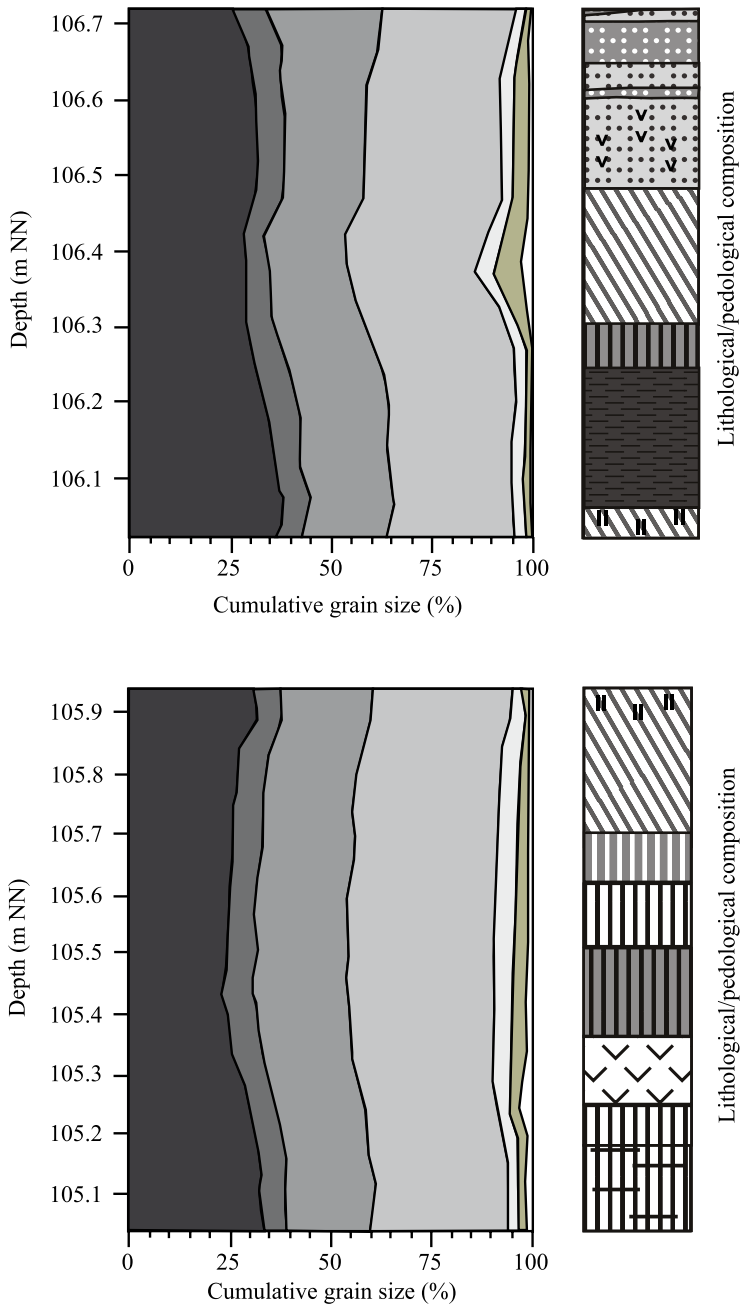


Fig. 12: Grain size distribution of the loess/palaeosol record of Inden-Altdorf. Lithological/pedological legend according to Figure 5. (T: clay, fU: fine silt, mU: medium silt, gU: coarse silt, fS: fine sand, mS: medium sand, gS: coarse sand, according to AG Boden, 2005)

Abb. 12: Korngrößenverteilung in der Löss/Paläoboden-Sequenz von Inden-Altdorf. Lithologisch-pedologische Legende gemäß der Darstellung in Abbildung 5. (Korngrößenklassen gemäß AG Boden 2005)

Luminescence dating (for labelling and position of the samples cp. Fig. 5) yielded an ITL-age of 120 ± 12 ka for the lowermost sample out of the lamellic Bt horizon (unit V, sample WW 1). Sample WW 2 obtained within the bleached stagnic horizon (unit 4) yielded an ITL-age of 99.4 ± 11 ka. For sample WW 5 an ITL-age of 74.9 ± 7.3 ka below the Ah horizon and 72.3 ± 6.8 ka above the Ah-horizon (sample WW 7) was determined. As for the Elsbach valley section ITL-measurements applied to the samples from the Inden-Altdorf section have to be viewed critically due to a possible overestimation of the true deposition age.

5 Discussion

In both investigated sequences, the lowermost Bt horizon, which presumably correlates with the last interglacial, is overlain by further weak Bt horizons of truncated Luvisols, stagnic and humic horizons, most likely correlating with the Lower Weichselian.

The age estimations obtained in the present study provide a chronostratigraphical frame for the period mentioned above, but the data set is small so far, and the ITL-ages are not totally reliable at this stage of the study. Additional measurements using the ITL-approach as well as measurements on the feldspar fraction have recently been conducted to evaluate the presented data set. Beside luminescence dating, for the first time, ratios derived from multi element analyses are included in the interpretation of loess/palaeosol records from the Lower Rhine area. The ratios show that the geochemical units (cp. Figs. 9, 11) partially exceed beyond horizon boundaries as derived from field observations and thus indicate polygenetic soil formation, which has to be further investigated by means of soil micromorphology.

The element ratios obtained for the lower unit of the Elsbach valley record show Bt features superimposed by secondary clay illuviation, which was also noticed in the field in terms of clay coatings. It could be hypothesised that

(i) relocation of a well developed Bt horizon occurred followed by postsedimentary pedogenetic processes; (ii) relocation of pre-weathered soil sediment (showing no Bt features, e.g. Bw, Cw horizons) was followed again by postsedimentary pedogenetic processes leading to the formation of Bt features or (iii) input or relocation of “unweathered”, calcareous and laminated sediments as parent material was superimposed by soil formation. Here, investigations on thin sections would be helpful to clarify the formation scenario.

The results obtained for the lower part of the Inden-Altdorf record indicate secondary (postsedimentary) pedogenetic processes in terms of clay illuviation as well.

The overlying sequence in both records is characterized by a distinct maximum of the Ti/Ca ratios (Unit II in the Elsbach valley record, Unit IV in the Inden-Altdorf record). In the Elsbach valley this peak is developed within an AhE horizon, in Inden-Altdorf within a weak humic Bt horizon. The element ratios, especially the Ti/Ca ratio as well as the ITL data indicate an input of allochthonous (pre-weathered) soil sediments. Secondary pedogenetic processes such as clay enrichment are reflected in the K/Ti and the K/Rb ratios, and are attended by decreasing clay contents in the overlying units. The observed unconformities on top of the lowermost Bt features support the assumption of allochthonous soil sediment relocation.

In contrast to Inden-Altdorf a weakly developed humic Bt horizon below the unconformity at 70.9 m (cp. Fig. 3) is described for the Elsbach valley record superimposing the underlying Bt-features. The ITL age of 118 ± 11 ka (sample FR 2) indicates a Late Eemian or Early Weichselian depositional age. Within the Inden-Altdorf sequence the sediments of the bleached stagnic horizon, where archaeological findings were imbedded yielded an age of 99 ± 11 ka, indicating a Lower Weichselian age.

The uppermost unit of the Elsbach valley section is characterised by the most intensive weathering within the whole sequence as displayed in the Ti/Ca ratio. Especially the high values of the K/Rb ratio imply the (re-) deposition of soil sediments (cp. section 3.2, section 4). The precipitation of secondary carbonate (leading to a masking of the Ti-derived weathering index) indicates leaching of carbonates from the hanging layers. For the parent material the ITL age of 87.1 ± 8.3 ka out of the rust spotted humic horizon is available, allowing a correlation with the Lower Weichselian. Distinct reworking processes are noticed in the uppermost part of the record as well as in the analytical sequence. The OSL age of 30.9 ± 2.9 ka indicates sediment accumulation during increased geomorphogenic activity towards the onset of MIS 2, in which older sediments and soils were relocated. The layer intercalated between the sandy reworked loess and soil sediments and the uppermost humic horizon most likely contains reworked soil sediments of the Middle Weichselian.

In the Inden-Altdorf section on top of the uppermost humic horizon, superimposed by a weak humic Bt horizon, the ITL age of 72.3 ± 6.8 ka within the reworked layer indicates a deposition of the parent material at the onset of MIS 4. Based on the Ti/Ca and Sr/Rb ratio, an increase in carbonate content can be assumed, which could be due to secondary precipitation from the hanging, calcareous loess sediments or reflects an input of weakly weathered mate-

rial. Clay enrichment corresponding with the macroscopically indentified weak Bht horizon is reflected by the K/Ti and the K/Rb ratios, which increase in the uppermost part of the underlying humic horizon.

In summary multiple sediment re-deposition and polygenetic pedological processes have to be considered for both records displaying the complexity of the investigated sequences. This leads to difficulties in correlation with existing stratigraphical schemes in the Lower Rhine area.

SCHIRMER (at last 2010) describes the MIS 5 pedocomplex as Rocourt Solcomplex, consisting of four Bt horizons, three humic and three stagnic horizons on top of each Bt horizon. The pedocomplex was denominated after the well known type locality Rocourt in the northwest of Liège (Belgium) by GULLENTOPS (1954).

However, focusing on the Eemian to Early Weichselian period, only few luminescence data are available for the Lower Rhine area. The published luminescence ages are mainly based on IRSL-dating of feldspars or on thermoluminescence (TL), measured with multiple aliquot protocols (e.g. ZÖLLER et al. 1988; ZÖLLER 1989; JANOTTA 1991; FRECHEN et al. 1992; HENZE 1998). A detailed discussion of different luminescence dating protocols for the investigated records is in preparation.

Based on field evidence the soil sediments on top of the uppermost humic horizon in Inden-Altdorf most likely correlate with the lower Keldach loess as described by SCHIRMER (e.g. 2002), which is also defined as Niedereschbach Zone in the Rhine-Main area (SEMML 1968). In the record of the Elsbach valley the uppermost unconformity on top of the reworked soil sediments of the Middle Weichselian most likely corresponds with the so called Eben-unconformity with the Eben Zone sensu SCHIRMER (e.g. 2003) on top. Comparable distinct erosional phases dating to the early Upper Weichselian are described for example by SEMML (1989) and MEYER & ROHDENBURG (1982). A detailed correlation of the lower part of the sequences remains uncertain. The humic horizons most likely correlate with the Mosbacher Humuszonen of the Lower Weichselian sensu SCHÖNHALS et al. (1964) which are correlated to the Pesch, Holz and Titz humus zones (SCHIRMER, e.g. 2002). These humic zones partially show basal B(t) horizons. The uppermost humic layers in the records under study possibly correlates with the (re-worked) “Titz” humus zone, in Garzweiler followed by the rust spotted “Holz” humus zone with the “Holz” soil underneath. The stratigraphical relevance of the weak humic Bt horizon on top of the uppermost humic horizon in Inden as well as the weak humic Bt horizon on top of the distinct Bt features in Garzweiler needs further clarification.

Following Schirmer's description and interpretation the Rocourt Solcomplex is developed as relatively thin pedocomplex in flat relief positions whereas soil divergence occurs towards the slope toe and in small depressions (SCHIRMER 2010: 37). In the latter positions the most complete stratigraphical records can be observed.

So called syn-solcomplex erosion results in a truncation of Luvisols, which is associated with the onset of cold periods (breviglacials sensu SCHIRMER 1999) leaving erosional remnants of the pedocomplex behind. Within these cold periods dust accumulation occurred resulting in a separation of the fossil soils by thin loess sediments. It is assumed

that small depressions as well as foot slope positions remain more protected from erosion than other geomorphological positions (SCHIRMER 2010: 34). The results presented here do not support this observation: The occurrence of soil sediments in slope positions as demonstrated for the records under study indicate that spreading of sequences does not generally reflect the climate conditions during soil formation but possibly represent erosional events. Both records are located in some distance to the (palaeo-) watershed position, hence were affected by active slope formation processes in transition periods from stable to unstable morphodynamic conditions. The soil horizons possibly do not represent relics of in situ formation, but originate from soil sediments as indicated by discordant bedding. Especially in foot slope positions and depressions, which are characterised by enhanced water percolation, pedogenesis should lead to an even stronger alteration of accumulated sediments resulting in a greater variety of diagnostic soil characteristics than observed.

The interplay of morphogenetic processes according to the relief position with the polygenetic superimposition of truncated palaeosols stresses the need for a comprehensive geomorphological/pedological analysis of comparable sequences for a sound chronostratigraphical and palaeoclimatical interpretation (cp. FRECHEN, TERHORST & RÄHLE 2007; STEPHAN 2000).

6 Conclusion

The geomorphological and palaeoclimatological interpretation of pedocomplexes of the Eemian and Lower Weichselian is a complex task not only leading to problems in chronostratigraphical correlation of archaeological records incorporated in these layers. The multi-element screening is a promising tool to characterise sediments and soils within loess/palaeosol records of the Lower Rhine area.

The applicability of luminescence techniques to create a more reliable chronostratigraphical frame for the time period under investigation still needs further research, especially for loess sediments with equivalent doses in or close to the OSL-saturation level. The applied ITL-approach does not argue against the observed litho- and pedostratigraphy. However, possible sensitivity changes not detected and corrected might pose a problem for the interpretation of obtained ages. Possibly, the application of the single aliquot regeneration and added dose procedure (SARA) within the ITL-approach as suggested by BUYLAERT et al. (2006) can help to investigate the reliability of the ages presented here.

For the archaeological find layer at the site of Inden-Altdorf it is concluded that it did not occur in autochthonous position but rather was incorporated in soil sediments of Lower Weichselian age. This conclusion contrasts the interpretation of the supervising archaeologists (cp. THISSEN 2007; PAWLICK & THISSEN 2011). Despite the archaeological evidence, in the publication by PAWLICK & THISSEN (2011:71) the find layer and the upper part of the interglacial soil are described as "reworked" by M. Kehl based on field evidence and micromorphological studies. In addition preliminary IRSL-data produced by M. Frechen yield Lower Weichselian ages. These details are not being further discussed by

PAWLICK & THISSEN (2011) but clearly support the conclusions drawn here.

The results show that within the Lower Weichselian of the Lower Rhine area multiple sediment deposition and/or relocation events are documented, delivering the parent material for polygenetic soil formation.

Main objectives of future studies should be the accurate differentiation of primary sediments, in situ soils and relocated soil sediments prior to stratigraphical correlation, using a wide methodological spectrum. In addition, the morphological position and the palaeorelief in the surrounding of investigated loess/palaeosol sequences require more attention in future studies.

7 Acknowledgments

Funding of the "Stiftung Archäologie im Rheinischen Braunkohlerevier" in context of the project "Paläolithikum im Indetal" (Proposal number 173) is appreciated. Furthermore we thank the two reviewers for helpful comments to improve the manuscript and Dr. Johanna Lomax, Vienna, for linguistic improvements.

8 References

- AG BODEN (2005): Bodenkundliche Kartieranleitung (5. Auflage). – 438 S.; Hannover (BGR).
- AHORNER, L. (1962): Untersuchungen zur quartären Bruchtektonik der Niederrheinischen Bucht. – Eiszeitalter und Gegenwart, 13: 24–105.
- BOENIGK, W. & FRECHEN, M. (1995): Lumineszenz-Datierungen an kolluvialen Sedimenten des Elsbachtals. – Bonner Jahrbücher, 195: 299–312.
- BOKHORST, M.P., BEETS, C.J., MARKOVIĆ, S.B., GERASIMENKO, N.P., MATVIJSHINA, Z.N. & FRECHEN, M. (2009): Pedo-chemical climate proxies in Late Pleistocene Serbian-Ukrainian loess sequences. – Quaternary International, 198: 113–123.
- BØTTER-JENSEN, L., MCKEEVER, S.W.S. & WINTLE, A.G. (2003): Optically Stimulated Luminescence Dosimetry. – 404 S.; Amsterdam (Elsevier).
- BRUNNACKER, K. (1967): Grundzüge einer Löß- und Bodenstratigraphie am Niederrhein. – Eiszeitalter und Gegenwart, 18: 142–151.
- BUGGLE, B., GLASER, B., ZÖLLER, L., HAMBACH, U., MARKOVIĆ, S., GLASER, I. & GERASIMENKO, N. (2008): Geochemical characterization and origin of Southeastern and eastern European loesses (Serbia, Romania, Ukraine). – Quaternary Science Reviews, 27: 1058–1075.
- BUGGLE, B., GLASER, B., HAMBACH, U., GERASIMENKO, N. & MARKOVIĆ, S. (2010): An evaluation of geochemical weathering indices in loess-paleosol studies. – Quaternary International, 240: 12–21.
- BUYLAERT, J. P., MURRAY, A. S., HUOT, S., VRIEND, M. G. A., VANDENBERGHE, D., DE CORTE, F. & VAN DEN HAUTE, P. (2006): A comparison of quartz OSL and isothermal TL measurements on Chinese loess. – Radiation Protection Dosimetry, 119: 474–478.
- BUYLAERT, J.P., MURRAY, A.S., VANDENBERGHE, D., VRIEND, M., DE CORTE, F. & VAN DEN HAUTE, P. (2008): Optical dating of Chinese loess using sand-sized quartz: Establishing a time frame for Late Pleistocene climate changes in the western part of the Chinese Loess Plateau. – Quaternary Geochronology, 3: 99–113.
- CHOI, J.H., MURRAY, A.S., CHEONG, C.S., HONG, D.G. & CHANG, H.W. (2006): Estimation of equivalent dose using quartz isothermal TL and the SAR procedure. – Quaternary Geochronology, 1: 101–108.
- DERBYSHIRE, E., KEMP, R & MENG, X (1995): Variations in loess and palaeosols properties as indicators of palaeoclimatic gradients across the Loess Plateau of North China. – Quaternary Science Reviews, 14: 681–697.
- FISCHER, P. (2010): Zur mittel- und jungquartären Relief- und Bodenentwicklung der nordwestlichen Kölner Bucht – Detailuntersuchungen der lössbedeckten Mittelterrassenlandschaft. – Dissertation Universität zu Köln, 253 S.; Köln. <http://kups.ub.uni-koeln.de/volltexte/2010/3030/>.
- FRECHEN, M., BOENIGK, W. & WEIDENFELLER, M. (1995): Chronostratigraphie des „Eiszeitlichen Lößprofils“ in Koblenz-Metternich. – Mainzer geowissenschaftliche Mitteilungen, 24: 155–180.

- FRECHEN, M., BRÜCKNER, H. & RADTKE, U. (1992): A comparison of different TL-techniques on loess samples from Rheindahlen (F.R.G.). – *Quaternary Science Reviews*, 11: 109–113.
- FRECHEN, M., TERHORST, B. & RÄHLE, W. (2007): The Upper Pleistocene loess/palaeosol sequence from Schatthausen in North Baden-Württemberg. – *E&G Quaternary Science Journal*, 56 (3): 212–227.
- GALBRAITH, R.F., ROBERTS, R.G., LASLETT, G.M., YOSHIDA, H. & OLLEY, J.M. (1999): Optical dating of single and multiple grains of quartz from Jinmium Rock Shelter, Northern Australia: Part I, Experimental design and statistical models. – *Archaeometry*, 41: 339–364.
- GALLET, S., JAHN, B. & TORII, M. (1996): Geochemical characterization of the Luochuan loess-palaeosol sequence, China, and its paleoclimatic implications. – *Chemical Geology*, 133: 157–172.
- GULLENTOPS, F. (1954): Contribution à la chronologie du Pleistocene et des formes du relief en Belgique. – *Mémoires de l' Institut géologique de l' Université de Louvain*, 18: 125–252.
- HENZE, N. (1998): Kennzeichnung des Oberwürmloesses in der Niederrheinischen Bucht. – *Kölner Forum für Geologie und Paläontologie*, 1: 212 S.; Geologisches Institut der Universität zu Köln.
- HOODA, P. [ed.] (2010): *Trace Elements in Soils*. – 616 S.; Chippenham, Wiley.
- JAIN, M., MURRAY, A.S. & BØTTER-JENSEN, L. (2007): Dose response, thermal stability and optical bleaching of the 310°C isothermal TL signal in quartz. – *Radiation Measurements*, 42: 1285–1293.
- JANOTTA, A. (1991): Thermolumineszenzdatierungen als chronometrischer Beitrag zur stratigraphischen Beschreibung von Lößprofilen. – *Düsseldorfer Geographische Schriften*, 30: 116 S.
- KABATA-PENDIAS, A. (2010): *Trace Elements in Soils and Plants*. – 4. ed., 520 S.; Boca Raton (CRC Press).
- KELS, H. (2007): Bau und Bilanzierung der Lössdecke am westlichen Niederrhein. – Dissertation Universität Düsseldorf: 206 S.; Düsseldorf. <http://docserv.uni-duesseldorf.de/servlets/DocumentServlet?id=3628>.
- KELS, H., KEHL, M., LEHMKUHL, F., TEGTMEIER, U. & THISSEN, J. (2009): Naturwissenschaftliche Untersuchungen zum mittelpaläolithischen Camp von Inden-Altdorf. – *Archäologie im Rheinland*, 2008: 36–39.
- KOSTER, E. A. (2005): Recent Advances in Luminescence Dating of Late Pleistocene (Cold-Climate) Aeolian Sand and Loess Deposits in Western Europe. – *Permafrost and Periglacial Processes*, 16: 131–143.
- LÖHR, H. & BRUNNACKER, K. (1974): Metternicher und Eltviller TuffHorizont im Würmlöß am Mittel und Niederrhein. – Notizblatt des hessischen Landesamtes für Bodenforschung., 102: 168190.
- LUI, T. (1985): *Loess and the Environment*. – 251 S.; Beijing (China Ocean Press).
- LUI, T. (1991): *Loess, Environment and Global Change*. – 288 S. Beijing (Beijing Science Press).
- MEYER, B. & ROHDENBURG, H. (1982): Paläoböden der südniedersächsischen Lößgebiete. – *Geologisches Jahrbuch*, F 14: 298–309.
- MURRAY, A.S., WINTLE, A.G. (2000): Luminescence dating of quartz using an improved single-aliquot regenerative-dose protocol. – *Radiation Measurements*, 32: 57–73.
- PAAS, W. (1961): Rezente und fossile Böden auf niederrheinischen Terrassen und deren Deckschichten. – *Eiszeitalter und Gegenwart*, 12: 165–230.
- PAAS, W. (1968a): Gliederung und Altersstellung der Lösse am Niederrhein. – Fortschritte in der Geologie von Rheinland und Westfalen, 16: 185–196.
- PAAS, W. (1968b): Stratigraphische Gliederung des Niederrheinischen Lösses und seiner fossilen Böden. – *Decheniana*, 121 (1/2): 9–38.
- PAWLIK, A. F. & THISSEN, J. (2011): The 'Palaeolithic Prospection in the Inde Valley' Project. – *Quaternary Science Journal* (Eiszeitalter und Gegenwart), 60: 66–77.
- PÉCSI, M. & RICHTER, G. (1996): Löss – Herkunft, Gliederung, Landschaften. – *Zeitschrift für Geomorphologie*. N. F., Suppl.- Bd., 98: 391 S.; Berlin, Stuttgart.
- PRESCOTT, J.R. & HUTTON, J.T. (1994): Cosmic ray contributions to dose rates for luminescence and ESR dating: large depth and long time variations. – *Radiation Measurements*, 23: 497–500.
- PREUSSER, F., DEGERING, D., FUCHS, M., HILGERS, A., KADEREIT, A., KLASEN, N., KRIBETSCHKE, M., RICHTER, D. & SPENCER, J. (2008): Luminescence dating: Basics, methods and applications. – *E&G Quaternary Science Journal*, 57 (1/2): 95–149.
- REMY, H. (1960): Der Löß am unteren Mittel- und Niederrhein. – *Eiszeitalter und Gegenwart*, 11: 107–120.
- ROBERTS, H. M. (2008): The development and application of luminescence dating to loess deposits: a perspective on the past, present, future. – *Boreas*, 37: 483–507.
- ROHDENBURG, H. & MEYER, B. (1966): Zur Feinstratigraphie und Paläopedologie des Jungpleistozäns nach Untersuchungen an südniedersächsischen und nordhessischen Lössprofilen. – *Mitteilungen der Deutschen Bodenkundlichen Gesellschaft*, 5: 1–137.
- SCHIRMER, W. (1999): Kaltzeiten und Warmzeiten im Löß. – In: BECKER-HAUMANN, R. & FRECHEN, M. [eds.]: *Terrestrische Quartärgeologie*. – 81–100; Köln (Logabook).
- SCHIRMER, W. (2000a): Rhein loess, ice cores and deep-sea cores during MIS 2–5. – *Zeitschrift der Deutschen Geologischen Gesellschaft*, 151: 309–332.
- SCHIRMER, W. (2000b): Eine Klimakurve des Oberpleistozäns aus dem rheinischen Löss. – *Eiszeitalter und Gegenwart*, 50: 25–49.
- SCHIRMER, W. (2002): Compendium of the Rhein loess sequence. – In: IKINGER, A. & SCHIRMER, W. [eds.]: *Loess units and solcomplexes in the Niederrhein and Maas area*. – *Terra Nostra*, 2002 (1): 8–23.
- SCHIRMER, W. (2003): Die Eben-Zone im Oberwürmloß zwischen Maas und Rhein. – In: SCHIRMER, W. [ed.]: *Landschaftsgeschichte im Europäischen Rheinland*. GeoArchaeoRhein, 4: 351–416.
- SCHIRMER, W. (2010): Interglacial complex and solcomplex. – *Central European Journal of Geosciences*, 2: 32–40.
- SCHIRMER, W. & KELS, H. (2002): Browncoal opencast mine Garzweiler. – In: IKINGER, A. & SCHIRMER, W. [eds.]: *Loess units and solcomplexes in the Niederrhein and Maas area*. – *Terra Nostra*, 2002 (1): 57–65, 102–104.
- SCHÖNHALS, E., ROHDENBURG, H. & SEMMEL, A. (1964): Ergebnisse neuerer Untersuchungen zur Würmloß-Gliederung in Hessen. – *Eiszeitalter und Gegenwart*, 15: 199–206.
- SCHULZ, W. (2007): Die Kolluvien der westlichen Kölner Bucht: Gliederung, Entstehungszeit und geomorphologische Bedeutung. – Dissertation Universität zu Köln: 218 S.; Köln. <http://kups.ub.uni-koeln.de/1965/>.
- SEMMEL, A. (1968): Studien über den Verlauf jungpleistozäner Formung in Hessen. – *Frankfurter Geographische Hefte*, 45: 133 S.
- SEMMEL, A. (1989): The importance of loess in the interpretation of geomorphological processes and for dating in the federal Republic of Germany. – *Catena*, Suppl., 15: 179–188.
- SINGHVI, A. K., BLUSZCZ, A., BATEMAN, M. D. & SOMESHWAR RAO, M. (2001): Luminescence dating of loess-palaeosol sequences and coversands: methodological aspects and palaeoclimatic implications. – *Earth-Science Reviews*, 54: 193–211.
- SMALLEY, I. J., JEFFERSON, I. F., DIJKSTRA, T. A. & DERBYSHIRE, E. (2001): Some major events in the development of the scientific study of loess. – *Earth Science Reviews*, 54: 5–18.
- SMYKATZ-KLOSS, B. (2003): Die Lößvorkommen des Pleiser Hügellandes bei Bonn und von Neustadt/Wied sowie der Picardie: Mineralogisch-geochemische und geomorphologische Charakterisierung, Verwitterungs-Beeinflussung und Herkunft der Lösse. – Dissertation Universität Bonn: 343 S.; Bonn. <http://hss.ulb.uni-bonn.de/90/2003/0308/0308.htm>.
- SMYKATZ-KLOSS, W., SMYKATZ-KLOSS, B., NAGUIB, N. & ZÖLLER, L. (2004): The reconstruction of paleoclimatological changes from mineralogical and geochemical compositions of loess and alluvial loess profiles. – In: SMYKATZ-KLOSS, W. & FELIX-HENNINGSSEN, P. (eds): *Palaeoecology of Quaternary Drylands*. Lecture Notes in Earth Sciences, 102: 101–118.
- STEPHAN, S. (2000): Bt-Horizonte als Interglazial-Zeiger in den humiden Mittelbreiten: Bildung, Mikromorphologie, Kriterien. – *Eiszeitalter und Gegenwart*, 50: 95–106.
- THISSEN, J. (2006): Mit dem Bagger in die Altsteinzeit – „Prospektion Paläolithikum im Indetal“ – Archäologie im Rheinland, 2005: 28–30.
- THISSEN, J. (2007): Ein Camp des Micoquien im Indetal bei Altdorf. – Archäologie im Rheinland, 2006: 42–45.
- UTHMEIER, T. (2006): Am Ufer lauert der Tod – Jagdplätze des Neandertalers in der niederrheinischen Bucht: Ergebnisse einer archäologischen Prospektion der Abbaukanten im rheinischen Braunkohlerevier. – In: UELSBERG, G. (ed.): Roots/Wurzeln der Menschheit: 269–288.
- WINTLE, A.G. & MURRAY, A.S. (2006): A review of quartz optically stimulated luminescence characteristics and their relevance in single-aliquot regeneration dating protocols. – *Radiation Measurements*, 41: 369–391.
- ZÖLLER, L. (1989): Geomorphologische und geologische Interpretation von Thermolumineszenz-Daten. – Bayreuther geowissenschaftliche Arbeiten, 14: 103–112.
- ZÖLLER, L., STREMME, H. E. & WAGNER, G. A. (1988): Thermolumineszenz-Datierung an Löß-Paläoboden-Sequenzen von Nieder-, Mittel- und Oberrhein. – *Chemical Geology*, 73: 39–62.
- ZÖLLER, L. & SEMMEL, A. (2001): 175 years of loess research in Germany – long records and “unconformities”. – *Earth-Sciences Reviews*, 54: 19–28.

Holzreste von spätglazialen Kiefern aus der tiefgründigen und tonreichen Permanentrutschung ‚Spiegelberg‘, Kanton Schwyz [Schweiz]

Conradin Zahno, Markus Gasser, Ruth Drescher-Schneider, Jakob Gasser, Christian Schlüchter

How to cite: ZAHNO, C.; GASSER, M.; DRESCHER-SCHNEIDER, R.; GASSER, J.; SCHLÜCHTER, C. (2012): Pine samples of late glacial age found in the sediments of the deep and clay-rich landslide ‘Spiegelberg’, Schwyz (Switzerland) – E&G Quaternary Science Journal, 61 (1): 64–68. DOI: 10.3285/eg.61.1.05

Kurzfassung: Die Hauptstrasse Nr. 8 zwischen Schwyz und Sattel verläuft durch aktive und tiefgründige Permanentrutschungen. Im lehmigen, matrix-gestützten Gehängeschutt der Rutschung ‚Spiegelberg‘ wurde zwischen 1979–81 die Gütschbrücke erstellt (LK: 690.314/211.943; 670 m ü.M.) und unter Anwendung von Gründungsschutzschächten im unterlagernden Fels fundiert. Beim Aushub des Schutzeschachtes für den Pfeiler WL-Nord wurden in der Tiefe von 25 m bzw. 38 m unter Oberkante Terrain zwei Nadelbaumfragmente gefunden. Letzterer Holzfund lag wenige Meter über der Felsoberfläche. Die ¹⁴C-Altersdatierung der Holzfunde (beide *Pinus sylvestris*) ergaben kalibrierte Altersspannen zwischen 11.690–11.270 cal. a BP (2σ) am Übergang vom Grönland Stadial 1 (GS-1; ‚Jüngere Dryas‘) zum Holozän bzw. 13.830–13.640 cal. a BP (2σ) zu Beginn der spätglazialen Wärmeschwankung GI-1c (Grönland Interstadial 1c; ‚Alleroed‘). Die vorliegenden Daten zeigen, dass die Hanginstabilitäten bei ‚Spiegelberg‘ nach dem Zerfall des letzteiszeitlichen Muota/Reussgletschers zu Beginn des Spätglazials eingesetzt haben mussten, und die Waldkiefer schon kurz nach den Kälterückschlägen des GI-1d („Aegelsee-Schwankung“) bzw. des GS-1 am nördlichen Alpenrand präsent war.

Pine samples of late glacial age found in the sediments of the deep and clay-rich landslide ‘Spiegelberg’, Schwyz [Switzerland]

Abstract: The main road H8 between Schwyz and Sattel crosses active landslide areas. The Gütsch bridge (Swiss coordinates: 690'314/211'943; 670 m asl.) was built in loamy matrix-supported sediments of the landslide area ‘Spiegelberg’ between 1979–81. Wood pieces were found during excavation of the foundation well for pillar ‘WL-Nord’ of which two samples were collected from 25 m and 38 m below surface, respectively. The bedrock surface i.e. the foundation base, was reached in 40 m below surface. The wood samples (both *Pinus sylvestris*) yielded calibrated radiocarbon ages between 11.690–11.270 cal. a BP (2σ) at the transition of the Greenland Stadial 1 (GS-1; ‘Younger Dryas’) to the Holocene and between 13.830–13.640 cal. a BP (2σ) i.e. the early interstadial GI-1c (Greenland Interstadial 1c; ‘Alleroed’), respectively. The data indicate that the slope instability at the SW slope of the Engelstock was initiated after the decay of the local Muota/Reuss Glacier at the beginning of the late glacial period. Our dating results demonstrate the presence of Pine at the northern alpine border shortly after the cold pulses GI-1d (i.e. ‘Aegelsee oscillation’) and GS-1, respectively.

Keywords: H8 Schwyz–Sattel, Steinen, Engelstock, subalpine molasse, landslide area, ¹⁴C-dating, late glacial, vegetation history

Addresses of authors: C. Zahno, Institut für Geologie, Universität Bern, Baltzerstrasse 1+3, CH-3012 Bern. Aktuelle Adresse: Sunnebergliweg 6, CH-6403 Küsnacht. E-Mail: conradin.zahno@gmx.net; M. Gasser, Tiefbauamt Kanton Schwyz, Abteilung Kunstbauten, Postfach 1251, CH-6431 Schwyz; R. Drescher-Schneider, Institut für Pflanzenwissenschaften der Karl-Franzens-Universität Graz, Holteigrasse 6, A-8010 Graz; J. Gasser, Kerngasse 4, CH-6442 Gersau; C. Schlüchter, Institut für Geologie, Universität Bern, Baltzerstrasse 1+3, CH-3012 Bern.

1 Einleitung

Die Hauptstrasse Nr. 8 Ingenbohl–Pfäffikon über den Sattelpass ist die wichtigste Verkehrsverbindung zwischen dem inneren und dem äusseren Teil des Kantons Schwyz (Abb. 1). Ab 1961 erfolgte der planmässige Ausbau des Strassenzugs, wobei geotechnische Herausforderungen in bekannten rutschgefährdeten Gebieten am Engelstock zwischen Schwyz und Sattel bautechnisch zu bewältigen waren (GASSER 1983a, 1983b).

Die Ausdehnung sowie die geotechnischen Eigenschaften der Rutschmassen wurden im Rahmen des Strassenausbauprojektes Hauptstrasse Nr. 8 Ingenbohl–Pfäffikon und einer Dissertation (YAVUZ 1996) untersucht. Die Ergebnisse dieser Arbeiten bilden die Grundlage für die vorliegende ergänzende Studie. Bisher konnte die Frage nach dem Al-

ter der Rutschungen von YAVUZ (1996) nicht angegangen werden, da geeignetes Probenmaterial für radiometrische Altersdatierungen wie eingeschuppte Holzreste oder überfahrene Humushorizonte, obwohl in Sondierprotokollen beschrieben, nicht mehr verfügbar waren.

Die zwischen 1979–81 gebaute Gütschbrücke (Hauptstrasse Nr. 8 km 7.840, Objekt Nr. 1373-2, ca. 670 m ü.M.) überbrückt das Tobel bei ‚Gütsch‘ und musste durch die Rutschmasse ‚Spiegelberg‘ mittels Gründungsschutzschächten im Fels fundiert werden (Abb. 1, Abb. 2). Dabei kamen Baumfragmente zum Vorschein, von denen J. Gasser zwei Holzproben aus grosser Aushubtiefe sammelte, dokumentierte und privat archivierte. Auf der Basis dieser Holzstücke wird die offene Frage nach dem zeitlichen Beginn der Hanginstabilitäten neu aufgegriffen und versucht, mittels ¹⁴C-Datierungen einzugrenzen.

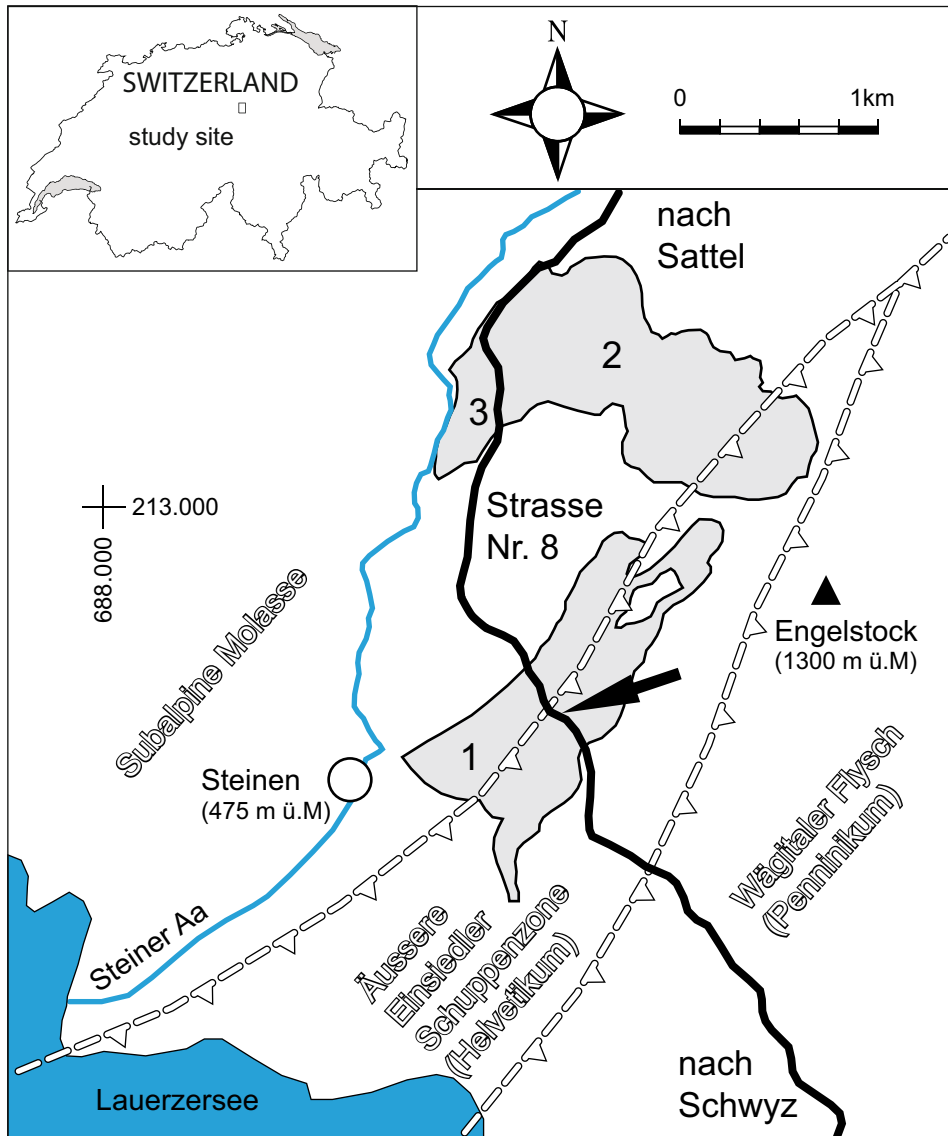


Abb. 1: Übersichtskarte mit dem Standort des 'Widerlager Nord' (Gütschbrücke) zwischen Sattel und Schwyz (Pfeil) sowie die tektonische Situation. Grau hinterlegte Flächen: 1 Rutschung 'Spiegelberg', 2 Rutschung 'Sattel' mit Teilrutschung 'Höchweid' (3) (nach YAVUZ & SCHINDLER 1997). Strichlierte Linien zeigen die Überschiebungen des nördlichen Alpenrandes.

Fig. 1: Overview and tectonic sketch map of the study area and location of the pillar 'Widerlager Nord' (Gütsch bridge) between Sattel and Schwyz (arrow). Given in grey are the landslide areas: 1 'Spiegelberg', 2 'Sattel', 3 'Höchweid' (nach YAVUZ & SCHINDLER 1997). Dashed lines indicate northern alpine frontal thrustplanes.

2 Geologisch-tektonischer Rahmen

Die Rutschmassen von 'Sattel', 'Höchweid' und 'Spiegelberg' überlagern den gegen NNW aufgeschobenen tektonischen Alpennordrand (Abb. 1). Von Nord nach Süd, bzw. von unten nach oben besteht der tektonische Schichtstapel aus den Einheiten der subalpinen Molasse, den helveticischen Gesteinen der Äusseren Einsiedler Schuppenzone und dem penninischen Wägitaler Flysch. Die Schichtflächen der Gesteine fallen durchwegs 30–60° gegen SSE ein (HANTKE & KURIGER 2003; PFIFFNER 2009).

3 Rutschung 'Spiegelberg'

Die ausgedehnte und tiefgründige Permanentrutschung 'Spiegelberg' reicht von 1150 m ü.M. (WNW Engelstock) bis östlich des Dorfes Steinen (470 m ü.M.) (Abb. 1). Die Rutschung ist rund 2.25 km lang, maximal 700 m breit und ist in einzelne, teils aktivere Rutschareale gegliedert. Die mittlere Geländeneigung beträgt 14° (YAVUZ & SCHINDLER 1997).

Die auf Wassereinwirkung empfindliche Rutschmasse aus einem lehmigen, matrixgestützten Gehängeschutt neigt zu plastischer Deformation und langsamen Kriech-



Abb. 2: Aushub eines Gründungsschutzschachtes mit einem elektrisch betriebenen Schreitbagger. Foto: J. Gasser, April 1980.

Fig. 2: Excavation of a fundation well. Photo: J. Gasser, April 1980.

bewegungen. Für die Periode zwischen 1992–93 konnten oberflächliche Verschiebungsbeträge von 2.5–8.5 cm a⁻¹ (in der Lage) und von -7 cm bis +10 cm (in der Höhe) photogrammetrisch ermittelt werden (YAVUZ 1996). Inklinometermessungen vor Baubeginn (SoLEXPERTS AG 1978) sowie

Tabelle 1: Probenbeschreibung.

Table 1: Sample description.

Labor Nr.	Koordinaten ^{a)} E [m]	N [m]	Probenmaterial	Entnahmetiefe [m u. OKT]	Bemerkung ^{b)}	Dendro-Analyse
B-9498	690.314	211.943	<i>Pinus sylvestris</i>	38	Gehängelehm; örtlich durchnässt; Rutschzone im slope indicator	Stammfragment ca. 6x2 cm; weder Kern noch Waldkante erhalten; Kern rund 8 cm entfernt, d.h. Stammdurch- messer von mindestens ca. 22 cm; ausgeglichenes Wachstum; 19 Jahrringe mit mittlerer Breite von 1.612 mm erfasst
B-9499	690.314	211.943	<i>Pinus sylvestris</i>	25	Gehängelehm	Teil einer ovalen Stammscheibe mit gerade noch erhaltenem Kern; mittlerer Durchmesser ca. 7 cm; wiederholte Phasen von Druckholzbildung; keine Waldkante erhalten; 66 Jahrringe mit mittlerer Breite von 1.038 mm erfasst

^{a)} Schweizer Landeskoordinaten (LK)

^{b)} gemäss Begutachtungsprotokoll BUSER 1980

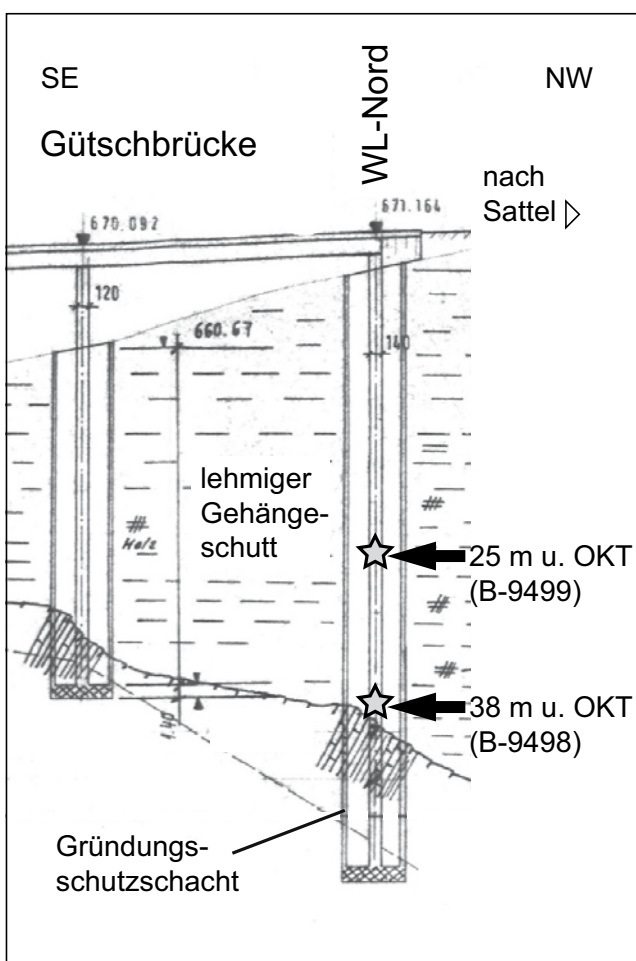


Abb. 3: Längsschnitt Gütschbrücke 1: 500 (Ausschnitt, nicht massstäblich). Die Holzreste wurden dem Aushub des Gründungsschutzschachtes WL-Nord entnommen. Modifiziert aus BUSER (1980).

Fig. 3: Longitudinal section of the Gütsch bridge 1: 500 (not at scale). The wood fragments were found in the fondation well for pillar 'WL-Nord'. Modified from BUSER (1980).

die Langzeitüberwachung des erstellten Gründungsschutzschachtes WL-Nord zwischen 1982 und 2010 (TIEFBAUAMT KANTON SCHWYZ 2010) zeigen keine signifikanten Rutschbewegungen.

4 Lage der Holzfundstücke, Dendro-Analyse und ^{14}C -Altersdatierung

Die zwei Holzfundstücke wurden beim Aushub für den Gründungsschutzschacht des Pfeilers WL-Nord in 25 m bzw. 38 m unter Oberkante Terrain (u. OKT) gefunden (Tab. 1, Abb. 3, Abb. 4). Der Fels liegt rund 40 m u. OKT. Auf der geneigten Felsoberfläche wurde Wasser beobachtet.

Bei beiden Holzfundstücken handelt es sich um *Pinus sylvestris* (Waldkiefer). Die Bestimmung der Holzproben wurde von F. Schweingruber, Eidgenössische Forschungsanstalt WSL, vorgenommen.

Die Jahrringbilder der Holzproben wurden von K. Nicolussi, Universität Innsbruck, analysiert. Aufgrund der kurzen Jahrringserie bzw. des stark gestörten Wachstums konnten jedoch keine Jahrringdatierungen durchgeführt werden. Die Resultate der Dendro-Analyse sind in der Tab. 1 festgehalten.

Die Holzstücke wurden von R. Fischer, Radiocarbon-Labor des Physikalischen Institutes der Universität Bern, durch Zählung der β -Zerfälle (beta counting) analysiert und die konventionellen ^{14}C -Alter berechnet. Für die Kalibrierung der konventionellen ^{14}C -Alter in Kalenderjahre wurde das Programm CALIB Version 5.0.2 verwendet. Die Laborresultate sowie die kalibrierten Altersspannen mit doppelter Standardabweichung (2σ) sind der Tab. 2 zu entnehmen.

5 Diskussion und Schlussfolgerungen

Aus den vorliegenden Deformationsmessreihen vom Standort des WL-Nord lassen sich keine tiefgreifenden, aktiven Gleithorizonte ableiten (v.a. BUSER 1978). Die Rutsch-

Tabelle 2: Resultate der ^{14}C -Datierung.

Table 2: Conventional and calibrated radiocarbon ages.

Labor Nr.	^{14}C -Alter		$\delta^{13}\text{C}$
	konventionell [^{14}C a BP]	kalibriert ^a [cal. a BP]	
B-9498	11.870±40	13.640-13.830	-25.3±0.2
B-9499	9.990±40	11.270-11.690	-24.6±0.2

^a Für die Kalibration der konventionellen ^{14}C -Alter in Kalenderjahre wurde das Programm CALIB Version 5.0.2 (<http://calib.qub.ac.uk/calib/>) in Verbindung mit STUIVER & REIMER (1993) und in Kombination mit dem INTCAL04 Kalibrationsdatensatz (REIMER et al. 2004) verwendet. Die kalibrierten ^{14}C -Altersbereiche sind angegeben mit den Extrema der zweifachen Standardabweichung (2 σ).



Abb. 4: Fotos der beprobenen Holzfundstücke (*P. sylvestris*).

(A) B-9499 (25 m u. OKT), (B) B-9498 (38 m u. OKT).

Fig. 4: Photographs of the investigated wood samples (*P. sylvestris*).

(A) B-9499 (25 m below surface), (B) B-9498 (38 m below surface).

masse ‚Spiegelberg‘ scheint im Bereich des WL-Nord einen bodenmechanischen Gleichgewichtszustand erreicht zu haben. Der Vermerk im Begutachtungsprotokoll von BUSER (1980), wonach über der Felsoberfläche eine aus Messungen ableitbare, aktive basale Gleitzone existiert (Tab. 1) kann mit den heute zur Verfügung stehenden Daten nicht nachvollzogen werden. Die Luftbildanalysen von YAVUZ (1996) zeigen jedoch, dass sich die Rutschung ‚Spiegelberg‘ bereichsweise mit mittlerer Intensität (2–10 cm a⁻¹) deformed. Die derzeit massgebenden Gleithorizonte innerhalb der Rutschmasse müssen im Übergangsbereich der wei-

chen Deckschichten zu steifer gelagerten Lockergesteinen der Rutschmasse vermutet werden.

Die ^{14}C -Altersdatierung der Holzfunde ergaben kalibrierte Altersspannen zwischen 11.690–11.270 cal. a BP (2 σ) und 13.830–13.640 cal. a BP (2 σ). Die erstere Waldkieferprobe datiert am Übergang des Grönland Stadial 1 (GS-1; Jüngere Dryas') zum Holozän (11.700 a vor 2000; LOWE et al. 2008). Das tiefer liegende Waldkieferstamm-Fragment kam zu Beginn der spätglazialen Wärmeschwankung GI-1c (Grönland Interstadial 1c; ‚Allerød‘) zur Ablagerung (13.950 a vor 2000; LOWE et al. 2008).

Auf Basis der älteren und nur wenige Meter über der Felsoberfläche gefundenen Holzprobe ist zu folgern, dass die Hangbewegungen bei ‚Spiegelberg‘ spätestens seit dem Beginn der Allerød-Wärmephase aktiv sind. Dies unterstützt die Vermutung von YAVUZ & SCHINDLER (1997), wonach die Hanginstabilitäten am Engelstock zwischen Schwyz und Sattel nach der Eisfreiwerdung des Schweizer Mittellandes vor ca. 14.600 ^{14}C a BP (LISTER 1988; SCHLÜCHTER 1988; WESSELS 1989; MAGNY et al. 2003; IVY-OCHS et al. 2008) und frühestens nach dem Abschmelzen des lokalen Muota/Reussgletschers im Raum Schwyz einsetzen.

Die Interpretation der Jahrringbilder der Holzproben bekräftigt die Vorstellung, wonach die Hangdeformation nicht graduell, sondern eher in kurzfristig auftretenden Phasen verstärkter Rutschintensität abließ (vgl. Probe B-9499 in Tab. 1).

Im Vergleich mit der Vegetationsentwicklung des Schweizer Mittellandes ist das ältere Kiefernholzfundstück kaum jünger als die erste deutliche Kiefernausbreitung zu Beginn der regionalen Pollenzone CHb-4a um ca. 12.000 ^{14}C a BP, die mit dem Beginn der Wärmephase des ‚Allerød‘ korreliert (WELTEN 1982; KÜTTEL 1989; LOTTER & ZBINDEN 1989; LOTTER et al. 1992). Der Holzfund gehört wohl zu den frühen spätglazialen *Pinus*-Hölzer der Schweiz nördlich der Alpen, jedoch nicht zu den ältesten, die aus dem Raum Zürich bekannt sind und bis ins GI-1e („Bølling“) zurück datieren (vgl. SCHAUB et al. 2008). Erwähnenswert ist jedoch der Fundort unmittelbar am nördlichen Alpenrand und die Folgerung, dass die SW-Flanke des Engelstock bis mindestens auf 670 m ü.M. mit *P. sylvestris*, mit Stammdurchmesser von mindestens ca. 22 cm, bestockt war (vgl. Tab. 1).

Die Datierung des jüngeren *Pinus*-Holzstückes mit stark gestörtem Wachstum ist entsprechend dem ^{14}C -Plateau relativ ungenau (Tab. 2), liegt jedoch am Übergang zur regionalen Pollenzone CHb-4c (vgl. LOTTER et al. 1992) am Klimaübergang zwischen der ‚Jüngeren Dryas‘ und dem ‚Präboreal‘, basierend auf der Korrelation von Sauerstoffisotopenprofilen an Seesedimentkernen aus Gerzensee und Leysin zum GRIP-Eisbohrkern (SCHWANDER et al. 2000).

Die vorliegenden Daten zeigen, dass *P. sylvestris* schon kurz nach dem Ende der spätglazialen Kälterückschläge GI-1d („Aegelsee-Schwankung“, 12.300–12.000 ^{14}C a BP; LOTTER et al. 1992) und GS-1 am nördlichen Alpenrand präsent ist.

Dank

Wir bedanken uns bei René Fischer (Radiocarbon-Labor, Universität Bern) für die Datierung der Holzproben. Fritz Schweingruber (Eidgenössische Forschungsanstalt WSL)

sowie Kurt Nicolussi (Universität Innsbruck) sind für die Dendro-Analysen herzlich gedankt. E. Vural Yavuz (Technische Universität Istanbul) danken wir für die nützlichen Informationen und Unterlagen zur Rutschung ‚Spiegelberg‘. Diese Untersuchung wurde vom Schweizerischen Nationalfonds (Projekt Nr. 200020–118038) mitfinanziert.

Literatur

- GASSER, J. (1983a): Der Ausbau der Hauptverkehrsstrasse T8 im Kanton Schwyz. – Bau, 4/83: 17–22.
- GASSER, J. (1983b): Die Hauptstrassen im Kanton Schwyz. – Schweizer Journal, 4/83: 32–34.
- HANTKE, R. & KURIGER, E. (2003): Überblick über die Geologie des Kantons Schwyz und seiner Nachbargebiete. – In: LIENERT, S. (ed.): Geologie und Geotope im Kanton Schwyz: 9–34; Berichte der schwyzerischen Naturforschenden Gesellschaft, Heft 14.
- IVY-OCHS, S., KERSCHNER, H., REUTHER, A., PREUSSER, F., HEINE, K., MAISCH, M., KÜBIK, P.W. & SCHLÜCHTER, C. (2008): Chronology of the last glacial cycle in the European Alps. – Journal of Quaternary Science, 23(6–7): 559–573.
- KÜTTEL, M. (1989): Züge der Jungpleistozänen Vegetations- und Landschaftsgeschichte der Zentralschweiz. – Revue de Paléobiologie, 8(2): 525–614.
- LISTER, G.S. (1988): A 15.000-year isotopic record from Lake Zürich of deglaciation and climatic change in Switzerland. – Quaternary Research, 29: 129–41.
- LOTTER, A.F. & ZBINDEN, H. (1989): Late-Glacial pollen analysis, oxygen-isotope record, and radiocarbon stratigraphy from Rotsee (Lucerne), Central Swiss Plateau. – Eclogae geologicae Helvetiae, 82(1): 191–202.
- LOTTER, A.F., EICHER, U., SIEGENTHALER, U. & BIRKS, H.J.B. (1992): Late-glacial climatic oscillations as recorded in Swiss lake sediments. – Journal of Quaternary Science, 7(3): 187–204.
- LOWE, J.J., RASMUSSEN, S.O., BJÖRCK, S., HOEK, W.Z., SEFFENSEN, J.P., WALKER, M.J.C., YU, Z.C. & the INTIMATE group (2008): Synchronisation of palaeoenvironmental events in the North Atlantic region during the Last Termination: a revised protocol recommended by the INTIMATE group. – Quaternary Science Reviews, 27: 6–17.
- MAGNY, M., THEW, N. & HADORN, P. (2003): Late-glacial and early Holocene changes in vegetation and lake-level at Hautrive/Rouges-Terres, Lake Neuchâtel (Switzerland). – Journal of Quaternary Science, 18: 31–40.
- PFIFFNER, O.A. (2009): Geologie der Alpen. – 359 S.; Bern (Haupt Verlag).
- REIMER, P.J., BAILLIE, M.G.L., BARD, E., BAYLISS, A., BECK, J.W., BERTRAND, C.J.H., BLACKWELL, P.G., BUCK, C.E., BURR, G.S., CUTLER, K.B., DAMON, P.E., EDWARDS, R.L., FAIRBANKS, R.G., FRIEDRICH, M., GUILDERSON, T.P., HOGG, A.G., HUGHEN, K.A., KROMER, B., McCORMAC, G., MANNING, S., RAMSEY, C.B., REIMER, R.W., REMMELE, S., SOUTHON, J.R., STUIVER, M., TALAMO, S., TAYLOR, F.W., VAN DER PLICHT, J. & WEYHENMEYER, C.E. (2004): INTCAL04 terrestrial radiocarbon age calibration, 0–26 cal kyr BP. – Radiocarbon, 46: 1029–1058.
- SCHAUB, M., KAISER, K.F., FRANK, D.C., BÜNTGEN, U., KROMER, B. & TALAMO, S. (2008): Environmental change during the Alleroed and Younger Dryas as reconstructed from Swiss tree-ring data. – Boreas, 37: 74–86.
- SCHLÜCHTER, C. (1988): The deglaciation of the Swiss Alps: a paleoclimatic event with chronological problems. – Bulletin de l’Association Française pour l’Etude du Quaternaire, 2: 141–145.
- STUIVER, M. & REIMER, P.J. (1993): Extended ¹⁴C data base and revised CALIB 3.0 ¹⁴C Age calibration program. – Radiocarbon, 35: 215–230.
- SCHWANDER, J., EICHER, U. & AMMANN, B. (2000): Oxygen isotopes of lake marl at Gerzensee and Leysin (Switzerland), covering the Younger Dryas and two minor oscillations, and their correlation to the GRIP ice core. – Palaeogeography, Palaeoclimatology, Palaeoecology, 159: 203–214.
- WELTEN, M. (1982): Pollenanalytische Untersuchungen im Jüngeren Quartär des nördlichen Alpenvorlandes der Schweiz. – Beiträge zur Geologischen Karte der Schweiz N.F., 162: 174 p.
- WESSELS, M. (1989): Natural environmental changes indicated by Late Glacial and Holocene sediments from Lake Constance, Germany. – Palaeogeography, Palaeoclimatology, Palaeoecology, 140: 421–432.
- YAVUZ, E.V. (1996): Analyse der Bewegung grosser, tonreicher Rutschgebiete am Beispiel des Gebietes Engelstock–Sattel–Steinen (SZ). – Dissertation ETH Zürich Nr. 11706, 186 S.
- YAVUZ, E.V. & SCHINDLER, C. (1997): Tonreiche Rutschungen im Grenzbereich subalpine Molasse – Flysch zwischen Sattel und Lauerzersee (Kt. Schwyz): Entstehung, Zusammensetzung und Bewegungsablauf. – Bulletin angewandte Geologie, 2(2): 123–149.

Geotechnische Berichte und Messreihen:

- BUSER, DR. HUGO (1978): T8 Hirschen–Matti, Baubegleitung Slope-Indicator-Messungen (KB 15, KB 17). Aktennotiz der Besprechung vom 07.07.1978.
- BUSER, DR. HUGO (1980): Begutachtung der Aushubetappen der Brückenfundamente – Schächte der Brücke Güttsch (Situation 1: 500, Schachtprofile 1: 100, Längsschnitt 1: 500). Ausführung T8 Ingenbohl–Pfäffikon, Teilstrecke Hirschen–Matti, Plan Nr. 80-731 vom 10.09.1980.
- SOLEXPERTS AG (1978): Sattel, Hirschen–Matti. Digitilt Slope Indicator, Deformationsmessungen des Hanges (12.5.1978 bis 29.08.1978, Messrohr Nr. 15 und Nr. 17).
- TIEFBAUAMT KANTON SCHWYZ (2010): H8 Schwyz–Sattel, Güttsch–Brücke, km 7.875, Objekt Nr. 1373-2. Deformationsmessungen der Schachtringe beim WL-Nord (Messreihe vom 29.03.1982 bis 16.06.2010).

Zur periglaziären Bildung und Überformung rinnenartiger Strukturen im Jungmoränengebiet Süd-Holsteins

Alf Grube

How to cite: GRUBE, A. (2012): Zur periglaziären Bildung und Überformung rinnenartiger Strukturen im Jungmoränengebiet Süd-Holsteins – E&G Quaternary Science Journal, 61 (1): 69–81. DOI: 10.3285/eg.61.1.06

Kurzfassung: Der weichselkaltzeitliche Binnensander-Bereich Bargfeld-Stegen (Schleswig-Holstein) nördlich von Hamburg ist durch intensive periglaziäre Überprägung charakterisiert. Hierbei treten rinnenartige Hohlformen (Rinnen), von bis zu 26 m Breite und 3,5 m Tiefe in den Vordergrund. Häufige Gemeinsamkeiten dieser Rinnen sind ein flach-konvexes Rinnenprofil, flache Basisflächen bzw. ein Einschneiden der Rinne bis zu einer Grenzfläche (ehem. Permafrostfläche), eine bindige Füllung mit aufgearbeitetem oder umgelagerten Till, ein diapir-artiges Aufdringen von Teilen der Rinnenfüllung im oberen Bereich und im Randbereich, Unterschneidungen und andere fluviatile Kennzeichen an den Rinnenflanken sowie homogen mit Sand gefüllte Sekundär-Rinnen im zentralen oberen Teil der Strukturen. Sie sind bevorzugt an Hängen im Winkel zur Haupt-Eisvorstossrichtung sowie im Randbereich der vorhandenen Deck-Till-Verbreitung vorhanden. Es kommen verschiedene Entstehungsmöglichkeiten in Betracht. Die Strukturen dürften maßgeblich während der jüngeren Weichsel-Kaltzeit unter Frostbodenklima durch die Wirkung periglaziär-fluviatiler Prozesse (Abluation) in Verbindung mit Solifluktionsprozessen, gebildet worden sein.

Periglacial generation and shaping of channel-like structures in the Weichselian moraine landscape of south Holstein

Abstract: The Bargfeld-Stegen sandur area (Schleswig-Holstein) north of Hamburg is characterized by an intense periglacial shaping. Channel-like features, hereinafter referred to as channels, up to 26 meters wide and 3.5 meters deep, as periglacial forms are incisive. Similar features can be observed in Itzehoe, Tangstedt (Norderstedt) and Schalkholz. Common features of these channels are: a usually shallow-convex cross section, an infill including re-deposited till, undercutting and other fluvial characteristics at the flanks, flat base eroded down to a boundary surface (permafrost), a diapir-like uplift of channel fillings in the upper channel parts and at the channel flanks, the parallel channel courses, sand-filled secondary channels and a linear progression of channels, preferably diagonally to the ice movement. The structures seem to appear mainly in slope positions in the marginal zones of the regional till-cover. Different forms of their generation have to be considered. They were probably mainly formed during the periglacial climate (Weichselian) by periglacial-fluvial processes (ablation) combined with solifluction.

Keywords: *periglacial, periglacial channels, solifluction, ablation, Weichselian periglacial*

Address of author: A. Grube, Geologischer Dienst Schleswig-Holstein, Landesamt für Landwirtschaft, Umwelt und ländliche Räume des Landes Schleswig-Holstein (LLUR), Hamburger Chaussee 25, D-24220 Flintbek. E-Mail: alf.grube@llur.landsh.de

1 Einleitung

Im Rahmen der geologischen Landesaufnahme in Schleswig-Holstein konnten seit 1999 Informationen zum oberflächennahen geologischen Bau bzw. zur Genese vor allem periglazialer Sedimente und Strukturen im Jungmoränengebiet des südlichen Holstein gewonnen werden. Der Binnensander-Bereich bei Bargfeld-Stegen ist durch intensive periglaziäre Überprägung charakterisiert. Bei den in der Literatur beschriebenen fossilen Periglazial-Formen Norddeutschlands und der Niederlande (vgl. EISSMANN 1981, LIEDTKE 1993, SEMMEL 1985, VANDENBERGHE 1983) wird, mit Ausnahme von weiträumigen Trockental-Bildungen, zu denen zahlreiche Arbeiten vorliegen (z.B. HANNEMANN 1963; vgl. Literatur bei HENNING 1973), wenig auf Hohlformen eingegangen. Im vorliegenden Beitrag werden kleinräumigere, rinnenartige Hohlformen von bis zu 26 m Breite und 3,5 m Tiefe als weitere typische Periglazial-Formen beschrieben und diskutiert. Diese weisen teilweise eine

deutliche Längserstreckung auf, es wurden Längen von mehreren Dutzend Metern beobachtet, vermutlich sind sie generell deutlich länger. Sie sind bevorzugt in Sandersedimente eingeschnitten. Im Folgenden wird dabei von Rinnen gesprochen, wobei formal von rinnenartigen Strukturen gesprochen werden müsste, da diese im Verhältnis z. B. zu elsterkaltzeitlichen Rinnen verhältnismäßig klein sind.

2 Material und Methoden

Neben der Auswertung von Archivunterlagen wurden geologische Sondierungen mittels Peilstangen- und Rammkerngerät niedergebracht. Weiterhin konnten Grundwasserbohrungen des Geologischen Landesamtes Schleswig-Holstein (u.a. BOCK 1981), Baugrubenbohrungen sowie Bohrungen der Altlastenuntersuchungen des Umweltamtes des Landkreises Stormarn für die Konstruktion des Geologischen Modells verwendet werden. Die vorhandenen Aufschlüsse wurden während des Abbaus der letzten Jahre

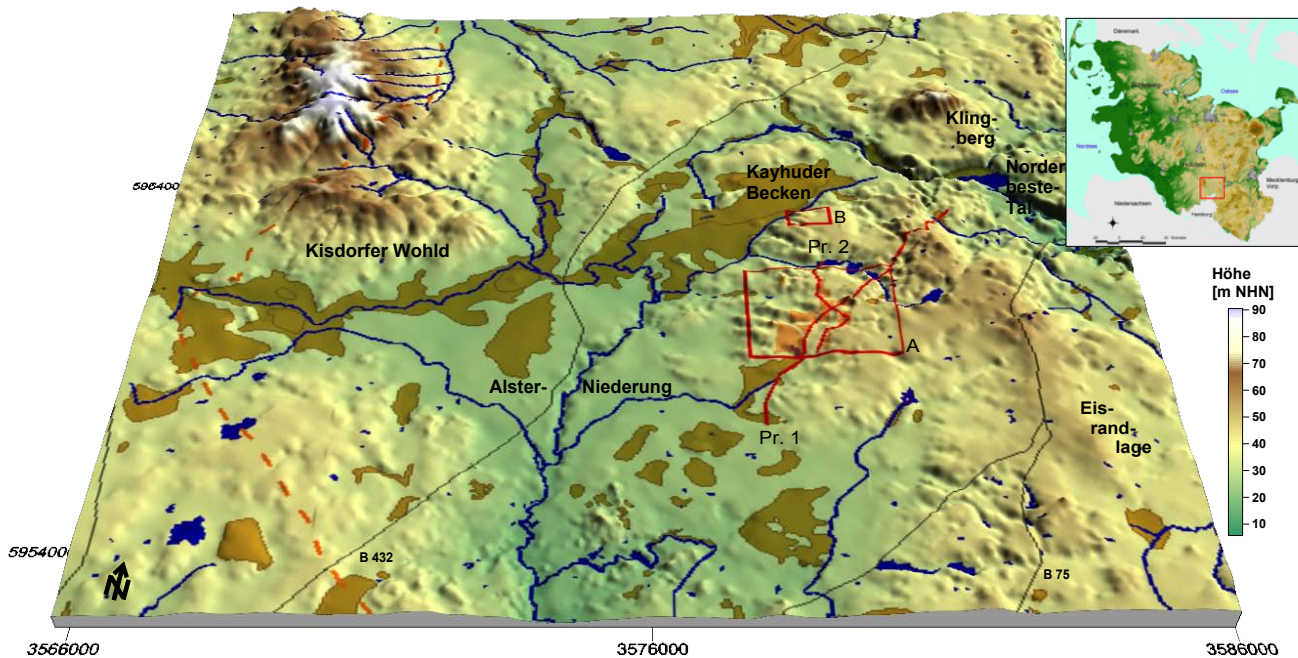


Abb. 1: Digitales Geländemodell auf Basis des DGM1 (LVA SH): Weiteres Untersuchungsgebiet; Moorflächen (braun), Abbauflächen (orange), Grenze der Maximalausdehnung der Weichselvereisung (rot gestrichelt), Profilschnitte 1 und 2 (rote Linien) und Lage der Abb. 6 (A, B, rot umrandet).

Fig. 1: Digital terrain model on basis of DGM1 (LVA SH): Wider investigation area; bogs (brown), gravel pits (orange), outermost limit of Weichselian ice margin (red dashed), cross sections 1 and 2 (red lines) and location of fig. 6 (A, B, framed red).

sukzessive mittels Aufgrabung und Eimmessung aufgenommen. Die Qualität der Aufnahmen ist unterschiedlich, da einige Strukturen aufgrund ihrer Lage in meterhohen frischen Abbauwänden nur schlecht zugänglich waren. Zur Rekonstruktion der Richtungen der Gletschervorstöße bei den Tills wurden nach dem Verfahren von RICHTER (1932) Geschiebe-Einregelungsmessungen durchgeführt. Die Schüttungsrichtung der Sande wurde ebenfalls ermittelt. Ab ca. 1999 erfolgte eine Aufnahme der Aufschlusswände in unregelmäßigen Abständen. Ergänzt wurden die Untersuchungen im Rahmen von zwei Diplomarbeiten am Geologisch-Paläontologischen Institut der Universität Hamburg (BAUKE 2008; SULKOWSKI 2008), die die generellen Lagerungsverhältnisse im weiteren Umfeld der hier beschriebenen Strukturen untersuchten. Im Bereich einer Rinne wurden Georadar-Messungen in Kooperation mit Mitarbeitern des Geologisch-Paläontologischen Institutes der Universität Hamburg durchgeführt (vgl. POTILLO et al. 2005).

Ähnliche Strukturen wie im Bereich Bargfeld-Stegen wurden im Rahmen der Landesaufnahme vereinzelt bei Itzehoe, Norderstedt und Schalkholz beobachtet, hier jedoch nicht näher dokumentiert.

3 Geologie des weiteren Untersuchungsgebiets

3.1 Geomorphologie

Das Untersuchungsgebiet liegt ca. 10 km östlich der maximalen Vereisungsgrenze der Weichsel-Kaltzeit (vgl. Abb. 1). Die Höhenunterschiede liegen im weiteren Untersuchungsgebiet zwischen ca. +5 und +80 m NHN. Der Bereich liegt am westlichen Rand eines Hochrückens der Stormarner Jungmoränenlandschaft, der bis über +60 m

NHN aufragt und der in etwa von Bargteheide nach Sülfeld verläuft. Nach TODTMANN (1952) handelt es sich dabei um ein System von zusammengesetzten Randschlagnen, die auf einer warthezeitlichen Hochlage gebildet worden sind. Die markante Randschlange der Weichsel-Kaltzeit wird wenig nördlich des Untersuchungsgebietes durch das subglazial angelegte Tal der Norderbeste unterbrochen. Der Randschlange nach Westen vorgelagert finden sich mächtigere Sanderablagerungen, die örtlich von Geschiebelehmen und -mergeln durchstoßen werden und die eine leicht wellige Landschaft bilden. Die durchschnittlichen Höhen im Bereich der Sanderfläche liegen zwischen ca. +35 und +45 m NHN. Im Westen des engeren Untersuchungsgebietes folgt zunächst das Kayhuder Gletscherzungengebiet, welches den Übergang zur großräumigen Talung der Alster bildet. Beim Kayhuder Zungenbecken handelt es sich um ein glaziales Becken mit Schmelzwasserablagerungen, welches heute ein Niedermoor mit aufgesetztem Hochmoor zeigt. Eine morphologisch deutlich sichtbare Umrandung des Beckens ist nicht überall vorhanden, die Höhendifferenz zwischen dem Beckeninneren und der Umrandung liegt generell im Osten höher als im Westen. Eine glazitische Verstellung ist für die südwestliche Umrandung des Zungenbeckens nachgewiesen (BOCK 1981, POTILLO et al. 2005). Die westlich des Beckenrandes gelegenen Bereiche bei Wakendorf sind nach STEPHAN (2004) ebenfalls gestaucht.

3.2 Geologischer Überblick

Informationen zum tieferen Untergrund liegen aus einer Tiefbohrung vor, die in Bargfeld-Stegen niedergebracht wurde. Demnach wurde in der Endteufe von 606 m der Hamburger Ton angetroffen, im Hangenden folgten die Oberen Braunkohlensande sowie der Glimmerton (Reinbek-, Lan-

genfeld- und Gram-Stufe). Diese miozänen Einheiten erreichen alle eine größere Mächtigkeit, die durch die Trog-Position westlich der Salzstruktur Sülfeld hervorgerufen wird. Bargfeld-Stegen liegt im Bereich einer Hochlage der Quartärbasis. Kaolinsande (Pliozän/Quartär) im Hangenden des Miozäns erreichen eine Mächtigkeit von ca. 30 m, ihr Top ragt bis zu Normalnull auf. Westlich, nördlich und östlich fällt die Quartärbasis zu einem pleistozänen Rinnensystem hin ab (Duvenstedter und Bargteheider Rinne), das auf tiefer als -400 m NHN einschneidet. Im Hangenden der Kaolinsande folgen Ablagerungen des Abschnittes Saale-Kaltzeit bis Holozän. An der Oberfläche bzw. in geringer Tiefe treten weichselkaltzeitliche Schmelzwassersande (Binnensander) auf, die im Norden und Osten von einem bis zu mehrere Meter mächtigen Deck-Till der Weichsel-Kaltzeit überlagert werden (vgl. Geologische Übersichtskarte BRANDES et al. 1977, ALAI-OMID et al. 1988). Dieser Till, vermutlich ursprünglich ein Abschmelz-Till, ist meist erheblich periglaziär überprägt worden (Abschn. 4.2).

4 Ergebnisse

4.1 Geologie

4.1.1 Weiterer Untersuchungsraum

Abb. 1 und 2 geben eine Übersicht über den weiteren Untersuchungsraum. Im Nordosten befindet sich eine ausgedehnte Niedertau-Landschaft bei Sülfelder Tannen (vgl. GRUBE 2010), die beim Abschmelzen eines Gletschers im Lee der großen Randlage entstanden ist. Die westlich der Niedertau-Landschaft gelegene markante weichselkaltzeitliche Randlage ist in ihrem Aufbau durch Geschiebebergel, Sande und Beckensedimente dominiert, es ist eine

glazitektonische Verstellung nachgewiesen. Im Topbereich der Randlage sind Kames-Ablagerungen aus der Deglaziations-Phase erhalten geblieben. Der Bereich westlich der Randlage zeigt einen sehr wechselhaften Aufbau, auf den im Abschnitt 4.1.2 näher eingegangen wird. Es handelt sich zuoberst um Sandersedimente, die teilweise von einem Deck-Till überlagert werden. Die Sandersedimente sind über Jahrzehnte intensiv lagerstättentechnisch genutzt worden. Südlich des engeren Untersuchungsgebietes treten in einer großen Niederung, in der der Hansdorfer und der Duvenstedter Brook angelegt sind, bis zu mehr als 10 m mächtige Beckenablagerungen im Hangenden eines Tills auf. Hier finden sich auch lokal kleine Dünne sowie Moorbildungen. Ältere warmzeitliche Ablagerungen wurden bisher nicht kartiert. Auch eine moderne Till-Stratigraphie steht noch aus, sodass im Profilschnitt (Abb. 2) keine klare stratigraphische Gliederung angegeben werden kann.

4.1.2 Engerer Untersuchungsraum

Hier sollen die oberflächennahen Sedimente im Vordergrund der Betrachtung stehen. Die Mächtigkeit der auftretenden glazifluviaten Ablagerungen, der in die Sandersablagerungen eingeschalteten bindigen Zwischenmittel sowie des Deck-Tills sind verhältnismäßig heterogen. Die Basis der Sandersande wird durch einen mächtigen bindigen Till gebildet, der sehr kreidereich ist. Er wird hier der Weichsel-Kaltzeit zugeordnet (ggf. Ellund-Vorstoß, vgl. STEPHAN 2003), da er großräumig oberflächennah auftritt. Der Till zeigt in den Aufschlüssen der Fa. Timm nördlich der L 82 stärkere glazitektonische Störungen (Abb. 3). Örtlich finden sich im Liegenden des Tills in Senkenposition glazilimnische Ablagerungen. Der Kreide-reiche Till bzw.

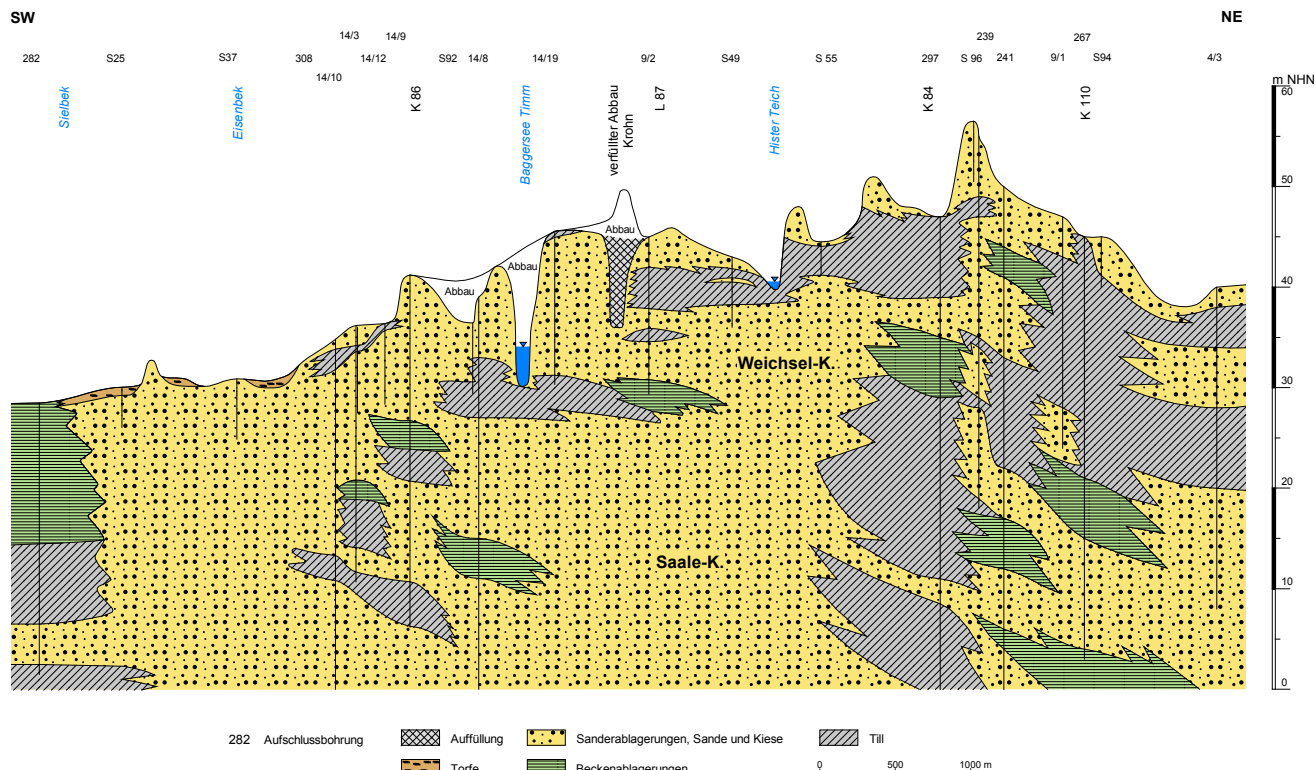


Abb. 2: Profilschnitt 1 durch das weitere Untersuchungsgebiet.

Fig. 2: Cross section 1 through the study area.

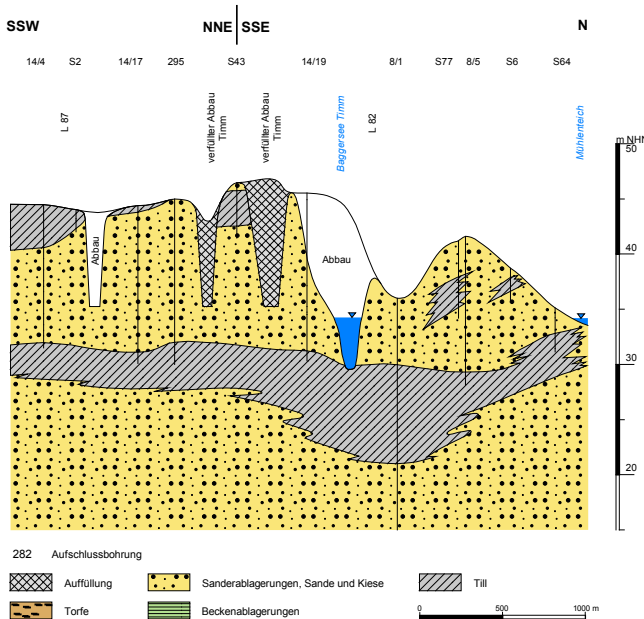


Abb. 3: Profilschnitt 2 durch das engere Untersuchungsgebiet.

Fig. 3: Cross section 2 through closer investigation area.

die glazilimnischen Bildungen sind Grundwasserhemmer, so dass die Grundwasseroberfläche wenige Meter oberhalb der Oberkante des Tills liegt. Im Hangenden folgen Sanderablagerungen, die durch drei Kies- und Sandfirmen (K. Timm, W. Krohn und C. & W. Borchert) im Nass- und Trockenverfahren gewonnen werden bzw. wurden. Die Mächtigkeit der Sanderablagerungen liegt durchschnittlich zwischen 6 und 12 m (BAUKE 2008; SULKOWSKI 2008). Es handelt sich um typische, schräg geschichtete Sanderablagerungen mit Kiesanteilen von bis zu ca. 8 %. Die Schüttung der Sanderablagerungen erfolgte generell nach Richtung Westen.

Vielerorts bildet ein stärker geklüfteter Deck-Till das Hangende der Sandersande (vgl. Abb. 3). Dieser liegt meist direkt und ohne größere Störungen oder Bildung eines Scher-Tills den Sanderablagerungen auf. So wurden beim Sandabbau durch die Fa. Timm (nördlich der L 82) ca. 2 m mächtige, stark kalkhaltige glazilimnische Schluffe im Liegenden eines ca. 1 m mächtigen Tills (gekläuft, gewöhnliches „Verwitterungsbild“) angetroffen. Der Deck-Till ist von der westlichen Seite der Randlage zwischen Elmenhorst und Sülfeld ausgehend nach Westen zunächst flächenhaft verbreitet (Grundmoränenlandschaft), dünn dann in Richtung Bargfeld-Stegen hin aus und ist hier nur noch lückenhaft vorhanden (Abb. 2). Entweder ist hier eine Vereisungsgrenze erreicht oder der Till wurde weiter westlich erodiert. Dieser Übergangsbereich, in dem der Deck-Till ausbeißt oder geringmächtiger wird, wird auch schwerpunktmaßig durch die Kiesindustrie genutzt. In der Marginalzone der Randlage Elmenhorst-Sülfeld besitzt der Till Mächtigkeiten von teilweise mehr als 5 m. Großflächig wird der Till 1–3 m mächtig. Häufig ist die Mächtigkeit des Deck-Tills im Bereich von Aufwölbungen der Erdoberfläche am größten (Fluting-ähnliche Strukturen).

An wenigen Stellen im Bereich Bargfeld-Stegen finden sich größere Till-Mächtigkeiten, die im unteren Bereich nur

geringe oder keine periglaziäre Beeinflussung des Deck-Tills zeigen. In einem solchen Geschiebemergel-Abschnitt konnten an zwei Stellen Geschiebelängsachsenmessungen durchgeführt werden (Südrand des Abbaus Krohn in Bargfeld-Stegen). Der Till ist hier verhältnismäßig bindig. Er wird hier teilweise mehr als 3 m mächtig. Der obere Teil ist braun, der untere hellbraun und etwas sandiger. Die Messung der Längsachsen erfolgte im unteren, weitgehend ungestörten Teil des Tills (Hauptrichtung der Klüftung 105–110°). Es wurde eine Vorstoßrichtung des Gletschers aus Ost-Nordost ermittelt (Durchschnittswert von 50 Messungen: 78°).

Lokal sind im Hangenden des Deck-Tills noch glazifluviatile Ablagerungen oder Kames-Bildungen vorhanden. Diese sitzen bevorzugt der Randlage auf.

4.2 Periglaziäre Überprägung

Verbreitet findet sich eine Periglazial-Decke von bis zu mehreren Dezimetern Mächtigkeit im Hangenden des Tills bzw. der Sanderablagerungen. Diese zeigt eine Verarmung an Ton- und Schluff-Anteilen, eine Anreicherung grober Komponenten, eine teilweise Einregelung von Geschieben (vertikale Aufrichtung) sowie Kryoturbations-Erscheinungen. Die intensive periglaziäre Überprägung ist im Verbreitungsbereich von Deck-Till am deutlichsten sichtbar. Kryoturbationen reichen hier bis in eine Tiefe von ca. 3,5 m, z. B. an der Ostwand des Abbaus der Fa. Krohn östlich von Bargfeld-Stegen (Abb. 4). Sie reichen hier bis in die liegenden Sande hinein, an der Basis des Tills finden sich Tropfenbodenstrukturen. Der obere Teil des Deck-Tills bzw. die Periglazial-Decke sind teilweise besonders stein-/blockreich, was auf periglaziäre Auswaschung und Ausblasung (Steinsohlenbildung) zurückgeht. Vielerorts wurden Frost-/Eiskeile beobachtet (Abb. 5). Diese reichen häufig ca. 2,5 bis 3 m tief, weisen eine generell schmale Form auf und sind mit lokalem, sandigen Material gefüllt. Die auffälligste Überprägung, die Rinnenbildung, wird gesondert im folgenden Abschnitt dargestellt.

4.3 Rinnenbildung

Bei den Kartierarbeiten wurden ungewöhnliche Rinnen angetroffen (Abb. 6). Diese unterscheiden sich zwar in Bezug auf ihre Größe, Geometrie, Internstruktur und Füllung, dürften aber meist auf ähnliche Weise entstanden sein. Die in den Rinnen enthaltenen Sedimente sind sämtlich kalkfrei. Die Rinnen sind in mehr oder weniger flach liegende, schräg geschichtete Sanderablagerungen eingeschnitten. Diese liegenden glazifluviatilen Ablagerungen zeigen an einigen Stellen im Umfeld der Rinnen Störungen, die offenbar mit der Bildung der Rinnen zusammenhängen. Die Rinnen sind aufgrund ihrer vorwiegend sandigen Füllung im Oberflächenbereich in Bohrungen häufig kaum von den umgebenden Sanden zu unterscheiden. Ihr Verlauf und Details der Formung konnten nur bei Vorhandensein von Aufschlüssen erkannt und dokumentiert werden. Da ihre Längserstreckung daher nur ansatzweise erfasst wurde, sollte diese bei den nach dem Abbau verbliebenen Rinnen möglichst durch geophysikalische Verfahren kartiert werden. Neben den bisher nur kleinräumig in den Aufschlüssen

beobachteten Rinnen-Strukturen, muss mit einer weiteren Verbreitung entsprechender Formen gerechnet werden.

In Abb. 7 sind die kartierten Rinnen vereinfacht dargestellt. Teilweise wird in den Rinnen umgelagertes Till-Material angetroffen. Dieses zeigt eine typische Till-Textur, teilweise noch ein Parallel-Gefüge, was auf eine geringere Transportentfernung hindeutet. Es tritt auch schluffig-sandiges Material (meist mittel bis stark schluffige Sande, Korngrößenverteilung wie Till) auf, welches als periglaziar „aufgearbeiteter Till“ interpretierbar ist. Da der humose Oberboden während der Kartierung teilweise bereits abgeräumt war, konnten die oberflächennahen Bereiche nicht immer komplett dokumentiert werden.

Einzelbeschreibungen:

Die **Rinnen-Struktur 1** (Abb. 8, 7c) ist mit einer Breite von ca. 12 m und 3,5 m Tiefe eine der größten Formen. Das Rinnenprofil ist, abgesehen von den Verstellungen in den liegenden Sanden (s. u.), normal-konvex ausgebildet. Unterhalb der eigentlichen Rinne scheinen die anstehenden Sandersande bis ca. 2 m seitlich gestört zu sein. Zwei flügelartige Sandbereiche links und rechts am unteren Ende der Rinne zeigen dabei eine flache Unterseite, die der ehemaligen Permafrost-Oberfläche entsprechen könnte (Abb. 8; „gestörte Bereiche“). Vermutlich erfolgten alle genannten Verstellungen der liegenden bzw. benachbarten Sande in zumindest teilweise gefrorenem Boden. Im östlichen Flankenbereich sind schluffige Ablagerungen schollenartig in die Sande eingeschaltet. Die Rinnenfüllung wird vorwiegend durch umgelagerten Till im unteren und aufgearbeiteten Till im hangenden Teil aufgebaut. Der umgelagerte Till zeigt eine Diapir-artige Aufwölbung im Zentrum der Rinne. Wie bei anderen Rinnen auch, ist im oberen, zentralen Rinnenbereich eine sekundäre Rinne mit parallel geschichteten Sanden in den aufgearbeiteten Till eingeschnitten. Den oberen Abschluss bildet eine flächenhafte periglaziar Deckschicht, die westlich der Rinnen-Struktur starke Kryoturbationen zeigt. Hier setzt auch ein Frostkeil an, der die gesamten aufgeschlossenen Sandersande durchschlägt.

Die **Rinnen-Struktur 2** (Abb. 7c) liegt nördlich der Hohlform 19. Das Zentrum der Hohlform wird überwiegend

durch einen rinnenartig eingesenkt Bereich von umgelagertem Till eingenommen. Oberhalb folgt geringmächtiger aufgearbeiteter Till. Am nördlichen Rinnenrand sind geringmächtige Sande ausgebildet. Der aufgearbeitete Till setzt sich flächenhaft beidseitig der Hohlform fort, im Hangenden folgen dabei schluffige Sande. Abgedeckt wird die Hohlform von der flächenhaft verbreiteten periglaziären Deckschicht.

Die **Rinnen-Struktur 19** (Abb. 7c) liegt benachbart zur Hohlform 2. Die Sandersande, in die die Rinnen eingeschnitten sind, fallen leicht nach Norden hin ein. Das Zentrum der Hohlform wird ganz überwiegend durch einen rinnenartig eingesenkt Bereich von umgelagertem sowie aufgearbeitetem Till eingenommen. Am nördlichen Rinnenrand sind an den Flanken geringmächtige Sande ausgebildet. Im Hangenden folgen schluffige Sande über die gesamte Hohlformbreite. Abgedeckt wird die Hohlform von der flächenhaft verbreiteten periglaziären Deckschicht.

Die **Rinnen-Struktur 3** zeigt eine verhältnismäßig komplexe Füllung. Sie liegt benachbart zur Hohlform 4 (Abb. 7c). Die Sandersande, in die die Rinne eingeschnitten ist, fallen leicht nach Norden hin ein. Die tief eingekernte Rinne hat eine angenäherte U-Form. Der untere Teil der Rinne ist mit weitgehend söhlig liegenden, schluffigen Sanden gefüllt, charakteristisch sind Unterschneidungen in diesem Teil der Hohlform (N-Flanke). Diese zeugen von einer fluviatilen Genese des unteren Teils der Hohlform (Abb. 9b). Mittig eingeschaltet in die Sande findet sich auch ein größeres Geröll. Darüber folgt ein unregelmäßiger Block von aufgearbeitetem Till, der fast die gesamte Rinnenbreite ausfüllt. Im Hangenden folgen schluffige Sande. In diese ist eine sekundäre Rinne eingeschnitten, die im untersten Teil mit schluffigen Sanden gefüllt ist, darüber folgt umgelagarter Till. Dieser schließt die Rinnenfüllung ab, er zieht sich flächenhaft in die benachbarte Hohlform 4 hinein und keilt nach Norden hin aus. Abgedeckt wird die Hohlform von der flächenhaft verbreiteten periglaziären Deckschicht, die hier verhältnismäßig mächtig ist.

Die **Rinnen-Struktur 4** liegt zwischen den Hohlformen 3 und 18 (Abb. 7c und 9c), wobei der Übergang zur Rinne 19 flach ist. Die liegenden Sandersande fallen leicht nach



Abb. 4: Intensive Kryoturbation, die bis ins Liegende des Deck-Tills reichen.
Fig. 4: Intensive cryoturbation reaches below the covering till.



Abb. 5: Eis-/Frostkeil-Pseudomorphe, die bis tief in die liegenden Sandersablagerungen reicht.
Fig. 5: Frostcrack/ice-wedge cast that cuts deep into the underlying sandur sediments.

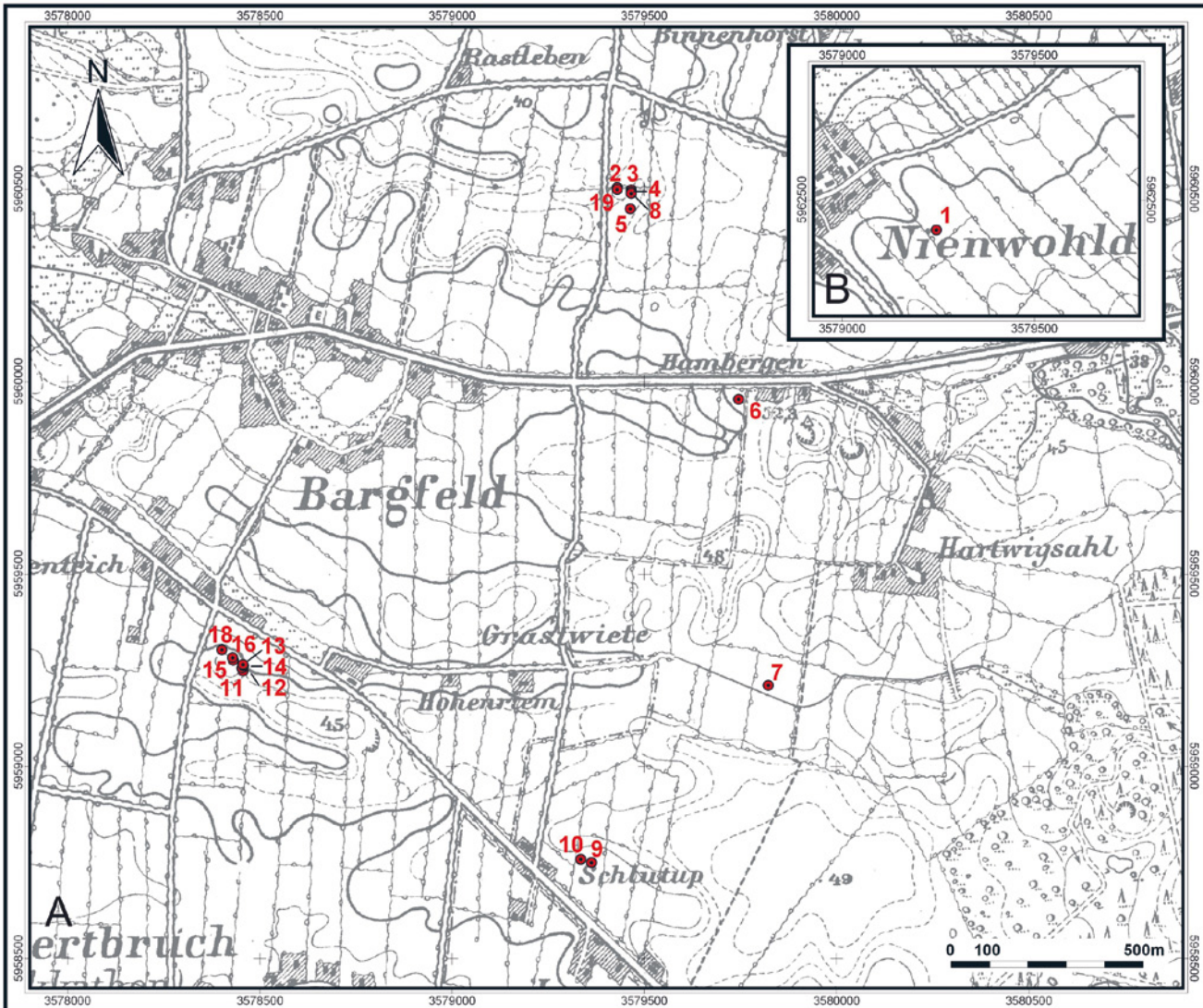


Abb. 6: Vorkommen der Rinnen-Strukturen im Untersuchungsgebiet (Preuß. Erstaufnahme, Blatt 2227 Bargteheide, Ausgabejahr 1878).

Fig. 6: Location map of the channels (1st Prussian ed., sheet 2227 Bargteheide, ed. 1878).

Norden hin ein. Die Hohlform zeigt eine verhältnismäßig flache Form, die Basisfläche ist durch stufenartige Formen auffallend unruhig gestaltet. Der interne Aufbau ist einfach. Im unteren Teil sind schluffige Sande aufgeschlossen, im Hangenden folgt aufgearbeiteter Till, der auch flächenhaft in den benachbarten Hohlformen 3 und 19 vorkommt. Abgedeckt wird die Hohlform von der periglazären Deckenschicht.

Die Rinnen-Struktur 8 liegt südlich benachbart zu der Hohlform 4 (Abb. 9c). Die Sandersande, in die die Rinne eingeschnitten ist, fallen leicht nach Norden hin ein. Die Struktur ist die breiteste der drei benachbarten Hohlformen. Der stehen gebliebene Sockel von Sandersanden zwischen dieser Hohlform und der benachbarten Hohlform 4 ist abgeflacht, was auf eine parallele Ausformung hindeutet. Das deutet sich auch durch den im Basisbereich der Hohlform 4 vorkommenden Sandhorizont an, der sich mit etwa ähnlicher Mächtigkeit in der Hohlform 4 fortsetzt. Das Zentrum der Hohlform wird ganz überwiegend durch einen rinnenartig eingesenkten Bereich von aufgearbeitetem Till eingenommen. Dieser setzt sich flächenhaft beidseitig der Hohlform fort, wobei im oberen Flankenbereich

der Struktur sowie oberhalb der bindigen Rinnenfüllung (zentral) schluffige Sande auftreten. Abgedeckt wird die Hohlform von der flächenhaft verbreiteten periglazären Deckschicht, die hier auffallend viele und große Geschiebe führt.

Die Rinnen-Struktur 5 (Abb. 7b) war an der Geländeoberfläche deutlich zu erkennen. Durch flächenhafte Georadar-Messungen (vgl. POTILLO et al. 2005) ist eine Länge der Struktur von ca. 25 Metern nachgewiesen. Die Struktur verläuft in Nord-Südrichtung. Vermutlich setzt sie sich nach Norden, in den nicht abgebauten Bereich hinein, fort. Das Liegende der Rinnen-Struktur wird durch Till gebildet, seitlich setzen bindige Sande ein. Die Rinne besitzt - im Gegensatz zu fast allen anderen Rinnen - eine vorwiegend sandige Füllung (meist Mittelsande). Sie zeigt dabei eine heterogene Internstruktur. Der untere Teil der Rinne ist mit deutlich geschichteten, bindig-sandigen Ablagerungen (Beckensedimente) verfüllt. An der Basis der Struktur treten einzelne Geschiebe auf. Die Füllung der Rinne besteht aus Fein-Mittelsanden, die teilweise hohe Anteile bindigen Materials führen können (Wasser führend). Die Sande sind teilweise deutlich verstellt. Zum Hangen-

Tab. 1: Angaben zu den Rinnen.

Tab. 1: Statistics concerning channel structures.

Nr.	Rechtswert [Mitte]	Hochwert [Mitte]	Breite [m]	Tiefe [m]	beobachtete Länge [m]	Exposition Wand	Orientierung
1	3579245	5962422	12	3,5	k. A.	E-W	k. A.
2	3579430**	5960504**	3	3	k. A.	N-S	k. A.
3	3579466	5960498	3	3,5	k. A.	N-S	k. A.
4	3579466	5960493	3,5	3	k. A.	N-S	k. A.
5	3579464	5960449	14	3,5	25	E-W	N-S
6	3579746	5959954	2,5	1,5	k. A.	E-W	k. A.
7	3579823	5959210	6	1,7	6	E-W	NNE-SSW
8	3579466	5960489	5,5	3,5	k. A.	N-S	k. A.
9 ¹⁾	3579363	5958749	5	3	30	N-S	WNW - ESE
10 ¹⁾	3579335	5958758	8,5	3			
11 ²⁾	3578457	5959247	14,5	4	30	E-W, NE-SW, NW-SE	N-S
12 ²⁾	3578454	5959255	13	3			
13 ²⁾	3578458	5959261	6	2			
14 ²⁾	3578457	5959264	26	4			
15 ³⁾	3578431	5959275	4,5	1,75	7	N-S	W-E
16 ³⁾	3578430	5959282	4,5	1,75			
17*	3578399	5959290	3,5	1,50	k. A.	E-W	k.A.
18	3578402	5959302	4	1,5	2	N-S	k.A.
19**	3579430	5960499	4,5	3,5	k. A.	N-S	k. A.

1), 2), 3) - jeweils zusammenhängend

* nicht näher dokumentiert; ** ungefähre Lage

k. A. = keine Angabe; Rinnen nur im Anschnitt in der Grubenwand beobachtet

den hin nimmt der bindige Anteil ab, im oberen Drittel der Struktur treten reine Feinsande auf. Die Rinne zeigt eine asymmetrische Unterfläche. Sie weist, abgeleitet aus der flächenhaften Georadar-Vermessung, an der Westseite eine stärkere Neigung als an der Ostseite auf. In der flächenhaften Erfassung mittels Georadar wurden auch unregelmäßige Vertiefungen im Längsverlauf sichtbar, ähnlich dem Profil einer subglazialen Rinne. An der östlichen Flanke der Rinne sind flächenhaft vorwiegend stark sandige Schluffe (bzw. Geschiebemergel) vorhanden, die deutlich geschichtet sind. Sie sind teilweise als Solifluktionsbildung zu interpretieren. Die Schüttung der Sedimente in der Rinne ist generell nach Norden ausgerichtet. Die Schüttungsrichtung in den liegenden, schluffigen und weniger einheitlichen Sanden liegt zwischen 75° und 110° (Einfallen bis 25°). In den hangenden Fein- bis Mittelsanden (Einfallen bis 20°) liegt sie zwischen 80° und 110°. Die schluffigen Sande und Schluffe können als Beckenbildungen gedeutet werden, die nachträglich verstellten worden sind. Hierbei dürfte Toteisdynamik eine größere Rolle gespielt haben. Die Sandschollen sind in gefrorenem Zustand transportiert worden. Abgedeckt wird die Hohlform von der flächenhaft verbreiteten periglaziären Deckschicht.

Die flache Rinnen-Struktur 6 (Abb. 7b) ist in einen liegenden Till eingeschnitten. Dieser ist hier sehr gleichförmig mit einem Meter Mächtigkeit vorhanden. Im Hangenden des Tills folgt eine Lage aufgearbeiteten Tills, der im Bereich der Rinne ausgeräumt ist. Die Basisfläche dieses Horizontes fällt zur Rinne hin ab. Der im Liegenden des relativ homogenen Tills folgende sandige Scher-Till ist wenige Dezimeter mächtig und wird nicht mehr durch die eingeschnittene Rinne berührt. Das Profil der Rinne

hat eine konvexe Form. Im Basisbereich der Rinne findet sich eine geringmächtige Lage schluffig-sandigen Materials. Die Rinne selbst ist vorwiegend mit schluffig-sandigen Sedimenten verfüllt, das sich in die Fläche fortsetzt, in der Hohlform jedoch eine größere Mächtigkeit erreicht. Abgedeckt wird die Hohlform von der flächenhaft verbreiteten periglaziären Deckschicht.

Die Rinnen-Struktur 7 (Abb. 7a) ist in die liegenden glazifluviatilen, hier weitgehend söhlig liegenden Sandersande eingeschnitten. Sie weist eine leichte Asymmetrie auf (flachere Flanke im Osten). Sie ist vorwiegend mit aufgearbeitetem Till verfüllt, der verhältnismäßig homogen ist. Im Zentrum sind Sande in Form einer sekundären, flachen Rinne verbreitet. Diese Sande nehmen an der Oberfläche der Gesamtstruktur die größte Fläche ein. Sie sind deutlich geschichtet.

Die Rinnen-Struktur 9 (10) (Abb. 7b) unterscheidet sich von den anderen, da sie nicht so deutlich ausgeprägt ist. Sie dürfte im nördlichen Abschnitt durch eine Frost-/Eiskeilstruktur vorgeprägt worden sein. Die Frost-/Eiskeil-Pseudomorphose liegt an der Basis der Rinne und reicht mehr als 1,5 m tief in die liegenden Sandersande. Die Rinnen-Struktur ist sehr flach und ist mit aufgearbeitetem Till verfüllt, der sich zu beiden Seiten in die Fläche fortsetzt. In den Till sind Schollen von sandig-schluffigen Sedimenten eingestreut. Bei der nicht abgebildeten Rinne 10 handelt es sich um die Fortsetzung der Rinne 9. Diese Rinne wurde nur hinsichtlich ihrer Ausmaße erfasst, sie ist deutlich breiter, gleich tief und vergleichbar aufgebaut.

Bei der Rinnen-Struktur 11 (12 / 13 / 14) handelt es sich um die größte Rinne im Untersuchungsbereich (Abb. 7c und 9 e-d), die längere Zeit im Abbau über eine Länge

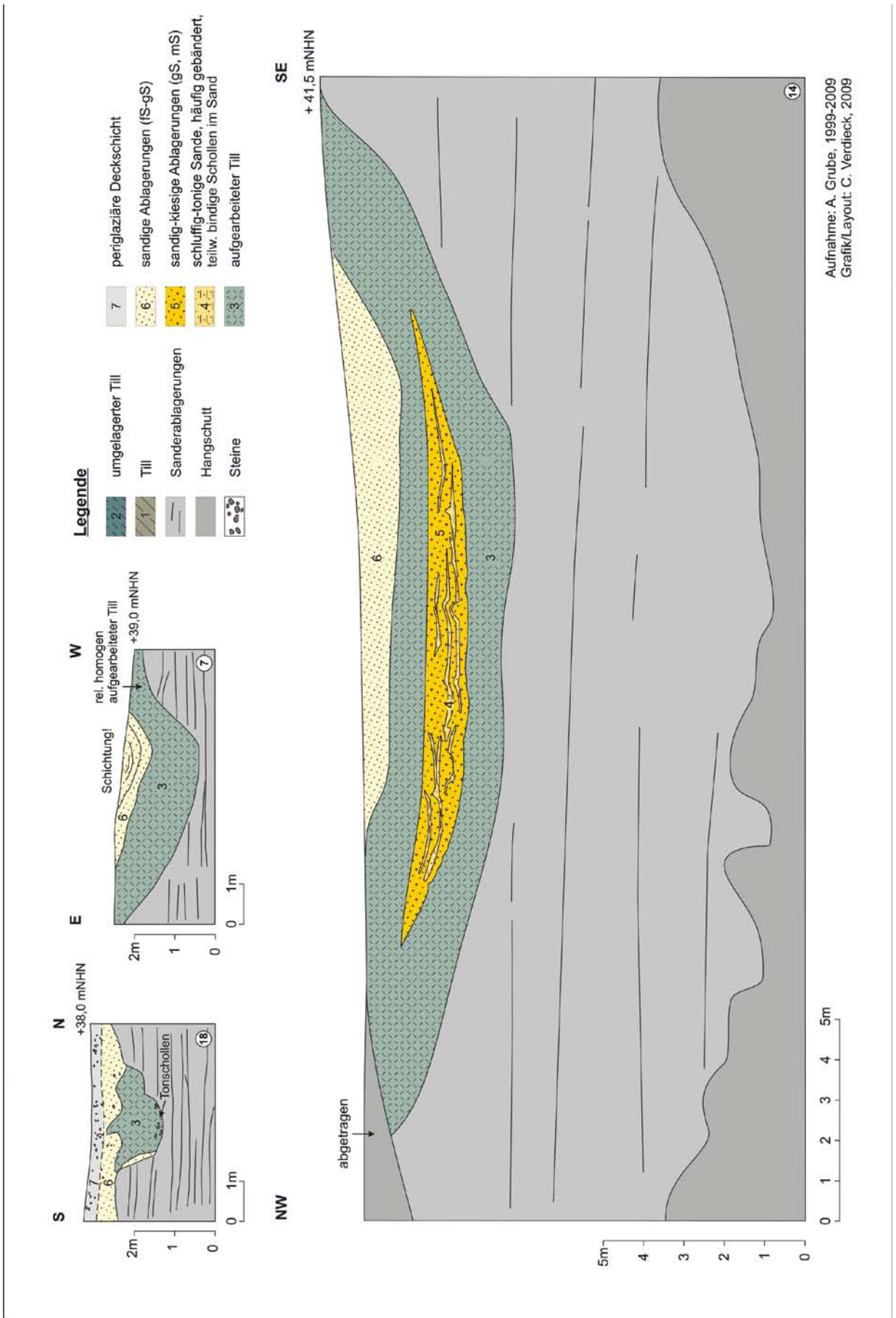


Abb. 7a: Vereinfachte Querprofilaufnahmen verschiedener rinnenartiger Strukturen (End-Koordinaten in Tab. 1).
Fig. 7a: Cross profiles of different channel structures (coordinates in tab. 1).

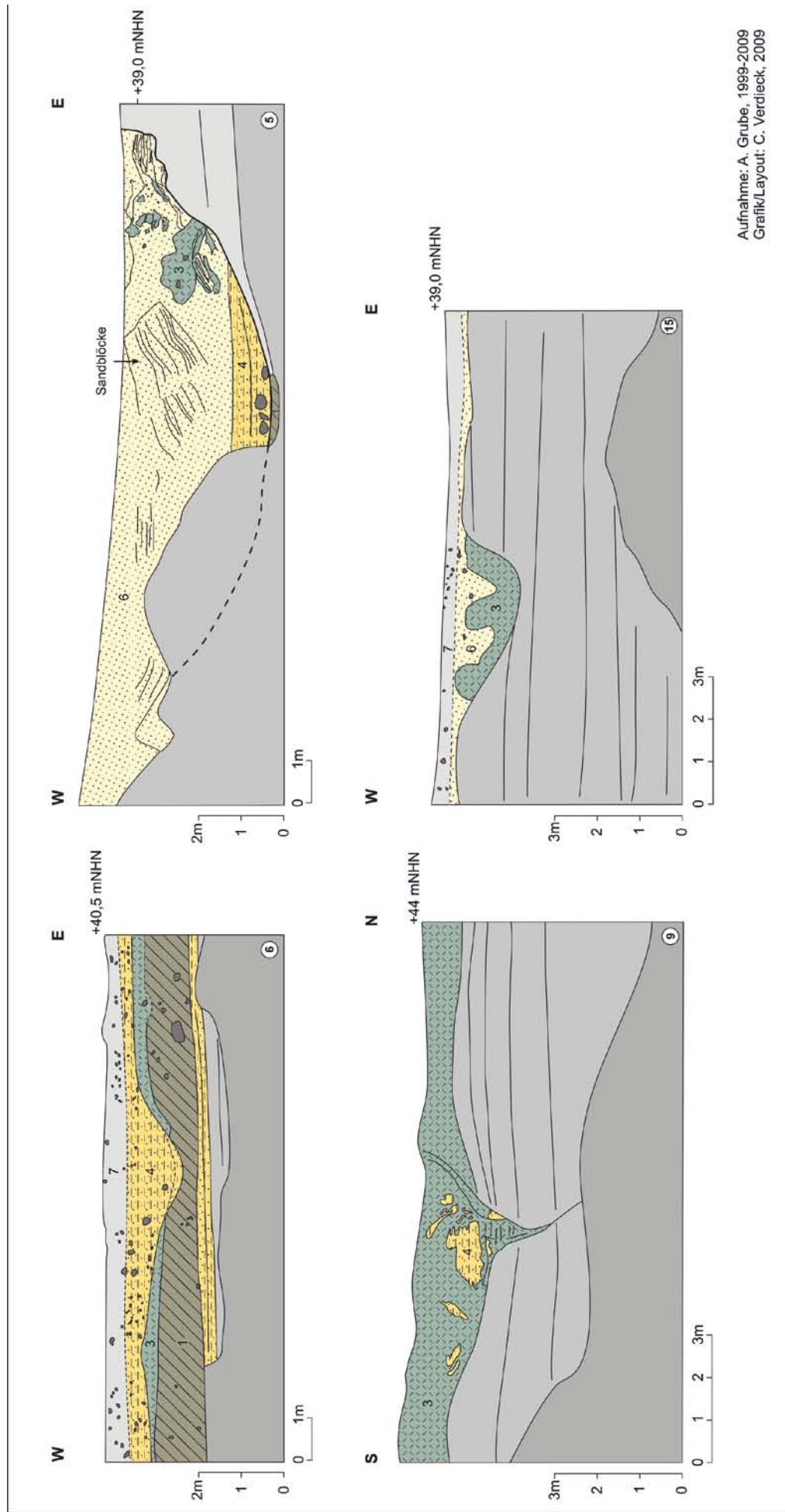


Abb. 7b: Vereinfachte Querprofileaufnahmen verschiedener rinnenartiger Strukturen.
Fig. 7b: Cross profiles of different channel structures.

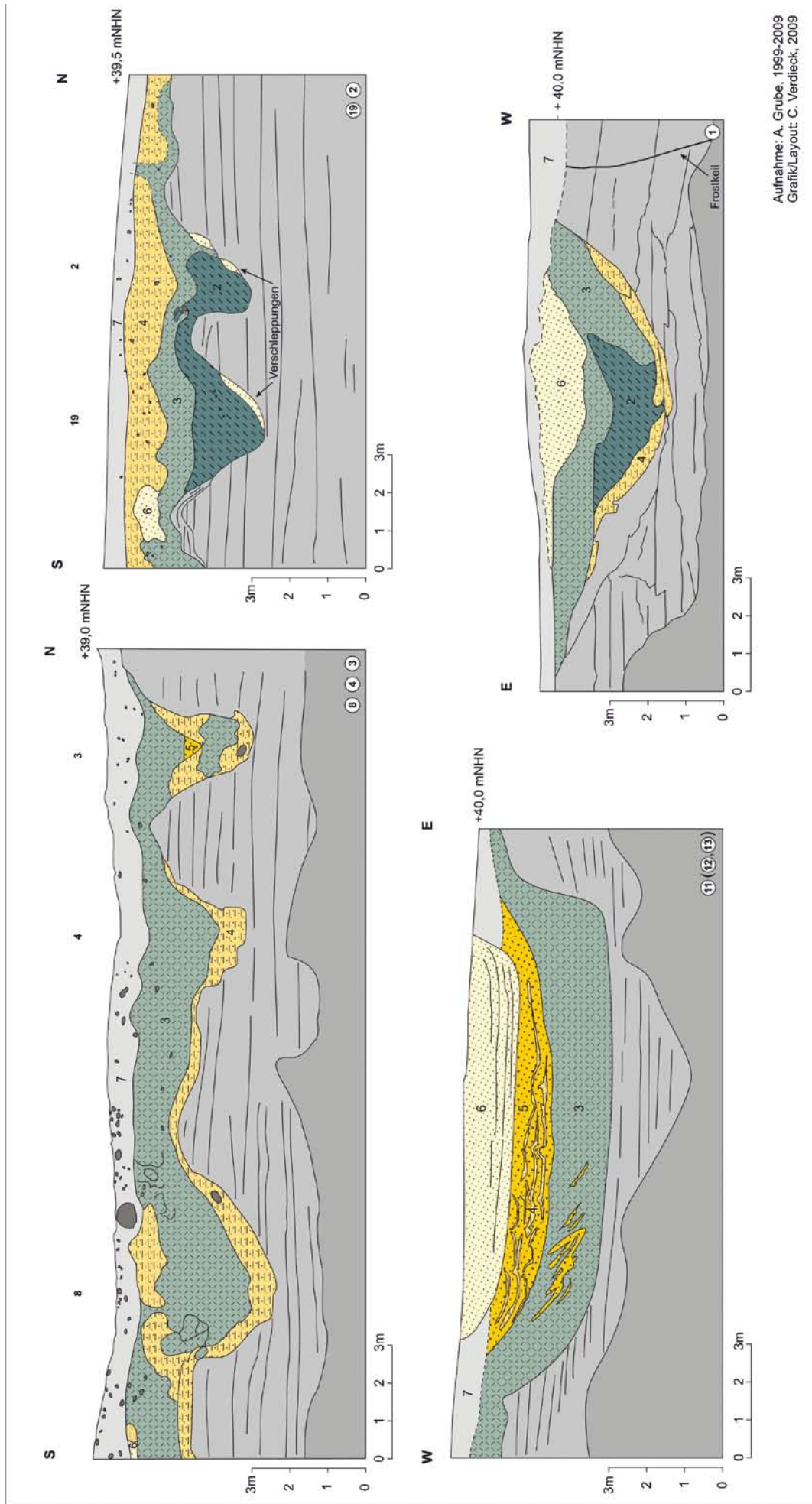


Abb. 7c: Vereinfachte Querprofilaufnahmen verschiedener rinnenartiger Strukturen.
Fig. 7c: Cross profiles of different channel structures.

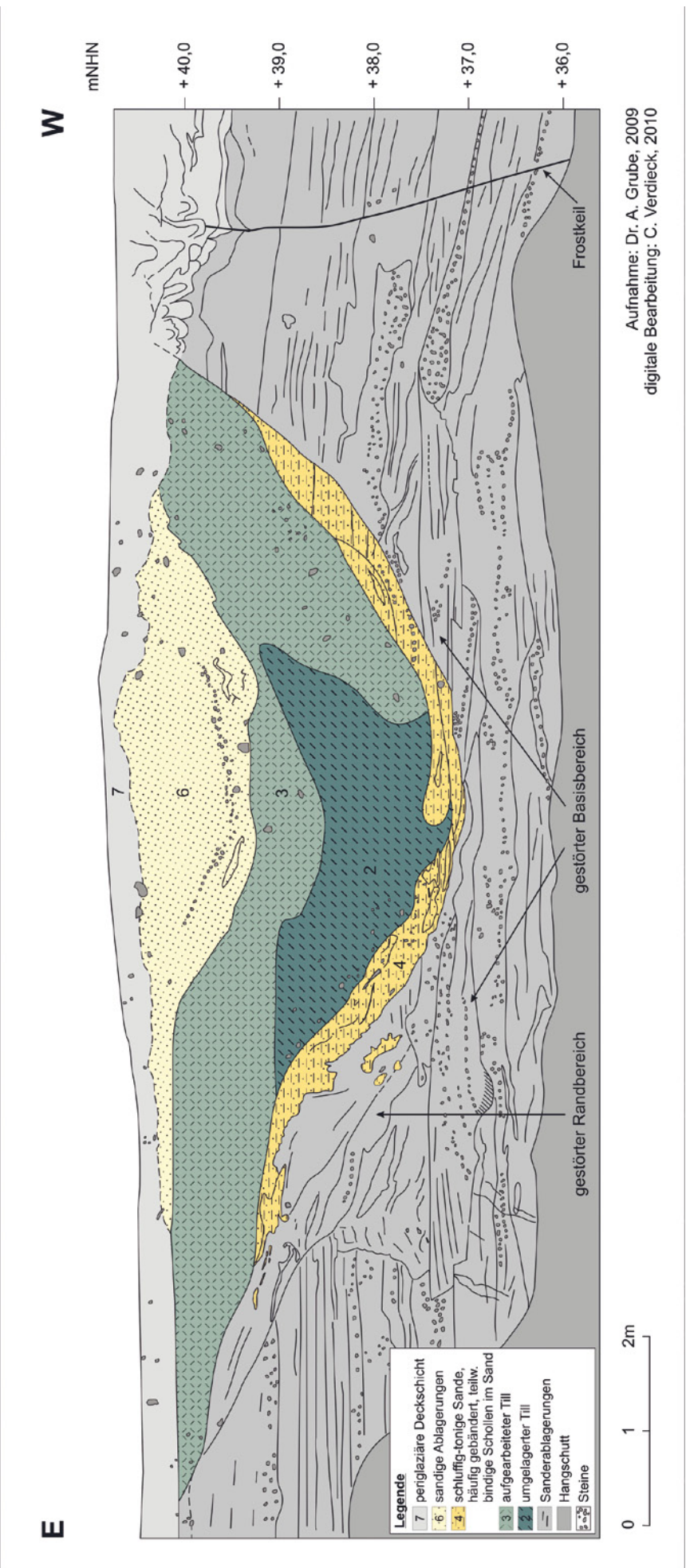


Abb. 8: Detailquerschnitt Rinnen-Struktur 1.
Fig. 8: Crossprofile channel 1.

von ca. 30 m verfolgt werden konnte. Ihre ursprüngliche Länge konnte aufgrund des bereits erfolgten Abbaus im nordöstlich anschließenden Bereich nicht festgestellt werden (Rest-abbau). Hierbei änderte sich die Breite der Form, weniger jedoch die Internstruktur. Die Rinnen-Struktur besitzt eine ungefähr N-S-gerichtete Erstreckung. Sie ist bis zu ca. 26 m breit und 3,5 m tief. Die Oberfläche der Struktur liegt bei ca. +40 m NHN. Die Sohle ist im Anschnitt 11 mit einer Breite von ca. 5 m auffallend eben, mit einem geringfügigen Gefälle zur östlichen Flanke.

Die Rinne ist vorwiegend mit schluffigen Sanden gefüllt. Im westlichen Bereich sind ca. 0,5 m unterhalb der Hohlformsohle bis zu ca. 0,15 m mächtige schluffige Bänder vorhanden, deren Mächtigkeit nach Osten hin abnimmt bzw. die im östlichen Bereich der Hohlform dann fehlen. Der untere Teil der Hohlform ist mit aufgearbeitetem Till gefüllt (siehe Abb. 9f). In diesen Till ist über die gesamte Hohlform ein schluffiger Horizont eingeschaltet, in dem besonders im westlichen Bereich der Rinne verstellte Sandlinsen (helle Sande) vorkommen. Es folgen schluffig-sandige Ablagerungen, in die dunkle Schluffbänder (periglaziar erheblich verstellt; wellenartige Struktur) eingeschaltet sind (Abb. 9e). Auf einem Großteil des Rinnenquerschnittes ist bis an die Oberfläche schließlich eine sekundäre Rinnen-Struktur eingeschnitten. Diese weist flach einfallende bis söhlige Mittelsande auf. Die oberen Randbereiche der Rinne 11 zeigen auf der Ost-Seite leichte Stauchungen bzw. Quetschungen („Ausweichen“ der bindigeren Sedimente). Die Verstellungen könnten durch Kompression durch die zentrale, ca. 0,7 m mächtige, rinnenartige sekundäre Rinnen-Struktur eingetreten sein. Die randlichen Verstellungen (Pressungen) weisen darauf hin, dass die sekundäre Rinnenbildung in unkonsolidiertem Sediment stattfand, was auf ein zeitlich nicht allzu weit auseinander liegendes Einschneiden hindeutet. Die Aufnahme der Rinnen-Struktur 11-14 im Nordteil (14) zeigt einen der Internstruktur der Rinne 11 vergleichbaren Aufbau. Leider war die Struktur aufgrund der Höhe der frischen Abbauwand nicht genauer zu dokumentieren. Nach Norden wird die gesamte Rinne offenbar flacher. Auch weist sie keine ebene Unterseite mehr auf. Die Rinnenfüllung ist unverändert, auch die sekundäre, mit horizontal gelagerten Sanden gefüllte Rinne setzt sich über die gesamte Länge der Struktur hin fort.

Die Rinnen-Struktur 15/16 (B: 4,5 m, T: 1,7) verläuft ungefähr parallel zur Struktur 11-14, d. h. in Nord-Süd-Richtung. Die Rinne (Abb. 7b) ist ebenso verhältnismäßig flach ausgebildet. Die Rinne ist im unteren Teil flächig mit aufgearbeitetem Till gefüllt, der bis in die Nähe der periglaziären Deckschicht aufragt. Seine Verbreitung ist auf die Rinne beschränkt, im Gegensatz z. B. zu Rinnen-Strukturen 4 und 19. In den Till sind zwei unregelmäßige, rinnenartige Vertiefungen mit Sanden relativ steil eingeschnitten. Nicht ausgeschlossen werden kann auch eine diapirartige Aufwölbung des Tills. Abgedeckt wird die Hohlform von der flächenhaft verbreiteten periglaziären Deckschicht.

Die Rinnen-Struktur 17/18 (und 19) ist verhältnismäßig flach ausgebildet (Abb. 7a). Im nördlichen (rechten) Flankenbereich findet sich ein stufenartiger Versatz. Ob die flachen benachbarten Rinnen zusammenhängen oder ggf. sogar eine vernetzte Struktur bildeten, konnte nicht festgestellt werden. Ähnlich wie die Rinne 15/16 zeigt die Rinne eine überwiegende Verfüllung mit aufgearbeitetem Till, der hier eine rötliche Färbung besitzt. Im Basisbereich sind kleine, bindige Schollen (Ton) eingeschaltet. An der linken Flanke der Rinne sind sandige Ablagerungen vorhanden. Die hangenden sandigen Ablagerungen greifen unregelmäßig in die Till-Oberfläche ein. Ein diapirartiges Aufdringen des Tills mit einer leichten Südvergenz des Diaps ist zu erkennen. Abgedeckt wird die Hohlform von der flächenhaft verbreiteten periglaziären Deckschicht, die in diesem Gebiet relativ geringmächtig ist.

5 Diskussion

Die intensive periglaziäre Überprägung des Sanderbereiches Bargfeld-Stegen ist nicht ungewöhnlich, auf dieses generelle Phänomenen auch im Jungmoränenbereich Schleswig-Holsteins hat bereits DÜCKER (1954) hingewiesen. Der Binnensander von Bargfeld-Stegen liegt relativ weit von der diskutierten Maximalausdehnung der Weichsel-Vereisung (qw0-Vorstoss, MÜLLER 2004) im westlich gelegenen Kisdorfer Wohld (JANETZKO 2002; STEPHAN 2011) entfernt. Der liegende Till wird hier diesem ersten Vorstoß zugeordnet. Die Kryoturbationen durchschlagen teilweise den oberen Till, der einer jüngeren (der zweiten?) Weichsel-Vereisung zugeordnet wird. Die tief reichende Formung

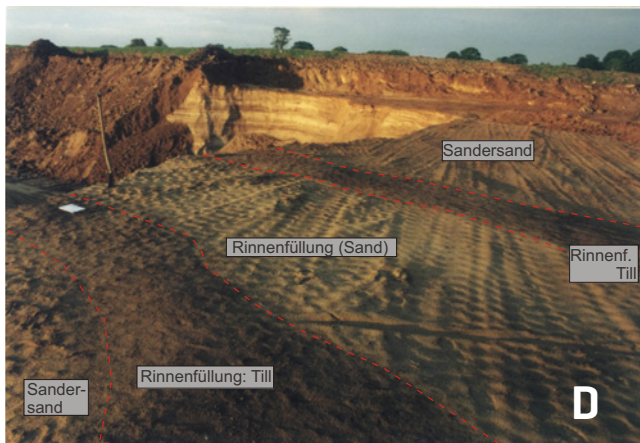




B



C



D



E



F



G



H

Abb. 9: Photos der Strukturen.

Fig. 9: Photos of structures.

A – Rinne 1 / channel 1

B – Rinne 3 / channel 3

C – Rinnen 8-4-3 / channels 8-4-3

D – Rinne 7 (Aufsicht) / channel 7 (top view)

E – Rinne 11 / channel 11

F – Rinne 11 – westliche Flanke / channel 11 – western flank

G – Rinne 11 – obere Ostflanke / channel 11 – upper eastern flank

H – Rinne 14 / channel 14

der Kryoturbationen (mehr als 3,5 m) weist auf eine hochglaziale Bildung bei Permafrost hin (VANDENBERGHE 1983). Es kann davon ausgegangen werden, dass der Deck-Till im Untersuchungsgebiet während der Hauptvereisungsphase der Weichsel vor ca. 25.000 Jahren abgelagert wurde. Damit würde für die Überprägung eine Zeitspanne von mindestens 10 ka zur Verfügung gestanden haben.

Erfasst wurden relativ zahlreiche Rinnen auf einer im Verhältnis zur Gesamtfläche des Binnensanders kleinen Kartierfläche. Sie unterscheiden sich hinsichtlich der Petrographie von ihrer Umgebung, da sie häufig bindige (Teil-)Füllungen enthalten. Die Rinnen sind insgesamt gesehen recht heterogen strukturiert. Sie zeigen einen unregelmäßigen Verlauf. Auch die Dimensionen der Hohlformen sind unterschiedlich. Die Struktur 5 könnte glazitektonisch initiiert worden sein, und soll deshalb hier nicht mit diskutiert werden. Die erfassten Rinnen zeigen, trotz ihrer Individualität, einige Gemeinsamkeiten:

- meist sanft geneigtes, konvexes Querprofil
- häufig flache Basisfläche bzw. Einschneiden der Rinne bis zu einer Grenzfläche
- meist an der heutigen Erdoberfläche nicht zu erkennen
- häufig bindige (Teil-)Füllungen der Rinnen (aufgearbeiteter oder umgelagerter Till u.a.)
- vielfach Unterschneidungen und andere fluviatile Formen an den Rinnenflanken
- teilweise Diapir-artiges Aufdringen des aufgearbeiteten Tills und anderer Rinnenfüllungen im oberen Bereich und im Randbereich der Rinnen
- mehrere Rinnen zeigen eine verhältnismäßig homogenem Sand gefüllte Sekundär-Rinne im oberen Zentrum der Struktur, d.h. eine spätere Überprägung der Haupt-Rinne
- beobachtete Verstellungen an der Sohle der Strukturen bzw. innerhalb der liegenden Sanderablagerungen, in die die Rinnen einschneiden deuten auf eine Anlage in Dauerfrostboden hin.

Als Ursache der Rinnen-Strukturen kommen glazogene, glazifluviatile bzw. kaltzeitlich-fluviatile sowie periglaziäre Einflüsse in Frage. Eine zentrale Frage bezüglich der Genese der beschriebenen Rinnen-Strukturen ist die nach einer möglichen glazialen Genese. Die Rinnen könnten als Exarations-Spuren aufgefasst werden. Gegen eine glaziale Genese sprechen jedoch u. a. die generell flache Ausprägung, die teilweise deutliche Schichtung innerhalb der Rinnen, die typischen periglaziären Verstellungen (u. a. Kryoturbation, Diapirbildung) in den Rinnen (auch in tieferen Abschnitten) sowie der Verlauf der Rinnen quer bzw. im deutlichen Winkel zur Haupt-Vorstoßrichtung des Eises. Gegen eine rein glazifluviatile oder kaltzeitlich-fluviatile Formung sprechen vor allem die meist abgeflachte bis ebene Sohle der meisten Rinnen-Strukturen und die relativ große Breite der Rinnen im Verhältnis zur geringen Tiefe. Teilweise könnten die Rinnen jedoch glazifluviatil oder subglazial initiiert worden sein, d.h. der (sub-)glazialen Entwässerung gedient haben. Die teilweise fluviatile Formung in gefrorenem Boden ist durch das steile Einschneiden einiger Rinnen belegt. Im unteren Teil einiger Rinnen finden sich zudem häufiger Kiese und Steine.

Teilweise sind Ähnlichkeiten der hier beschriebenen Strukturen mit „Riesenfrosttaschen“ bzw. „Lehmsträngen“ (GOLTE & HEINE 1974, EISSLAMM 1981) vorhanden. Letztere scheinen jedoch seltener trogartig geformt sowie netzartig verbunden zu sein. Sie sind zudem deutlich kleiner, auch ihre Füllung scheint von den hier beschriebenen Rinnen abzuweichen. Insgesamt tendiert ihre Form und Füllung eher in Richtung Kryoturbation. Ähnlichkeiten sind gegeben in Bezug auf die Größe der Formen und das Vorkommen in sandigem Substrat.

Die hier favorisierte, vorwiegend durch periglaziäre Prozesse bedingte Genese der Rinnen passt zur erwähnten intensiven periglaziären Überprägung im Raum Bargfeld-Stegen. Die Strukturen dürften vorwiegend unter Frostbodenklima durch die Wirkung periglaziär-fluviatiler Prozesse, in Verbindung mit Solifluktions-Prozessen geschaffen worden sein. Dafür spricht zunächst, dass einige der Rinnen verhältnismäßig flach und breit sind. Bei der Formung ist Abluation der Hauptprozess, ein denudativer Spülprozess (Abspülung) auf Hängen. Die teilweise flache Ausbildung der Rinnensohle könnte mit einer unterlagernden Permafrostschicht zusammenhängen, bis zu der das Einschneiden stattfand. Es finden sich Verstellungen der liegenden Sanderablagerungen, in die die Rinnen einschneiden. Trotz dieser beobachteten lokalen Störungen in den liegenden Schmelzwassersanden (z. B. Rinnen 1 und 11; Abb. 8 und 7c), behielten diese Ablagerungen weitgehend ihr ursprüngliches Ablagerungsgefüge bis in Erdoberflächennähe (häufig wenige Dezimeter unter GOK). Beides deutet darauf hin, dass die Rinnen in einen Permafrostkörper eingeschnitten worden sind.

Die periglaziären rinnenartigen Strukturen scheinen bevorzugt im Randbereich der Deck-Till-Verbreitung aufzutreten. Das Vorkommen des Deck-Tills bedingt, dass das anfallende Niederschlags- und Schmelzwasser während Auftauphasen des Permafrosts weniger gut versickern konnte und dadurch vorwiegend oberflächlich abfloss. Hierdurch könnte die Bildung von Rinnen begünstigt worden sein. Die Strukturen wurden durch periglaziäre Massenverlagerung (Soliflaktion) und glazifluviatile Prozesse verfüllt. Durch den Wechsel von Till, Sanden und schluffig-sandigen Ablagerungen kann von verschiedenen Verfüllungsphasen ausgegangen werden. Während der Wiederverfüllung wurden die Sedimente verschiedentlich periglaziär überformt, u. a. durch den Aufbau eines zu Diapir-Strukturen führenden Druckregimes. Der solifluidale Einfluss ist in den meisten Rinnen durch das Vorkommen von umgelagertem und aufgearbeitetem Till belegt. Das an der ehemaligen Oberfläche verbreitete, generell eher fleckenhaft vorkommende und geringmächtige bindige Sediment (Till) konnte solifluidal leicht bewegt werden. Textur und Gefüge der in den Rinnen vorhandenen Tills sind teilweise nur wenig verändert, was ggf. auf kurze Transportentfernungen hindeutet. Die Rinnen verlaufen, nach den bisher vorliegenden Informationen, häufig in einer ungefähren Nord-Süd-Richtung. Dieses könnte teilweise mit der Sonnen-Exposition zusammenhängen, die zu einer bevorzugten Schmelzwasser- und Solifluktions-Aktivität an südexponierten Hängen führte.

Zur genaueren Analyse der Genese und Struktur der in der vorliegenden Arbeit vorgestellten Rinnen sind nähere flächenhafte geologische Untersuchungen mit geophysikalischer Unterstützung notwendig.

6 Danksagung

Der Firma Timm (Bargfeld-Stegen), insbesondere den Herren Timm sen. und jun. sowie Kurt Brüggmann, der Fa. Willy Krohn GmbH (Sieck) und der Fa. C. & W. Borchert (Hamburg; Herr Poersch, besonders Peter Lattke) sei für die zuvorkommende Behandlung und die praktische Hilfe bei den Feldarbeiten sowie die Genehmigung zur Einsicht in firmeneigene Unterlagen gedankt. Christina Verdieck (LLUR) sei für die digitale Umsetzung der Rinnen-Zeichnungen, Frau Maike Schirk (LLUR) für die Erstellung der Profilschnitte herzlich gedankt. Herrn Jürgen Ehlers (Hamburg) und Herrn Stefan Wansa (Halle/Saale) danke ich besonders für die kritisch-konstruktive Durchsicht und Verbesserung des Manuskriptes.

7 Literatur

- ALAI-OMID, M., CHRISTENSEN, S., KOSACK, B. & LANGE, W. (1988): Grundzüge der Geologie des Kreises Stormarn. – Die Heimat, 95 (1): 18-31.
- BAUKE, Chr. (2008): Geologie und Sedimentologie im Raum Bargfeld-Stegen (Schleswig-Holstein). – Department Geowissenschaften, Universität Hamburg, Diplomarbeit Dipl.-Geologen-Hauptprüfung, Teile I + II; 73 S., Anhang [unveröff.].
- BOCK, W. (1981): Schichtenfolge, Grundwasserphysik und Grundwasserbeschaffenheit in Bargfeld-Stegen (TK 2227). – Hydrogeologisches Gutachten, Geologisches Landesamt Schleswig-Holstein vom 23.04.1981; 11 S. und Anhänge.
- BRANDES, H., HÖFLE, H.C., JORDAN, H., LEPPER, J., MENGELEING, H., MERKT, J., MEYER, K.-D., REUTER, G., TÜXEN, J., VINKEN, R., VOSS, H.-H., GRUBE, F. & LANGE, W. (1977): Geologische Übersichtskarte 1:200.000 – CC 3176 (HH-Ost). – Bundesanstalt für Geowissenschaften und Rohstoffe [Hrsg.], Hannover.
- DÜCKER, A. (1954): Die Periglazial-Erscheinungen im holsteinischen Pleistozän. – Göttinger Geographische Abhandlungen, 16: 5-54, Anhang.
- EISSMANN, L. (1981): Periglaziäre Prozesse und Permafroststrukturen aus sechs Kaltzeiten des Quartärs. – Altenberger Naturwissenschaftliche Forschungen, 1: 1-127, Anhang.
- GOLTE, W. & K. HEINE (1974): Fossile Riesen-Eiskeilnetze am Niederrhein. – Eiszeitalter und Gegenwart, 25: 132-140.
- GRUBE, A. (2010): Sülfelder Tannen – eine einmalige Niedertau- und Kamme-Landschaft der Weichsel-Kaltzeit (Kreise Stormarn und Segeberg). – Natur- und Landeskunde, 117 (7-9): 93-101.
- HANNEMANN, M. (1963): Anlage und Entwicklung weichseleiszeitlicher glaziger und periglazier Täler in Südostbrandenburg. – Berichte der Geologischen Gesellschaft in der DDR, 8: 617-636.
- HENNING, I. (1973): Zur periglazialen Talententwicklung im norddeutschen Jungmoränengebiet. – Schriften des Naturwissenschaftlichen Vereins für Schleswig-Holstein, 43: 25-28.
- JANETZKO, P. (2002): Der Kisdorfer Wohld – eine Landschaft im Aufbruch. – LANU-Jahresbericht, 2002: 152-155.
- LIEDTKE, H. (1993): Phasen periglaziär-geomorphologischer Prägung während der Weichseleiszeit im norddeutschen Tiefland. – Zeitschrift für Geomorphologie, Neue Folge, Suppl.-Bd., 93: 69-94.
- MÜLLER, U. (2004): Weichsel-Frühglazial in Nordwest-Mecklenburg. – Meyniana, 56: 81-115.
- POTILLO, R., GRUBE, A., BETZLER, C. & REISS, S. (2005): Georadaruntersuchungen zur Erkundung von Sand- und Kieslagerstätten in Norddeutschland. – Bericht für die Verbände Nord, Industrieverband Sand, Kies, Mörtel, Transportbeton Nord e.V., Hamburg, 15 S. [unveröff.].
- RICHTER, K. (1932): Die Bewegungsrichtungen des Inlandeises, rekonstruiert aus den Kritzen und Längsachsen der Geschiebe. – Zeitschrift für Geschiebeforschung, 8: 62-66.
- SEMMLER, A. (1985): Periglazialmorphologie. – Erträge der Forschung, 231: 1-116; Darmstadt.
- STEPHAN, H.-J. (2003): Zur Entstehung der eiszeitlichen Landschaft Schleswig-Holsteins. – Schriften des Naturwissenschaftlichen Vereins für Schleswig-Holstein, 67: 101-118.
- STEPHAN, H.-J. (2004): Karte der Stauchgebiete und Haupt-Gletscherrandlagen in Schleswig-Holstein 1:500.000. – Meyniana, 56: 149-154.
- STEPHAN, H.-J. (2011): Geschiebestratigraphische Untersuchungen im Bereich der Stauchmoräne Kisdorfer Wohld, Südholstein und in ihrem Hinterland. – Geschiebekunde aktuell, Sonderheft 9: 113-124.
- SULKOWSKI, N. (2008): Geologie und Sedimentologie im Raum Bargfeld-Stegen (Schleswig-Holstein). – Department Geowissenschaften, Universität Hamburg, Diplomarbeit, Dipl.-Geologen-Hauptprüfung, Teile I + II; 67 S., Anhang [unveröff.].
- TODTMANN, E. M. (1952): Über Schwankungen des weichselzeitlichen Eisrandes im südlichen Holstein. – Abhandlungen und Verhandlungen des Naturwissenschaftlichen Vereins zu Bremen, 33: 89-106.
- VANDEMBERGHE, J. (1983): Some periglacial phenomena and their stratigraphical position in Weichselian deposits. – Polarforschung, 53 (2): 97-107.

A permafrost glacial hypothesis – Permafrost carbon might help explaining the Pleistocene ice ages

Roland Zech

How to cite: ZECH, R. (2012): A permafrost glacial hypothesis – Permafrost carbon might help explaining the Pleistocene ice ages. – E&G Quaternary Science Journal, 61 (1): 84–92. DOI: 10.3285/eg.61.1.07

Abstract: Over the past several ~100 ka glacial-interglacial cycles, the concentration of atmospheric CO₂ was closely coupled to global temperature, which indicates the importance of CO₂ as a greenhouse gas. The reasons for changes in atmospheric CO₂ have mainly been sought in the ocean, but remain elusive. Moreover, the mid-Pleistocene transition from the ‘41 ka world’ during the early Pleistocene before ~0.7 Ma to the ~100 ka ice age cycles is poorly understood. The classical Milankovitch theory of summer insolation forcing at high northern latitudes can not fully explain the Pleistocene ice age rhythm. Based on the recent findings that the amount of soil organic carbon stored in high-latitude permafrost regions has been greatly underestimated and the simple logic that permafrost regions and respective carbon pools were likely much larger during glacials than during interglacials, a ‘permafrost glacial hypothesis’ is proposed: (i) Gradual sequestration of CO₂ in permafrost soils during coolings and rapid release of CO₂ and methane during terminations, respectively, provide important positive feedbacks for the climate. (ii) Integrated annual insolation at the southern and thus most sensitive permafrost boundary may act as a trigger for global climate changes. (iii) The mid-Pleistocene transition might be readily explained with permafrost extents reaching ~45°N during the long-term Pleistocene cooling, resulting in a transition from high-latitude obliquity (~41 ka) to mid-latitude eccentricity (~100 ka) forcing.

Eine Permafrost Hypothese – Kohlenstoff in Permafrostböden könnte helfen, die pleistozänen Eiszeiten zu erklären

Kurzfassung: Während der letzten ~100 ka Glazial-Interglazial-Zyklen war die Konzentration des Treibhausgases CO₂ in der Atmosphäre eng mit der globalen Temperatur gekoppelt. Die Gründe für die CO₂-Konzentrationsschwankungen wurden bislang vor allem im Ozean vermutet, bleiben aber rätselhaft. Darüberhinaus gibt es nur spekulative Erklärungsansätze für den mittelpaläozänen Übergang von den 41 ka Eiszeitzyklen im Frühpaläozän vor ~0.7 Ma zu den ~100 ka Eiszeitzyklen danach. Die klassische Milankovitch Theorie der Sommerinsolation in hohen nördlichen Breiten kann die Abfolge der pleistozänen Eiszeiten nicht vollständig erklären.

Basierend auf jüngsten Erkenntnissen, dass die Menge des organischen Bodenkohlenstoffs in Permafrostgebieten massiv unterschätzt wurde, und der simplen Logik, dass Permafrostgebiete und die entsprechende Kohlenstoffspeicherung in den Eiszeiten vermutlich wesentlich größer waren als in den Warmzeiten, soll hier eine „Permafrost Hypothese“ vorgestellt werden: (i) Langsame Anreicherung von Kohlenstoff in Permafrostböden während Abkühlungsphasen, sowie rasche Freisetzung von CO₂ und Methan während Erwärmungsphasen, sind entscheidende positive Rückkopplungsprozesse für das Klima. (ii) Änderungen der integrierten annualen Insolation an der südlichen, und damit sensitiven Permafrostgrenze könnten als externe Auslöser für globale Klimaveränderungen fungieren. (iii) Der mittelpaläozäne Wechsel der Eiszeitzyklen könnte implizit damit erklärt werden, dass Permafrostgebiete im Laufe der langfristigen pleistozänen Abkühlung Breiten von ~45°N erreichten. Dort verschwindet das für höhere nördliche Breiten charakteristische aus der Schiefe der Ekliptik resultierende ~41 ka Signal der annualen Insolation, und es dominiert allein das ~100 ka Signal der orbitalen Ekzentrizität.

Keywords: Pleistocene, ice ages, Milankovitch, insolation forcing, permafrost, Siberia

Address of author: R. Zech, Geological Institute, ETH Zurich, Sonneggstr. 5, 8092 Zurich, Switzerland. E-Mail: godotz@gmx.de, Phone: +41 44 632 2184, Fax +41 44 632 1080

1 Introduction

Recent studies have suggested that much more soil organic carbon is stored in northern permafrost regions than hitherto assumed, possibly as much as 1670 Pg C (SCHUUR et al. 2008; TARNOCAI et al. 2009). On the one hand, such high figures imply that the role of permafrost for soil organic matter preservation may have been underestimated, particularly in view of low biomass production in such cold ecosystems. On the other hand, these revised carbon pool estimates have fueled concerns that anthropogenic warming leads to thawing of permafrost, enhanced mineralization of soil organic carbon, and release of CO₂ and methane into the atmosphere (KHVOROSTYANOV et al. 2008; SCHAEFER

et al. 2011; SCHUUR et al. 2008; ZIMOV, SCHUUR & CHAPIN III 2006). While the temperature-sensitivity of soil carbon mineralisation and the related feedbacks to climate change remain somewhat controversial on a global scale (BOND-LAMBERTY & THOMSON 2010; DAVIDSON & JANSSENS 2006), there is little doubt that thawing permafrost will emit on the order of several hundred Pg carbon over the next few centuries, and will thus more than off-set enhanced carbon sequestration by expanding biomass (GRUBER et al. 2004; KHVOROSTYANOV et al. 2008; SCHAEFER et al. 2011; SCHUUR et al. 2008). It should be noted that carbon emissions from thawing permafrost are a particularly strong positive feedback mechanism, because part of the carbon is released as methane, which has a higher greenhouse gas potential

than CO₂. Permafrost carbon dynamics are thus already widely acknowledged to be important for the global carbon cycle today.

However, scientific attention has much less focused on the possible role of permafrost carbon dynamics on glacial-interglacial timescales. This largely stems from the very limited number of suitable outcrops to study past changes in permafrost carbon pools. Outcrops along the Russian Arctic coast and from Alaska rarely span more than several ten thousand years, are often heavily affected by cryoturbation and have hiatus (MUHS et al. 2003; REYES, FROESE & JENSEN 2010; SCHIRRMEISTER et al. 2002; WETTERICH et al. 2008). The only published permafrost profile so far that likely continuously spans two glacial cycles is the loess-paleosol sequence ‘Tumara’ in northeast Siberia (M. ZECH et al. 2010; ZECH, ZECH & GLASER 2007; ZECH et al. 2008). In order to circumvent any shortcomings stemming from dating uncertainties and to obtain a direct proxy of paleo-temperatures for the Tumara Sequence, we have recently analyzed the compound-specific deuterium/hydrogen ratios on extracted alkanes (R. ZECH et al. 2010; ZECH et al. 2011). The respective results now unambiguously (i.e. totally independent of the age control) corroborate that more organic carbon was sequestered at this site during glacials than during interglacials, supporting the logic that cold,

glacial conditions favored intensive permafrost, waterlogging, and soil organic matter preservation (Fig. 1).

Although it is very challenging to up-scale the observed local permafrost carbon dynamics, several hundred Pg ‘excess carbon’ might have been stored in the vast non-glaciated plains in Siberia that became affected by permafrost during glacials (Fig. 2) (R. ZECH et al. 2010; ZECH et al. 2011). Apart from the obvious drawback, namely that more comparable outcrops should be studied to come up with robust estimates for permafrost carbon stock changes, one needs to keep in mind that thawing and landscape erosion during interglacials undoubtedly leads to soil carbon mineralization and destruction of much of the evidence for glacial-interglacial permafrost dynamics in many places. In that sense, the Tumara Paleosol Sequence might be special, because probably no major hiatus occurred, and the glacial sediments are still frozen and well-preserved today. In any case, the most accurate estimates for permafrost carbon stock changes on glacial-interglacial timescales will probably have to come from models. The only model estimate published so far for soil carbon released from the vast, non-glaciated Siberian permafrost regions during the last deglaciation (~17–12 ka BP, before present) indicates that more than 1000 Pg C could have been released (ZIMOV et al. 2009). Modeling the complex physical and biogeochemi-

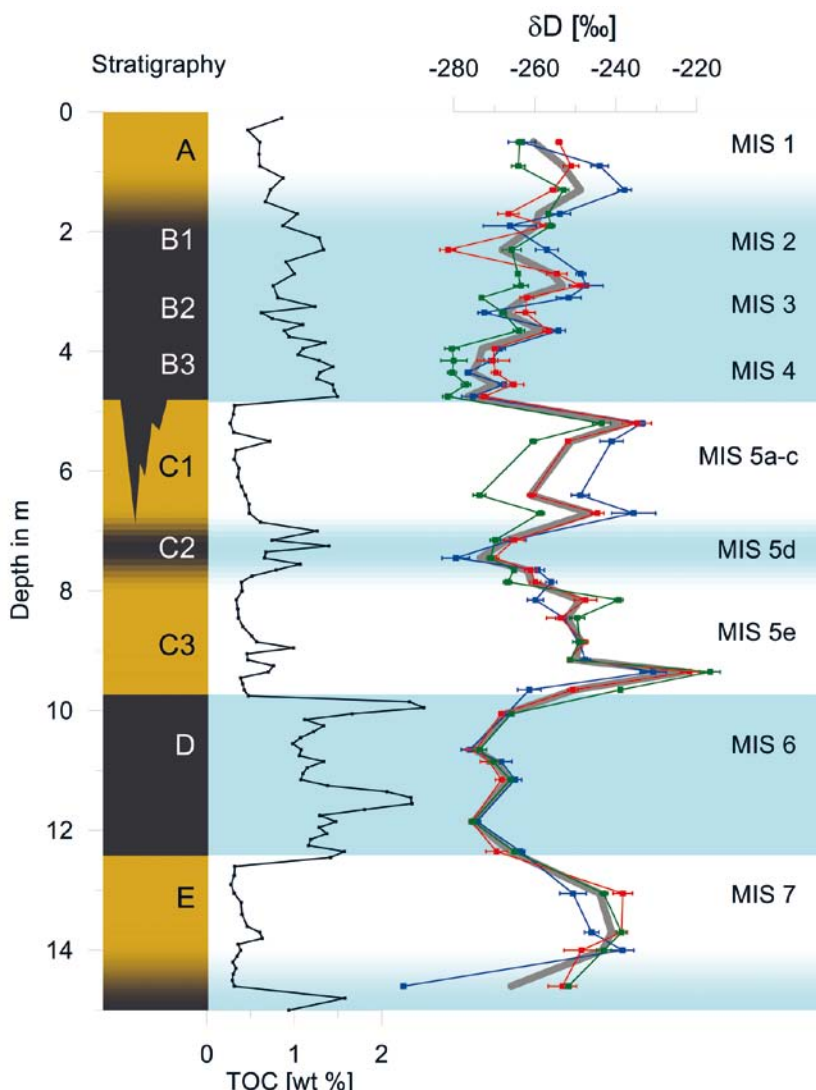


Fig. 1: Stratigraphy and analytical results for the loess-paleosol sequence ‘Tumara’. The stratigraphy illustrates the alternation between organic-rich, dark grey units B and D, and bright brown organic-poor units A, C and E. TOC = total organic carbon concentration. δD = deuterium/hydrogen isotope ratios (blue: n-Alkan C27, red: n-C29, green: n-C31, error bars: standard deviation of triplicate measurements, grey: average of all three alkanes). The tentative correlation with marine isotope stages (MIS) is shown to the right (modified from R. ZECH et al. 2010; ZECH et al. 2011).

Abb. 1: Stratigraphie und Analysenergebnisse für das Löss-Paleoboden-Profil „Tumara“. Die Stratigraphie illustriert die Abfolge der organikreichen, dunkelgrauen Horizonte B und D, und der hellbraunen, organikarmen Horizonte A, C und E. TOC = Bodenkohlenstoffkonzentration. δD = Deuterium/Wasserstoff Isotopenverhältnis (blau: n-Alkan C27, rot: n-C29, grün: n-C31, Fehlerbalken: Standardabweichung der Dreifachmessungen, grau: Mittelwert aller drei Alkane). Die Korrelation mit den Marinischen Isotopen Stadien (MIS) ist rechts dargestellt (verändert nach R. ZECH et al. 2010; ZECH et al. 2011).

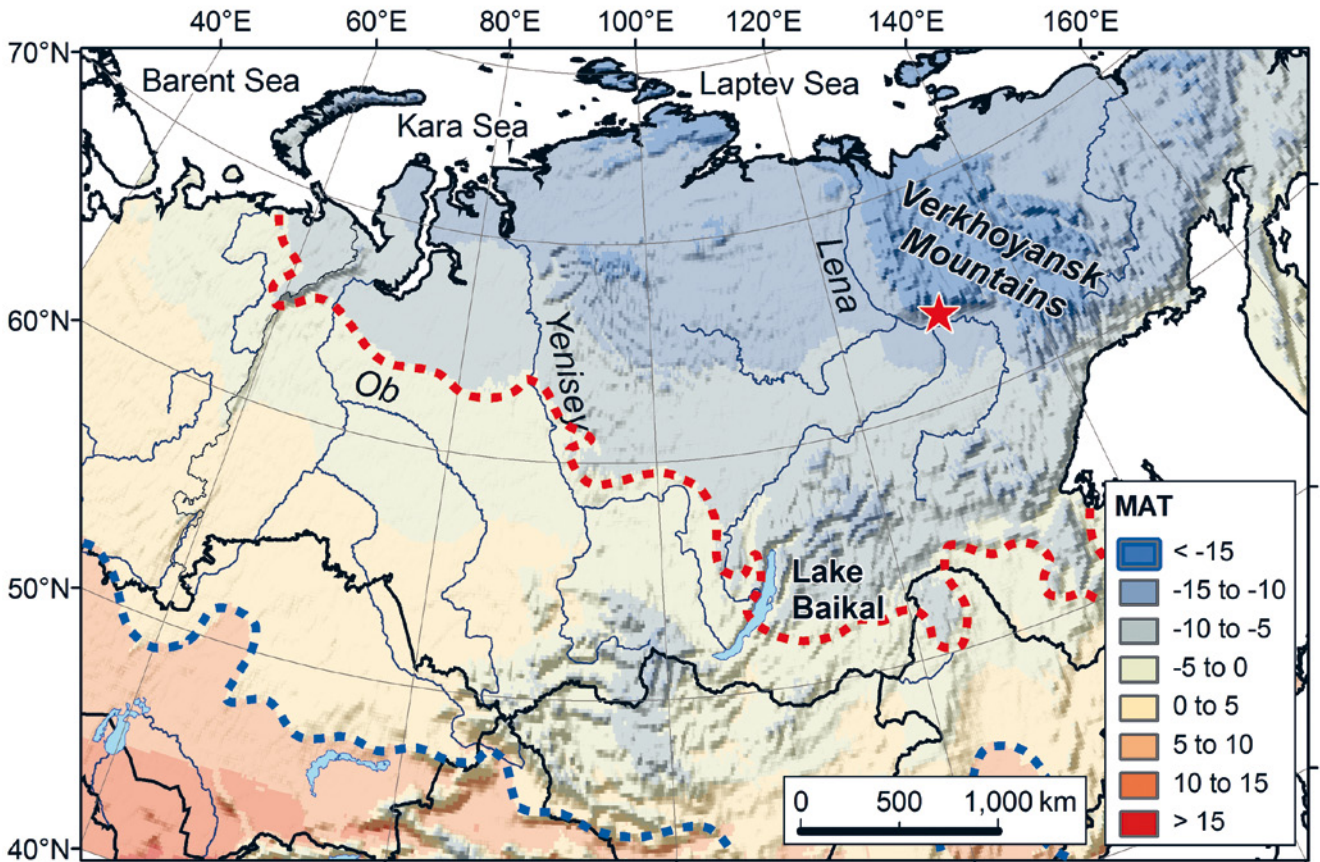


Fig. 2: Location of the Tumara Sequence (red star) and mean annual temperatures (MAT in °C) in Siberia (NEW et al., 2002). The -5°C isotherm (red dashed line) approximately marks the southward extent of continuous permafrost today (TARNOCAI et al. 2009). Discontinuous permafrost exists until MAT 0°C, and the +5°C isotherm (dashed blue line) indicates the approximate southward expansion of continuous permafrost during glacials assuming a 10°C temperature reduction (from R. ZECH et al. 2010; ZECH et al. 2011).

Abb. 2: Lage des Tumara Profils (roter Stern) und mittlere annuelle Temperaturen (MAT in °C) in Sibirien (NEW et al. 2002). Die -5°C Isotherme (rote, gestrichelte Linie) markiert ungefähr die heutige südliche Grenze des kontinuierlichen Permafrostes (TARNOCAI et al. 2009). Diskontinuierlicher Permafrost gibt es bis MAT ~0°C, und die +5°C Isotherme (gestrichelte blaue Linie) markiert ungefähr die südliche Ausdehnung des kontinuierlichen Permafrostes während der Eiszeiten (unter Annahme einer 10°C Temperaturerniedrigung, nach R. ZECH et al. 2010; ZECH et al. 2011).

cal processes in permafrost soils is challenging, and future studies are necessary to evaluate this enormous figure.

Nonetheless, it is an interesting and worthwhile endeavor to pursue the potential consequences of assuming such large amounts of permafrost carbon being sequestered repeatedly in permafrost regions during each glacial. In the following, I will (i) briefly recap the state of knowledge concerning Pleistocene climate and the role of carbon dioxide, and then show that (ii) permafrost carbon might have contributed significantly to the observed glacial-interglacial changes in atmospheric CO₂ concentrations without violating existing proxy evidence from carbon isotopes. (iii) I speculate that integrated annual insolation forcing of the permafrost carbon dynamics might have acted as trigger for global changes and (iv) suggest that the mid-Pleistocene transition could be readily explained with the southern permafrost boundary reaching mid-latitudes during the course of the Pleistocene cooling trend.

2 State of knowledge – ‘burden’ and ‘helper’ scenarios

As we know from Antarctic ice cores, the ~100 ka rhythm of glacials and interglacials during the past ~800 ka was closely coupled to the global carbon cycle (LUETHI et al.

2008; PETIT et al. 1999; SHACKLETON 2000). While low concentrations of atmospheric CO₂ (~180 to 200 ppm) coincided with and most likely caused glacial periods, high concentrations (~250 to 300 ppm) were characteristic for the interglacials. The prevailing notion to explain the glacial-interglacial changes in atmospheric CO₂ concentrations is that the oceans were the principal driver and acted as net carbon sink during glacials (ARCHER et al. 2000; BROECKER 1982; KOHFELD & RIDGWELL 2010; SIGMAN & BOYLE 2000; SIGMAN, HAIN & HAUG 2010). This shall here be referred to as ‘ocean hypothesis’. Such a notion indeed appears unequivocal at first glance given the enormous size of the carbon pool in the ocean (~60 times the atmospheric carbon). Particularly changes in the Southern Ocean circulation have recently been invoked to control atmospheric CO₂, because up-welling of deep ocean water masses mainly occurs around Antarctica, where thus CO₂ from remineralized marine organic material is vented back into the atmosphere (FISCHER et al. 2010; SIGMAN, HAIN & HAUG 2010; TOGGEWEILER, RUSSELL & CARSON 2006).

Virtually all current glacial hypotheses and climate-carbon models, regardless of their favorite mechanisms and their specific model set-ups, not only build on the assumption that physical and/or biological changes in the ocean led

to the sequestration of carbon dioxide in the deep glacial ocean, they also assume that the terrestrial carbon pools during glacials were smaller, and thus the ocean had to take up even more than just the ~200 Pg C from the atmosphere (~100 ppm change). Reduced carbon storage on land is in agreement with the intuitive view that net production of terrestrial biomass is lower during glacials, because lower temperatures, lower atmospheric CO₂, and increased glacial aridity are less favorable conditions for plant growth. Quantitative estimates based on vegetation models indicate that the ‘burden’ may have been on the order of ~600–800 Pg C (FRANÇOIS et al. 1998; JOOS et al. 2004; KAPLAN et al. 2002), although much larger figures have been proposed as well (ADAMS & FAURE 1998). Estimates of 300 to 700 Pg C have been derived from ~0.32‰ more negative marine carbon isotopes (BIRD, LLYOD & FARQUHAR 1996; DUPLESSY et al. 1988) that are commonly interpreted to document a net transfer of (isotopically negative) terrestrial carbon to the ocean.

There are, however, various reasons to doubt the currently widely accepted burden scenario:

1. Even when taking all possible physical and biological changes in the ocean into account, current carbon models are unable to convincingly explain the full range of glacial-interglacial changes in atmospheric CO₂ (ARCHER et al. 2000; BROVKIN et al. 2007; FISCHER et al. 2010; KOHFELD & RIDGWELL 2010; TAGLIABUE et al. 2009).
2. The ‘ocean hypothesis’ suggests that a large pool of ‘old’ radiocarbon was trapped in the glacial deep ocean, yet there has been no success so far in finding this pool (BROECKER & BARKER 2007; DE POL-HOLZ et al. 2010; SKINNER et al. 2010).
3. Models have not yet included permafrost carbon – a largely underestimated terrestrial carbon pool that was most likely even much larger during glacials.

It should be noted that earlier studies have already raised doubts concerning the burden scenario. ZENG (2003; 2007) has suggested that the assumed terrestrial burden might have been too large, because organic carbon buried below ice sheets has been ignored. Zeng also emphasized that a ‘helper scenario’, i.e. a net release of terrestrial carbon during terminations, would not be implausible. The recent estimates of huge amounts of carbon stored in permafrost soils, and particularly the potential release of more than 1000 Pg C from thawing permafrost regions in Siberia during the last deglaciation (ZIMOV et al. 2009) may now need to be considered in the overall balance as well and fuel the debate.

3 Reconciling permafrost carbon dynamics with the global carbon cycle

The uncertainties regarding the amount of ‘excess’ soil carbon storage in permafrost regions during glacials may be very large, but nonetheless it is certainly a justified endeavor to explore the potential consequences of large changes in permafrost carbon with regard to the global carbon cycle on glacial-interglacial timescales.

To begin with, if one took the 1000 Pg C released from thawing permafrost during terminations at face value as

hitherto unrecognized additional terrestrial carbon pool change, this amount would massively affect the global climate. When considered in isolation of other terrestrial pools, most of the released permafrost carbon would be taken up by the ocean within a few millennia, and only about 10%, i.e. ~100 Pg C, would remain in the atmosphere (ARCHER et al. 2004). Still, this would be equivalent to ~50 ppm atmospheric CO₂ and thus be a significant contribution to the carbon balance on glacial-interglacial timescales.

A more balanced approach additionally has to consider that carbon released from thawing permafrost would partly be captured in other terrestrial carbon pools that increase during terminations, for example via plant and peat re-growth in formerly glaciated areas. Given the large uncertainties related to all involved carbon pools, it is probably impossible at this point to provide a robust calculation, but simply balancing the proposed 1000 Pg C permafrost carbon (ZIMOV et al. 2009) against estimates of ~600 to 800 Pg C for terrestrial carbon based on vegetation models (excluding permafrost) (FRANÇOIS et al. 1998; JOOS et al. 2004; KAPLAN et al. 2002) leaves a net release of ~200 to 400 Pg C of terrestrial carbon into the atmosphere-ocean system during termination. Note that this balance is not including hundreds of Pg C that may have been buried below glacial ice sheets and also released during terminations (ZENG 2003; 2007), but that it also ignores the onset of peat formation after deglaciation, particularly in formerly glaciated areas of Siberia and North America (JONES & YU 2010; MACDONALD et al. 2006). Nonetheless, our back-of-the-envelope calculation suggests that the ‘burden’ for the ocean may have been strongly overestimated, and that a ‘helper’ scenario may be realistic.

Would such a helper scenario be in contradiction with marine and ice core proxies?

3.1 Carbon isotopic signals during deglaciation

Negative carbon isotopic excursions of ~0.5‰ δ¹³C in ice core CO₂ (LOURANTOU et al. 2010) and many ocean records (SPERO & LEA 2002) during the termination, as well as the simultaneous ~200‰ drop in atmospheric Δ¹⁴C (BROECKER & BARKER 2007; HUGHEN et al. 2006) have generally been interpreted as evidence for the release of (isotopically depleted and old) carbon that was trapped in the deep ocean during glacials. Apart from the fact that this supposedly trapped large deep ocean carbon pool has not been found so far (BROECKER & BARKER 2007; DE POL-HOLZ et al. 2010; SKINNER et al. 2010), one should keep in mind that the isotopic signature of this pool would be very similar to permafrost carbon (BROVKIN et al. 2002). It may thus be worth pursuing the idea of massive permafrost carbon release during terminations instead of, or at least in combination with deep ocean carbon.

Back-of-the-envelope calculations could be based on a net-release of 200 to 400 Pg C permafrost carbon (~27‰ δ¹³C and radiocarbon dead, i.e. -1000‰ Δ¹⁴C) into the glacial atmosphere (~400 Pg C, ~7‰ δ¹³C and ~400‰ Δ¹⁴C). As the ocean will take up ~90% of the released permafrost carbon on millennial timescales, the mass balance needs to be made with the remaining 10%, i.e. ~20 to 40 Pg C. This yields

a ~1 to 2‰ drop in atmospheric (and upper ocean) $\delta^{13}\text{C}$ and a ~70 to 140‰ drop $\Delta^{14}\text{C}$, which is in reasonable agreement with the observations. More sophisticated calculations and modeling studies, similar to the one by KOEHLER et al. (2006), would of course be promising to refine those numbers and put better constraints on the permafrost carbon pool changes.

3.2 Carbon isotopic signals during the LGM

The ~0.32‰ more negative mean ocean $\delta^{13}\text{C}$ during the last glacial has traditionally been suggested to reflect a net carbon transfer of 300 to 700 Pg C from the terrestrial biosphere to the ocean (BIRD, LLYOD & FARQUHAR 1996; DUPLESSY et al. 1988). The hypothetical helper scenario above, however, would imply a net terrestrial carbon storage of 200 to 400 Pg during glacials, which would leave the ocean (and atmosphere) more enriched by ~0.2–0.4‰. Two considerations might help to reconcile these apparent discrepancies.

First, the widely used value of -0.32‰ was derived from a relatively limited set of ocean sediment cores, and although a more recent synthesis undoubtedly corroborates more negative values in the deep ocean during glacials, it also shows that large differences exist between individual records, and that the signal is much less clear in intermediate and surface ocean waters (OLIVER et al. 2010). Above ~2000 m water depth, the oceans may have been more $\delta^{13}\text{C}$ positive during glacials (see also CURRY & OPPO 2005; MATSUMOTO et al. 2002). An independent piece of evidence for more positive surface waters might in fact come from the ice core $\delta^{13}\text{CO}_2$. The LGM and Holocene $\delta^{13}\text{CO}_2$ values are almost identical, although the isotopic fractionation between the surface ocean and the atmosphere changed by ~0.5‰ due to lower temperatures and increased salinity (KÖHLER, FISCHER & SCHMITT 2010; LOURANTOU et al. 2010). Whereas KOEHLER et al. (2010) invoke sea ice, iron fertilization and ocean circulation effects (which are all highly uncertain, see e.g. KOHFELD & RIDGWELL 2010) to offset the temperature and salinity effect, it might also be possible to reconcile the ice core $\delta^{13}\text{CO}_2$ observations with more $\delta^{13}\text{C}$ positive surface ocean waters and a helper rather than a burden scenario (see also TAGLIABUE et al. 2009).

Second, and more importantly, it is not trivial to infer past isotopic changes in dissolved inorganic carbon from $\delta^{13}\text{C}$ measured in foraminifera, because many other factors, such as ocean chemistry, ocean circulation and vital effects, need to be considered (e.g. OLIVER et al. 2010). Culture experiments, for example, indicate that the glacial rise in surface ocean carbonate ion concentrations can account for at least a 0.25–0.5‰ drop in shell $\delta^{13}\text{C}$ (SPERO et al. 1997). LEA et al. (1999) further elaborate on this issue and predict anomalies in shell $\delta^{13}\text{C}$ between -0.3 and -0.9‰. Both studies acknowledge that similar corrections may not be valid for the deep ocean isotope records, but one could argue that changes in the biological pump, deep ocean chemistry, and ocean circulation leave plenty of possible explanations for a negative bias of the deep ocean $\delta^{13}\text{C}$ record.

In summary, a significant permafrost carbon contribution to the glacial-interglacial carbon balance is not necessarily contradicting existing carbon isotope proxies and might in fact help reconciling many observations.

4 Integrated annual insolation as external forcing for permafrost and trigger for global climate change

In the following, we shall hypothetically assume that the permafrost carbon contributions are large enough to dominate the net terrestrial carbon fluxes and to affect atmospheric CO_2 . This specific helper scenario could be coined ‘permafrost scenario’. To provide again a rough quantitative estimate, the net terrestrial carbon of ~200 to 400 Pg C released during the last termination (from the above back-of-the-envelope calculation) would be equivalent to ~100 to 200 ppm atmospheric CO_2 . Particularly in view of the fact that part of the permafrost carbon is released as methane and thus as efficient greenhouse gas, these large numbers suggest that permafrost carbon dynamics could be sufficient to trigger global climate changes. One needs to keep in mind, of course, that ~90% of the emitted carbon will be taken up by the ocean within a few millennia. Thus, other mechanisms, such as previously suggested physical and biological changes in the ocean, ultimately still need to explain most of the ~100 ppm glacial-interglacial changes in atmospheric CO_2 . In that sense, permafrost carbon dynamics should be considered only a hitherto unrecognized, additional mechanism. Importantly, however, permafrost carbon dynamics may not only be a positive feedback, but also act as trigger for climate change, with many of the other mechanisms acting as amplifiers.

But what in turn could be the forcing for permafrost carbon dynamics? One can argue that permafrost carbon dynamics are most sensitive to changes of the southern permafrost boundary, because the existence of permafrost exerts an important control on the drainage of soil water and thus soil organic matter preservation, whereas the depth of the active layer in permafrost regions is of secondary importance. And as mean annual temperatures determine the existence of permafrost, the search for the external forcing leads us to the mean or integrated annual insolation at the southern permafrost boundary.

At high latitudes (>45°N), integrated annual insolation is mainly controlled by the orbital parameter obliquity (HUYBERS 2006) (Fig. 3). Decreasing/low obliquity can accordingly be expected to favor the expansion of permafrost and enhanced carbon sequestration every ~41 ka. Increasing/high obliquity, on the other hand, favors permafrost thawing and soil carbon mineralization. This forcing could readily explain the ice-age rhythm in the ‘41 ka world’ during the early Pleistocene (~1–2 Ma), which was characterized by ~41 ka glacial-interglacial cycles (HUYBERS 2006; RAYMO & NISANCIOLU 2003) (Fig. 4).

5 The mid-Pleistocene transition

But what could have caused the mid-Pleistocene transition, i.e. the transition from the ‘41 ka world’ to longer, approximately 100 ka glacial cycles (CLARK, ALLEY & POLLARD 1999; HUYBERS 2006; RAYMO & NISANCIOLU 2003; TZIPERMAN & GILDOR 2003) (Fig. 4)? After the explanation of the glacial-interglacial changes in atmospheric CO_2 , this is in fact the second ‘holy grail’ in Quaternary paleoclimatology. It has recently been recognized that the ~100 ka glacial cycles are probably ~80 or ~120 ka cycles and thus related to the orbit-

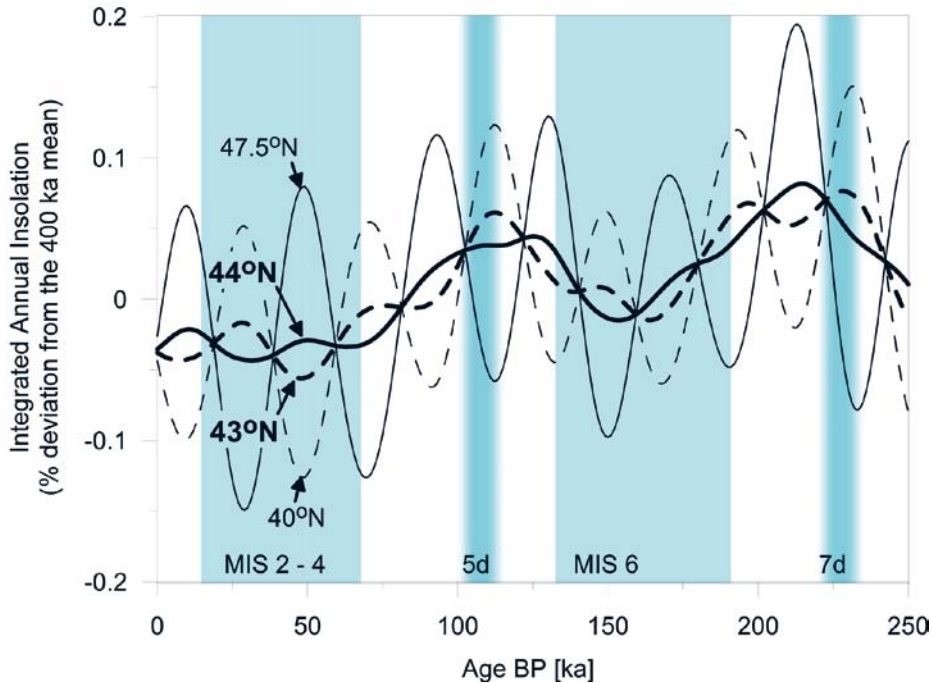


Fig. 3: Integrated annual insolation for 47.5, 44, 43 and 40°N (BERGER & LOUTRE 1991). The 400 ka means are ~9.4, 9.9, 10.0, and 10.4 GJ/m².

Abb. 3: Integrierte annuelle Insolation für 47.5, 44, 43 und 40°N (BERGER & LOUTRE 1991). Die 400 ka Mittelwerte sind ~9.4, 9.9, 10.0, und 10.4 GJ/m².

al parameter obliquity rather than eccentricity (HUYBERS 2007), yet adequate and convincing explanations for the ‘skipped obliquity cycles’ remain elusive. In the following, I outline how the permafrost glacial hypothesis provides an intriguingly simple and elegant concept that could explain the transition.

As long as the southern permafrost boundary is north of ~45°N, the insolation forcing of permafrost carbon dynamics is directly and only controlled by obliquity (Fig. 3). While this was probably the case before the transition and could explain the 41 ka world, the overall long-term cooling trend during the Pleistocene must have reached a threshold, when expansion of permafrost areas during glacials reached latitudes south of ~45°N. Note that today, continuous permafrost regions in Siberia already extend to ~55°N (TARNOCAI et al. 2009) (Fig. 2), and that during the last glacial, permafrost regions undoubtedly extended southward beyond 45°N. Integrated annual insolation south of ~45°N shows the opposite signal compared to north of ~45°N, because obliquity (the tilt of the Earth’s axis) basically controls the amount of insolation that reaches high latitudes rather than the equator. The exact latitude where the sign of the obliquity forcing flips may in fact be between 43 and 44°N (Fig. 3), but the crux is that once the Pleistocene cooling was sufficient for glacial permafrost areas to reach mid-latitudes, the southern permafrost boundary and the related carbon dynamics became insensitive (or at least less sensitive) to changes in obliquity. The external forcing that remains is then eccentricity. I suggest that as a consequence, obliquity cycles (glacial terminations) were skipped during the Middle and Late Pleistocene, when they coincided with decreasing annual insolation at mid-latitudes due to eccentricity. Only the next obliquity maximum that coincided with increasing eccentricity kicked off the warming feedbacks related to thawing permafrost and CO₂ and methane releases. The result are glacial terminations every ~80 or 120 ka during the Late Pleistocene, i.e. exactly the observed succession of the ice ages (HUYBERS 2007) (Fig. 4).

6 Conclusions

Recent studies have shown that the amount of soil organic carbon in permafrost regions has been greatly underestimated today, and very likely even more so during past glacials. Permafrost plays a very important role for the hydrological conditions in soils, and thus also for changes in mineralization versus preservation of organic material. This leads to the formulation of a permafrost glacial hypothesis:

- (i) The amount of soil organic carbon released from thawing permafrost during glacial terminations at least partly compensated the carbon sequestered by expanding biomass, facilitating the explanation of glacial-interglacial changes in atmospheric CO₂ concentrations.
- (ii) Carbon isotopic records derived from marine sediments and ice cores might be more easily reconciled when taking permafrost carbon dynamics into account. In any case, they do not necessarily contradict a net release of terrestrial carbon during terminations. Thus the ‘terrestrial burden’ may not only have been overestimated, the possibility of a ‘helper scenario’ should also not be ruled out.
- (iii) Integrated annual insolation forcing, which likely affects permafrost carbon dynamics most effectively at the southern permafrost boundary, provides an external forcing for permafrost carbon dynamics on orbital timescales.
- (iv) The long Pleistocene cooling trend implies the expansion of permafrost regions to mid-latitudes at some point in the past. If this occurred during the mid-Pleistocene transition, it could automatically explain the transition from obliquity forcing (dominant north of ~45°N) to longer ~80 or 120 ka ice age cycles, because permafrost carbon dynamics at mid-latitudes are dominantly forced by eccentricity.

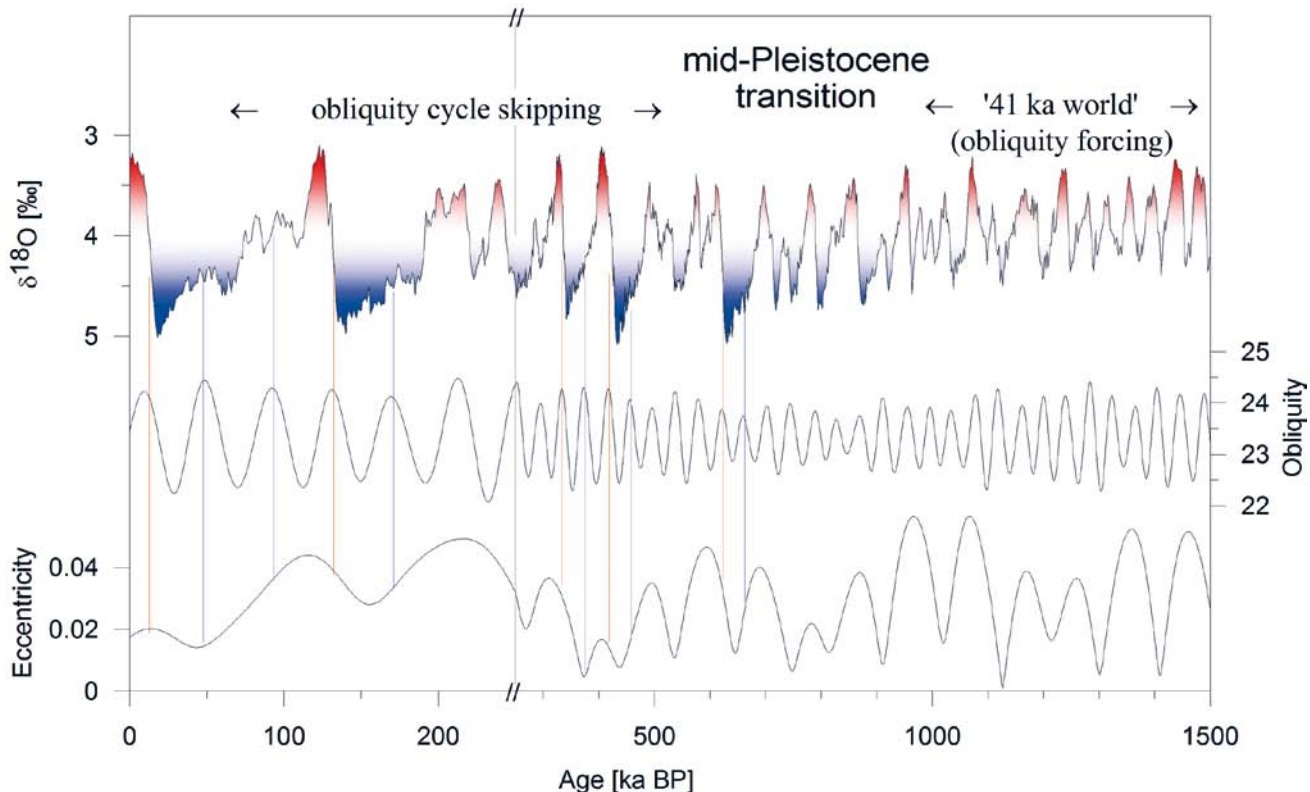


Fig. 4: Outline of the permafrost glacial hypothesis explaining the obliquity cycle skipping after the mid-Pleistocene transition. The marine $\delta^{18}\text{O}$ stack illustrates changes in global ice volume and global temperatures (LISIECKI & RAYMO 2005), obliquity and eccentricity the relevant orbital forcing parameters (BERGER & LOUTRE 1991). Blue lines mark prominent examples where obliquity cycles were skipped. Red lines mark subsequent obliquity maxima that coincided with increasing eccentricity and that therefore triggered major terminations.

Abb. 4: Darstellung der pleistozänen Eiszeitenabfolge und deren potentielle Erklärung mit Hilfe der Permafrost Hypothese. Die marine $\delta^{18}\text{O}$ Kurve illustriert die Änderungen des globalen Eisvolumens und der globalen Temperaturen (LISIECKI & RAYMO 2005), die Schiefe der Ekliptik und die Ekzentrizität, die relevanten orbitalen Insolationsparameter (BERGER & LOUTRE 1991). Blaue Linien markieren exemplarisch Fälle, in denen ein 41 ka Zyklus ausfiel. Rote Linien markieren nachfolgende Maxima in der Schiefe der Ekliptik, welche mit steigender Ekzentrizität einhergingen und damit das Ende einer Eiszeit einleiteten.

Although the permafrost glacial hypothesis may seem to challenge much of the current knowledge and existing hypotheses at first glance (particularly the paradigm that the glacial ocean acted as net sink for CO_2), many marine proxies and findings from global carbon models might in fact be reconciled more easily when permafrost is taken into account.

Two approaches seem to be most appropriate to evaluate the permafrost glacial hypothesis. The first one could be to further investigate the potential carbonate ion or pH effect on shell $d^{13}\text{C}$ in benthic foraminifera, in order to come up with new estimates for mean ocean $d^{13}\text{C}$ changes and thus net terrestrial carbon budgets on glacial-interglacial timescales. The second approach could be to develop more sophisticated soil carbon – climate models that explicitly include permafrost dynamics and peatland growth, in order to obtain more robust estimates of the amount of organic carbon stored at high latitudes during glacials. I hope this manuscript inspires respective research in the near future.

Acknowledgements

I thank M. Zech, Y. Huang, J. Russell, T. Eglinton, N. Gruber and J. Zech for discussions. Support through a SNF Post-Doc fellowship is gratefully acknowledged.

References

- ADAMS, J.M. & FAURE, H. (1998): A new estimate of changing carbon storage on land since the last glacial maximum, based on global land ecosystem reconstruction. – *Global and Planetary Change*, 16: 3–24.
- ARCHER, D., WINGUTH, A., LEA, D. & MAHOWALD, N. (2000): What caused the glacial/interglacial atmospheric pCO_2 cycles? – *Review of Geophysics*, 38: 159–189.
- ARCHER, D., MARTIN, P., BUFFETT, B., BROVKIN, V., RAHMSTORF, S. & GANOPOLSKI, A. (2004): The importance of ocean temperature to global biogeochemistry. – *Earth and Planetary Science Letters*, 222: 333–348.
- BERGER, A. & LOUTRE, M.F. (1991): Insolation values for the climate of the last 10 million of years. – *Quaternary Sciences Review*, 10: 297–317.
- BIRD, M.I., LLYOD, J. & FARQUHAR, G.D. (1996): Terrestrial carbon-storage from the last glacial maximum to the present. – *Chemosphere*, 33: 1675–1685.
- BOND-LAMBERTY, B. & THOMSON, A. (2010): Temperature-associated increases in the global soil respiration record. – *Nature*, 464: 579–582.
- BROECKER, W. (1982): Glacial to interglacial changes in ocean chemistry. – *Progress in Oceanography*, 2: 151–197.
- BROECKER, W. & BARKER, S. (2007): A 190% drop in atmosphere's $\Delta^{14}\text{C}$ during the "Mystery Interval" (17.5 to 14.5 kyr). – *Earth and Planetary Science Letters*, 256: 90–99.
- BROVKIN, V., HOFMANN, M., BENDTSSEN, J. & GANOPOLSKI, A. (2002): Ocean biology could control atmospheric $\delta^{13}\text{C}$ during glacial-interglacial cycle. – *Geochemistry, Geophysics, Geosystems*, 3.
- BROVKIN, V., GANOPOLSKI, A., ARCHER, D. & RAHMSTORF, S. (2007): Lowering glacial atmospheric CO_2 in response to changes in oceanic circulation and marine biogeochemistry. – *Paleoceanography*, 22: 1–14.

- CLARK, P.U., ALLEY, R.B. & POLLARD, D. (1999): Northern Hemisphere Ice-Sheet Influences on Global Climate Change. – *Science*, 286: 1104–1111.
- CURRY, W.B. & OPPO, D.W. (2005): Glacial water mass geometry and the distribution of $\delta^{13}\text{C}$ of ΣCO_2 in the western Atlantic Ocean. – *Paleoceanography*, 20: PA1017. Doi:10.1029/2004PA001021.
- DAVIDSON, E.A. & JANSSENS, I.A. (2006): Temperature sensitivity of soil carbon decomposition and feedbacks to climate change. – *Nature*, 440: 165–173.
- DE POL-HOLZ, R., KEIGWIN, L., SOUTHON, J., HEBBELN, D. & MOHTADI, M. (2010): No signature of abyssal carbon in intermediate waters off Chile during deglaciation. – *Nature Geoscience*, 3: 192–195.
- DUPLESSY, J.C., SHACKLETON, N.J., FAIRBANKS, R.G., LABEYRIE, L., OPPO, D. & KALLEL, N. (1988): Deepwater Source Variations During the Last Climatic Cycle and Their Impact on the Global Deepwater Circulation. – *Paleoceanography*, 3: 343–360.
- FISCHER, H., SCHMITT, J., LÜTHI, D., STOCKER, T.F., TSCHUMI, T., PAREKH, P., JOOS, F. et al. (2010): The role of Southern Ocean processes in orbital and millennial CO_2 variations – A synthesis. – *Quaternary Science Reviews*, 29: 193–205.
- FRANÇOIS, L.M., DELIRE, C., WARNANT, P. & MUNHOVEN, G. (1998): Modeling the glacial-interglacial changes in the continental biosphere. – *Global and Planetary Change*, 16: 37–52.
- GRUBER, N., FRIEDLINGSTEIN, P., FIELD, C.B., VALENTINI, R., HEIMANN, M., RICHEY, J.E., ROMERO-LANKAO, P. et al. (2004): The vulnerability of the carbon cycle in the 21st century: An assessment of carbon-climate-human interactions. – In: FIELD, C. B. & RAUPACH, M. R. (eds.): *Toward CO_2 Stabilization: Issues, Strategies, and Consequences*: 45–76; Washington, D.C. (Island Press).
- HUGHEN, K., SOUTHON, J., LEHMAN, S., BERTRAND, C. & TURNBULL, J. (2006): Marine-derived ^{14}C calibration and activity record for the past 50,000 years updated from the Cariaco Basin. – *Quaternary Science Reviews*, 25: 3216–3227.
- HUYBERS, P. (2006): Early Pleistocene Glacial Cycles and the Integrated Summer Insolation Forcing. – *Science*, 313: 508–511.
- HUYBERS, P. (2007): Glacial variability over the last two million years: an extended depth-derived age model, continuous obliquity pacing, and the Pleistocene progression. – *Quaternary Science Reviews*, 26: 37–55.
- JONES, M.C. & YU, Z. (2010): Rapid deglacial and early Holocene expansion of peatlands in Alaska. – *Proceedings of the National Academy of Sciences*, 107: 7347–7352.
- JOOS, F., GERBER, S., PRENTICE, I.C., OTTO-BLIESNER, B.L. & VALDES, P.J. (2004): Transient simulations of Holocene atmospheric carbon dioxide and terrestrial carbon since the Last Glacial Maximum. – *Global Biogeochemical Cycles*, 18: GB2002. Doi:10.1029/2003GB002156.
- KAPLAN, J.O., PRENTICE, I.C., KNORR, W. & VALDES, P.J. (2002): Modeling the dynamics of terrestrial carbon storage since the Last Glacial Maximum. – *Geophysical Research Letters*, 29. Doi:10.1029/2002GL015230.
- KHVOROSTYANOV, D.V., CIAIS, P., KRINNER, G. & ZIMOV, S.A. (2008): Vulnerability of east Siberia's frozen carbon stores to future warming. – *Geophysical Research Letters*, 35. Doi:10.1029/2008GL033639.
- KOHFELD, K.E. & RIDGWELL, A.J. (2010): Glacial-interglacial variability in atmospheric CO_2 . – In: SALTZMAN, E. & QUERE, C. L. (eds.): *Surface ocean – lower atmospheres processes*. – *Geophysical Monograph Series*: 251–286; Washington D.C. (AGU).
- KÖHLER, P., FISCHER, H. & SCHMITT, J. (2010): Atmospheric $\delta^{13}\text{CO}_2$ and its relation to $p\text{CO}_2$ and deep ocean $\delta^{13}\text{C}$ during the late Pleistocene. – *Paleoceanography*, 25: PA1213. Doi:10.1029/2008PA001703.
- KÖHLER, P., FISCHER, H., SCHMITT, J. & MUNHOVEN, G. (2006): On the application and interpretation of Keeling plots in paleo climate research – deciphering $\delta^{13}\text{C}$ of atmospheric CO_2 measured in ice cores. – *Biogeosciences*, 3: 539–556.
- LEA, D.W., BIJMA, J., SPERO, H.J. & ARCHER, D. (1999): Implications of a carbonate ion effect on shell carbon and oxygen isotopes for glacial ocean conditions. – In: FISCHER, G. & WEFER, G. (eds.): *Use of Proxies in Paleoceanography: Examples from the South Atlantic*: 513–522; Berlin, Heidelberg (Springer).
- LISIECKI, L.E. & RAYMO, M.E. (2005): A Pliocene-Pleistocene stack of 57 globally distributed benthic $\delta^{18}\text{O}$ records. – *Paleoceanography*, 20: PA1003. Doi:10.1029/2004PA001071.
- LOURANTOU, A., LAVRIC, J., KÖHLER, P., BARNOLA, J.-M., PAILLARD, D., MICHEL, E., RAYNAUD, D. et al. (2010): Constraint of the CO_2 rise by new atmospheric carbon isotopic measurements during the last deglaciation. – *Global Biogeochemical Cycles*, 24: GB2015. Doi:10.1029/2009GB003545.
- LUETHI, D., LE FLOCH, M., BEREITER, B., BLUNIER, T., BARNOLA, J.-M., SIEGENTHALER, U., RAYNAUD, D. et al. (2008): High-resolution carbon dioxide concentration record 650,000–800,000 years before present. – *Nature*, 453: 379–382.
- MACDONALD, G.M., BEILMAN, D.W., KREMENETSKI, K.V., SHENG, Y., SMITH, L.C. & VELICHKO, A.A. (2006): Rapid Early Development of Circumarctic Peatlands and Atmospheric CH_4 and CO_2 Variations. – *Science*, 314: 285–288.
- MATSUMOTO, K., OBA, T., LYNCH-STIEGLITZ, J. & YAMAMOTO, H. (2002): Interior hydrography and circulation of the glacial Pacific Ocean. – *Quaternary Science Reviews*, 21: 1693–1704.
- MUHS, D.R., AGER, T.A., BETTIS III, E.A., McGEEHIN, J., BEEN, J.M., BEGET, J.E., PAVICH, M.J. et al. (2003): Stratigraphy and palaeoclimatic significance of Late Quaternary loess-palaeosol sequences of the Last Interglacial-Glacial cycle in central Alaska. – *Quaternary Science Reviews*, 22: 1947–1986.
- NEW, M., LISTER, D., HULME, M. & MAKIN, I. (2002): A high-resolution data set of surface climate over global land areas. – *Climate Research*, 21: 1–25.
- OLIVER, K.I.C., HOOGAKKER, B.A.A., CROWHURST, S., HENDERSON, G.M., RICKABY, R.E.M., EDWARDS, N.R. & ELDERFIELD, H. (2010): A synthesis of marine sediment core $\delta^{13}\text{C}$ data over the last 150 000 years. – *Climate of the Past*, 6: 645–673.
- PETIT, J.R., JOUZEL, J., RAYNAUD, D., BARKOV, N.I., BARNOLA, J.-M., BASILE, I., BENDER, M. et al. (1999): Climate and atmospheric history of the past 420,000 years from the Vostok ice core, Antarctica. – *Nature*, 399: 429–436.
- RAYMO, M.E. & NISANCIOLU, K. (2003): The 41 kyr world: Milankovitch's other unsolved mystery. – *Paleoceanography*, 18: Doi:10.1029/2002PA000791.
- REYES, A.V., FROESE, D.G. & JENSEN, B.J.L. (2010): Permafrost response to last interglacial warming: field evidence from non-glaciated Yukon and Alaska. – *Quaternary Science Reviews*, 29: 3256–3274.
- SCHAFFER, K., ZHANG, T., BRUHWILER, L. & BARRETT, A.P. (2011): Amount and timing of permafrost carbon release in response to climate warming. – *Tellus*, 63B: 165–180.
- SCHIRRMEISTER, L., SIEGERT, C., KUNITZKY, V., GROOTES, P. & ERLENKEUSER, H. (2002): Late Quaternary ice-rich permafrost sequences as a paleoenvironmental archive for the Laptev Sea Region in northern Siberia. – *International Journal of Earth Sciences*, 91: 154–167.
- SCHUTTER, E.A.G., BOCKHEIM, J., CANADELL, J.G., EUSKIRCHEN, E., FIELD, C.B., GORYACHKIN, S.V., HAGEMANN, S. et al. (2008): Vulnerability of Permafrost Carbon to Climate Change: Implications for the Global Carbon Cycle. – *Bioscience*, 58: 701–714.
- SHACKLETON, N.J. (2000): The 100,000-Year Ice-Age Cycle Identified and Found to Lag Temperature, Carbon Dioxide, and Orbital Eccentricity. – *Science*, 289: 1897–1902.
- SIGMAR, D.M. & BOYLE, E.A. (2000): Glacial/interglacial variations in atmospheric carbon dioxide. – *Nature*, 407: 859–869.
- SIGMAR, D.M., HAIN, M.P. & HAUG, G.H. (2010): The polar ocean and glacial cycles in atmospheric CO_2 concentration. – *Nature*, 466: 47–55.
- SKINNER, L.C., FALLON, S., WAELBROECK, C., MICHEL, E. & BARKER, S. (2010): Ventilation of the Deep Southern Ocean and Deglacial CO_2 Rise. – *Science*, 328: 1147–1151.
- SPERO, H.J. & LEA, D.W. (2002): The Cause of Carbon Isotope Minimum Events on Glacial Terminations. – *Science*, 296: 522–525.
- SPERO, H.J., BIJMA, J., LEA, D.W. & BEMIS, B.E. (1997): Effect of seawater carbonate concentration on foraminiferal carbon and oxygen isotopes. – *Nature*, 390: 497–500.
- TAGLIABUE, A., BOPP, L., ROCHE, D.M., BOUTTES, N., DUTAY, J.-C., ALKAMA, R., KAGEYAMA, M. et al. (2009): Quantifying the roles of ocean circulation and biogeochemistry in governing ocean carbon-13 and atmospheric carbon dioxide at the last glacial maximum. – *Climate of the Past*, 5: 695–706.
- TARNOCAI, C., CANADELL, J.G., SCHUUR, E.A.G., KUHRY, P., MAZHITOVA, G. & ZIMOV, S. (2009): Soil organic carbon pools in the northern circumpolar permafrost region. – *Global Biogeochemical Cycles*, 23: GB2023. Doi:10.1029/2008GB003327.
- TOGGWEILER, J.R., RUSSELL, J.L. & CARSON, S.R. (2006): Midlatitude westerlies, atmospheric CO_2 , and climate change during the ice ages. – *Paleoceanography*, 21: Doi:10.1029/2005PA001154.
- TZIPERMAN, E. & GILDOR, H. (2003): On the mid-Pleistocene transition to 100-kyr glacial cycles and the asymmetry between glaciation and deglaciation times. – *Paleoceanography*, 18: Doi:10.1029/2001PA000627.
- WETTERICH, S., KUZMINA, S., ANDREEV, A.A., KIENAST, F., MEYER, H., SCHIRRMEISTER, L., KUZNETSOVA, T. et al. (2008): Palaeoenvironmental dynamics inferred from late Quaternary permafrost deposits on Kurngash Island, Lena Delta, Northeast Siberia, Russia. – *Quaternary Science Reviews*, 27: 1523–1540.

- ZECH, M., ZECH, R. & GLASER, B. (2007): A 240,000-year stable carbon and nitrogen isotope record from a loess-like palaeosol sequence in the Tumara Valley, Northeast Siberia. – *Chemical Geology*, 242: 307–318.
- ZECH, M., ZECH, R., ZECH, W., GLASER, B., BRODOWSKI, S. & AMELUNG, W. (2008): Characterisation and palaeoclimate of a loess-like permafrost palaeosol sequence in NE Siberia. – *Geoderma*, 143: 281–295.
- ZECH, M., ANDREEV, A., ZECH, R., MUELLER, S., HAMBACH, U., FRECHEN, M. & ZECH, W. (2010): Quaternary vegetation changes derived from a loess-like permafrost palaeosol sequence in northeast Siberia using alkane biomarker and pollen analyses. – *Boreas*, 39: 540–550.
- ZECH, R., HUANG, Y., ZECH, M., TAROZO, R. & ZECH, W. (2010): A permafrost glacial hypothesis to explain atmospheric CO₂ and the ice ages during the Pleistocene. – *Climate of the Past Discussions*, 6: 2199–2221.
- ZECH, R., HUANG, Y., ZECH, M., TAROZO, R. & ZECH, W. (2011): High carbon sequestration in Siberian permafrost loess-paleosols during glacials. – *Climate of the Past*, 7: 501–509.
- ZENG, N. (2003): Glacial-interglacial atmospheric CO₂ changes – the Glacial Burial Hypothesis. – *Advances in Atmospheric Sciences*, 20: 677–693.
- ZENG, N. (2007): Quasi-100 ky glacial-interglacial cycles triggered by sub-glacial burial carbon release. – *Climate of the Past*, 3: 135–153.
- ZIMOV, N.S., ZIMOV, S.A., ZIMOVA, A.E., ZIMOVA, G.M., CHUPRYNIN, V.I. & CHAPIN, F.S., III (2009): Carbon storage in permafrost and soils of the mammoth tundra-steppe biome: Role in the global carbon budget. – *Geophysical Research Letters*, 36: L02502. DOI:10.1029/2008GL036332.
- ZIMOV, S.A., SCHUUR, E. & CHAPIN III, F.S. (2006): Permafrost and the Global Carbon Budget. – *Science*, 312: 1612–1613.

DEUQUA-Tagung 2012

Umwelt – Mensch – Georisiken im Quartär

Die 36. Hauptversammlung der Deutschen Quartärvereinigung DEUQUA e.V. findet vom 16. bis 20. September 2012 an der Universität Bayreuth statt (Vorexkursion: 15.-16.9.12; Nacherkursion: 21.-23.9.12). Das Rahmenthema lautet „Mensch – Umwelt – Georisiken im Quartär“. Ausrichter ist der Lehrstuhl Geomorphologie in Kooperation mit BayCEER (www.bayceer.uni-bayreuth.de).

Bayreuth und seine nähere Umgebung sind für einzigartige Vorkommen aus früheren geologischen Epochen bekannt. Vor diesem Hintergrund ist die Landschaftsentwicklung unseres Raumes besonderes Anliegen. Der Lehrstuhl hat insbesondere im letzten Jahrzehnt der Quartärforschung inhaltlich und methodisch hohe Priorität verliehen und sich stark mit der internationalen Quartärforschung vernetzt. Die Mitarbeiter, die mit innovativen Methoden quartärwissenschaftliche Themen in großer Breite bearbeiten, freuen sich darauf, mit der Ausrichtung der Tagung neue Akzente zu setzen. Dazu dienen Sitzungen zu den unten genannten Schwerpunktthemen sowie freie Themen.

Neben mehreren eintägigen Exkursionen in die Umgebung werden in einer 2-tägigen Vorexkursion zu neuen „Highlights“ aus dem Quartär Ostbayerns sowie in einer 3-tägigen Nacherkursion nach Tschechien bisher weniger bekannte Erkenntnisse und Fragestellungen präsentiert, wie Morphotektonik und Neotektonik im Westteil der böhmischen Masse, Neovulkanismus einschließlich quartärem Vulkanismus, Lössstratigraphie und jungpleistozäne Umwelt, holozäne Klimgeschichte und Extremereignisse.

Schwerpunktthemen

(Stand 13. Januar, 2012)

- Fortschritte der Quartärstratigraphie
 - Löss & terrestrische Archive
 - Endogene Prozesse (Neotektonik & Vulkanismus)
 - Steinzeitliche Menschen und Umweltwandel
 - Quartäre Landschaftsentwicklung – ein Schlüssel zum Verständnis aktueller Georisiken
- Ort: Campus der Universität Bayreuth, Gebäude Geowissenschaften I+II

Kontakt & Adresse

DEUQUA 2012
c/o Lehrstuhl Geomorphologie
Geographisches Institut
Universität Bayreuth
95440 Bayreuth
Telefax: ++49 (0)921 / 552314

Vorläufiges Tagungsprogramm

15.-16.9.12

Vorexkursion

(A) Neue Highlights aus dem Quartär Ostbayerns – Deckenschichten, Auensedimente, Moore, Tektonik im Löss (Leitung: Völkel/Leopold/Niemeyer/Raab) ab Regensburg

16.9.2012

15:00 Stadtführung (Neptunbrunnen am Hauptmarkt); ab 18:00 Icebreaker in der Paläobotanischen Sammlung Rossmann (Uni Campus)

17.9.2012

9:00 Eröffnung, Vorträge, Posterpräsentationen Teil 1
18:30 Öffentlicher Abendvortrag

18.9.2012

8:30 Vorträge, Posterpräsentationen Teil 2
19:00 Gemeinsames Abendessen in einer traditionellen Kleinbrauerei mit Fränkischem Kabarett

19.9.2012

8:30 Vorträge, Posterpräsentationen Teil 3
17:00 Mitgliederversammlung & Stadtführung für Nichtmitglieder

20.9.2012

8:00 Tagesexkursionen
(B) Europäische Wasserscheide, Flussgeschichte, Bruchsollzone, Trebgasttal
(C) Mit der "Eiszeit" ins Quartär und den "Dinos" zu den Anfängen Europas - der Geopark Bayern-Böhmen
(D) Steinzeit auf der Frankenalb
(E) Geologische Highlights Oberfrankens
(F) Flussgeschichte des Ober- und Mittelmais

21.-23.9.2012

Nacherkursion
(G) Tschechien (Neotektonik, Neovulkanismus, Holozän, Löss; Leitung: Cilek/Lisa/Peterek/Zöller).

Anmeldung

Anmeldungen von Vortrags- und Posterbeiträgen (mit Kurzfassung) werden bis zum 01.06.2012 erbeten. Das Organisationskomitee behält sich vor, Vortragesanmeldungen in die Postersession zu verschieben.
Verbindliche Anmeldung zur Tagung bis 01.07.12.

Nähtere Informationen zu den Exkursionen, den Schwerpunktthemen und dem aktuellen Tagungsprogramm, sowie online Anmeldung unter:
www.bayceer.uni-bayreuth.de/deuqua2012

Ludwig Zöller (Bayreuth)



AUS DEM INHALT

Nachweis des Europäischen Waldelefanten *Elephas antiquus* [FALCONER & CAUTLEY, 1847] bei Neubrandenburg in Mecklenburg-Vorpommern (NE-Deutschland) – Fundbericht
Stefan Meng [Greifswald]

Findling Trissow
Hans-Jörg Altenburg [Utzedel]

Klassifikation und Aufbau ausgewählter Vorkommen glazilimnischer Sedimente nördlich der Pommerschen Eisrandlage im brandenburgischen Abschnitt der Erdgasfernleitung OPAL1
Olaf Juschus [Berlin], Norbert Schlaak [Cottbus]

Steine am Stolper Turm
Karl-Jochen Stein [Waldsee]

Die Blekinge-Region – Gesteine im Anstehenden und als Geschiebe
Hans-Jörg Altenburg [Utzedel]

88 Seiten, 17 x 24 cm, Softcover
www.geologische-beitraege.de

Für 8,50 Euro beim Verlag oder direkt bei den Herausgebern bestellbar.
Manuskript-Einreichungen sind gerne gesehen. Bitte schreiben Sie an:
redaktion@geologische-beitraege.de



Geozon Science Media
Postfach 3245
D-17462 Greifswald
Germany

Tel. 03834-80 14 80
Fax 03834-80 14 81
E-Mail: info@geozon.net
www.geozon.net



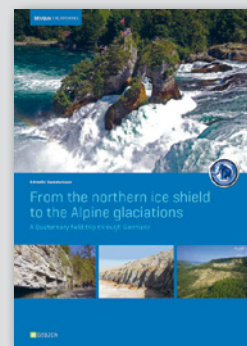
Eiszeitlandschaften in Mecklenburg-Vorpommern
ISBN 978-3-941971-05-9
34,- Euro



Zur Landschafts- und Gewässergeschichte der Müritz
ISBN 978-3-941971-00-4
29,- Euro



Glaciations and periglacial features in Central Europe
ISSN 0424-7116
54,- Euro



From the northern ice shield to the Alpine glaciations
ISBN 978-3-941971-06-6
29,- Euro

IN VORBEREITUNG

Die spätpleistozäne und holozäne Gewässernetzentwicklung im Bereich der Pommerschen Haupteisrandlage Mecklenburgs
Sebastian Lorenz · ISBN: 978-3-941971-03-5

Die Bauern- und Waldarbeiterdörfer im Naturpark und seinem Umfeld
Förderverein Naturpark Nossentiner/Schwinzer Heide e.V. · ISBN 978-3-941971-07-3



Geozon Science Media
Postfach 3245
D-17462 Greifswald
Germany

Tel. 03834-80 14 80
Fax 03834-80 14 81
E-Mail: info@geozon.net
www.geozon.net

Radiocarbon Dating shouldn't take ages



BETA

Beta Analytic
Radiocarbon Dating
Since 1979

- Results in as little as 2-3 days
- ISO 17025-accredited measurements
- Outstanding customer service

Australia Brazil China India Japan UK USA

Visit www.radiocarbon.com for details

Instruction to Authors

Basically the manuscript shall be submitted in electronic form and has to include the name and the address of the first author. Please use a standard word processor in .rtf, .odt or .doc-format (LaTeX files on request). As character set please use the standard fonts Times Roman, Helvetica or Courier with 1.5 line spacing.

For the submission please use our online system at www.quaternary-science.net. After the login you can upload your manuscript as well as separate figures and tables.

Manuscript style

The acceptable languages are English and German. Manuscripts in German have to contain an English subtitle, an abstract in English and English keywords. The rules of the new German spelling reform apply to German texts.

Manuscripts should be arranged in the following order:

- I Short but concise title
- II Full names, full address and e-mail
- III 5 to 10 keywords that describe the contents of your paper
- VI An abstract of up to 200 words in German and English.
The translated abstract should carry the translated title in square brackets,
- V Clearly structured text. For chapter numbering use Arabic numerals.
- VI The reference list has to be arranged alphabetically and should be conform to the examples given below.

References have to be insert in the text as brief quotations, the name of the author has to be set in small CAPITALS, the year of publication in brackets e.g. MÜLLER (2006). If more than one publication of the same author in the same year is cited, identify each citation as follows: MÜLLER (2006a, 2006b). Where three or more authors are listed in the reference list, please cite in the text as MÜLLER et al. (2006). Papers with up to three authors should be cited as MÜLLER & MEYER (2006) or MÜLLER, MEYER & SCHULZ (2006). If a special page or figure of a paper should be cited, use following citation style: MÜLLER (2006: 14) or MÜLLER (2006, Fig. 14).

Scientific names of flora and fauna (*gender, sub-gender, species, sub-species*) have to be written in *italics*. Use small CAPITALS for the author (*Armeria maritima* WILLD.)

- Do not justify your text, use a ragged left alignment.
- Do not use automatic hyphenation.
- Do not use any automatic formatting.
- Do not use pagination.

Do not insert images, tables and photos into the text, it should be added as separate files. Captions of figures and tables in German and English should be placed at the end of the manuscript.

Illustrations

Supply each figure as a separate file with the name of the author. Illustrations should be reducible to a column width (8.4 cm) or type area (17.2 x 26 cm). The lettering has to be easy readable after reduction. Where a key of symbols is required, include this in the figure, not in the caption of the figure. Avoid fine lines (hairlines) and grey-shading/ halftones. All figures may be colored. There are no additional costs.

For printing all illustrations have to be supplied electronically. Please use for pixel-based images (photos) the .tif-format with a resolution of at least 450 dpi and for vector-based illustrations (graphs, maps, tables) the .eps-format. Greatly reduced .jpg-files or .pdf-files or figures included in word-documents are not accepted.

References [examples]

Papers:

- SCHWARZBACH, M. (1968): Neue Eiszeithypothesen. – Eisezeitalter und Gegenwart, 19: 250–261.
- EISSMANN, L. & MÜLLER, A. (1979): Leithilinen der Quartärenentwicklung im norddeutschen Tiefland. – Zeitschrift für Geologische Wissenschaften, 7: 451–462.
- ZAGWIJN, W.H. (1996): The Cromerian Complex Stage of the Netherlands and correlation with other areas in Europe. – In: TURNER, C. (ed.): The Middle Pleistocene in Europe: 145–172; Rotterdam (Balkema).
- MAGNY, M. & HAAS, J.N. (2004): A major widespread climatic change around 5300 cal. yr BP at the time of the Alpine Iceman. – Journal of Quaternary Science, 19: 423–430. DOI: 10.1002/jqs.850

Books:

- EHLERS, J. (1994): Allgemeine und historische Quartärgeologie. – 358 S.; Stuttgart (Enke).

Please do not use abbreviations of the journal names.

Specimen copies

Authors receive no printed specimen copies. The electronic version is available as download free.

For further questions about the submission of manuscripts please contact the production editor (imprint).

Autorenhinweise

Das Manuskript ist grundsätzlich in elektronischer Form einzureichen und muss mit Namen und Adresse des Erstautoren versehen sein. Bitte benutzen Sie eine Standard-Textverarbeitung im .rtf, .odt oder .doc-Format (LaTeX-Daten auf Anfrage). Als Zeichensatz verwenden Sie bitte die Standard-Fonts Times Roman, Helvetica oder Courier mit einem 1,5-fachen Zeilenabstand.

Zur Einreichung nutzen Sie bitte unser Online Submission System unter www.quaternary-science.net. Nach dem Login steht Ihnen hier eine Upload-Funktion für das Manuskript und die Abbildungs-Dateien zur Verfügung.

Manuskriptform

Als Publikationssprachen sind Englisch und Deutsch zugelassen. Manuskripte in deutscher Sprache müssen einen englischen Untertitel tragen sowie eine englische Kurzfassung und englische Keywords beinhalten. Für die deutschen Texte gelten die Regeln der neuen Rechtschreibreform.

Die Manuskripte sollen folgendem Aufbau entsprechen:

- I Kurze, aber prägnante Überschrift
- II Ausgeschriebener Vor- und Nachname, Post- und E-Mail-Adresse
- III 5 bis 10 englische Keywords, die den Inhalt des Manuskriptes widerspiegeln.
- IV Deutsche und englische Kurzfassung des Textes mit einer Länge von bis zu 200 Wörtern. Der englische Untertitel des Manuskriptes ist der englischen Kurzfassung in eckigen Klammern voranzustellen.
- V Klar gegliederter Text. Kapitelnummernierungen sind mit arabischen Ziffern zu versehen.
- VI Alphabetisch geordnete Literaturliste. Die Zitierweise muss der unten angegebenen Form entsprechen.

Im fortlaufenden Text sind Literaturhinweise als Kurzzitate einzufügen, der oder die Autorennamen sind in KAPITÄLCHEN-Schrift zu setzen, das Erscheinungsjahr in Klammern, z. B. MÜLLER (2006). Werden von einem Autor mehrere Arbeiten aus einem Jahr zitiert, so sind diese durch Buchstaben zu unterscheiden: MÜLLER (2006a, 2006b). Bei mehr als drei Autoren kann et al. verwendet werden: MÜLLER et al. (2006). Arbeiten mit bis zu drei Autoren werden folgendermaßen zitiert: MÜLLER & MEYER (2006) oder MÜLLER, MEYER & SCHULZ (2006). Sind mit der Zitierung bestimmte Seiten oder Abbildungen gemeint, müssen diese genau angegeben werden: MÜLLER (2006: 14) oder MÜLLER (2006: Fig. 14).

Die wissenschaftlichen Namen von Pflanzen und Tieren (*Gattungen, Untergattungen, Arten, Unterarten*) sind kursiv zu schreiben. Die den biologischen Namen folgenden Autoren werden in KAPITÄLCHEN gesetzt (*Armeria maritima* WILLD.).

Bitte keinen Blocksatz verwenden, sondern linksbündigen Satz.
Bitte keine automatische Silbentrennung verwenden.
Bitte alle automatischen Formatierungen in Ihrer Textbearbeitung deaktivieren.

Bitte keine Seitenzählung.

Abbildungen, Tabellen und Fotos nicht in den Text einbauen, sondern separat als Datei beifügen. Abbildungsunterschriften in Deutsch und Englisch am Ende des Manuskripttextes platzieren.

Abbildungen

Bitte fügen Sie jede Abbildung als separate Datei mit einem eindeutigen Namen bei. Alle Grafiken müssen eine Verkleinerung auf Spaltenbreite (= 8,4 cm) oder Satzspiegel (= 17,2 x 26 cm) zulassen. Die Beschriftung muss nach der Verkleinerung noch gut lesbar sein. Sollte eine Legende nötig sein, so binden Sie diese in die Abbildung ein. Bitte vermeiden Sie Haarlinien oder Grauwerte. Alle Abbildungen können farbig sein. Es entstehen keine Mehrkosten.

Für die Drucklegung müssen alle Abbildungen in elektronischer Form eingereicht werden. Bitte verwenden Sie für pixelbasierte Abbildungen (Fotos) das .tif-Format mit einer Auflösung von mindestens 450 dpi und für vektorbasierte Abbildungen (Diagramme, Maps, Tabellen) das .eps-Format. Stark reduzierte jpg oder .pdf-Dateien sowie in Text-Dokumente eingebundene Abbildungen werden nicht akzeptiert.

Zitierweise (Beispiele)

Aufsätze:

- SCHWARZBACH, M. (1968): Neue Eiszeithypothesen. – Eiszeitalter und Gegenwart, 19: 250–261.
- EISSMANN, L. & MÜLLER, A. (1979): Leitlinien der Quartär-entwicklung im norddeutschen Tiefland. – Zeitschrift für Geologische Wissenschaften, 7: 451–462.
- ZAGWIJN, W.H. (1996): The Cromerian Complex Stage of the Netherlands and correlation with other areas in Europe. – In: TURNER, C. (ed.): The Middle Pleistocene in Europe: 145–172; Rotterdam (Balkema).
- MAGNY, M. & HAAS, J.N. (2004): A major widespread climatic change around 5300 cal. yr BP at the time of the Alpine Iceman. – Journal of Quaternary Science, 19: 423–430. DOI: 10.1002/jqs.850

Monographische Werke, Bücher:

- EHLERS, J. (1994): Allgemeine und historische Quartärgeo- logie. – 358 S.; Stuttgart (Enke).

Bitte keine Abkürzungen der Zeitschriftentitel verwenden.

Belegexemplare

Es werden keine gedruckten Belegexemplare verschickt. Die elektronische Version steht zum kostenlosen Down-load zur Verfügung.

Bei weiteren Fragen zur Manuskriteinreichung wenden Sie sich bitte an die technische Redaktion (s. Impressum).

German Quaternary Association

The German Quaternary Association (DEUQUA) eV is an association of German-speaking Quaternary Scientists. The aim of the association is to promote the Quaternary Science, to represent it in public, to intensify the contact to applied science as well as to advice public and political boards in quaternary issues.

Furthermore, the association has set itself the task of operating the contacts between the Quaternary Scientists and related organizations at home and abroad.

The DEUQUA published annually several editions of "E&G – Quaternary Science Journal". In that journal research results from the field of Quaternary Science are published. In addition, developments in the DEUQUA are announced in the "Geoscience messages" (GMIT). GMIT is published quarterly.

Every two years, the German Quaternary Association held the DEUQUA-Conference. At this conference the latest research results of the Quaternary Science are presented and discussed.

Committee / Vorstand



PRESIDENT / PRÄSIDENTIN

MARGOT BÖSE
Freie Universität Berlin
Malteserstr. 74–100
D-12249 Berlin, Germany
Tel.: +49 [0]30-838-70 37 3
E-Mail: m.boese [at] fu-berlin.de

VICE PRESIDENTS / VIZEPRÄSIDENTEN

CHRISTOPH SPÖTL
Institut für Geologie und Paläontologie
Universität Innsbruck
Innrain 52
A-6020 Innsbruck, Austria
Tel.: +43 [0]512-507-5593
Fax: +43 [0]512-507-2914
E-Mail: christoph.spoetl [at] uibk.ac.at

LUDWIG ZÖLLER
Fakultät II – Lehrstuhl für Geomorphologie
Universität Bayreuth
Universitätsstraße 30
D-95440 Bayreuth, Germany
Tel.: +49 [0]921-55 2266
Fax: +49 [0]921-55 2314
E-Mail: ludwig.zoeller [at] uni-bayreuth.de

TREASURER / SCHATZMEISTER

JÖRG ELBRACHT
Landesamt für Bergbau, Energie und Geologie
Stilleweg 2
D-30655 Hannover, Germany
Tel.: +49 [0]511-643-36 13
E-Mail: joerg.elbracht [at] lbg.niedersachsen.de

EDITOR-IN-CHIEF / SCHRIFTLEITUNG (E&G)

HOLGER FREUND
ICBM – Geoecology
Carl-von-Ossietzky Universitaet Oldenburg
Schleusenstr. 1
D-26382 Wilhelmshaven, Germany
Tel.: +49 [0]4421-94 42 00
E-Mail: holger.freund [at] uni-oldenburg.de

ARCHIVIST / ARCHIVAR

STEFAN WANSA
Landesamt für Geologie und Bergwesen
Sachsen-Anhalt
Postfach 156
D- 06035 Halle, Germany
Tel. +49 [0]345-5212-12 7
E-Mail: wansa [at] lagb.mw.sachsen-anhalt.de

ADVISORY BOARD / BEIRAT

CHRISTIAN HOSELMANN
Hessisches Landesamt für Umwelt und Geologie
Postfach 3209
D-65022 Wiesbaden, Germany
Tel.: +49 [0]611-69 39 92 8
E-Mail: christian.hoselmann [at] hlug.hessen.de

DANIELA SAUER

Institut für Bodenkunde und Standortslehre
Universität Hohenheim
Emil-Wolff-Str. 27
D-70593 Stuttgart, Germany
Tel.: +49 [0]711-459-22 93 5
E-Mail: d-sauer [at] uni-hohenheim.de

FRANK PREUSSER

Department of Physical Geography and
Quaternary Geology
Stockholm University
10961 Stockholm, Sweden
Tel. +46 8 674 7590
E-Mail: frank.preusser@natgeo.su.se

REINHARD LAMPE

Institut für Geographie und Geologie
Ernst-Moritz-Arndt-Universität Greifswald
Friedrich-Ludwig-Jahn-Straße 16
D-17487 Greifswald, Germany
Tel.: +49 [0]3834-86-45 21
E-Mail: lampe [at] uni-greifswald.de

BIRGIT TERHORST

Geographisches Institut
Universität Würzburg
Am Hubland
D-97074 Würzburg, Germany
Deutschland
Tel. +49 [0]931-88 85 58 5
E-Mail: birgit.terhorst [at] uni-wuerzburg.de

Deutsche Quartärvereinigung

Die Deutsche Quartärvereinigung (DEUQUA) e.V. ist ein Zusammenschluss deutschsprachiger Quartärwissenschaftler und wurde 1949 gegründet. Der Verein hat zum Ziel, die Quartärwissenschaft zu fördern, sie in der Öffentlichkeit zu vertreten, den Kontakt zu angewandter Wissenschaft zu intensivieren sowie öffentliche und politische Gremien in quartärwissenschaftlichen Fragestellungen zu beraten. Des Weiteren hat der Verein sich zur Aufgabe gemacht, die Kontaktpflege der Quartärforscher untereinander und zu verwandten Organisationen im In- und Ausland zu betreiben.

Die DEUQUA veröffentlicht jährlich mehrere Ausgaben von „E&G – Quaternary Science Journal“. Dort werden Forschungserkenntnisse aus dem Bereich der Quartärwissenschaft publiziert. Zusätzlich werden Entwicklungen in der DEUQUA vierteljährlich in den Geowissenschaftlichen Mitteilungen (GMIT) bekannt gemacht.

Im zweijährigen Turnus veranstaltet die Deutsche Quartärvereinigung e.V. die DEUQUA-Tagung. Diese bietet ein Forum, in welchem aktuelle Forschungsergebnisse aus dem Bereich der Quartärwissenschaften vorgestellt und diskutiert werden.

Reorder / Nachbestellung

The volumes 6–7, 11–17, 19–28 and 30–58 are currently available. All other volumes are sold out. A reduced special price of 10,- € per edition is up to and including volume 55. The regular retail price applies from vol. 56/1–2. The complete content is searchable at www.quaternary-science.net.

1951-2006

Vol. 6–7, 11–17, 19–28, 30–55 each volume 10,— €

2007	Topics	Price
Vol. 56 No 1-2	Special issue: Stratigraphie von Deutschland – Quartär	54,- €
Vol. 56 No 3	Pfälzerwald, pollen types and taxa, Oberösterreich, Riß-Iller, Schatthausen	27,- €
Vol. 56 No 4	Nußloch, Rangsdorfer See, Lieth/Elmshorn, Gardno Endmoräne/Debina Cliff	27,- €

2008	Topics	Price
Vol. 57 No 1-2	Special issue: Recent progress in Quaternary dating methods	54,- €
Vol. 57 No 3-4	Special issue: The Heidelberg Basin Drilling Project	54,- €

2009	Topics	Price
Vol. 58 No 1	Surface Exposure Dating, Bodensee, Living Fossil, Hochgebirgsböden	27,- €
Vol. 58 No 2	Special issue: Changing environments – Yesterday, Today, Tomorrow	27,- €

2010	Topics	Price
Vol. 59 No 1-2	Baltic Sea Coast, Rodderberg Crater, Geiseltal, Wettersteingebirge, Møn, Argentina	54,- €

2011	Topics	Price
Vol. 60 No 1	Special issue: Loess in Europe	27,- €
Vol. 60 No 2-3	Special issue: Glaciations and periglacial features in Central Europe	54,- €
Vol. 60 No 4	Special issue: Quaternary landscape evolution in the Peribaltic region	27,- €

2012	Topics	Price
Vol. 61 No 1	Calcareous Alps Austria, Löss, Holzreste Schweiz, Rinnen-Strukturen, Permafrost carbon	27.- €

The prices are understood plus shipping costs. VAT is included.

Subscription / Abonnement

Title: E&G – Quaternary Science Journal

Print-ISSN: 0424-7116

Issues per volume: 2

Prices (EUR) print per volume

End customers: 50,46 € (Free for DEUQUA-Members)
Wholesalers, booksellers: 32,80 €
Scientific libraries: 47,94 €
VAT is not included.

Postage [EUR] per volume

within Germany: 2,50 €
World (Surface): 6,80 €
World (Airmail): 7,70 €

Special offer

Libraries which subscribe our journal can receive the volumes 1951–2006 for free. Only shipping costs have to be paid.

Order address

Geozon Science Media
P.O. Box 3245
D-17462 Greifswald
Germany

tel.: +49 (0)3834-80 40 80
fax: +49 (0)3834-80 40 81
e-mail: info (at) geozon.net
web: www.geozon.net

Contents

- DOI 10.3285/eg.61.1.01
3 **Sediment imprint of the severe 2002 summer flood in the Lehnsmühle reservoir, eastern Erzgebirge (Germany)**
Lucas Kämpf, Achim Brauer, Peter Dulski, Karl-Heinz Feger, Frank Jacob, Eckehard Klemt
- DOI 10.3285/eg.61.1.02
16 **Effects of deglacial sedimentation pulse, followed by incision: A case study from a catchment in the Northern Calcareous Alps (Austria)**
Diethard Sanders
- DOI 10.3285/eg.61.1.03
32 **Rhine loess at Schwalbenberg II – MIS 4 and 3**
Wolfgang Schirmer
- DOI 10.3285/eg.61.1.04
48 **Formation and geochronology of Last Interglacial to Lower Weichselian loess/palaeosol sequences – case studies from the Lower Rhine Embayment, Germany**
Peter Fischer, Alexandra Hilgers, Jens Protze, Holger Kels, Frank Lehmkühl, Renate Gerlach
- DOI 10.3285/eg.61.1.05
64 **Holzreste von spätglazialen Kiefern aus der tiefgründigen und tonreichen Permanentrutschung „Spiegelberg“, Kanton Schwyz (Schweiz)**
Conradin Zahna, Markus Gasser, Ruth Drescher-Schneider, Jakob Gasser, Christian Schlüchter
- DOI 10.3285/eg.61.1.06
69 **Zur periglaziären Bildung und Überformung rinnenartiger Strukturen im Jungmoränengebiet Süd-Holsteins**
Alf Grube
- DOI 10.3285/eg.61.1.07
84 **A permafrost glacial hypothesis – Permafrost carbon might help explaining the Pleistocene ice ages**
Roland Zech